



Computer-aided design methodology for separation processes with ionic liquids

Chen, Yuqiu

Publication date:
2020

Document Version
Publisher's PDF, also known as Version of record

[Link back to DTU Orbit](#)

Citation (APA):
Chen, Y. (2020). *Computer-aided design methodology for separation processes with ionic liquids*. Technical University of Denmark.

General rights

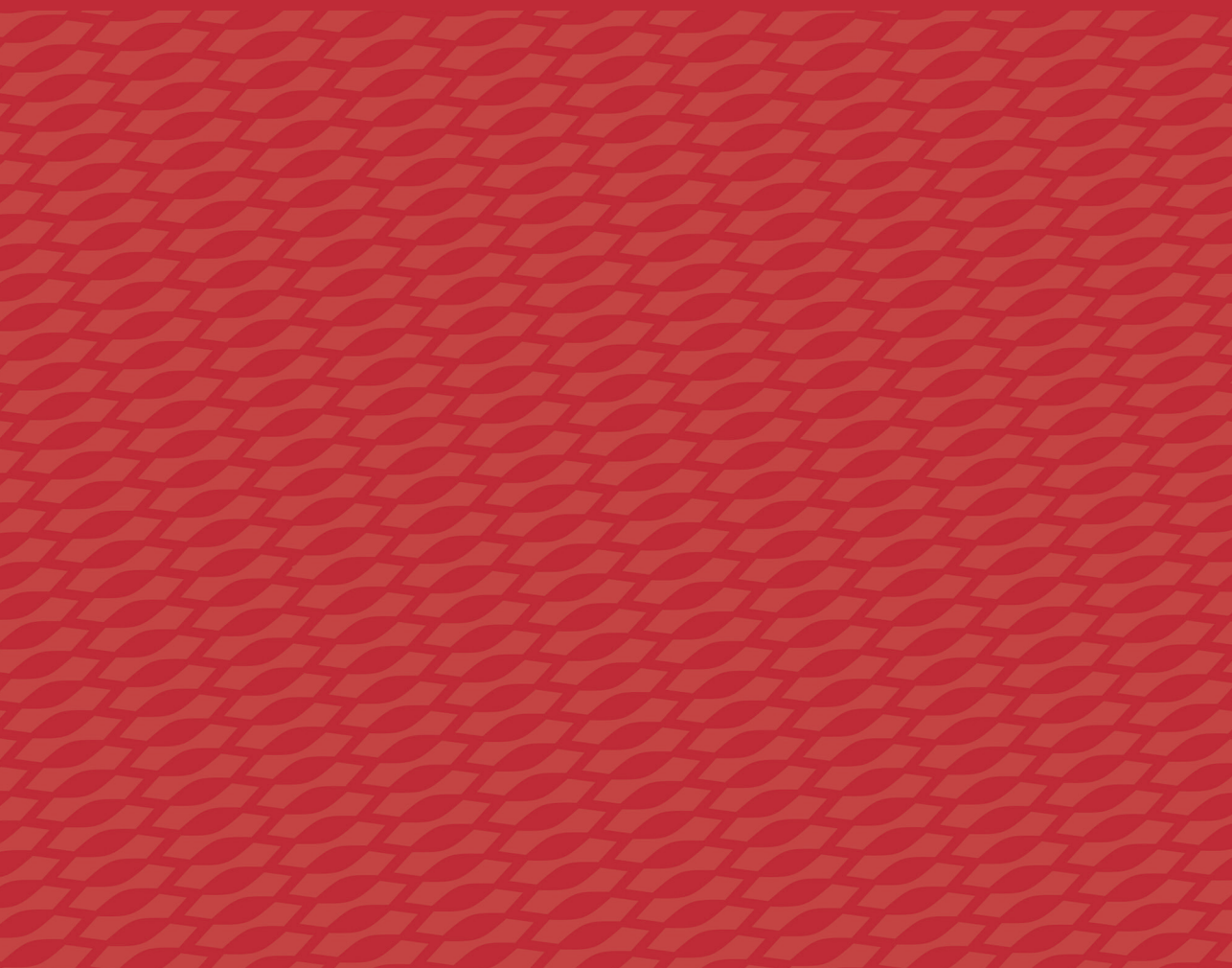
Copyright and moral rights for the publications made accessible in the public portal are retained by the authors and/or other copyright owners and it is a condition of accessing publications that users recognise and abide by the legal requirements associated with these rights.

- Users may download and print one copy of any publication from the public portal for the purpose of private study or research.
- You may not further distribute the material or use it for any profit-making activity or commercial gain
- You may freely distribute the URL identifying the publication in the public portal

If you believe that this document breaches copyright please contact us providing details, and we will remove access to the work immediately and investigate your claim.

Computer-aided design methodology for separation processes with ionic liquids

Yuqiu Chen
PhD Thesis
2020





Computer-aided design methodology for separation processes with ionic liquids

Yuqiu Chen

PhD Thesis

2020

DTU Chemical Engineering

Department of Chemical and Biochemical Engineering



Computer-aided design methodology for separation processes with ionic liquids

Doctor of Philosophy Thesis

Yuqiu Chen

October 2020

KT-Consortium

Department of Chemical and Biochemical Engineering

Technical University of Denmark

Technical University of Denmark

Anker Engelundsvej 1

Building 101A

DK-2800, Kgs. Lyngby

Denmark

CVR-nr.30060946

Phone:(+45) 45 25 25 25

Email:dtu@dtu.dk

www.dtu.dk

PREFACE

This thesis is submitted as a fulfillment of the requirements for the degree of Doctor of Philosophy (Ph.D.) in Chemical Engineering at the Technical University of Denmark (DTU).

The PhD project has been carried out at the KT Consortium research group of the Department of Chemical and Biochemical Engineering, DTU from November 1st, 2017 until October 31st, 2020, under the supervision of Professor John M. Woodley (from Process and Systems Engineering (PROSYS)) and Professor Georgios M. Kontogeorgis (from Center for Energy Resources Engineering (CERE)) at the Department of Chemical and Biochemical Engineering, Technical University of Denmark. The Ph.D. thesis work has been funded by the China Scholarship Council and KT Consortium from Chemical and Biochemical Engineering Department at Technical University of Denmark.

First of all, I would like to take this opportunity to express my deepest appreciation and sincere gratitude to my supervisors Prof. John M. Woodley and Prof. Georgios M. Kontogeorgis for their insightful guidance, teaching, support and encouragement during these three eventful years. Their positive criticism, motivation and confidence in me has greatly improved my technical and personal skills. I will always be grateful to them for their valuable time over these years.

I would like to genuinely thank my former supervisor, Prof. Rafiqul Gani for not only giving me this opportunity to work on this challenging and innovative project, but also for sharing his own viewpoint and perspectives about Process Systems Engineering. His guidance has been very inspiring to broaden my thought process.

I would also like to express my gratitude to Nipun and Xinyan, who have always been available for technical conversations and support. I am also thankful to Eva, who has always been there to help me. I also acknowledge my former and current colleagues at KT Consortium and CERE at DTU. Also, a special thanks to Saeed, Alay, Yingjun, Xianglei, Olivia, Spardha, Hao, Jiahuan, Meng, Xiaodong, for many helpful discussions, suggestions and support.

Finally, I would like to thank my parents, my sisters Yumin and Yubing, as well as my uncle Riping for their unlimited support and understanding over the past three years.

Thank-you once again to all!

Yuqiu Chen

October 2020

Kongens Lyngby, Denmark

ABSTRACT

In the process industries, separation represents a fundamental step to reach the products quality and purity required by the market. Its efficiency could promote the development of industry to reap great energy and environmental benefits. Therefore, any new separation technologies or intensified process designs allowing energy efficient and sustainable operations are highly desirable, especially for energy intensive and difficult separation processes. Separations of close-boiling and azeotropic mixtures as well as many gas separations are representatives of high energy consuming processes, while the downstream separation in bioprocesses is usually difficult and expensive because of recovery of targeted products from dilute aqueous solutions. In response to increasing energy and environmental challenges, several new innovative separation technologies and intensified process designs have been widely studied. Among them, separation technologies using ILs as solvents are being paid more attention due to its attractive properties such as non-volatility, inflammability exhibiting good solubility and selectivity for a wide range of organic and inorganic chemicals. Nonetheless, some challenges need to be addressed before taking their place in industrial applications, such as how to lower the price of ILs and reduce their viscosities, and particularly how to design/screen suitable ILs for different separation systems.

The main objective of this work is to develop a systematic computer-aided design method that is able to rapidly and reliably screen suitable ILs with desired properties as well as meet specific objectives. Since the performance of this non-experimental based design method largely depend on the predictive property models; group contribution (GC)-based property models covering various ILs are developed. Alongside, a comprehensive UNIFAC-IL-Gas model that combines IL-gas and other IL-solute systems is also proposed to predict the thermodynamic behaviors of the studied IL containing systems. In all cases, property models are validated by using 20-30% of data points as test datasets. These models can be easily integrated in the computer-aided design method of ILs, and they can also be used to predict properties of ILs that have not yet been synthesized. This is essential to find new high-performance ILs for different industry applications. Unlike experimental-based or other trial-and-error solvent screening methods that are usually time consuming and expensive, the design method of ILs proposed in this work is both cost- and time-efficient due to the fact that this methodology is completely based on the predictive property models.

On the other hand, ILs are introduced to the intensified process designs including hybrid process schemes, integrated solvent and process design, and *in situ* product removal (ISPR). Furthermore, different design methodologies are proposed accordingly for each of the intensified process design involving ILs. These IL-based intensified process designs along with associated algorithms, knowledge bases and tools are, respectively, tested with different case studies. (1) Hybrid process schemes with ILs: separation of aqueous solutions and production of aldehydes by bio-oxidation of alcohols. (2) Integrated IL and process design: separation of ethanol-water, separation of acetone-methanol, and CO₂ capture process. (3) IL-based ISPR design: biobutanol production from acetone-butanol-ethanol (ABE) fermentation. For all intensified process designs, the computer-aided design method of ILs as well as the physical and thermodynamic property models are included. In each of the case study, new IL(s) and optimized process operations are achieved using proposed design methodologies.

Besides all the case studies described above, the proposed computer-aided design method of ILs is also used to design optimal ILs for some other applications: for removing acid gas (e.g. CO₂, H₂S) from shale/natural gas, for recovering bio-isoprene from fermentation off-gas, and as electrolyte additives in lithium titanate (LTO) batteries. In all studied cases, the designed ILs provide better process performance when compared to their corresponding benchmark solvents or additives.

RESUME PÅ DANSK

I procesindustrien er separation et grundlæggende trin for at opnå produktkvalitet og renhed, som markedet kræver. Dens effektivitet kunne fremme industriens udvikling og resultere i store energi- og miljøfordele. Derfor er enhver ny adskillesesteknologi eller intensiveret procesdesign, der tillader energieffektivitet og bæredygtig drift, meget eftertragtet især til energi intensive og vanskelige separationsprocesser. Separationer af tæt kogende og azeotrope blandinger samt mange gasseparationer er repræsentanter for høj energiforbrugende processer, mens downstream separation i bioprocesser er normalt vanskelig og dyr på grund af fremskaffelse af målprodukterne fra fortyndede vandige opløsninger. Som reaktion på stigende energi- og miljøudfordringer bliver flere nye innovative adskillesesteknologier og intensiverede procesdesign bredt undersøgt. Blandt dem er fokus på adskillesesteknologier der bruger IL'er som opløsningsmidler. På grund af dets attraktive egenskaber såsom ikke-flygtighed og brændbarhed som udviser god opløselighed og selectivity for en bred vifte af organiske og uorganiske kemikalier. Ikke desto mindre skal nogle udfordringer løses før de kan bruges i industrien, såsom hvordan man sænker prisen på IL'er og reducerer deres viskositet, og især hvordan man designer/udvælger passende IL'er til forskellige separationssystemer.

Hovedformålet med dette stykke arbejde er at udvikle en systematisk computerstøttet designmetode, der er i stand til at hurtig og pålidelig udvælge passende IL'er med ønsket egenskaber og opfylder specifikke mål. Da ydeevne af denne ikke-eksperimentelle baserede designmetode afhænger i høj grad af de predictive property modeller, er gruppebidrag (GC)-baserede property modeller, der dækker forskellige IL'er, udviklet. Sideløbende er en omfattende UNIFAC-IL-Gas-model, der kombinerer IL-gas og andre IL-oplysning systemer, også forslået til at forudsige den termodynamiske opførsel af de undersøgte systemer med IL. I alle tilfælde valideres property modeller ved brug af 20-30% af datapunkterne som test datasæt. Disse modeller kan let integreres i den computerstøttede designmetode for IL'er, og de kan også bruges til at forudsige egenskaber for IL'er, der endnu ikke er blevet syntetiseret. Dette er essentiel for at finde nye high-performance IL'er til forskellige industrielle applikationer. I modsætning til eksperimentelt baseret eller andre trial and error solvent udvælges metoder, som mange gang er tidskrævende og dyre, er design metoden for IL'er foreslået i denne opgave både omkostnings- og tidseffektiv, på grund af det faktum at, denne metode er helt baseret på de predictive property modeller.

På den anden side bliver IL'er introducerede til de intensified process designs, herunder hybrid process schemes, integreret opløsningsmiddel og procesdesign samt *in situ* product removal (ISPR). Desuden foreslås forskellige designmetoder for hver af de intensiverede procesdesign der involverer IL'er. Disse IL-baserede intensiverede procesdesign sammen med de tilhørende algoritmer, baggrundsviden og værktøjer bliver henholdsvis testet med forskellige casestudier. (1) Hybrid process schemes med IL'er: adskillelse af vandige opløsninger og produktion af aldehyder ved bio-oxidation af alkoholer. (2) Integreret IL og procesdesign: adskillelse af ethanol-vand, adskillelse af acetone-methanol og CO₂ opsamlingsproces. (3) IL-baseret ISPR-design: produktion af biobutanol fra fermentation af acetone-butanol-ethanol (ABE). For alle intensiverede procesdesigner er den computerstøttet designmetode for IL'er såvel som de fysiske og termodynamiske property modeller inkluderet. I hver af casestudierne er de nye IL(er) og optimerede proces operationer fremskaffede ved hjælp af foreslået designmetoder.

Udover alle de førnævnte casestudier bliver den foreslået computerstøttet designmetode for IL'er også brugt til at designe optimale IL'er til nogle andre anvendelser: fjernelse af acid gas (f.eks. CO₂, H₂S) fra skifergas/naturgas, genvinding af bio-isoprene fra fermentation af off-gas og som elektrolyt tilsætningsstof i lithium titanate (LTO) batterier. I alle undersøgte tilfælde giver de designede IL'er bedre procesydelse sammenlignet med tilsvarende benchmark opløsningsmidler eller tilsætningsstof.

CONTENTS

PREFACE	I
ABSTRACT	II
RESUME PÅ DANSK	IV
CONTENTS	VI
ABBREVIATIONS	VIII
SYMBOLS	XI
1 INTRODUCTION	13
1.1 BACKGROUND AND MOTIVATION	14
1.2 PROJECT OBJECTIVES.....	17
1.3 THESIS STRUCTURE.....	17
1.4 DISSEMINATION OF THE PHD PROJECT RESULTS	18
2 DATABASE AND MODEL LIBRARY	20
2.1 DATABASE ESTABLISHMENT	21
2.2 PROPERTY MODEL DEVELOPMENT.....	25
2.3 UNIFAC-IL MODEL EXTENSION	34
2.4 CHAPTER SUMMARY	53
3 DESIGN METHODOLOGIES	54
3.1 HYBRID PROCESS DESIGN WITH IONIC LIQUIDS	55
3.2 INTEGRATED IONIC LIQUID AND PROCESS DESIGN	80
3.3 IONIC LIQUID-BASED <i>IN-SITU</i> PRODUCT REMOVAL DESIGN.....	97
3.4 CHAPTER SUMMARY	117
4 GAS SEPARATIONS	119
4.1 SHALE GAS PURIFICATION	120
4.2 NATURAL GAS SWEETENING.....	133
5 BIO-ISOPRENE RECOVERY	146
5.1 BIO-ISOPRENE RECOVERY	147
6 APPLICATIONS IN ELECTROCHEMISTRY	161
6.1 ADDITIVES IN LTO BATTERIES.....	162
7 CONCLUSIONS	175
7.1 CONCLUSIONS	176
8 FUTURE PERSPECTIVES	179
8.1 FUTURE PERSPECTIVES.....	180
REFERENCES	182
APPENDIX A	196
GROUP CONTRIBUTION PARAMETERS FOR GC-BASED PROPERTY MODELS	196
APPENDIX B	202

GROUP INTERACTION PARAMETERS FOR UNIFAC-IL-GAS MODEL	202
APPENDIX C	217
VAPOR PRESSURE CALCULATION METHODS FOR GASES INVOLVED IN UNIFAC-IL-GAS MODEL	217
APPENDIX D	218
KINETICS MODEL OF ABE FERMENTATION PROCESS	218

ABBREVIATIONS

AARD	average absolute relative deviation
ABE	acetone-butanol-ethanol
ABS	aqueous biphasic system
ACC	annual capital cost
BA	butyric acid
[C ₁ mmIm][DMP]	1, 2, 3-trimethylimidazolium dimethylphosphate
[C ₁ Py][DMP]	1-methylpyridinium dimethylphosphate
[C ₁ Py][TFA]	1-methylpyridinium trifluoroacetate
[C ₂ mPy][BF ₄]	1-ethyl-3-methylpyridinium tetrafluoroborate
[C ₁ OHPy][TFA]	3-hydroxy-1-methylpyridinium trifluoroacetate
[C ₂ Py][BF ₄]	1-ethylpyridinium tetrafluoroborate
[C ₃ mPy][BF ₄]	3-methyl-1-propylpyridinium tetrafluoroborate
C ₄ mIm][CF ₃ SO ₃]	1-butyl-3-methylimidazolium trifluoroacetate
[C ₄ mim][Cl]	1-butyl-3-methylimidazolium chloride
[C ₄ mIm][Tf ₂ N]	1-butyl-3-methylimidazolium bis(trifluoromethylsulfonyl)imide
[C ₆ mIm][Tf ₂ N]	1-hexyl-3-methylimidazolium bis(trifluoromethylsulfonyl)imide
CaLB	Candida antarctica lipase B
CAMD	computer-aided molecular design
CAIL	computer-aided ionic liquid design
CAPEX	total capital expenditure
COSMO-RS	Conductor-like Screening Model for Real Solvents
CPA	cubic-plus-association
DC	direct cost
DEA	diethanolamine
DEPG	dimethyl ethers of polyethylene glycol
DIPA	diisopropylamine
Dnb	di-n-butylphthalate
NRTL	nonrandom two-liquid model
EC	ethylene carbonate
EDS	extractive desulfurization system
EMC	ethyl carbonate
[emIm][BF ₄]	1-ethyl-3-methylimidazolium tetrafluoroborate
[emIm][CF ₃ SO ₃]	1-ethyl-3-methylimidazolium trifluoromethanesulfonate
EOS	equation of state
FOC	fixed operating cost
FCI	fixed capital investment
GC	group contribution
MAPE	mean absolute percentage error
[mmIm][DMP]	1, 3-dimethylimidazolium dimethylphosphate
[mIm][BF ₄]	1-methylimidazolium tetrafluoroborate
[mmpy][eFAP]	1,3-dimethylpyridinium tris(pentafluoroethyl) trifluorophosphate

MEP	2C-methyl-D-erythritol 4-phosphate
MVA	mevalonic acid
[hmIm][Tf ₂ N]	1-hexyl-3-methylimidazolium bis(trifluoromethylsulfonyl)imide
IC	indirect cost
ILs	ionic liquids
ISPR	<i>in situ</i> product removal
LLE	liquid-liquid extraction
LTO	lithium titanate
MAS	monoethanolamine aqueous scrubbing
MDEA	methyldiethanolamine
MEA	monoethanolamine
MINLP	mixed integer nonlinear programming
[mmIm][DMP]	1, 3-dimethylimidazolium dimethylphosphate
[N1,8,8,8][Oct]	1-methyltriocylammonium octanoate
NN	neural network
NRTL	non-random two liquid
OA	oleyl alcohol
OL	operating labor
[omPy][CF ₃ SO ₃]	3-methyl-1-octylpyridinium trifluoromethanesulfonate
OPEX	total operating expenditure
PEC	purchased equipment cost
PR	Peng-Robinson
PSA	pressure swing absorption
PWS	pressure water scrubbing
QC	quantum chemical
QSPR	quantitative structure property relationships
RK	Redlich-Kwong
RO	reverse osmosis
SAFT	statistical associating fluid theory
SCD	surface charge density
SCN	thiocyanate
SEC	specific energy consumption
SEI	solid electrolyte interphase
SRK	Soave-Redlich-Kwong
TP	tricesyl phosphate
TEA	triethanolamine
TEC	total energy consumption
[thtdp][phos]	trihexyltetradecylphosphonium bis(2,4,4-trimethylpentyl)phosphinate)
[TDA][Mchb]	tetrakis(decyl)-ammonium 1-methyl-1-cyclohexanoate
[TDPH][TCB]	trihexyltetradecylphosphonium tetracyanoborate
[TDPH][phos]	tetradecyl(trihexyl)-phosphonium bis-2,4,4-trimethylpentyl-phosphinate
TRC	total removal cost
UNIFAC	universal quasichemical functional-group activity coefficients

[VAIM][TFSI]	3-(2-amino-2-oxoethyl)-1-vinylimidazolium bis(trifluoromethyl-sulfonyl)amide
VC	vinylene carbonate
VLE	vapor-liquid equilibrium
VOC	variable operating cost
XPS	X-ray photoelectron spectroscopy
* Anions/Cations	see Table 2.1

SYMBOLS

p_i^s	vapor pressure of pure component i (Pa)
P	pressure (bar, MPa, Pa)
T	temperature (K)
x_i	mole composition of component i in liquid.
y_i	mole composition of component i in vapor
γ_i	activity coefficient
γ_i^∞	infinite dilution activity coefficient of component i
H_{iA}	Henry's law constant of component i in solvent A (Pa)
M_i	molar mass of component i (g.mol ⁻¹)
η	viscosity (Pa.s, cP)
V	molar volume (m ³ .mol ⁻¹)
C_{pi}	heat capacity of component i (J.mol ⁻¹ .K ⁻¹)
λ	thermal conductivity (W.m ⁻¹ .K ⁻¹)
σ_f	surface tension (N.m ⁻¹)
ϕ_i^V	fugacity coefficient in the vapor phase.
T_c	critical temperature (K)
ρ	density (kg.m ⁻³ , g.cm ⁻³)
R_k	van der Waals group volume (cm ³ .mol ⁻¹)
Q_k	van der Waals group area (cm ² .mol ⁻¹)
r_i	dimensionless molecular van der Waals volume.
q_i	dimensionless molecular van der Waals surface area.
Γ_k	group residual activity coefficient
$\Gamma_k^{(i)}$	residual activity coefficient of group k in a reference solution containing only compounds i
X_m	fraction of group m in the mixture
ψ_{nm}	group interaction parameter
a_{nm}	interaction energy between groups n and m
E_{misfit}	misfit energy of two molecules
α'	energy factor
σ	charge density (Coulomb.m ⁻²)
a_{eff}	contacted surface area (m ²)
E_{hb}	hydrogen interaction energy (Coulomb)

E_{vdW}	interaction energy attributing to van der Waals force
$p_i(\sigma)$	probability distribution of σ , called “ σ -profiles”
μ_s^x	chemical potential of compound x in system s
μ_x^x	chemical potential of compound x in the reference state of the pure compound
$\mu_{c,s}^x$	additional combinatorial term of chemical potential of compound x in system s
$\mu_s(\sigma)$	chemical potential of a surface segment with SCD σ
T_b	boiling point (K)
P_c	critical pressure (bar)
V_c	critical volume ($\text{cm}^3 \cdot \text{mol}^{-1}$)
c_{HB}, σ_{HB}	adjustable parameters of the HB interaction energy
τ_{vdW}, τ'_{vdW}	element-specific parameters
A_i, B_i, C_i, D_i	group contribution parameters of property i
c_i	binary variables representing the cation
a_j	binary variables representing the anion
x_l	binary variables representing the chain l
v_b, v_{sl}	group valences of the cations and substituents, respectively
n_S^L, n_{Sl}^L	minimum numbers of the substituents specified to the cation base and each side chain l , respectively
n_S^U, n_{Sl}^U	maximum numbers of the substituents specified to the cation base and each side chain l , respectively
γ_i^*	unsymmetrical activity coefficient of component i
ir	annual interest rate

1 INTRODUCTION

In this chapter, first, an overview of the need for sustainable and innovative industrial technologies is explained. Then, technologies with ILs especially IL-based separation methods are introduced and described. Next, an overview of three intensified process design methods is discussed. Finally, main challenges of current applications of ILs are pointed out before introducing the main objectives of this work and the structure of this thesis.

Chapter structure:

- 1.1 Background and motivation
- 1.2 Project objectives
- 1.3 Thesis structure
- 1.4 Dissemination of the PhD project results

1.1 BACKGROUND AND MOTIVATION

The increasing energy and environmental challenges emphasize the need for new sustainable and innovative industrial technologies. As a fundamental step in process industries, separation process accounts for about 50% of US industrial energy use and 10-15% of the world's energy consumption.¹ Its efficiency could promote the development of industry and reap great energy and environmental benefits. Therefore, any new separation techniques or intensified process designs allowing energy efficient operations are highly desirable, particularly for those high energy consuming and difficult separation processes.²⁻⁵ Separation of close-boiling and azeotropic mixtures are representatives of energy intensive separation processes,⁶ while the downstream separation in bioprocesses is usually expensive and difficult due to the fact that targeted products need to be recovered from dilute aqueous solutions.^{7, 8} Thus, it is advantageous to develop new separation technologies and investigate new process intensification methods that are not only energy efficient but are sustainable as well.

In current process industries, extraction and distillation are usually applied for liquid-liquid separations, while absorption and adsorption are widely used in gas separation processes. In addition, filtration, evaporation, crystallization and precipitation are also common techniques used for various separation purposes (e.g. liquid-liquid separation, liquid-solid separation). Each separation technique described above has its own advantages and shortcomings. Among them, distillation has the least thermal efficiency, but it undertakes nearly 80% of vapor-liquid separation tasks.⁹ Therefore, any improvement of distillation technique could greatly improve the overall energy performance of the process industry.^{2, 3, 10} Extractive distillation is a very efficient distillation method used for mixtures having a low value of relative volatility. Similar to extraction and adsorption processes, solvent also plays a critical role in the extractive distillation process. In all cases, finding suitable solvents with good separation performance as well as meeting sustainable and environmental constraints is an important criteria.

Among many potential solvent candidates, ionic liquids (ILs) with unique properties such as non-volatility, inflammability, and tunability have increasingly received attention.¹¹ Unlike volatile organic solvents that can easily escape into the atmosphere, ILs have less loss and require less energy for regeneration,¹² which could significantly improve the safety and process performance. In addition, ILs also exhibit good solubility and selectivity for a variety of organic and inorganic chemicals.¹³ For these reasons, ILs are being considered as potential alternatives for replacing conventional organic solvents in many separation processes.¹⁴ So far, the application of ILs has been extensively studied in many fields, such as chemistry, pharmaceuticals and materials. In terms of their roles, ILs can be used as solvents in separations,¹⁴ media and/or catalysts in reactions¹⁵ and function materials such as electrolytes in batteries.¹⁶

Currently, adsorption, extraction and extractive distillation are three main separation techniques that ILs are involved in. Research of using ILs as solvents in adsorption mainly focuses on gas

separations such as CO₂ capture, acid gas removal and ammonia recovery. To date, many efforts on gas adsorption process with ILs have been made by researchers, especially Zhang's group from Institute of Process Engineering, Chinese Academy of Science and Lei's group from Beijing University of Chemical Technology. Recently, Shang et al.,¹⁷ reviewed the progress of gas separation with ILs and concluded that this separation technology has potential industrial applications, but it still has some challenging issues such as how to design/screening new ILs with better separation performance, and how to lower the price of ILs as well as reduce their viscosities. On the other hand, the use of ILs as solvents in extraction is widely studied for many liquid-liquid separations, particularly for the recovery of a wide range of bioproducts ranging from small organic compounds (e.g. phenolic acids, alkaloids, fats, essential oils, carotenoids, vitamins, amino acids) to more complex molecules (e.g. nucleic acids, proteins, enzymes, antibodies). Various ILs have been synthesized for such purposes by many researchers, especially Coutinho's group from University of Aveiro. Recently, a critical review on IL-mediated extraction and separation processes for bioactive compounds was published¹⁴ and it demonstrates that, if properly selected/designed, ILs can provide higher extraction yields and purification factors compared to conventional organic solvents. However, most of the current studies are limited to imidazolium cations and fluorinated anions (e.g. bis (trifluoromethylsulfonyl) imide, tetrafluoroborate, hexafluorophosphate), which are generally expensive, moderately toxic and has low biodegradability. Screening/design new ILs that are affordable, less toxic and biocompatible is a challenging but critical task in the coming years.

Unlike ILs in adsorption and extraction processes depending on their solubility and selectivity for targeted components, ILs in extractive distillations are expected to interact differently with the components of the mixture thereby changing their relative volatilities. Extractive distillation with ILs is mostly applied to separate close-boiling/azeotropic mixtures (e.g. ethanol-water, acetone-methanol). Much progress of this separation technology ranging from the molecular level to industrial scale has been made in the past decade. Lei et al., provided a comprehensive review on extractive distillation with ILs and found that extractive distillation with ILs has the best energy performance among all special distillation processes including extractive distillation (with ILs or organic solvents), azeotropic distillation (with organic solvents) and pressuring swing distillation.¹⁸ Meanwhile, they pointed out some unsolved issues covering limited experimental data, incomplete thermodynamic models, operations at high viscosity and intensified use of ILs are lacking.

In addition to finding new high-performance solvents, developing innovative process intensification methods is another strategy to improve process performance. One such example is to use hybrid separation schemes, which combine one or more separation techniques operating at their highest energy efficiencies. So far, hybrid distillation-membrane schemes have been applied in different processes including separation of azeotropic mixtures,^{19, 20} recovery of olefins,²¹⁻²⁵ and the separation of a mixture of alkanes.²⁶ In all cases, hybrid distillation-membrane schemes are able to bring energy savings. Integrated design method that

fully represents the strong interdependencies between solvent properties and process performance is another example of process intensification. Pereira et al., (2011)²⁷ and Burger et al., (2015)²⁸ optimized solvent structure and process operations for the separation of CO₂ and CH₄ by using an integrated design method. Zhou et al., (2015)²⁹ used an integrated design method to simultaneously optimize the solvent structure and process configurations for the Diels-Alder reaction. For all studied processes, improvements of both energy and capital performance are achievable by using integrated design methods.

In the past few decades, *in-situ* product removal (ISPR) that integrates the conversion step with the first product recovery step has been introduced as one possible tool for bioprocess intensification. Currently, ISPR technologies are being studied for the recovery of industrial chemicals, pharmaceuticals, fuels and food ingredients such as propionic acid (PA). Hecke et al., (2014)³⁰ reviewed the progress of ISPR in whole cell biotechnology and revealed that in many cases, ISPR can lead to significant process improvements including overall productivity, yield, and reduced process flows. Despite many efforts have been made by researchers, the application of ISPR still has some implementation issues, one of which is the low product removal efficiency of separation approaches. In this regard, IL-based liquid-liquid extraction (LLE) that allows efficient bioproducts recovery from dilute aqueous solutions may provide the potential alternative and are worth investigating.

From the literature study, we came to know that ILs have significant potential to replace conventional organic solvents in many separation processes. However, some challenges need to be addressed before taking their place in industrial applications, such as how to lower the price of ILs and reduce their viscosities, particularly how to design/screen suitable ILs for different separation systems. Herein this PhD project aims to develop a systematic computer-aided design method that is able to rapidly and reliably screen suitable ILs with desired properties as well as meeting a specific-task standard. Meanwhile, physical and thermodynamic property models of ILs are also developed to ensure the reliability of this design method. Unlike experimental-based or other trial-and-error methods that are usually time consuming and expensive, this non-experimental based design method is both cost- and time-efficient due to its dependence on predictive property models. On the other hand, introducing ILs to the intensified process design would greatly increase the diversity of process intensification methods and thereby bringing more possibilities to achieve process performance improvements. For example, IL-based separation technologies described above have both advantages such as high separation performance, low energy demands and shortcomings such as high cost, high viscosity. Conceivably, hybrid separation schemes involving ILs making each separation technology operating at their highest process efficiencies leads to more efficient process operations. Similarly, integrated IL and process design, and ISPR with IL-based extraction are another two intensification methods that have potential to improve performance of chemical and biochemical processes. To date, only a few studies regarding intensified process design with ILs can be found in the literature³¹, but they are highly worth investigating. In this PhD study,

we also explore the possibility of using ILs in different intensification methods and design methodologies are proposed accordingly for each of the intensified process design involving ILs.

1.2 PROJECT OBJECTIVES

Motivated by the needs, this PhD project aims to develop a systematic computer-aided design method that is able to rapidly and reliably screen suitable ILs with desired properties as well as meet specific-task standards, and introduce ILs to intensified process designs allowing energy-efficient and cost-effective separation operations.

The main objectives of this PhD thesis are as follows:

- To develop a systematic computer-aided IL design/screening method.
- To develop property models for estimating various properties of ILs.
- To develop UNIFAC-IL-Gas model for predicting the thermodynamic behaviors of IL containing systems.
- To develop design methodologies for different intensified process designs with ILs.
- To find high-performance ILs for different applications, particularly for energy intensive separations and difficult downstream separations in bioprocesses.

1.3 THESIS STRUCTURE

This PhD thesis consists of eight chapters, each of them is briefly described and Figure 1.1 presents a CAILD-based methodology framework summarizing the relationship between each involved chapter.

1. **Introduction.** In this chapter, the background and motivation for this PhD project is firstly stated, and then the main objectives and thesis structure is introduced.
2. **Database and Property Models.** A large number of experimental data collected from literature and a number of pseudo-experimental data are generated from a calibrated COSMO-RS model. Group contribution (GC)-based property models are developed for 7 properties of ILs, i.e. density, viscosity, heat capacity, surface tension, thermal conductivity, melting point temperature and electrical conductivity. A comprehensive UNIFAC-IL-Gas model is developed to various IL involved systems covering 13 gases, i.e. CO₂, SO₂, H₂S, NH₃, N₂O, CO, N₂, O₂, H₂, CH₄, C₂H₄, C₂H₆ and C₃H₈.
3. **Design Methodologies.** This chapter gives design methodologies developed for the intensification methods involving ILs, i.e. hybrid process schemes with ILs, integrated IL and process design and IL-based ISPR design.
4. **Gas Separations.** In this chapter, gas separations including shale gas purification using ILs and natural gas sweetening using IL-methanol mixture solvents are presented.

5. **Bio-isoprene recovery.** This chapter presents an IL-based bio-isoprene recovery process.
6. **Applications in electrochemistry.** In this chapter, using ILs as multi-functional additives in lithium titanate (LTO) batteries is presented.
7. **Conclusions.** The conclusions and achievements of this PhD project are presented in this chapter.
8. **Future Perspectives.** Future perspectives, and directions related to this work are provided in this chapter.

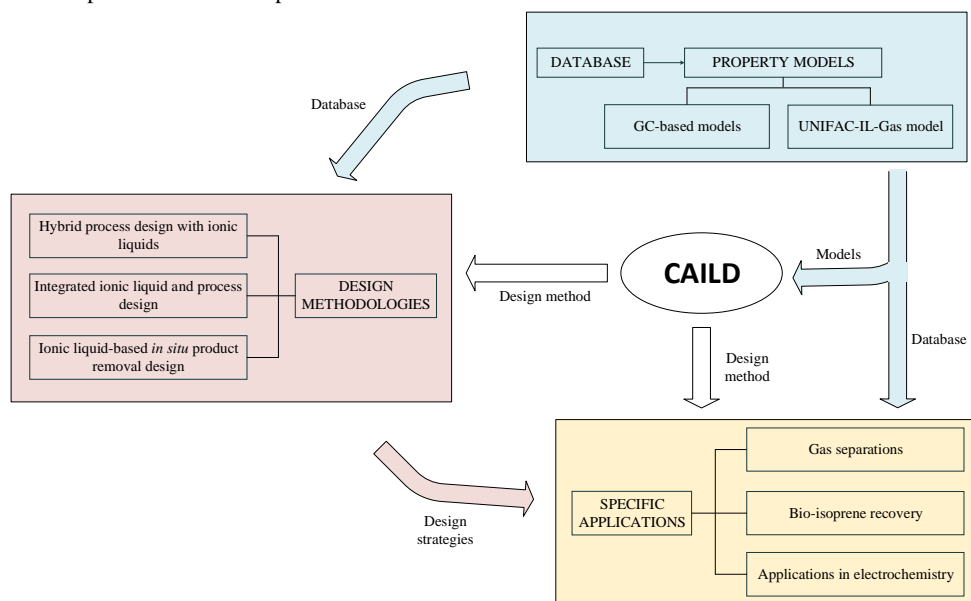


Figure 1.1 A CAILD-based methodology framework summarizing the relationship between each involved chapter

1.4 DISSEMINATION OF THE PHD PROJECT RESULTS

This section contains a list of publications and conference presentations related to this PhD project.

Publications

1. **Chen Y.,** Meng X., Cai Y., Kontogeorgis G.M. & Woodley J.M., 2020. “Natural gas upgrading using tailored ionic liquid-methanol mixture solvent with selective removal of H₂S and CO₂”, (Energy & Environmental Science) In preparation
2. **Chen Y.,** Garg N., Luo H., Kontogeorgis G.M. & Woodley J.M., 2020. “Ionic liquid-based in-situ product removal (ISPR) design for small molecule fermentation”, (Biotechnology Progress) Manuscript

3. Cai Y., **Chen Y.**, Xu T., Solms, N.V., Kontogeorgis G.M., Woodley J.M., Zhang S. & Thomsen K., 2020. "Computer-aided multifunctional ionic liquid design for electrolyte in LTO rechargeable batteries", (Advanced Functional Materials) Manuscript
4. **Chen Y.**, Liu X., Woodley J.M. & Kontogeorgis G.M., 2020. "Gas solubility in ionic liquids (ILs): UNIFAC-IL model extension", Industrial & Engineering Chemistry Research.
5. **Chen Y.**, Liu X., Kontogeorgis G.M. & Woodley J.M., 2020. "Ionic liquid-based bio-isoprene recovery process design", Industrial & Engineering Chemistry Research, 58, 4277-4292.
6. **Chen Y.**, Cai Y., Thomsen K., Kontogeorgis G.M. & Woodley J.M., 2020. "A group contribution-based prediction method for electrical conductivity of ionic liquids", Fluid Phase Equilibria, 509, 112462.
7. Liu X., **Chen Y.**, Zeng S., Zhang X., Zhang S., Liang X., Gani R. & Kontogeorgis G.M., 2020. "Structure optimization of tailored ionic liquids and process simulation for shale gas separation", AIChE Journal, 66, e16794.
8. **Chen Y.**, Koumaditi E., Gani R., Kontogeorgis G.M. & Woodley J. M., 2019. "Computer-aided design of ionic liquids for hybrid process schemes", Computers & Chemical Engineering, 130, 106556.
9. **Chen Y.**, Gani R., Kontogeorgis G.M. & Woodley J. M., 2019. "Integrated ionic liquid and process design involving azeotropic separation processes", Chemical Engineering Science, 203, 402-414.
10. **Chen Y.**, Kontogeorgis G.M. & Woodley J. M., 2019. "Group contribution-based estimation method for properties of ionic liquids", Industrial & Engineering Chemistry Research, 58, 4277-4292.
11. **Chen Y.**, Woodley J. M., Kontogeorgis G.M. & Gani R., 2018. "Integrated Ionic Liquid and Process Design involving Hybrid Separation Schemes", Computer Aided Chemical Engineering, 44, 1045-1050.
12. **Chen Y.**, Koumaditi E., Woodley J. M., Kontogeorgis G.M. & Gani R., 2018. "Integrated solvent-membrane and process design method for hybrid reaction-separation schemes", Computer Aided Chemical Engineering, 43, 851-856.

Contribution to international conferences

1. **Chen Y.**, Woodley J. M., Kontogeorgis G.M. & Gani R., 2018. "Integrated Ionic Liquid and Process Design involving Hybrid Separation Schemes", Type: Oral, presented at: *PSE-2018 conference, San Diego, California, USA.*
2. **Chen Y.**, Koumaditi E., Woodley J. M., Kontogeorgis G.M. & Gani R., 2018. "Integrated solvent-membrane and process design method for hybrid reaction-separation schemes", Type: Poster, presented at: *ESCAPE-28 conference, Graz, Austria.*

2 DATABASE AND MODEL LIBRARY

In this chapter, a comprehensive IL database covering a large number of experimental data collected from literature and a number of pseudo-experimental generated from a calibrated COSMO-RS model is presented. Based on this database, group contribution-based predictive models are developed for 7 properties of ILs and a UNIFAC-IL-Gas model is presented for various IL involved systems containing 13 gases.

Chapter structure:

2.1 Database establishment

2.2 Property model development

2.3 Thermodynamic model extension

2.4 Chapter summary

2.1 DATABASE ESTABLISHMENT

This chapter forms the basis of following publications:

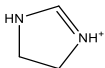
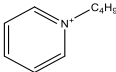
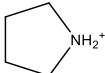
Chen, Y.; Kontogeorgis, G. M.; Woodley, J. M.: *Group Contribution-based estimation method for properties of ionic liquids. Industrial & Engineering Chemistry Research* 2019.

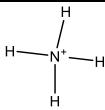
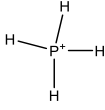
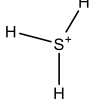
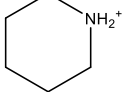
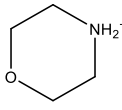
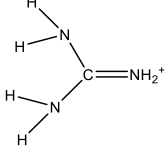
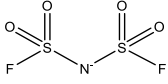
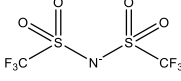
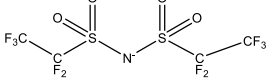
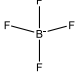
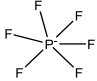
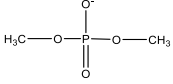
Chen, Y.; Cai, Y.; Thomsen, K.; Kontogeorgis, G. M.; Woodley, J. M.: *A group contribution-based prediction method for the electrical conductivity of ionic liquids. Fluid Phase Equilibria* 2020, 509, 112462.

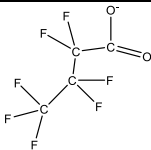
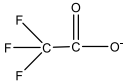
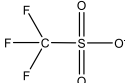
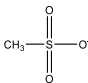
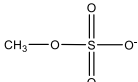
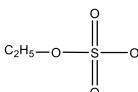
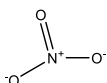
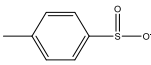
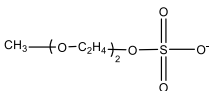
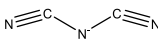
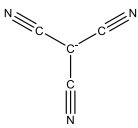
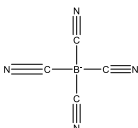
Chen, Y.; Liu, X.; Woodley, J. M.; Kontogeorgis, G. M.: *Gas solubility in ionic liquids: UNIFAC-IL model extension. Industrial & Engineering Chemistry Research* 2020.

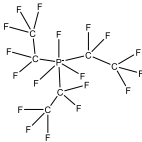
The database established in this work contains a large number of experimental data collected from literature and a number of pseudo-experimental data generated from a calibrated COSMO-RS model. For experimental data, a wide range of pure component property data covering 7 physical properties (i.e. density, heat capacity, viscosity, surface tension, thermal conductivity, melting point, and electrical conductivity) under different temperatures (and pressures) are included. Meanwhile, numerous Henry's law constant data and gas solubility data for various IL-gas systems covering 13 gases (i.e. CO₂, SO₂, H₂S, NH₃, N₂O, CO, N₂, O₂, H₂, CH₄, C₂H₄, C₂H₆, C₃H₈) are also involved. In addition, liquid-liquid phase equilibrium data and activity coefficient data for diverse IL-solute systems are collected as well during the database development. So far, most experimental data are limited to those ILs that are composed of well-known cations such as imidazolium, pyridinium and ammonium) and anions such as bis(trifluoromethylsulfonyl)imide, tetrafluoroborate and hexafluorophosphate. For this reason, a number of pseudo-experimental data of IL containing systems generated from a calibrated COSMO-RS model are used as an important supplement. In this database, all included ILs stem from 9 cation families and 42 anion families, as given in Table 2.1.

Table 2.1 Structure of cation and anion for ILs included in the database

Name	Abbreviations	Structure
Cations		
imidazolium	[Im] ⁺	
pyridinium	[Py] ⁺	
pyrrolidinium	[Pyr] ⁺	

ammonium	$[\text{NH}_4]^+$	
phosponium	$[\text{PH}_4]^+$	
sulfonium	$[\text{SH}_3]^+$	
piperidinium	$[\text{Pip}]^+$	
morpholinium	$[\text{Morp}]^+$	
guanidium	$[\text{Gua}]^+$	
Anions		
bis(fluorosulfonyl)amide	$[\text{TS}_2\text{N}]^-$	
bis(trifluoromethylsulfonyl)-amide	$[\text{Tf}_2\text{N}]^-$	
bis(perfluoroethylsulfonyl)imide	$[\text{Pf}_2\text{N}]^-$	
tetrafluoroborate	$[\text{BF}_4]^-$	
hexafluorophosphate	$[\text{PF}_6]^-$	
dimethylphosphate	$[\text{DMP}]^-$	

heptafluorobutyrate	$[\text{C}_3\text{F}_7\text{COO}]^-$	
trifluoroacetate	$[\text{TFA}]^-$	
trifluoromethanesulfonate	$[\text{TFO}]^-$	
methylsulfonate	$[\text{MeSO}_3]^-$	
methylsulfate	$[\text{MeSO}_4]^-$	
ethylsulfate	$[\text{EtSO}_4]^-$	
nitrate	$[\text{NO}_3]^-$	
tosylate	$[\text{TOS}]^-$	
2-(2-methoxyethoxy)ethylsulfate	$[\text{MDEGSO}_4]^-$	
chloride	$[\text{Cl}]^-$	Cl^-
bromide	$[\text{Br}]^-$	Br^-
iodide	$[\text{I}]^-$	I^-
dicyanamide	$[\text{DCA}]^-$	
tricyanomethanide	$[\text{TCM}]^-$	
tetracyanoborate	$[\text{TCB}]^-$	

formate	$[\text{CO}_2]^-$	$\begin{array}{c} \text{O} \\ \parallel \\ \text{HC}-\text{O}^- \end{array}$
acetate	$[\text{C}_1\text{CO}_2]^-$	$\begin{array}{c} \text{O} \\ \parallel \\ \text{H}_3\text{C}-\text{C}-\text{O}^- \end{array}$
propanoate	$[\text{C}_2\text{CO}_2]^-$	$\begin{array}{c} \text{O} \\ \parallel \\ \text{C}_2\text{H}_5-\text{C}-\text{O}^- \end{array}$
butanoate	$[\text{C}_3\text{CO}_2]^-$	$\begin{array}{c} \text{O} \\ \parallel \\ \text{C}_3\text{H}_7-\text{C}-\text{O}^- \end{array}$
hexanoate	$[\text{C}_5\text{CO}_2]^-$	$\begin{array}{c} \text{O} \\ \parallel \\ \text{C}_5\text{H}_{11}-\text{C}-\text{O}^- \end{array}$
octanoate	$[\text{C}_7\text{CO}_2]^-$	$\begin{array}{c} \text{O} \\ \parallel \\ \text{C}_7\text{H}_{15}-\text{C}-\text{O}^- \end{array}$
decanoate	$[\text{C}_9\text{CO}_2]^-$	$\begin{array}{c} \text{O} \\ \parallel \\ \text{C}_9\text{H}_{19}-\text{C}-\text{O}^- \end{array}$
tris(pentafluoroethyl)trifluorophosphate	$[\text{eFAP}]^-$	
dihydrogen phosphate	$[(\text{OH})_2\text{PO}_2]^-$	$\begin{array}{c} \text{O} \\ \parallel \\ \text{HO}-\text{P}-\text{O}^- \\ \\ \text{OH} \end{array}$
hydrogen carbonate	$[\text{OHCO}_2]^-$	$\begin{array}{c} \text{O} \\ \parallel \\ \text{HO}-\text{C}-\text{O}^- \end{array}$
ethyl phosphonate	$[\text{C}_2\text{PO}_3]^-$	$\begin{array}{c} \text{O} \\ \parallel \\ \text{C}_2\text{H}_5-\text{O}-\text{P}-\text{O}^- \\ \\ \text{H} \end{array}$
butyl phosphonate	$[\text{C}_4\text{PO}_3]^-$	$\begin{array}{c} \text{O} \\ \parallel \\ \text{C}_4\text{H}_9-\text{O}-\text{P}-\text{O}^- \\ \\ \text{H} \end{array}$
hexyl phosphonate	$[\text{C}_6\text{PO}_3]^-$	$\begin{array}{c} \text{O} \\ \parallel \\ \text{C}_6\text{H}_{13}-\text{O}-\text{P}-\text{O}^- \\ \\ \text{H} \end{array}$
octyl phosphonate	$[\text{C}_8\text{PO}_3]^-$	$\begin{array}{c} \text{O} \\ \parallel \\ \text{C}_8\text{H}_{17}-\text{O}-\text{P}-\text{O}^- \\ \\ \text{H} \end{array}$
thiocyanate	$[\text{SCN}]^-$	$^-\text{S}-\text{C}\equiv\text{N}$

lactate	[L] ⁻	
levulinate	[LEV] ⁻	
saccharinate	[SAC] ⁻	
succinamate	[SUC] ⁻	
tetrafluoroethanesulfonate	[TFES] ⁻	
bis(2,4,4-trimethylpentyl)phosphinate	[phos] ⁻	

2.2 PROPERTY MODEL DEVELOPMENT

This chapter forms the basis of following publications:

Chen, Y.; Kontogeorgis, G. M.; Woodley, J. M.: Group Contribution-based estimation method for properties of ionic liquids. Industrial & Engineering Chemistry Research 2019.

Chen, Y.; Cai, Y.; Thomsen, K.; Kontogeorgis, G. M.; Woodley, J. M.: A group contribution-based prediction method for the electrical conductivity of ionic liquids. Fluid Phase Equilibria 2020, 509, 112462.

Abstract

Properties of ionic liquids (ILs) are required for the design of products and processes involving ILs. Although innumerable ILs may be generated through the combination of a variety of cations, anions and substituents, only a small part of them have been reported to exist (have been synthesized). The available experimental data are generally limited and sometimes even contradictory. A detailed knowledge about the properties of ILs is critically important, especially for ILs not yet available. Based on the experimental data taken from our database, a series of group contribution models have been developed for estimating various properties of ILs.

2.2.1 Introduction

The increasing interest in ILs in chemical, biochemical and other industrial processes requires systematic knowledge of the properties of ILs in order to predict their behavior needed for product and process design involving these compounds. Therefore, study of property characterization and development of structure-property relationships for ILs is as important as the investigation of their applications. So far, only a limited number of ILs have been reported and the available experimental data of their properties is still scarce and restricted to some well-studied ILs, moreover, experimental data from different sources are sometimes contradictory. Considering the potential of ILs and their very large number, to measure the properties for all conceivable ILs is impractical. Therefore, theoretical or empirical methods are alternative and promising ways to achieve the required information on their properties.

To date, several methods for property estimation have been proposed for ILs in the form of empirical correlations³²⁻³⁶ or equation of state-based methods.³⁷⁻⁴¹ However, these proposed models require volume and molecular information for the prediction of density. Therefore, simple group-contribution based methods that avoids this information is more attractive since they can be easily used and they are also the basis of the development of computer aided molecular design (CAMD) methods,^{42, 43} which are useful techniques for confidently identifying optimal ILs containing desired properties for specific applications.⁴⁴

The purpose of this work is to develop reliable group contribution methods for the estimation of several properties (density, heat capacity, viscosity, surface tension, thermal conductivity, melting point, electrical conductivity) for ILs. The ultimate target is to be able to use the method not just for well-known ILs but also for the many ILs previously not-studied, which may be considered as potential solvents in practical applications. Together with discussions on the prediction accuracy and reliability of the proposed group contribution methods, a brief analysis regarding the effect of temperature (and pressure) as well as of the IL molecular structure on the studied properties is also provided. In addition, we also present comparisons with some literature methods when this is possible.

2.2.2 GC-based model development

Before using GC-based methods to build property models for ILs, an appropriate decomposition approach should be selected for the IL molecule. Currently, three main decomposition approaches, as shown in Figure 2.1, are generally used for this purpose.

- (I) The IL molecule is divided into one cation-based group and one anion group. This approach cannot reflect the structural variations of substituents in ILs.

- (II) The IL molecule is divided into several groups, but the skeletons of the cation and anion are treated as a one functional group. This approach cannot be easily extended due to its fixed combination of cations and anions.
- (III) The IL molecule is divided into several groups with the cation skeleton treated as a separate functional group. This approach enables the largest extension of the UNIFAC-IL model with an adequate consideration of the structural variation of cations, anions, and substituents in ILs. Meanwhile, it can significantly enlarge the design space and the flexibility for IL design in CAMD^{45,13}. With these considerations, this decomposition approach is employed for both experimental data extension (Section 4.1) and pseudo-experimental data extension (Section 4.2) in this work.

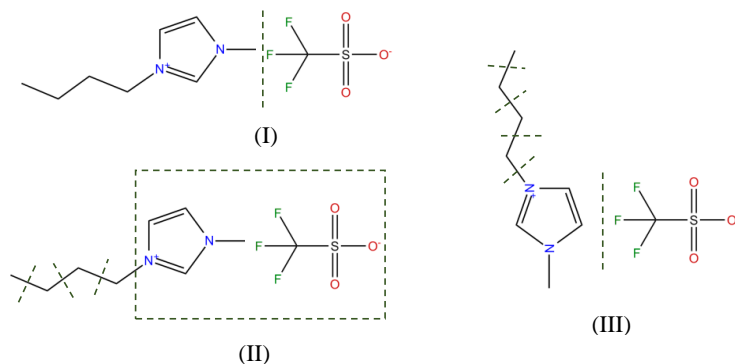


Figure 2.1 Three different decomposition methods of IL molecule: Exemplified for 1-butyl-3-methylimidazolium trifluoroacetate ($[C_4mIm]^+[CF_3SO_3]^-$)

Based on use of the decomposition method (III), a series of GC-based predictive models are developed for 7 physical properties of ILs including density, heat capacity, viscosity, surface tension, thermal conductivity, melting point, and electrical conductivity. These GC-based property models are summarized in Table 2.2. We can use these models not just for well-known ILs but also for those ILs that are previously unstudied, some of which may have practical applications in industry. To evaluate the performance of these GC-based property models, nearly 70% of the experimental physical property data (taken from our database) are used as training datasets for the model correlation, and then the remaining data are used as test datasets for the model prediction purpose. The resulting average absolute relative deviation (AARD) % of prediction for the test dataset highlights the performance of the proposed GC-based property models. To better illustrate the model performance, comparisons between the experimental and model calculated physical properties are presented in Figure 2.2. The group contribution parameters of these property models are provided in Appendix A.

Table 2.2 Group contribution-based physical property models proposed in this work

Property	Specific model	No.	Notation description
Density	$\rho = A_\rho + B_\rho \cdot T + C_\rho \cdot P$	2.1	Where ρ is the density in kg.m^{-3} ; T is the temperature in K; P is the pressure in MPa. A_ρ, B_ρ, C_ρ are GC parameters.
	$A_\rho = \sum_{i=1}^k n_i a_{i,\rho}$ $B_\rho = \sum_{i=1}^k n_i b_{i,\rho}$ $C_\rho = \sum_{i=1}^k n_i c_{i,\rho}$	2.2	Where κ is the total number of different groups in the molecule and n_i denotes the number of groups of type i , and the group contribution parameters are shown in Table A.1 of Appendix A.
	$C_{pL} = R(A_{C_{pL}} + B_{C_{pL}} \cdot (\frac{T}{100}) + D_{C_{pL}} \cdot (\frac{T}{100})^2)$	2.3	where C_{pL} represents the heat capacity in $\text{J.mol}^{-1}.\text{K}^{-1}$, T is the absolute temperature in K and R is the gas constant ($8.3145 \text{ J.mol}^{-1}.\text{K}^{-1}$). $A_{C_{pL}}, B_{C_{pL}}, D_{C_{pL}}$ are GC parameters.
Heat capacity	$A_{C_{pL}} = \sum_{i=1}^k n_i a_{i,C_{pL}}$ $B_{C_{pL}} = \sum_{i=1}^k n_i b_{i,C_{pL}}$ $D_{C_{pL}} = \sum_{i=1}^k n_i d_{i,C_{pL}}$	2.4	where n_i is the number of groups of type i and k represents the total number of different groups in the IL molecule. The group contributions parameters $a_{i,C_{pL}}, b_{i,C_{pL}}$ and $d_{i,C_{pL}}$ are obtained based on 3304 experimental data points, shown in Table A.2 of Appendix A.
Viscosity	$\ln \frac{\eta}{R_{0\eta}} = A_\eta + B_\eta \cdot \frac{100}{T} + D_\eta \cdot (\frac{100}{T})^2$	2.5	where η is the viscosity in Pa.s and T is the temperature in K. $R_{0\eta}$ is an adjustable parameter, also expressed in Pa.s. A_η, B_η and C_η are estimated by a group contribution method.
	$A_\eta = \sum_{i=1}^k n_i a_{i,\eta}$ $B_\eta = \sum_{i=1}^k n_i b_{i,\eta}$ $D_\eta = \sum_{i=1}^k n_i d_{i,\eta}$	2.6	where k is the total number of different groups in the molecule and n_i is the number of groups of type i . The group contributions $a_{i,\eta}, b_{i,\eta}$ and $d_{i,\eta}$ are generated based on 1090 experimental data points, shown in Table A.3 of Appendix A.

	$\ln \sigma = A_{\sigma} + B_{\sigma} \left(\frac{T}{100} \right) + D_{\sigma} \left(\frac{T}{100} \right)^2 \quad 2.7$	<p>where σ is the viscosity in $\text{N}\cdot\text{m}^{-1}$ and T is the temperature in K. Parameters A_{σ}, B_{σ} and D_{σ} are calculated by a group contribution method.</p>
Surface tension	$A_{\sigma} = \sum_{i=1}^k n_i a_{i,\sigma}$ $B_{\sigma} = \sum_{i=1}^k n_i b_{i,\sigma}$ $D_{\sigma} = \sum_{i=1}^k n_i d_{i,\sigma} \quad 2.8$	<p>where k is the total number of different groups in the molecule while n_i denotes the number of groups of type i, and the group contributions $a_{i,\sigma}$, $b_{i,\sigma}$ and $d_{i,\sigma}$ are obtained based on 1365 experimental data points, shown in Table A.4 of Appendix A.</p>
Thermal conductivity	$\lambda = C_{1\lambda} + C_{2\lambda} \cdot T + C_{3\lambda} \cdot T^2 \quad 2.9$ $C_{m\lambda} = \sum_{i=1}^k n_i c_{i,m\lambda} \quad 2.10$	<p>where λ is the thermal conductivity in $\text{W}\cdot\text{m}^{-1}\cdot\text{K}^{-1}$ and T is the temperature in K. Parameters $C_{m\lambda(m=1-3)}$ are calculated by a group contribution method.</p> <p>where k is the total number of different groups in the molecule and n_i is the number of groups of type i. Group contributions $c_{i,m\lambda}$ ($m = 1, 2, 3$) are obtained by the regression of experimental data shown Table A.5 of Appendix A.</p>
Melting point	$T_m = \sum_{c=1}^{k_c} n_c t_c + \sum_{a=1}^{k_a} n_a t_a + \sum_{g=1}^{k_g} n_g t_g \quad 2.11$	<p>where T_m is the melting point in K. Parameters n_c, n_a and n_g denote the number of cations, anions and side groups in the molecule while t_c, t_a and t_g represent the group contribution of the cations, anions and substituents for the melting point, respectively. These group contributions are obtained based on 225 experimental data points, shown in Table A.6 of Appendix A.</p>
Electrical conductivity	$\ln \frac{\eta}{R_{0\varepsilon}} = A_{\varepsilon} + B_{\varepsilon} \cdot \frac{100}{T} + D_{\varepsilon} \left(\frac{100}{T} \right)^2 \quad 2.12$	<p>where ε is the electrical conductivity in $\text{S}\cdot\text{m}^{-1}$ and T is the temperature in K. $R_{0\varepsilon}$ is an adjustable parameter, also expressed in $\text{S}\cdot\text{m}^{-1}$. A_{ε}, B_{ε} and C_{ε} are</p>

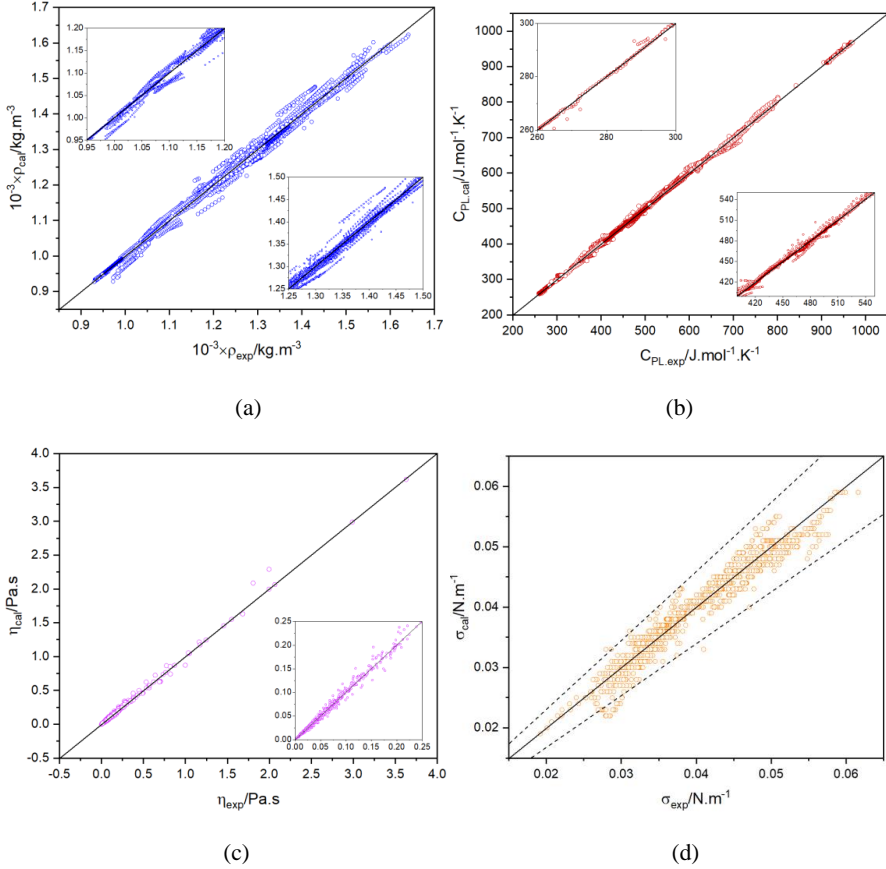
estimated by a group contribution method.

$$A_e = \sum_{i=1}^k n_i a_{i,e}$$

$$B_e = \sum_{i=1}^k n_i b_{i,e}$$

$$D_e = \sum_{i=1}^k n_i d_{i,e}$$

where k is the total number of different groups in the molecule and n_i is the number of groups of type i . The group contributions $a_{i,e}$, $b_{i,e}$ and $d_{i,e}$ are generated based on 1090 experimental data points, shown in Table A.7 of Appendix A.



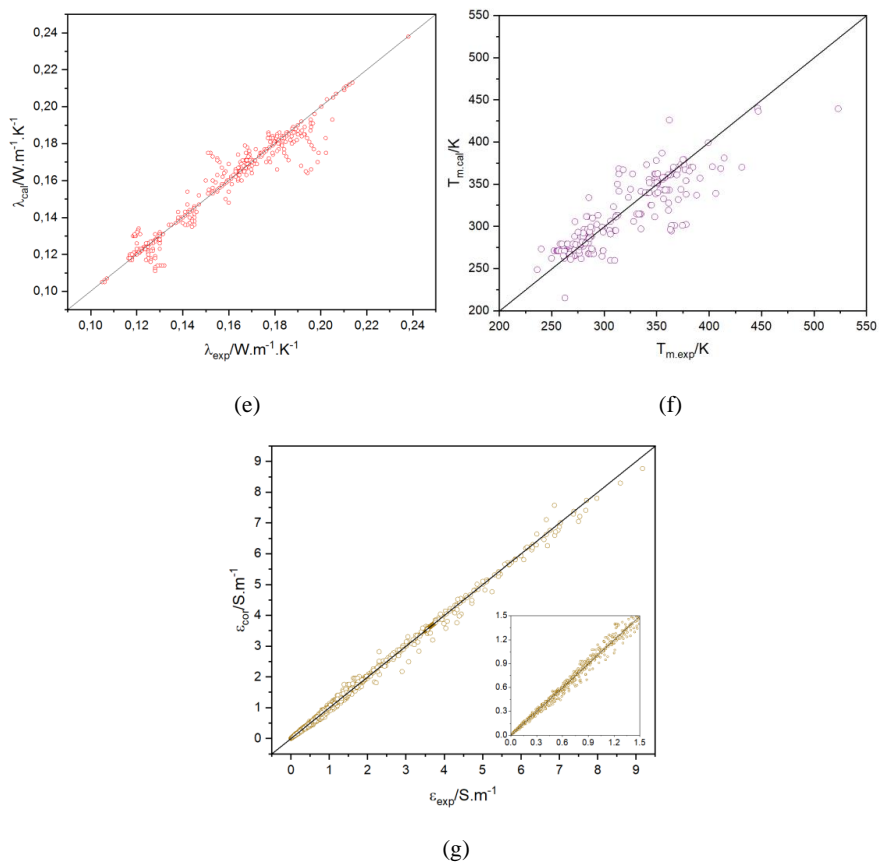


Figure 2.2 Plots of experimental versus model predicted physical properties of ILs (a) density; (b) heat capacity; (c) viscosity; (d) surface tension; (e) thermal conductivity; (f) melting point; (g) electrical conductivity

Table 2.3 summarizes the information of developing GC-based methods in this work. This information includes the number of experimental data points and the AARD% of each cation based ILs as well as all families for the studied physical properties. Meanwhile, we also compile the number of experimental data points in training and test datasets, the required related information, the AARD% and the maximum relative deviation of the property estimation methods for ILs (some methods are reported from literature), as given in Table 2.4. The comparisons highlight the performance (e.g. reliability and simplicity) of the GC-based property models developed in this work. These GC-based property models can predict the properties of both well-known ILs and for those never previously studied, which make it possible to develop computer-aided design method for ILs. These models can be further extended to new ILs that are not included in this study once their experimental data become available.

Table 2.3 Summary of the group contribution property models proposed in this work

Properties	Cation-based	Data points	Average Absolute Relative Deviation (%)
Density	Imidazolium-	5061	0.44
	Pyridinium-	990	0.63
	Pyrrolidinium-	457	0.97
	Alkyl ammonium-	204	1.59
	Phosphonium-	424	0.11
	Piperidinium-	224	0.19
	All families	7360	0.50
Heat capacity	Imidazolium-	2672	0.36
	Pyridinium-	442	0.99
	Pyrrolidinium-	88	0.07
	Alkyl ammonium-	31	0.40
	Phosphonium-	48	0.13
	Piperidinium-	23	0.11
	All families	3304	0.43
Viscosity	Imidazolium-	476	4.22
	Pyridinium-	280	3.27
	Pyrrolidinium-	65	3.58
	Alkyl ammonium-	149	3.35
	Phosphonium-	64	2.00
	Piperidinium-	56	2.89
	All families	1090	3.58
Surface tension	Imidazolium-	753	2.96
	Pyridinium-	281	2.13
	Pyrrolidinium-	114	1.50
	Alkyl ammonium-	111	4.39
	Phosphonium-	85	8.76
	Piperidinium-	21	0.66
	All families	1365	3.10
Thermal conductivity	Imidazolium-	309	2.94
	Pyridinium-	15	1.29
	Pyrrolidinium-	16	1.55
	Alkyl ammonium-	9	0.47
	Phosphonium-	32	0.82
	All families	381	2.4
Melting point	Imidazolium-	125	3.64
	Pyridinium-	23	5.87
	Pyrrolidinium-	22	5.48
	Alkyl ammonium-	41	7.05
	Phosphonium-	9	5.34
	Piperidinium-	5	3.80
	All families	225	4.74

Electrical conductivity	Imidazolium-	925	4.51
	Pyridinium-	212	4.35
	Pyrrolidinium-	208	3.19
	Alkyl ammonium-	77	2.65
	Phosphonium-	95	3.74
	Sulfonium-	22	2.63
	Piperidinium-	13	1.49
	Morpholinium-	26	1.03
All families		1578	3.62

Table 2.4 Comparisons between the methods proposed in this work and other methods reported from literature

Properties	Author(s)	Sets	Data Points	ILs	AARD (%)	RD _{max} (%)	Related Information Required
Density	Paduszynski-Domanska ⁴⁶	Training	13135	828	0.53	≈15.00	Molar mass
		Test	3695	200	0.45	≈12.50	Molar volume
		Total	16830	1028	0.51		
	This work	Training	5039	90	0.43	4.70	
		Test	2321	53	0.67	6.24	None
		Total	7360	143	0.49	4.60	
Heat capacity	Gardas-Coutinho ⁴⁷	Training	2396	19	0.36	2.43	
		Test	-	-	-	-	None
		Total	2396	19	0.36	2.43	
	This work	Training	2391	44	0.39	4.20	
		Test	913	17	0.62	4.70	None
		Total	3304	61	0.43	4.60	
Viscosity	Gardas-Coutinho ⁴⁸	Training	482	24	7.50	22.79	
		Test	-	-	-	-	None
		Total	482	24	7.50	22.79	
	This work	Training	778	56	3.36	27.50	
		Test	312	20	5.63	36.80	None
		Total	1090	76	3.58	27.70	
Surface tension	Gardas-Coutinho ⁴⁹	Training	361	40	5.75	15.58	Parachors Density
		Test	-	-	-	-	
		Total	361	40	5.75	15.58	
	This work	Training	952	72	2.87	19.92	
		Test	413	30	4.71	14.70	None
		Total	1365	102	3.10	22.10	
Thermal conductivity	Gardas-Coutinho ⁴⁸	Training	107	16	1.06	3.07	
		Test	-	-	-	-	None
		Total	107	16	1.06	3.07	
	This work	Training	381	64	2.4	6.94	
		Test	-	-	-	-	None

Melting point	Lazzús ⁵⁰	Total	381	64	2.4	6.94	None
		Training	200	200	7.97	25.17	
		Test	200	200	6.16	19.47	
		Total	400	400	7.07	25.17	
		Training	162	75	4.70	22.40	
	This work	Test	63	26	7.09	18.30	None
		Total	225	111	4.74	20.30	
		Training	307	15	4.57	16.01	
		Test	-	-	-	-	
		Total	307	15	4.57	16.01	
Electrical conductivity	This work	Training	1121	57	3.30	27.6	None
		Test	457	20	6.83	26.6	
		Total	1578	77	3.62	27.7	

2.3 UNIFAC-IL MODEL EXTENSION

This chapter forms the basis of following publication:

Chen, Y.; Liu, X.; Woodley, J. M.; Kontogeorgis, G. M.: Gas solubility in ionic liquids: UNIFAC-IL model extension. Industrial & Engineering Chemistry Research 2020.

Abstract

Prediction of thermodynamic behavior is essential for the early design stage of separation processes including solvent selection, process optimization and its performance evaluation. In order to better utilize ionic liquids (ILs) as solvents in gas separation processes, the UNIFAC-IL model of IL-liquid solute systems is extended to IL-gas systems by using experimental data from published works and pseudo-experimental data specifically generated from a calibrated COSMO-RS model. In this work, we consider in the model development a total number of 100 ILs from 6 cation families and 24 anion families, and 13 gases including CO₂, SO₂, H₂S, NH₃, N₂O, CO, N₂, O₂, H₂, CH₄, C₂H₄, C₂H₆, C₃H₈. The extended UNIFAC-IL-Gas model consists of two sub-models, namely the UNIFAC-IL-Gas (Exp.) model and the UNIFAC-IL-Gas (Pseudo-Exp.) model. The training and testing of the UNIFAC-IL-Gas (Exp.) model is based on 100% experimental data, while the training of the UNIFAC-IL-Gas (Pseudo-Exp.) model is based on pseudo-experimental data, but its testing is also based on 100% experimental data.

2.3.1 Introduction

The performance of an IL-based gas separation process, as well as other solvent-based separation processes, largely depends on the solvent thermodynamic properties which are strongly determined by its molecular structure. Therefore, the selection of a suitable IL with desired thermodynamic properties for a specific gas separation task is of great importance. Considering that numerous ILs are possible composed of different cations and anions, the experimental trial and error method for IL screening is inevitably very time consuming and cost

intensive, aside from being non-systematic. Therefore, predictive thermodynamic models that can support efficient, cost-effective and systematic selection of ILs are highly desirable.

A reliable predictive thermodynamic model can both identify structure-property relationships and provide the phase equilibria information of the systems. By far, predictive thermodynamic models including activity coefficient models (e.g. NRTL, UNIQUAC, UNIFAC),⁵¹⁻⁵⁹ equations of state models (e.g. GC EOS, CPA EOS, SAFT-based EOS)⁶⁰⁻⁶² and Ab initio methods (e.g. COSMO-RS, COSMO-SAC)⁶³⁻⁶⁵ have been introduced to the IL containing systems. Most recently, Dong et al., proposed a united COSMO-UNIFAC model that combines COSMO-SAC and UNIFAC models for systems containing ILs.^{66, 67} Among these thermodynamic models, COSMO-RS and UNIFAC are the two most commonly studied methods for modelling of IL-containing systems. The COSMO-RS model is a predictive method first proposed by Klamt and Eckert (2000)⁶⁸ and it only requires molecular structure information. Banerjee et al. (2006)⁶⁹ used this model to predict binary VLE of systems containing imidazolium-based ILs and their work confirms that the presence of ILs in the vapor phase can be neglected even at very low pressures. Zhang et al. (2008)⁷⁰ applied the COSMO-RS model to predict the Henry's law constants of CO₂ in 408 ILs and it was found that ILs selected by this method present enhanced capability of capturing CO₂, in contrast to ILs reported in literature. Based on the predicted selectivity and activity coefficient at infinite dilution using the COSMO-RS model, some suitable ILs are selected for extractive distillation processes and these screening ILs show better performance than their corresponding conventional solvents.⁶⁴ Zhou et al. (2012)⁷¹ used the COSMO-RS model to predict the mutual solubilities of 1500 ILs with water at 298.15 K and the influence of the types of anion and cation and substituent groups on the mutual solubility of IL-water was also investigated in their work. Although the use of COSMO-RS model does not require experimental information, it typically offers mostly qualitatively correct results.⁷² A way to improve the predictions from COSMO-RS is to use experimental data to calibrate the model and it is reported that all calibration models have better performance than the original COSMO-RS model.⁷³⁻⁷⁷

On the other hand, UNIFAC is usually preferred as it can provide reliable prediction results because the group interaction parameters in this model are regressed from experimental data. Additionally, UNIFAC is applicable for the thermodynamic prediction of those ILs for which experimental data is not unavailable, many of which may not even have been synthesized, although with potential practical application. Furthermore, UNIFAC can also be easily integrated into computer aided design methods (CAMD),^{44, 78} which have been suggested as one of the most efficient and systematic approaches to IL screening. To date, hundreds of UNIFAC group interaction parameters covering various IL groups (i.e. cations, anions) and conventional functional groups have been presented.^{53, 56, 58, 77, 79-81} Kato and Gmehling⁵³ studied the thermodynamic behavior of 119 IL-liquid solute systems using both the original and modified UNIFAC models and then Nebig and Gmehling⁸² revised and extended the modified UNIFAC model to the prediction of phase equilibria and excess properties for systems with ILs.

The results show that the original UNIFAC especially modified UNIFAC method allows the reliable prediction of IL containing systems. Lei et al. (2009)⁵², Lei et al. (2012)⁵⁸ and Roughton et al. (2012)⁷⁹ extended the UNIFAC model to IL-solute systems by using different IL molecular decomposition methods. Since these extended UNIFAC-IL models can predict well the VLE of the systems with ILs, they can be used for screening/design suitable ILs for specific separation tasks. Most recently, Zhou et al. (2020)⁷⁷ largely extended the UNIFAC model for IL-liquid solute systems by using experimental data collected from literature and computational data generated from calibrated COSMO-RS models. Remarkably, 39358 experimental data covering 21 conventional functional groups, 9 cation skeleton groups, and 29 anion groups was included in their work. In contrast, current UNIFAC-IL regression work of IL-gas systems is still limited to a few widely studied IL-CO₂ systems^{54, 76, 83} and a small number of other gases such as H₂, and gaseous hydrocarbon systems.^{59, 67, 76, 83-85} However, separation processes involving gases such as H₂S and SO₂ are widely encountered in chemical and petrochemical industries, and therefore an extension of the UNIFAC-IL model to such IL-gas systems is highly desirable.

In the past decade, more and more solubility data of different gases in various ILs have been tested, which make it possible to extend the UNIFAC-IL model to their corresponding IL-gas systems. Although the solubility of CO₂ in ILs has been widely studied, experimental data for other gases (e.g. H₂S, SO₂) in many ILs are still not available. Moreover, most solubility data for gases are limited to those ILs that are composed of well-known cations (i.e. imidazolium, pyridinium and ammonium) and anions (i.e. bis(trifluoromethylsulfonyl)imide, tetrafluoroborate and hexafluorophosphate). In order to extend the UNIFAC-IL model to those IL-gas systems which do not have experimental data, reliable computational data generated from a priori prediction methods must be supplemented. In this respect, one of the quantum chemical calculation-based models, COSMO-RS, has been successfully applied in the generation of computational data for many IL-solute systems. Nonetheless, COSMO-RS only offers qualitatively correct results in some cases due to the high deviation between experimental and COSMO-RS computational properties. For this reason, this model is usually calibrated or modified before its application so as to improve the reliability of these computational data.^{76, 77}

Based on the solubility database built by Lei et al.,⁸⁶ we develop in this work a new database combining experimental data and COSMO-RS data with the aim of achieving a systematic extension of the UNIFAC-IL model to IL-gas systems. Besides this database, a model extension strategy is also proposed in this work (see Section 2.3.3.1). Compared to the previously reported UNIFAC-IL model, the UNIFAC-IL-Gas model presented in this work covering many more IL-gas systems, and many ILs and gases is for the first time introduced to the UNIFAC-IL model. This extended UNIFAC-IL-Gas model can provide reliable predictions of gas solubility in ILs and it offers prospect of screening ILs for many gas separations prior to their corresponding experimental work. For example, the removal of acid gases especially SO₂ and H₂S is critical in the natural gas upgrading process, but currently screening suitable ILs for this

process is not possible due to the insufficient experimental data or the limitation of the current UNIFAC-IL model. Therefore, the UNIFAC-IL-Gas model proposed in this work is a solution in this direction. In most previous works, the IL-liquid solute system and IL-gas system are separately incorporated into the UNIFAC-IL-Gas model. In order to combine the IL-solute and IL-gas systems in a single UNIFAC-IL-Gas model, some interaction parameters between IL and conventional main groups regressed from IL- liquid solute systems by Roughton et al.⁷⁹ have been adopted in this work. That is to say, this UNIFAC-IL-Gas model is not limited to IL-solute or IL-gas systems, but can be applied to IL-solute-gas systems, which is very important for the study of IL-based mixture solvent application in gas separation processes. In addition, the cation, anion and substituents of IL molecule are treated as separate functional groups in this work (see Section 3.2), which allows a larger and more flexible IL design space while using this UNIFAC-IL-Gas model.

2.3.2 Thermodynamic models

2.3.2.1 The COSMO-RS model

As a predictive thermodynamic model combining quantum chemical calculations and statistical thermodynamic approaches, COSMO-RS has been widely used to calculate the activity coefficients for many mixtures since it was first proposed by Klamt and Eckert.⁶⁸ In this model, the activity coefficient of a compound i in a solvent S (γ_S^i) is computed from the chemical potential of the pure compound i (μ_i^i) and the chemical potential of i in the solvent S (μ_S^i), as shown in Eq.2.14.

$$\ln \gamma_S^i = (\mu_S^i - \mu_i^i)/RT \quad 2.14$$

where μ_S^i can be calculated from the integration of the chemical potential of a surface segment σ in the solvent S ($\mu_S(\sigma)$) over the surface of the compound i as follows.

$$\mu_S^i = \mu_{C,S}^i + \int p^i(\sigma) \mu_S(\sigma) d\sigma \quad 2.15$$

where $\mu_{C,S}^i$ is a combinatorial term describing the size and shape differences of different molecules in the solvent. $p^i(\sigma)$ is a surface composition function (see Eq. 2.16), also known as σ -profile, which represents the distribution of the polarization charges of each molecule and details of the relative amount of surface with polarity σ on the surface of the molecule. $\mu_S(\sigma)$, i.e. σ -potential, as a measure of the affinity of the solvent S to a surface of polarity σ , and is associated with the molecular surface interaction energies through a statistical thermodynamic procedure as described by Eqs.2.17-2.20.

$$p^i(\sigma) = \frac{n_{i(\sigma)}}{n_i} = \frac{A_{i(\sigma)}}{A_i} \quad 2.16$$

$$\mu_S(\sigma) = -\frac{RT}{a_{eff}} \times \ln \left[\int p_S(\sigma') \exp \left\{ \frac{a_{eff}}{RT} (\mu_S(\sigma') - e(\sigma, \sigma')) \right\} d\sigma' \right] \quad 2.17$$

$$E_{\text{misfit}}(\sigma, \sigma') = a_{\text{eff}} e_{\text{misfit}}(\sigma, \sigma') = a_{\text{eff}} \frac{\alpha'}{2} (\sigma + \sigma')^2 \quad 2.18$$

$$E_{\text{HB}}(\sigma, \sigma') = a_{\text{eff}} c_{\text{HB}} \min\{0, \min(0; \sigma_{\text{donor}} + \sigma_{\text{HB}}) \max(0; \sigma_{\text{acceptor}} - \sigma_{\text{HB}})\} \quad 2.19$$

$$E_{\text{vdW}}(\sigma, \sigma') = a_{\text{eff}} (\tau_{\text{vdW}} + \tau'_{\text{vdW}}) \quad 2.20$$

In Eq.2.16, $n_{i(\sigma)}$ represents the number of segments with charge density σ that have a surface area $A_{i(\sigma)}$, while n_i represents the total number of segments in a single molecule with a total surface area A_i . In Eqs.2.17-2.20, a_{eff} is the effective contact area and α' is an interaction parameter; interactions of electrostatics (E_{misfit}) and hydrogen bonding (E_{HB}) are described as functions of the polarization charges of two interacting surface segments σ and σ' . If the segments are located on a hydrogen bond donor or acceptor atom, these surface segments are expressed as σ_{donor} and σ_{acceptor} . c_{HB} and σ_{HB} are adjustable parameters of the hydrogen bond strength and the threshold for hydrogen bonding, respectively. The less specific van der Waals (E_{vdW}) interactions are also considered with the element specific vdW interaction parameters τ_{vdW} and τ'_{vdW} .

As described above, COSMO-RS is an a priori approach that can predict activity coefficients of compounds in liquid mixtures without experimental data as its calculation only relies on compounds' σ -profiles. To date, σ -profiles of many cations and anions of ILs, as well as thousands of conventional molecules, have been included in the COSMO-RS database. Moreover, the σ -profiles of those compounds not included can easily be derived from quantum chemical calculations. Since COSMO-RS allows efficient and fast thermodynamic calculations without experimental data, it has been applied to many liquids or liquid mixtures, especially for those systems for which experimental data is unavailable. For the same reason, the COSMO-RS model has also received attention for the prediction of gas solubility in ILs, where the ions are treated separately as an electroneutral mixture, and distinct COSMO files are generated.

2.3.2.2 The Original UNIFAC model

Original UNIFAC proposed by Fredenslund et al.,⁸⁷ is a functional group based semi-empirical prediction method, where the activity coefficient for each species in the system is split into two components; a combinatorial γ_i^{C} and a residual component γ_i^{R} . For the molecule i , the activity coefficients are broken down as:

$$\ln \gamma_i = \ln \gamma_i^{\text{C}} + \ln \gamma_i^{\text{R}} \quad 2.21$$

The combinatorial component of the activity is related to the entropic effects accounting for the size and shape of molecules, which can be expressed via the van der Waals volume (R_k) and surface area (Q_k) parameters for each functional group. The residual component of the activity is due to energetic interactions between groups present in the system, and represents the enthalpy contribution. It can be expressed as binary interaction parameters (α_{nm}, α_{mn}). γ_i^{C} and γ_i^{R} can be calculated by Eqs.2.22-2.26 and Eqs.2.27-2.32, respectively.

$$\ln \gamma_i^c = 1 - V_i + \ln V_i - 5q_i(1 - \frac{V_i}{F_i} + \ln(\frac{V_i}{F_i})) \quad 2.22$$

$$F_i = \frac{q_i}{\sum_j q_j x_j} \quad 2.23$$

$$V_i = \frac{r_i}{\sum_j r_j x_j} \quad 2.24$$

$$q_i = \sum_k v_k^{(i)} Q_k \quad 2.25$$

$$r_i = \sum_k v_k^{(i)} R_k \quad 2.26$$

where F_i and V_i represent auxiliary properties for component i ; the pure component parameters q_i and r_i , respectively, denote relative molecular van der Waals surface areas and molecular van der Waals volumes, which are obtained from the sum of the group area Q_k and group volume parameters R_k , respectively. $v_k^{(i)}$ is the number of groups of type k in molecule i .

$$\ln \gamma_i^R = \sum_k v_k^{(i)} (\ln \Gamma_k - \ln \Gamma_k^{(i)}) \quad 2.27$$

$$\ln \Gamma_k = Q_k(1 - \ln(\sum_m \theta_m \psi_{mk}) - \sum_m \frac{\theta_m \psi_{km}}{\sum_n \theta_n \psi_{nm}}) \quad 2.28$$

$$\theta_m = \frac{Q_m X_m}{\sum_n Q_n X_n} \quad 2.29$$

$$X_m = \frac{\sum_i v_m^{(i)} x_i}{\sum_i \sum_k v_k^{(i)} x_i} \quad 2.30$$

$$\psi_{nm} = \exp[-(\alpha_{nm}/T)] \quad 2.31$$

$$\psi_{mn} = \exp[-(\alpha_{mn}/T)] \quad 2.32$$

where Γ_k and $\Gamma_k^{(i)}$ denote the residual activity coefficient of group k and the residual activity coefficient of group k in pure component i , respectively; θ_m is the fraction of group m in a mixture of the liquid phase and X_m/X_n is the fraction of group m or n in the mixture; ψ_{nm} and ψ_{mn} are the group interaction parameters which can be calculated through Eqs.2.31 and 2.32 based on the value of UNIFAC group interaction parameters (α_{nm} , α_{mn}) between groups m and n .

Unlike COSMO-RS, the original UNIFAC model calculates the activity coefficient based on the van der Waals parameters (experiment-independent) of different functional subgroups and the binary interaction (experiment-dependent, temperature-independent) between the main groups of each component in the mixtures. Therefore, the predictive ability of the UNIFAC model is usually better than COSMO-RS, but its application, to some extent, is limited to systems where there are some available experimental data or parameters. Although the modified UNIFAC model^{88, 89} with temperature-dependent interaction parameters has also been proposed because it can improve the model's prediction performance, the temperature has no noticeable impact on the activity coefficient for some IL-solute systems, especially IL-gas systems. For this reason, the original UNIFAC model is considered for the UNIFAC-IL model

extension to IL-gas systems in this work. A large number of UNIFAC interaction parameters between conventional functional groups have been regressed and widely used.^{90, 91}

2.3.3 UNIFAC-IL-Gas model extension

2.3.3.1 Model extension strategy

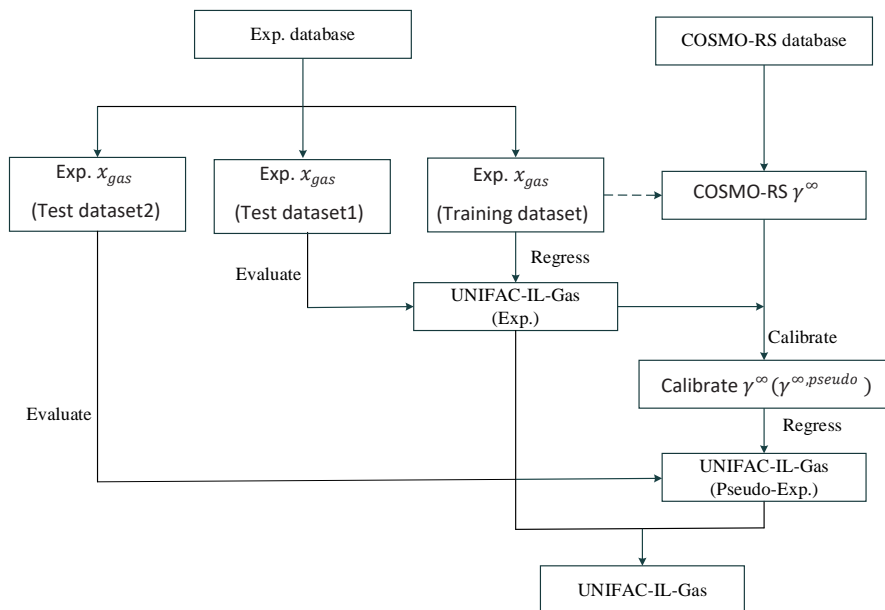


Figure 2.3 Hierarchical strategy for the extension of UNIFAC-IL-Gas model. (Exp. and Pseudo-Exp. indicate the source of data from experimental database and the calibrated COSMO-RS model)

Considering the large number of IL-gas systems in the UNIFAC-IL-Gas model extension, a hierarchical is proposed in this work (see Figure 2.3). Because testing is a very important part of the model extension, the experimental data coming from the Exp. database is divided into a training dataset and test datasets, and these datasets cover different IL-gas systems. Typically, 20-30% of data points are used for testing purposes. However, considering the limited number of experimental data for some systems, the percentage of the test dataset used will be adjusted accordingly (see Section 2.3.4). First, the UNIFAC-IL model is extended to the IL-gas systems by using experimental gas solubility data (i.e. the training dataset) from Exp. database and this UNIFAC-IL-Gas (Exp.) model is evaluated by using experimental data of Test dataset1 from Exp. database. Secondly, a wide range of computational infinite dilution activity coefficients (γ^∞) of different gases in various ILs are specifically generated from COSMO-RS model, and then these γ^∞ are calibrated by using calculated γ^∞ from validated UNIFAC-IL-Gas (Exp.) model. Next, these calibrated γ^∞ ($\gamma^{\infty,pseudo}$) are used for the regression of UNIFAC-IL-Gas

(Pseudo-Exp.) model and its predictive capability is further evaluated by using experimental data of Test dataset2 from Exp. database. Finally, an extended UNIFAC-IL-Gas model combining UNIFAC-IL-Gas (Exp.) and UNIFAC-IL-Gas (Pseudo-Exp.) model is obtained.

2.3.3.2 Model extension method

Since UNIFAC is a functional group based thermodynamic model, the IL molecule should be first decomposed appropriately into separate functional groups for the UNIFAC-IL model extension. Similar to the development of GC-based property models in Section 2.2, the decomposition approach (III), as shown in Figure 2.1, is also used in the UNIFAC-IL model extension. Overall, 13 gases, 7 cation groups, 24 anion groups and 3 substituent groups from the group decomposition are included in the proposed UNIFAC-IL model extension to IL-gas systems. The van der Waals volumes and areas R_k and Q_k of these groups are either taken from literature or calculated as follows:

$$R_k = \frac{V_k \times N_A}{V_{VW}} \quad 2.33$$

$$Q_k = \frac{A_k \times N_A}{A_{VW}} \quad 2.34$$

where V_k and A_k denote, respectively, the van der Waals group volumes and surface areas of group k in each molecule, which can be calculated from correlations with molecular volumes and surface areas or from quantum chemical calculations. N_A is the Avogadro's number with a value of $6.023 \times 10^{23}/mol$, and V_{VW} , A_{VW} are standard segment volume and surface area (of ethylene group in polyethylene) with values of $15.17 \text{ cm}^3/mol$, $2.5 \times 10^9 \text{ cm}^2/mol$, respectively. The values of R_k and Q_k for all the involved functional subgroups are summarized in Table 2.5. Most of the R_k and Q_k values are taken from previously published work and the remaining parameters obtained in this work are calculated from COSMO-RS.

Table 2.5 Group's information of R_k and Q_k involved in the extension of the UNIFAC-IL-Gas model (R_k and Q_k obtained in this work are calculated from COSMO-RS)

Group No.	Main group	Subgroup	R_k	Q_k	Reference
1	CO ₂	CO ₂	1.3000	1.1200	92
2	SO ₂	SO ₂	0.9011	0.8480	83
3	H ₂ S	H ₂ S	1.7933	1.5022	This work
4	NH ₃	NH ₃	1.2193	1.1786	This work
5	N ₂ O	N ₂ O	1.8465	1.5860	This work
6	CO	CO	1.0470	1.0600	59
7	N ₂	N ₂	0.9340	0.9750	85
8	O ₂	O ₂	1.1257	1.1940	85
9	H ₂	H ₂	0.528	0.664	59
10	CH ₄	CH ₄	1.1290	1.1240	92

11	C ₂ H ₄	C ₂ H ₄	1.5740	1.4880	92
12	C ₂ H ₆	C ₂ H ₆	1.8022	1.6960	93
13	C ₃ H ₈	C ₃ H ₈	3.2002	2.3460	This work
14	CH ₂	CH ₃	0.9011	0.8480	87
		CH ₂	0.6744	0.5400	87
		CH	0.4469	0.228	87
15	OH	OH	1.0000	1.200	90
16	CH ₂ O	CH ₃ O	1.1450	1.088	52
		CH ₂ O	0.9183	0.7800	52
17	[Im]	[Im]	1.9471	0.8660	79
		[mIm]	2.8482	1.7140	79
18	[Py]	[Py]	2.6670	1.5530	79
		[mPy]	3.5681	2.4010	79
19	[Pyr]	[mPyr]	3.3873	2.9093	79
20	[N]	[CH ₃ N]	1.1865	0.9400	79
		[C ₂ H ₅ N]	1.8609	1.4800	79
		[C ₃ H ₇ N]	2.5353	2.0200	79
		[C ₄ H ₉ N]	3.2097	2.5600	79
21	[P]	[CH ₃ P]	1.4931	0.9197	77
22	[TDPH]	[TDPH]	29.7600	16.1100	This work
23	[TMG]	[TMG]	3.2002	2.3459	This work
24	[Tf ₂ N]	[Tf ₂ N]	5.7738	4.9320	79
25	[BF ₄]	[BF ₄]	1.7856	1.4940	79
26	[PF ₆]	[PF ₆]	7.0615	6.5787	79
27	[DMP]	[DMP]	3.4127	3.2820	79
28	[C ₃ F ₇ CO ₂]	[C ₃ F ₇ COO]	6.7579	3.9692	This work
29	[TFA]	[CF ₃ COO]	3.1773	3.2200	79
30	[TfO]	[CF ₃ SO ₃]	3.4745	2.9796	79
31	[MeSO ₃]	[MeSO ₃]	2.7126	2.3701	94
32	[MeSO ₄]	[MeSO ₄]	3.4832	3.7280	79
33	[EtSO ₄]	[EtSO ₄]	4.1576	4.1760	79
34	[NO ₃]	[NO ₃]	1.6611	1.5289	94
35	[TOS]	[TOS]	5.4854	4.5884	94
36	[MDEGSO ₄]	[MDEGSO ₄]	6.6686	6.9840	79
37	[Cl]	[Cl]	0.7660	0.7200	79
38	[Br]	[Br]	0.9492	0.8320	79
39	[DCA]	[DCA]	2.4171	2.1337	94

40	[TCB]	[TCB]	4.3314	3.6652	94
41	[eFAP]	[eFAP]	9.4117	7.7294	94
42	[L]	[L]	3.1347	2.3066	This work
43	[LEV]	[LEV]	5.6143	3.6501	This work
44	[SAC]	[SAC]	8.0206	4.6397	This work
45	[SUC]	[SUC]	5.2374	3.3891	This work
46	[TFES]	[TFES]	6.1611	3.7065	This work
47	[phos]	[phos]	16.6847	8.5221	This work

Like many other UNIFAC-IL extensions, the interaction parameters between conventional main groups are taken directly from the original UNIFAC parameter matrix. Meanwhile, in order to combine the IL-solute and IL-gas systems in one UNIFAC-IL-Gas model, some interaction parameters between IL and conventional main groups regressed from IL-solute systems by Roughton et al.⁷⁹ have been adopted. That is to say, this model is not limited to IL-solute or IL-gas systems, but can be applied in IL-solute-gas systems, which is very important for the study of IL-based mixture solvent application in gas separation processes. In addition, the interaction parameters between IL main groups (i.e. cations and anions) are assumed to be zero considering the strong interaction and weak dissociation of ion pairs. We should note that the interaction parameters between different gases are not involved or considered in the current model extension, as such parameters are typically not available in UNIFAC-tables. Figure 2.4 presents the group interaction parameter matrix of the extended UNIFAC-IL-Gas model. In this work, we consider in the model extension a total number of 100 ILs (see Appendix) from 6 cation families and 24 anion, and 13 gases including CO₂, SO₂, H₂S, NH₃, N₂O, CO, N₂, O₂, H₂, CH₄, C₂H₄, C₂H₆, and C₃H₈.

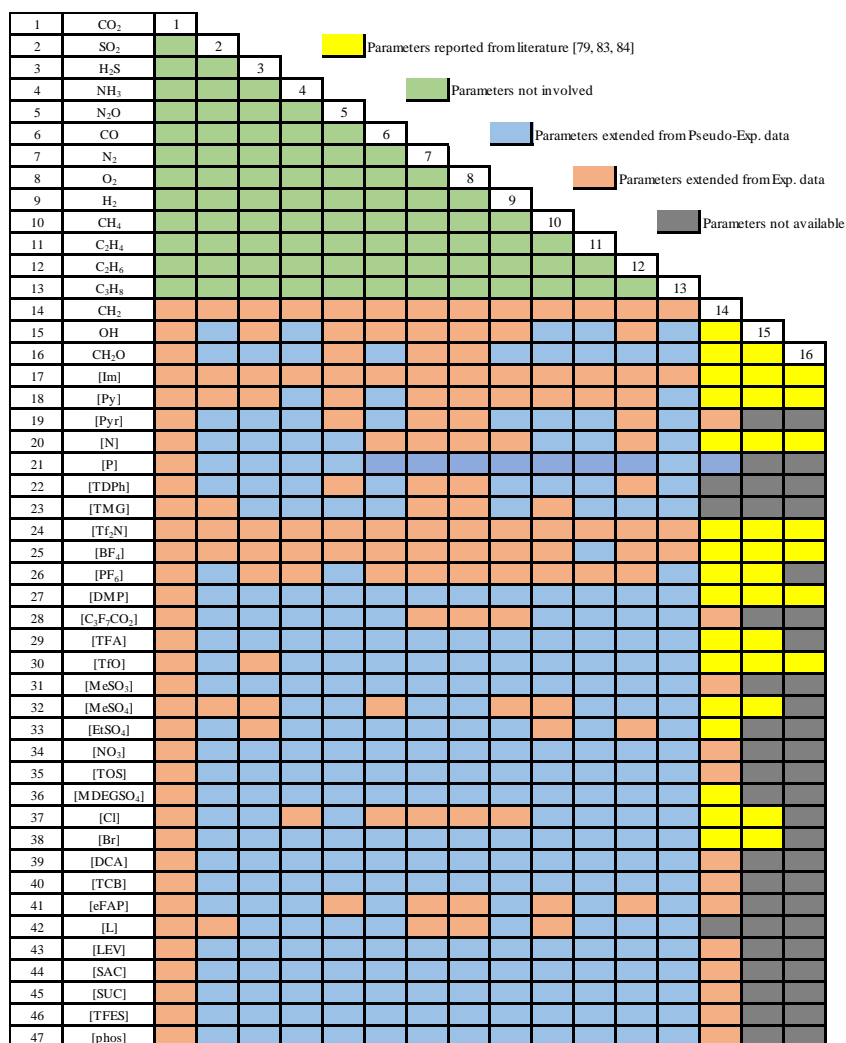


Figure 2.4 The extended UNIFAC-IL-Gas group interaction parameter matrix

Results and discussion

2.3.3.3 Experimental data extension

In this section, 7034 experimental gas solubility data in ILs with a range of temperature, 283.15-384.15K, and pressure, 0.05-973 bar taken from our IL database are applied for the UNIFAC-IL model extension. As shown in Figure 2.4, group interaction parameters with orange color in the extended UNIFAC-IL-Gas parameter matrix are regressed from IL-gas systems by minimizing the objective function, i.e. the average absolute relative deviation (AARD) %

between experimental and calculated gas solubility (mole fraction of gas in IL), as shown in Eq.2.35.

$$O.F. = AARD(\%) = \frac{1}{N} \sum_{i=1}^N \left| \frac{x_i^{exp} - x_i^{cal}}{x_i^{exp}} \right| \times 100\% \quad 2.35$$

where i represents the data point and N denotes the total number of the regressed data points. x_i^{cal} and x_i^{exp} are the gas solubility in ILs that can be directly taken from the experimental database and calculated from phase equilibrium equation (see Eq.2.36), respectively.

$$x_{gas} = \frac{y_{gas} P \varphi(T, P, y_{gas})}{\gamma_{gas} P_{gas}^s} \quad 2.36$$

In Eq. 23, the activity coefficient of gas (γ_{gas}) can be calculated from UNIFAC-IL-Gas model and the mole composition of gas in the vapor phase (y_{gas}) is assumed to be 1 due to the negligible vapor pressure of ILs. P represents the phase equilibrium pressure of the studied IL-gas system. The fugacity coefficient of gas ($\varphi(T, P, y_{gas})$) can be calculated by the Peng-Robinson equation of state, while the saturated vapor pressure of gas (P_{gas}^s) can be estimated from suitable correlations such as the Wagner, DIPPR, and Antoine equations. In this work, both DIPPR and Antoine equations were considered for different gases.

One of nonlinear programming solvers “lindoglobal” in GAMS (24.4.6) was used to solve this regression problem. Considering the complexity of this problem, the interaction parameters associated with the IL-CO₂ systems are regressed first, and then the interaction parameters associated with other IL-gas systems are regressed. To evaluate the reliability of the regressed interaction parameters, as well as the predictive performance of the extended UNIFAC-IL-Gas (Exp.) model, nearly 75% of the involved experimental data points (i.e. training dataset) are used for the regression, while a certain number of remaining data points (i.e. Test dataset1) are used for prediction purposes.

The AARD (%) between the experimental and calculated x_{gas} of different gases in ILs range from 12% for gaseous hydrocarbons (CH₄, C₂H₄, C₂H₆, C₃H₈) to 22% for the gas dataset covering CO, N₂, O₂, H₂ in the training dataset. As expected, the AARD (%) from the test dataset is higher than, but rather close to, its corresponding AARD (%) from the training dataset. The AARD (%) between the experimental and calculated x_{gas} of different gases in ILs for both the training and test datasets can be found in Table 2.6. To better illustrate the calculation results, comparisons between the experimental and calculated x_{gas} of all gases in ILs from the training and test datasets are presented in Figures 2.5 and 2.6, respectively. The resulting AARD (%) of prediction for the test dataset shows a reliable predictive ability of the extended UNIFAC-IL-Gas (Exp.) model. It should be noted that a very small number of calculated x_{gas} from both training and test datasets have values higher than 1. This can be explained by the fact that these datapoints have relatively high values of x^{exp} and their calculated γ_{gas} are less than their real γ_{gas} (see Eq.2.36). Such prediction results can also be found in the case of using COSMO-RS

model.⁹⁵ Although it's unable to use these calculated γ_{gas} (>1) to make accurate predictions, they indicate that the studied IL-gas systems have relatively high value of x^{exp} . The new obtained group interaction parameters with their values are provided in Appendix B.

Table 2.6 Summary of the extended UNIFAC-IL-Gases (Exp.) model for both training and test datasets

Gas dataset	Involved gases	Training dataset		Test dataset1	
		Data points	*AARD%	Data points	*AARD%
1	CO ₂	2345	14.5	1083	16.5
2	SO ₂ , H ₂ S, NH ₃ , N ₂ O	1533	12.7	395	19.2
3	CO, N ₂ , O ₂ , H ₂	681	22.1	96	35.0
4	CH ₄ , C ₂ H ₄ , C ₂ H ₆ , C ₃ H ₈	877	11.5	24	14.2

*AARD% of both training and test datasets are calculated from Eq.2.35

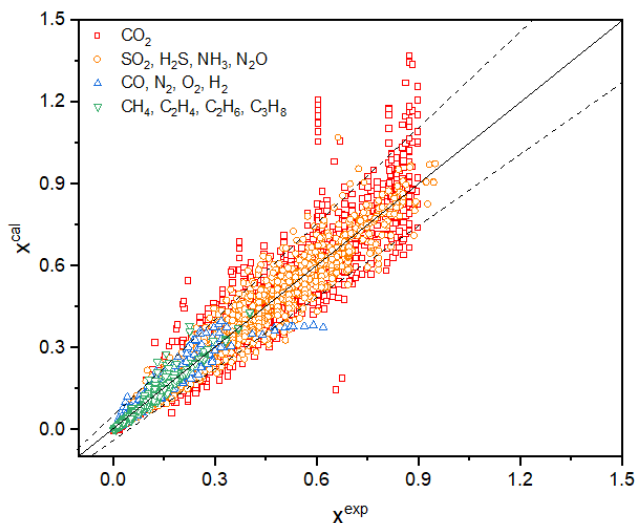


Figure 2.5 Comparison of experimental and UNIFAC-IL-Gas calculated gas solubilities of different gases in ILs from the training dataset

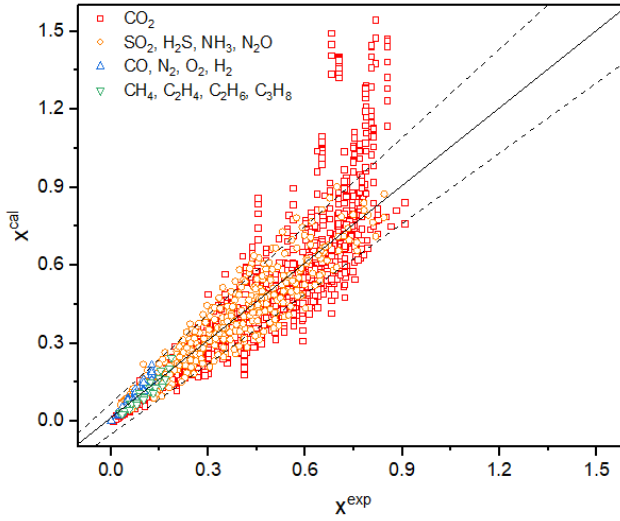


Figure 2.6 Comparison of experimental and UNIFAC-IL-Gas (Exp.) predicted gas solubilities of different gases in ILs from Test dataset1

2.3.3.4 Pseudo-experimental data extension

As mentioned above, computational data from the COSMO-RS calculation are very useful because of the insufficient experimental data for some important IL-gas systems. In this work, we only use the COSMO-RS model to generate computational data, but it is not included in the UNIFAC-IL-Gas model extension. Although gas solubility data can be generated directly from COSMO-RS calculations where the saturated vapor pressure is estimated by using the information of gas-phase energy, we use the pseudo-experimental data of infinite dilution activity coefficient since it allows consistent vapor pressure calculations (DIPPR or Antoine method) for both experiment and pseudo-experimental data based regression. To improve the reliability of the computational γ^∞ from COSMO-RS model, a number of calculated γ^∞ from validated UNIFAC-IL-Gas (Exp.) were used for calibrations. In this work, a linear calibrated COSMO-RS model involving temperature (T) was employed, as shown in Eq.2.37. This calibration method for the COSMO-RS model has been used previously and suggested in several published works.⁷³⁻⁷⁶ In the last part of this section, the testing results from Test dataset2 also verify the reliability of this calibration.

$$\gamma^{\infty,pseudo} = a\gamma^{\infty,COSMO-RS} + b + cT \quad 2.37$$

where $\gamma^{\infty,pseudo}$ and $\gamma^{\infty,COSMO-RS}$ are the calibrated γ^∞ and the γ^∞ calculated directly from COSMO-RS, respectively. The adjustable parameters (a , b and c) of this linear calibrated model can be obtained by minimizing:

$$AARD(\%) = \frac{1}{N} \sum_{i=1}^N \left| \frac{\gamma_i^{\infty,exp} - \gamma_i^{\infty,pseudo}}{\gamma_i^{\infty,exp}} \right| \times 100\% \quad 2.38$$

where $\gamma_i^{\infty,pseudo}$ and $\gamma_i^{\infty,exp}$ are the pseudo-experimental γ^{∞} and experimental γ^{∞} of data point i , respectively. N denotes the total number of the regressed data points. In this equation, $\gamma_i^{\infty,exp}$ are calculated from validated UNIFAC-IL-Gas (Exp.) model.

In this section, we will calibrate the computational data generated from COSMO-RS. The purpose of this calibration is to narrow the difference between experimental and computational data. To complement the insufficient amount of experimental data, a total of 6,610 $\gamma^{\infty,COSMO-RS}$ covering various IL-gas systems under different temperatures are computed directly from COSMOthermX software, where the σ -profiles of the IL functional groups and studied gases are taken from the IL Thermo database. The detailed information of $\gamma^{\infty,pseudo}$ and $\gamma^{\infty,COSMO-RS}$ for each gas is presented in Table 2.7. From the linear regression results, we can observe that all gases with calibration have lower AARD% between the COSMO-RS based computational γ^{∞} and UNIFAC-IL-Gas (Exp.) model based calculated γ^{∞} , and only 3 gases (i.e. O₂, C₂H₆, C₃H₈) have AARD% higher than 20%. These linear calibrations for each gas can be validated from the testing results of AARD% between experimental x_{gas} and calculated x_{gas} from calibrated γ^{∞} .

Table 2.7 Calibration of the COSMO-RS model for generating pseudo-experimental data. The calibration parameters refer to Eq.2.37

Gas	AARD% without calibration	Calibration parameters			AARD% with calibration	Number of data points used in calibration
		a	b	c		
SO ₂	4.5	1.0000	-0.0620	0.0002	4.0	30
H ₂ S	54.0	0.8000	0.6850	-0.0010	8.5	30
NH ₃	74.5	1.6000	0.3370	-0.0001	7.2	30
CO	54.1	1.1500	-0.4710	0.0006	8.5	60
N ₂	22.2	1.5000	0.7060	-0.0030	8.8	30
O ₂	59.0	1.5210	2.1930	-0.0060	10.4	30
H ₂	57.1	2.5820	0.1970	-0.0010	22.6	90
N ₂ O	19.5	0.8360	-0.2140	0.0006	3.8	60
CH ₄	35.3	0.6620	-0.1980	0.0080	16.6	60
C ₂ H ₄	20.3	0.6390	1.6460	-0.0030	14.7	40
C ₂ H ₆	37.2	0.7450	-1.3690	0.0050	31.7	90
C ₃ H ₈	44.5	0.8000	-1.1810	0.0070	36.8	40

Based on the pseudo-experimental data from the calibrated COSMO-model, the remaining unknown group interaction parameters (Marked in blue) in the extended UNIFAC-IL-Gas parameter matrix are regressed by minimizing the AARD % between the experimental and calculated gas solubility, as shown in Eq.2.39.

$$AARD(\%) = \frac{1}{N} \sum_{i=1}^N \left| \frac{\gamma_i^{\infty,pseudo} - \gamma_i^{\infty,cal}}{\gamma_i^{\infty,pseudo}} \right| \times 100\% \quad 2.39$$

where $\gamma_i^{\infty,pseudo}$ and $\gamma_i^{\infty,cal}$ are the pseudo-experimental and calculated γ^{∞} of data point i , respectively. N denotes the total number of the regressed data points.

Table 2.8 summarizes the AARD (%) between $\gamma_i^{\infty,pseudo}$ and $\gamma_i^{\infty,cal}$ of all pseudo-experimental data points. To evaluate the predictive performance of the obtained UNIFAC-IL-Gas (Pseudo-Exp.) model, a test dataset (i.e. Test dataset2) including 347 experimental data points is applied. The AARD (%) between the experimental x_{gas} and x_{gas} calculated from UNIFAC-IL-Gas (Pseudo-Exp.) model for the test dataset is also provided in Table 2.8. Compared to the extension of UNIFAC-IL-Gas (Exp.) model, the AARD (%) from pseudo-experimental data presents similar fitting results, but the predictive reliability of this UNIFAC-IL-Gas (Pseudo-Exp.) model is not as good as its corresponding UNIFAC-IL-Gas (Exp.) model. Nevertheless, pseudo-experimental data from the calibrated COSMO-RS model is still a good supplementary data source when experimental data are not available. To better illustrate the calculation results, comparisons between $\ln(\gamma_i^{\infty,pseudo})$ and $\ln(\gamma_i^{\infty,cal})$ of all pseudo-experimental data points are presented in Figure 2.7, and comparisons between the experimental and predicted x_{gas} from UNIFAC-IL-Gas (Pseudo-Exp.) model are given in Figure 2.8. The resulting AARD (%) of prediction for the test dataset shows an acceptable predictive performance of the extended UNIFAC-IL-Gas (Pseudo-Exp.) model. The values of these new group interaction parameters in UNIFAC-IL-Gas (Pseudo-Exp.) model are provided in Appendix B.

Table 2.8 Summary of the extended UNIFAC-IL-Gas (Pseudo-Exp.) model for both training and test datasets

Gas dataset	Involved gases	Training dataset (pseudo-experimental data)		Test dataset2 (experimental data)	
		Data points	AARD%	Data points	AARD%
2	SO ₂ , H ₂ S, NH ₃ , N ₂ O	2280	8.1	169	12.5
3	CO, N ₂ , O ₂ , H ₂	2090	9.6	88	35.1
4	CH ₄ , C ₂ H ₄ , C ₂ H ₆ , C ₃ H ₈	2240	13.5	86	22.8

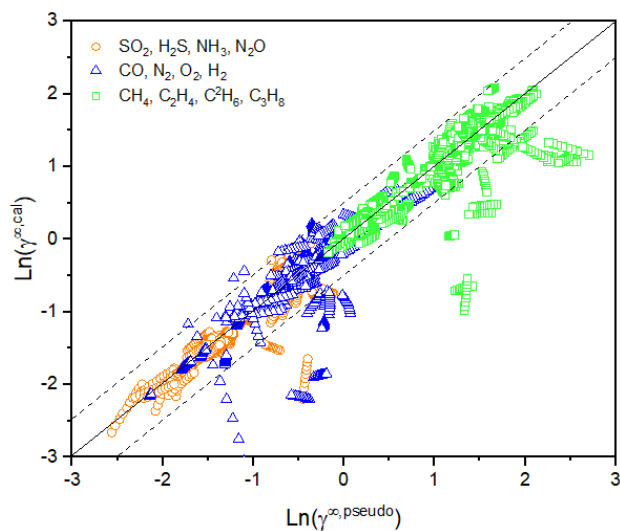


Figure 2.7 Comparison of the pseudo-experimental and model (UNIFAC-IL-Gas) calculated γ^∞ for different gases in ILs

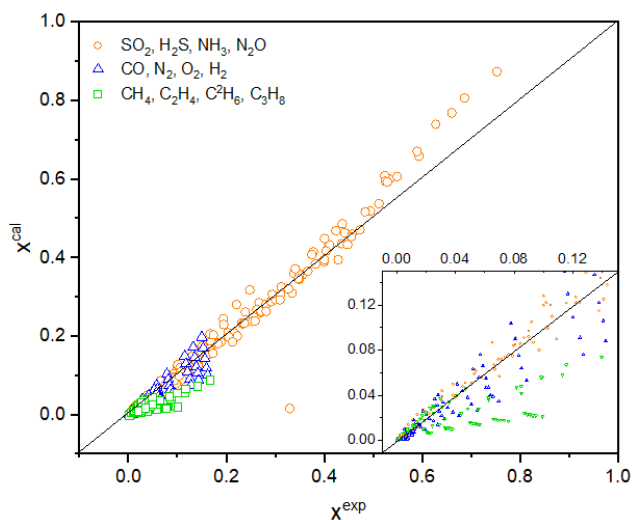


Figure 2.8 Comparison of the experimental and model (UNIFAC-IL-Gas) predicted gas solubility for different gases in ILs (experimental data are taken from Test dataset2)

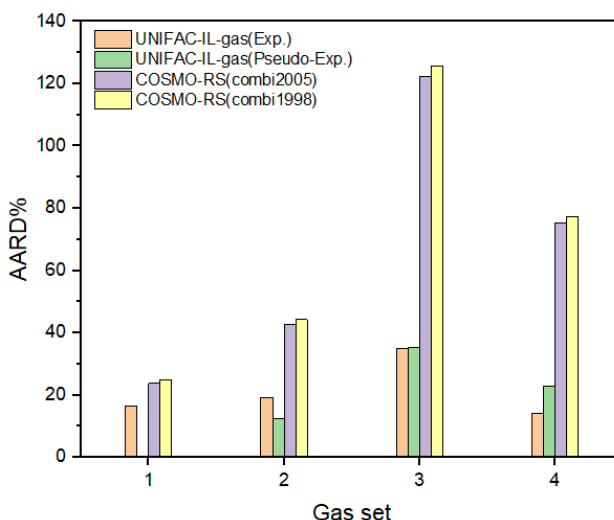


Figure 2.9 Comparisons between the prediction result (expressed as AARD%) from the UNIFAC-IL and COSMO-RS based model⁹⁵ for all studied gas datasets. (Gas dataset1: CO₂; Gas dataset2: SO₂, H₂S, NH₃, NO₂; Gas dataset3: CO, N₂, O₂, H₂; Gas dataset4: CH₄, C₂H₄, C₂H₆, C₃H₈)

Among all studied IL-gas systems, gases (CO, N₂, O₂, H₂) involved in the Gas dataset3 have relatively large deviation (about 30%) for both UNIFAC-IL-Gas (Exp.) and UNIFAC-IL-Gas (Pseudo-Exp.) models, as shown in Tables 2.6 and 2.8. This can be explained by the fact that these gases have lower vapor pressures compared with other studied gases, which usually leads to lower solubility in ILs, so their experimental data itself has higher deviation. Nevertheless, the extended UNIFAC model has much better predictive performance for CO, N₂, O₂ and H₂ than COSMO-RS, for which AARD is over 100% (see Figure 2.9). In addition, it is found that there is no significant difference in the deviation of IL systems with different cation or anion families. However, a small number of data points for some IL-CO₂ systems show very large deviations, as shown in Figures 2.3 and 2.4. This can be explained as follows: (1) the system pressure of some data points for CO₂-IL systems (e.g. 1-hexyl-3-methylimidazolium saccharinate and 1-hexyl-3-methylimidazolium tris(pentafluoroethyl)trifluorophosphate) is very low or very high; (2) the number of data points for some CO₂-IL systems (e.g. trihexyl tetradecyl phosphonium bis(2,4,4-trimethylpentyl)phosphinate, 1-butyl-3-methylimidazolium 2-(2-methoxyethoxy)ethylsulfate) is very small; (3) the experimental data of some CO₂-IL systems (mainly imidazolium dicyanamide) from different data sources has some deviations.

It is worth mentioning that the DIPPR and Antoine equations present different regression results for many IL-gas systems, especially for the gases with very low critical temperature. This can be explained by the fact that both the DIPPR and Antoine equations are sufficient for estimating

the vapor pressure below the critical temperature and they provide similar vapor pressure values in the range of certain temperatures (e.g. CO 68.15-132.92 K). However, hypothetical vapor pressure extrapolated from these equations cannot express some gas systems well at temperatures above the critical temperature. In fact, from a thermodynamic point of view, when the system temperature is higher than the critical temperature of the component, the liquid vapor pressure of the component no longer exists, and so, the vapor pressure (above the critical temperature) calculated from the DIPPR or Antoine equation is regarded as a pseudo-vapor pressure. In this work, the temperature of most studied IL-gas systems is much higher than the critical temperature of those involved gases and different vapor pressure equations present different regression results. This is one of the reasons why the AARD% of IL-gas systems is generally higher than for other IL-solutes systems. For this reason, we use either DIPPR or Antoine equation for different IL-gas systems based on their regression performance. It should be noted that when using this UNIFAC-IL-Gas model, the vapor pressure equation (DIPPR or Antoine) and coefficients must be consistent with the equation and coefficients used for each gas in this work. The details of the vapor calculation method and their corresponding equation parameters for all involved gases are provided in Appendix C.

On the other hand, although the computational data generated from COSMO-RS has errors of its own, a calibration method is used to calibrate these computational data for reducing the impact of such inherent errors. Most importantly, the UNIFAC-IL-Gas (Pseudo-Exp.) model extended from these calibrated computational data (i.e. pseudo-experimental data) is verified by Test dataset2 containing 100% experimental data. In order to compare the prediction performance of the extended UNIFAC-IL-Gas models with COSMO-RS models, the prediction results of AARD% from the UNIFAC-IL and COSMO-RS based models for 4 gas datasets covering all studied gases are plotted in Figure 2.9. The prediction results from different versions (combi2005 and combi1998) of the COSMO-RS model are taken from Lei's work.⁹⁵ Clearly, both UNIFAC-IL-Gas (Exp.) and UNIFAC-IL-Gas (Pseudo-Exp.) models have much better predictive performance than the COSMO-RS models, especially for the gases included in Gas dataset3 and dataset4. These comparisons highlight the reliability and applicability of the extended UNIFAC-IL-Gas model developed in this work. This model can be easily used for screening suitable ILs for many gas separations such as natural gas upgrading and NH₃ recovery prior to their corresponding experimental work.

2.3.4 Conclusions

A comprehensive database of IL gas-systems including experimental data from published works and pseudo-experimental data from calibrated COSMO-RS model has been developed. By using a hierarchical extension strategy, the UNIFAC-IL was extended to various IL-systems from a large number of experimental and pseudo-experimental data, and then a combined UNIFAC-IL-Gas model consisting of UNIFAC-IL-Gas (Exp.) and UNIFAC-IL-Gas (Pseudo-Exp.) was obtained. We should note that COSMO-RS model is only used to obtain pseudo-

experimental data, and it is not involved in the UNIFAC-IL-Gas model extension. Overall, 13 gases, 3 conventional functional groups, 7 cation skeleton groups, and 24 anion groups are considered in this extended model. The calculation results of both training and test datasets, presented as comparisons between the experimental/pseudo-experimental and calculated gas solubility from the UNIFAC-IL-Gas model, show the reliable predictive performance of the UNIFAC-IL-Gas model obtained in this work.

This UNIFAC-IL-Gas model can be applied in solvent screening, process optimization and evaluation in the design stage of gas separation processes involving ILs. Moreover, this model can also be used for IL-based mixture solvents design since it combines IL-gas and other IL-solute systems, giving significant opportunity to potentially expand the application of ILs in gas separation processes. Furthermore, the current UNIFAC-IL-Gas model can be updated, or further extended, to new gas-IL systems that are currently not included in this study, once their experimental data becomes available.

2.4 CHAPTER SUMMARY

A comprehensive IL database covering a large number of experimental data collected from literature and a number of pseudo-experiments generated from a calibrated COSMO-RS model is established. Then, group contribution (GC)-based property models are developed for estimating various properties of ILs including density, viscosity, heat capacity, surface tension, thermal conductivity, melting point temperature and electrical conductivity. More than 15000 experimental data points in a wide range of temperature (and pressure) covering nearly 300 ILs stem from 8 cation families, 34 anion families and 4 substituents are used. All property models are validated by using 20-30% of data points as test datasets. Alongside, a UNIFAC-IL-Gas model consisting of two sub-models, i.e. UNIFAC-IL-Gas (Exp.) model and UNIFAC-IL-Gas (Pseudo-Exp.) model, is also developed for the thermodynamic calculations of systems containing ILs. A large number of experimental data collected from literature and a number of pseudo-experimental data generated from a calibrated COSMO-RS model are involved in this model's development. Similarly, this model is tested by using 20-30% of experimental data points for each IL-gas system. Overall, 7 cation groups, 24 anion groups, and 3 substituent groups decomposed from 100 ILs as well as 13 gases including CO₂, SO₂, H₂S, NH₃, N₂O, CO, N₂, O₂, H₂, CH₄, C₂H₄, C₂H₆, C₃H₈ are covered in this thermodynamic model. The physical and thermodynamic property models proposed in this chapter are the basis of the development of our computer-aided design methodology for ILs.

3 DESIGN METHODOLOGIES

In this chapter, ILs are introduced to the intensified process designs. Based on the conceptual design of hybrid process schemes, integrated solvent and process design, and *in-situ* product removal (ISPR), different methodologies are, respectively, proposed for each of the intensified process design method.

Chapter structure and contents:

- 3.1 Hybrid process design with ionic liquids
- 3.2 Integrated ionic liquid and process design
- 3.3 Ionic liquid-based *in-situ* product removal design
- 3.5 Chapter summary

3.1 HYBRID PROCESS DESIGN WITH IONIC LIQUIDS

This chapter forms the basis of following publications:

Chen, Y.; Koumaditi, E.; Woodley, J.; Kontogeorgis, G.; Gani, R.: Integrated Solvent-Membrane and Process Design Method for Hybrid Reaction-Separation Schemes. In Computer Aided Chemical Engineering; Elsevier, 2018; Vol. 43; pp 851-856.

Chen, Y.; Koumaditi, E.; Gani, R.; Kontogeorgis, G. M.; Woodley, J. M.: Computer-Aided Design of Ionic Liquids for Hybrid Process Schemes. Computers & Chemical Engineering 2019, 106556.

Abstract

Hybrid process schemes that combine two (or more) units operating at their highest process efficiencies to perform one (or more) process tasks are considered as potentially innovative and sustainable processing options. Additionally, ILs, as well as certain organic chemicals, are good candidates for use as solvents in hybrid schemes that can replace energy-intensive processing steps. As successful design of solvent-based hybrid schemes depends on the specific properties of the solvent used, a hybrid process design method combining CAILD and process design-simulation to identify the optimal IL and its corresponding hybrid process specifications has been proposed. The application of this design method has been illustrated through case studies including the separation of aqueous solutions using an IL-based hybrid distillation scheme and the bio-oxidation of alcohols using a hybrid reaction-separation scheme with continuous product removal.

3.1.1 Introduction

Solvents and membranes have a wide range of applications in many chemical and related industries. Solvents can be used in a multipurpose role (e.g. reaction medium, extraction solvent) in different processing steps, such as chemical reaction and separation. For example, a reaction step usually carried out in one solvent and the separation step of product recovery requires another solvent or membrane.⁹⁶ Therefore, it is advantageous to investigate hybrid schemes that allow solvent or membrane-based processing units operating at their highest efficiencies to perform one or more process tasks.

Separation operations to obtain pure products is found in almost all processing routes producing a chemical product, where, the processes involved, like distillation, account for 10–15% of the world's energy consumption. More energy efficient methods to purify chemicals could greatly reduce carbon dioxide emissions as well as energy cost.¹ As an important separation technique in chemical process industry, distillation is energy intensive and has the least thermal efficiency. Nevertheless, nearly 80% of all vapor-liquid separations are performed by distillation. Its

efficiency could significantly contribute to the overall energy consumption in chemical process industries and therefore intensified separation designs that allow energy efficient operation are attractive.^{2,3} One such option is to use hybrid separation schemes, which combine one or more separation techniques operating at their highest energy efficiencies such that a target separation can be achieved at significantly lower energy consumption.⁹⁷

Bio-reactions, which involve the use of enzymes or living microorganisms for the production of chemical and biochemical substances, may often be carried out under mild conditions, they are highly specific, and involve high reaction rates, therefore, can act as possible alternatives for conventional synthesis routes. However, limitations of biocatalysts mostly related with product and/or substrate inhibition result in low productivity and highly diluted product, which leads in difficult downstream separations.^{7, 8, 30} In each case, the product needs to be removed as soon as it is formed in order to overcome these constraints and hence increase the product yields of the bio-catalytic process. Generally, recovery and purification stages in bioprocesses require numerous steps, associated with high chemicals and energy consumption, and usually represent 20–60% of the total cost, and even in some protein synthesis biological process this value may reach 90%.⁹⁸ For these bioprocesses, hybrid schemes that involve the intensification of the reaction and separation processes are able to lower energy consumption, improve reaction performance as well as reduce the complexity.

Together with organic chemicals, ILs are being considered as solvents for use in hybrid schemes replacing energy intensive processes. IL-based separation processes are generally energy efficient because of their non-volatility and therefore low energy consuming solvent recovery operations.^{12, 18} For the same reason, membrane-based separations are also promising alternatives for the energy intensive processes.⁹⁹ However, both IL-based and membrane-based separations are limited to low flux operations due to their operational and economic constraints (e.g. high viscosity or low flux rate, high cost). To overcome such limitations, hybrid schemes are promising innovative and sustainable processing options since processing units (e.g. reactor, column, membrane) are operating at their highest efficiencies in hybrid schemes. For example, reactive distillation (e.g. production of methyl acetate) integrates reaction and separation in a single operating unit resulting in reduced equipment sizes and lower operating cost. Distillation with membrane separation (e.g. n-butane from isobutane) is another example of combining unit operations to achieve lower energy consumption and improve quality of distillation cuts.

Although hybrid schemes have significant potential to contribute the development of the process industries, a main question is when such hybrid schemes can be applied, what characteristics the process problem should have, what the process specification should be and how much improvement can be expected. To find truly innovative and more sustainable solutions,³ proposed a computer-aided, multi-level, multi-scale method, where different hybrid schemes can be generated to test if any of them match the desired targets while also satisfying the process specifications. So far, hybrid schemes involving membrane-based separation with

distillation (i.e. Figure 3.2a) have been proposed for several separation processes, such as separation of azeotropic mixtures,^{19, 20} recovery of olefins,²¹⁻²⁵ and the separation of a mixture of alkanes.²⁶ In contrast, studies regarding the hybrid process design using ILs as solvents are still scarce.

To achieve the full potential of the hybrid process schemes, the selection of optimal solvents or membranes is of great importance due to fact that different solvents or membranes are usually present with very distinct properties and separation performances, especially for ILs that combine diverse cations, anions and substituents.¹⁰⁰ Currently, ILs are usually selected based on experiments which can be time consuming and cost-intensive since many thousands of ILs may be considered as potential solvents. Therefore, in order to find suitable ILs for specific tasks confidently and rapidly, systematic solvent screening method like computer-aided ionic liquid design (CAILD) is attractive.⁴⁴ To date, studies on CAILD are mainly focusing on the separation of azeotropic mixtures (e.g. ethanol-water, acetone-methanol) and the CO₂ capture process.^{79, 101-105} Most recently, CAILD method has been extended to the extractive desulfurization system (EDS) for fuel oils.⁹⁴

Hybrid schemes have potential to contribute significantly to the sustainability of the process industry through the use of CAILD for the optimal design of ILs. This work presents a hybrid process design method combining CAILD with process design-simulation to identify the optimal IL and its corresponding hybrid process specifications. As proof of concept, results from two case studies, i.e. separation of aqueous solutions using hybrid distillation schemes and bio-oxidation of alcohols using hybrid reaction-separation schemes, are presented.

3.1.2 Hybrid process design

In this work, a hybrid process design method that combines CAILD and process design-simulation to identify the optimal IL and its corresponding hybrid process specifications has been proposed (see Figure 3.1). First, hybrid schemes that have the potential to satisfy the demands of lower energy consumption and/or improve the reaction performance (for biochemical processes) are generated. For the hybrid schemes involving reaction process, a dynamic-state simulation should be performed first to evaluate the reaction performance. The design step can go to the downstream separations if the desired performance is achieved, otherwise the hybrid schemes should be regenerated. Second, based on the IL design target(s) for separation system(s) in the generated hybrid schemes, CAILD including the constraints of IL structure, thermodynamic and physical properties is employed to the optimal design of ILs, where UNIFAC-IL model and physical property models are introduced as the property prediction models. Third, optimal IL candidates identified from the solution of the MINLP-based CAILD problems are further evaluated by means of steady-state simulation in ASPEN Plus, in which the information of thermodynamic model, physical and critical properties of ILs are provided. Among this information, sub-models of four temperature-dependent properties (i.e. C_{pL} , σ , η , λ) are regressed based on a large number of collected experimental data in this

work. Finally, the final hybrid process design can be identified if the desired results of the hybrid scheme are achieved, otherwise the design target(s) of IL for CAILD should be adjusted accordingly.

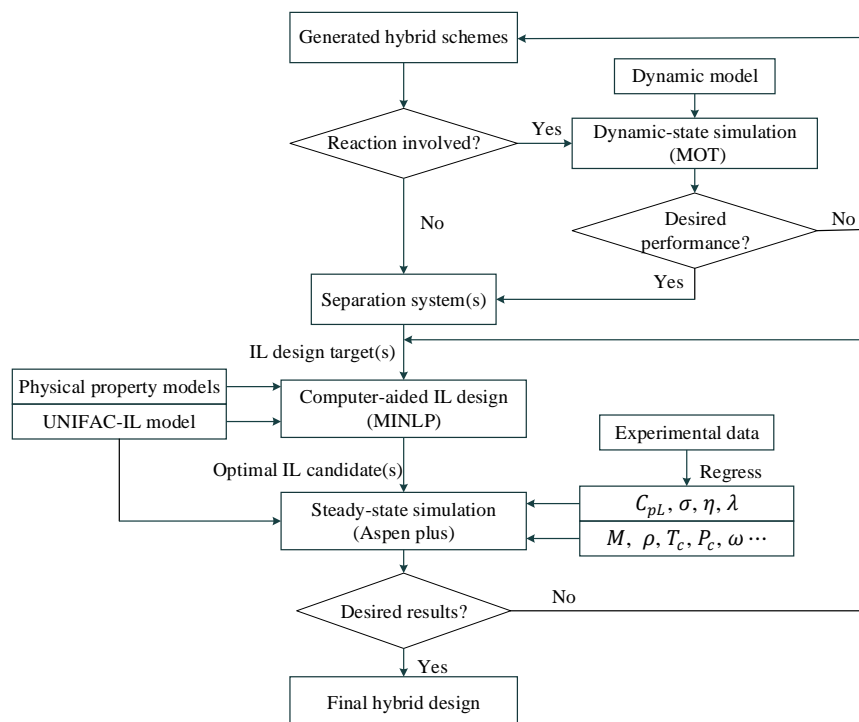


Figure 3.1 Framework of the computer-aided design of ionic liquids for hybrid process schemes

3.1.2.1 Generation of Hybrid Schemes

The generation of hybrid schemes is based on the method proposed by.³ Based on the identified “hot-spots” of a process, design targets for its improvement that overcome the “hot-spots” are set. Two hybrid schemes, i.e. hybrid distillation with ionic liquid (see Figure 3.2b) and hybrid reaction-separation scheme (see Figure 3.3), are investigated and further demonstrated by case studies in this work. In the hybrid distillation scheme, a traditional energy intensive distillation operation is replaced by a combination of not are energy intensive distillation operation with an IL-based extraction distillation. The result is that the same separation is achieved at much lower cost, better environmental impact and reduced waste. In the hybrid reaction-separation scheme, a typical bioreactor operation is combined with solvent-based product recovery giving a higher product yield and avoiding catalyst (enzyme) inhibition.

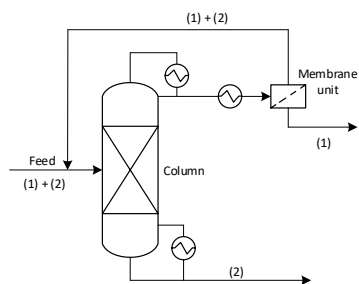


Figure 3.2a Hybrid distillation with membrane

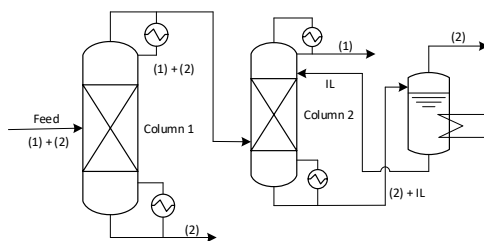


Figure 3.2b Hybrid distillation with IL

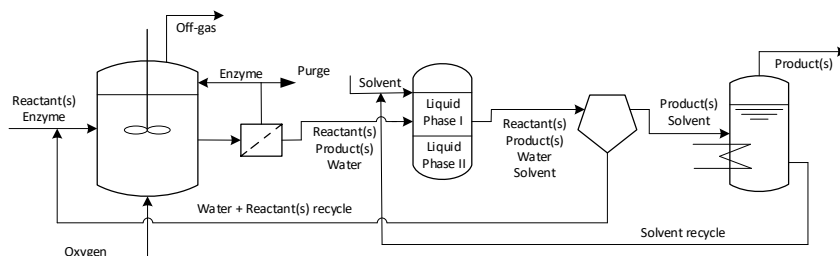


Figure 3.3 Hybrid bioreaction-separation scheme with continuous product removal

3.1.2.2 Computer-Aided Design of ILs

To achieve the full potential of the generated hybrid schemes using ILs as solvents, CAILD is used for the optimal design of ILs in this work. In CAILD, various functional groups (cations, anions and substituents) are combined subject to the constraints of IL structure, thermodynamic and physical properties. The optimal IL candidates can be identified by maximizing or minimizing the objective function (i.e. design target) in CAILD. The CAILD can be summarized as the following MINLP problem

$$\max/\min_z f_{\text{obj}}(z) \quad 3.1$$

s. t. IL structural constraints

thermodynamic property constraints

physical property constraints

where $f_{\text{obj}}(z)$ is the objective function and the vector z represents the molecular (IL) structure including the existence and the number of building blocks (cations, anions and substituents). For example, the objective function should be minimized when using Henry's constant as design target for the CO₂ capture process, while the objective function should be maximized when using relative volatility as design target for the distillation separation. The CAILD optimization problem has three main constraints: a) IL structural constraints that are introduced to ensure the feasibility (e.g. octet rule, bonding rule) and the complexity (e.g. numbers of

substituents) of the IL molecule, the detailed description of these constraints is expressed by Eq.3.7-3.13; b) Thermodynamic property constraints that are considered to find more attractive ILs for industrial applications. For example, in a liquid-liquid extraction process, the solubility of the designed IL in raffinate (e.g. aqueous phase) should be constrained to avoid the solvent loss; c) Physical property constraints that are included to ensure the applicability of designed ILs in practical operations. For example, to avoid solidification, the melting point temperature of the designed IL must be at least 5 K less than the temperature at every point in the whole process, and the viscosity should be relatively low (e.g. less than 0.05 Pa.s) with the consideration of the process operation.

Objective function

In order to obtain an attractive separation performance of hybrid distillation with IL (see Figure 2b), a reasonable design target should be set for the CAILD optimization problem. As a measure comparing the vapor pressures of the components in a liquid mixture of chemicals, relative volatility can indicate the ease or difficulty of using distillation to separate the more volatile components from the less volatile components in a mixture. Since the components are to be easily separated from each other with high relative volatility, the maximization of the relative volatility between component (1) and component (2) in the ternary system containing IL is selected as the objective function. In the present work, two types of relative volatility: infinite dilution activity coefficients (γ^∞) based relative volatility ($\alpha_{1,2}^\infty$) and solvent-to-feed ratio (S/F) based relative volatility ($\alpha_{1,2}^{S/F}$) are considered. They are defined in Eqs.3.2 and 3.3.

$$\alpha_{1,2}^\infty = \frac{\gamma_1^\infty P_1^{sat}}{\gamma_2^\infty P_2^{sat}} \quad 3.2$$

$$\alpha_{1,2}^{S/F} = \frac{\gamma_1^{S/F} P_1^{sat}}{\gamma_2^{S/F} P_2^{sat}} \quad 3.3$$

where P_1^{sat} and P_2^{sat} , respectively, represent the saturated pressure of component (1) and component (2). γ_1^∞ , γ_2^∞ are the infinite dilution activity coefficient of component (1) and component (2) while $\gamma_1^{S/F}$, $\gamma_2^{S/F}$ are the activity coefficient of component (1) and component (2) with certain S/F, respectively. In a ternary system containing IL, the IL interacts differently with the components of the mixture thereby causing their relative volatilities to change, and different ILs generally have different interaction with the components to be separated.

Together with relative volatility, the Hildebrand solubility parameter that can predict solvent-related properties is also considered as design target since compounds with similar solubility parameter are more likely to form a miscible solution.¹⁰⁶ In this work, a group contribution (GC)-based model developed by Roughton et al.⁷⁹ for predicting the Hildebrand solubility parameter of IL (δ_{IL}) is used, as given in Eq.3.4.

$$\delta_{IL} = \sum_{c=1}^{k_c} n_c \delta_c + \sum_{a=1}^{k_a} n_a \delta_a + \sum_{g=1}^{k_g} n_g \delta_g + b \quad 3.4$$

where parameters δ_c , δ_a and δ_g represent the group contributions from cations, anions and substituents for the Hildebrand solubility parameter while δ_c , δ_a and δ_g denote the number of cations, anions and substituents in the IL molecule, respectively. When using Hildebrand solubility parameter as design target in the CAILD optimization problem, the objective function is to minimize the difference between the solubility parameter of IL and the solubility parameter of the entrained component.

When choosing an IL as solvent for the product recovery (liquid-liquid extraction) in the proposed reaction-separation scheme (see Figure 3.3), its separation performance are generally described by solvent properties at infinite dilution such as distribution coefficient (D) and selectivity (S).^{102, 107, 108}

$$D = \frac{\gamma_{P,H_2O}^{\infty} M_{w,H_2O}}{\gamma_{P,IL}^{\infty} M_{w,IL}} \quad 3.5$$

$$S = \frac{\gamma_{R,IL}^{\infty}}{\gamma_{P,IL}^{\infty}} \quad 3.6$$

where γ_{P,H_2O}^{∞} is the infinite dilution activity coefficient of product P in the aqueous phase; γ_{P,H_2O}^{∞} , $\gamma_{R,IL}^{\infty}$ are the infinite dilution activity coefficients of product P and reactant R in the IL phase, respectively; in Eq.1, M_{w,H_2O} and $M_{w,IL}$ represent the molecular weights of water and IL, respectively. In this work, S and $\{D \times S\}$, respectively, are considered as the objective function in the CAILD optimization problem and both them should be maximized.

IL structural constraints

To ensure the feasibility and complexity of designed ILs, A detailed set of constraints proposed by ⁴⁴ is introduced, shown as in Eqs.3.7–3.13.

$$\sum_{i \in C} c_i = 1 \quad 3.7$$

$$\sum_{j \in A} a_j = 1 \quad 3.8$$

$$\sum_{l=1}^N x_l - \sum_{i \in C} c_i v_i = 0 \quad 3.9$$

$$\sum_{i \in C} (2 - v_i) c_i + \sum_{l=1}^N \sum_{k \in S} (2 - v_{kl}) x_l n_{kl} = 2 \quad 3.10$$

$$\sum_{k \in S} (2 - v_{kl}) x_l n_{kl} = 1 \quad 3.11$$

$$n_S^L \leq \sum_{l=1}^N \sum_{k \in S} x_l n_{kl} \leq n_S^U \quad 3.12$$

$$n_{Sl}^L \leq \sum_{k \in S} x_l n_{kl} \leq n_{Sl}^U \quad 3.13$$

where C , A , S are the sets of cations, anions and substituents, respectively; the cations are represented by the binary variable of c_i and the anions are represented by the binary variables of a_j . The vector x_l of binary variables represent the side chains l , while the vector n_{kl} of integer variables denotes the number of substituents of type k in the side chain l . Group valences of the cations and substituents, respectively, described by vectors of v_i and v_{sl} . As

shown in Eqs.3.7 and 3.8, only one cation and one anion is available in each IL molecule. The octet rule that ensures the consistency between the number of side chains and the free valence of the cation is described by Eq.3.9. Meanwhile, Eqs.3.10 and 3.11 are utilized to ensure that any two adjacent groups are not linked by more than one covalent bond. As given in Eqs.3.12 and 3.13, minimum and maximum numbers of substituents n_S^L , n_{Sl}^L and n_S^U , n_{Sl}^U are, respectively, specified to the cation and each side chain l with the consideration of the size and complexity of designed IL candidates.

Thermodynamic property constraints

To find ILs with attractive process performance, some thermodynamic property constraints are necessary. For the ILs used in hybrid distillation, constraint of relative volatility that ensures the possibility of the separation process should be considered. On the other hand, when IL is selected as the solvent for liquid-liquid extraction in a dilute aqueous solution, the constraints of distribution coefficient, selectivity and solvent loss (Sl) should be introduced to the CAILD problem. In this work, Sl is described as the following equation

$$Sl = \frac{1}{\gamma_{IL,H_2O}^\infty} \quad 3.14$$

where γ_{IL,H_2O}^∞ represents the infinite dilution activity coefficient of solvent (IL) in the aqueous phase.

To predict the thermodynamic behavior of the IL containing system, different types of methods have been introduced and extended. They can be summarized as conductor-like screening model (COSMO)-based priori thermodynamic methods including COSMO-RS,^{64, 68, 109-112} COSMO-SAC,¹¹²⁻¹¹⁴ equations of state like GCLF and PC-SAFT,¹¹⁵⁻¹¹⁷ and activity coefficient based methods such as UNIQUAC, NRTL and UNIFAC.^{51, 52, 54, 57, 58, 79, 118}

In this work, UNIFAC is considered as the thermodynamic method because of its reliable predictions and easy integration with the use of CAILD. Proper decomposition of ILs is required for the application of UNIFAC method, here the decomposition approach where the IL is divided into cation, anion, and substituents separately is employed since it can improve the design space and the flexibility of the CAILD optimization problem.⁹⁴

Physical property constraints

Properties of ILs (ILs), especially the melting point and the viscosity, are important for the optimal design of ILs. For example, to avoid solidification of the solvent, the melting point temperature (T_m) of the designed IL must be at least 5 K less than the temperature at every point in the whole process (T_p) while the viscosity (η) has significant impact on the process operation. Therefore, constraints ensure the applicability of the designed ILs are added to these two properties (see Eqs.3.15 and 3.16).

$$T_p - T_m < 5 \text{ (K)} \quad 3.15$$

$$\eta < 0.05 \text{ (Pa.s)} \quad 3.16$$

Several types of methods such as quantum chemistry-based method¹¹⁹⁻¹²², empirical correlations,¹²³⁻¹²⁶ GC-based methods,^{46, 48, 127} and corresponding states principle-based equations,^{38, 128} have been developed for the physical property predictions of ILs. Among them, GC-based methods are preferred since it can be easily integrated with the use of CAILD. For this reason, two GC-based estimation methods developed in Section 2.2 are used to calculate T_m and η of ILs.

3.1.2.3 Process Design-Simulation

Hybrid distillation with ionic liquid

As shown in Figure 3.2b, two separation techniques (a conventional distillation and an IL-based distillation) are combined in the proposed hybrid scheme involving IL-based distillation. Both distillations have their regions of efficient operations. For conventional distillation, this should have significant energy savings and for IL-based distillation it reduces the amount of IL and also improves the column operation (e.g. low viscosity). So replacing the part of the separation where conventional distillation has very low driving force (or requires most of the energy) with a IL-based distillation that has higher separation efficiency in this region will ensure both the separation techniques are operating at their high efficiency regions. The hybrid scheme has better energy efficient and economical performance than any of the separation techniques on their own.

To evaluate the process performance of the hybrid distillation scheme using IL identified from the solution of the CAILD problems, detailed process simulations are performed in Aspen Plus. To date, ILs are still not included to the component database in Aspen Plus and therefore they should be defined as pseudo-components. For the purpose of these definition, properties of ILs such as molecular weights, densities and critical properties need to be specified. Likewise, information of the thermodynamic method for the IL containing system is also required.

Critical properties of ILs can be calculated using the fragment contribution-corresponding states method developed by,¹²⁹ as following equations

$$T_b = 198.2 + \sum_{i=1}^k n_i \Delta T_{b,i} \quad 3.17$$

$$T_c = \frac{T_b}{0.5703 + 1.0121 \sum_{i=1}^k n_i \Delta T_{c,i} - (\sum_{i=1}^k n_i \Delta T_{c,i})^2} \quad 3.18$$

$$P_c = \frac{M}{(0.34 + \sum_{i=1}^k n_i \Delta P_{c,i})^2} \quad 3.19$$

$$V_c = 28.8946 + 14.75246 \sum_{i=1}^k n_i \Delta V_{c,i} + \frac{6.03853}{\sum_{i=1}^k n_i \Delta V_{c,i}} \quad 3.20$$

$$\omega = \frac{T_b T_c}{(T_c - T_b)(0.7 T_c)} \log\left(\frac{P_c}{P_b}\right) - \frac{T_c}{(T_c - T_b)} \log\left(\frac{P_c}{P_b}\right) + \log\left(\frac{P_c}{P_b}\right) - 1 \quad 3.21$$

In Eqs.3.17–3.20, n_i denotes the number of fragment i that appears in the IL molecules; $\Delta T_{b,i}$, $\Delta T_{c,i}$, $\Delta P_{c,i}$, and $\Delta V_{c,i}$ represent the fragment increments of fragment i for the normal boiling temperature (T_b), critical temperature (T_c), critical pressure (P_c), critical volume (V_c), respectively; M is the molar mass in g.mol⁻¹. In Eq.3.21, ω is the acentric factor and P_b is the atmospheric pressure in bar.

To calculate the temperature-dependent properties such as heat capacity, surface tension, viscosity and thermal conductivity, prediction sub-models of these properties in Aspen Plus (Eqs.3.22-3.25) are extracted and further regressed based on a wide range of experimental data taken from our IL database.

$$C_{pL} = C_{1pL} + C_{2pL}T + C_{3pL}T^2 + C_{4pL}T^3 + C_{5pL}/T^2 \quad 3.22$$

$$\sigma = C_{1\sigma} + C_{2\sigma}T + \dots + C_{10\sigma}T^9 \quad 3.23$$

$$\ln \eta = C_{1\eta} + C_{2\eta}/T + C_{3\eta} \ln T + C_{4\eta}T^2 + C_{5\eta}/T^2 \quad 3.24$$

$$\lambda = C_{1\lambda} + C_{2\lambda}T + C_{3\lambda}T^2 + C_{4\lambda}T^3 + C_{5\lambda}T^4 \quad 3.25$$

where, T is the absolute temperature in K; heat capacity C_{pL} (J.mol⁻¹.K⁻¹), surface tension σ (N.m⁻¹), viscosity η (Pa.s) and thermal conductivity λ (W.m⁻¹.K⁻¹) can be calculated from their corresponding modeling parameters C_{mpL} , $C_{m\sigma}$, $C_{m\eta}$ and $C_{m\lambda}$ ($m = 1, 2, 3 \dots$), respectively.

As in the design stage of CAILD, UNIFAC is also selected as the thermodynamic method in Aspen Plus for process simulation. In this work, group volume parameters (R_k), surface area parameters (Q_k) as well as interaction parameters (α_{mn} , α_{nm}) of UNIFAC-IL model are taken from the published works by.^{79, 91} In their work, parameters R_k , Q_k were calculated based on the rules of Bondi¹³⁰ and parameters α_{mn} , α_{nm} were regressed on the basis of experimental data containing activity coefficients of different solutes at infinite dilution in various ILs. These parameters were validated by comparing experimental and calculated ternary VLE data of various binary aqueous mixtures (ethanol–water, 1-propanol–water and 2-propanol–water) with different ILs.

Hybrid reaction-separation scheme

Hybrid reaction-separation scheme is an intensified process operation where the conversion of the reactant(s) is completed in the reactor and the product recovery is performed externally with a separate loop where separation technique of liquid-liquid extraction is used, as presented in Figure 3.3. Bio-reactions are considered in this hybrid scheme, meaning that the medium of the reactor contains large amounts of water. In liquid-liquid extraction, the solvent should be able to extract the product (s) from the dilute water solution and separate it from the reactants. Meanwhile, the reactant (s) should remain dissolved in the aqueous phase and then recycled back to the reactor after decantation. After liquid-liquid extraction, the product (s) and the solvent are further separated in a flash evaporator, where the product s are recovered and the

solvent is regenerated. In this case, a heavy solvent with very low volatility and water immiscibility is needed to achieve the separation target and therefore hydrophobic ILs are the potential solvent candidates. CAILD is selected as the solvent screening method and the feasibility of the product recovery with the identified ILs from solution of CAILD problem is evaluated by the liquid-liquid equilibrium (LLE) calculation of the studied IL containing system performed in Aspen Plus.

A dynamic-state simulation is required to evaluate the possibility of improving reaction performance by the continuous product removal from reactor (Figure 3.4). For this reason, a dynamic model that describes the behavior of the reaction system is developed for the dynamic-state simulation. The model aims to be applicable for any kind of reaction process catalyzed by enzymes with low substrate concentrations and low yields. Aerobic bio-reactions are also taken into consideration in this model and therefore the presence of the vapor phase is due to possible aeration requirements.

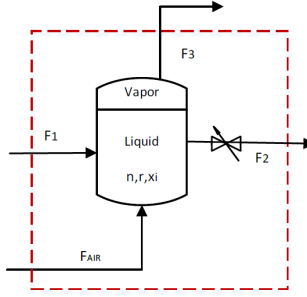


Figure 3.4 Schematic representation of the modelled reactor

In Figure 3.4, F_1 , F_2 , F_{AIR} and F_3 refer to the inlet and outlet molar flow rates of the liquid (F_1 , F_2) and the vapor phase (F_{AIR} , F_3) (kmol/h), respectively. F_1 , F_2 can be controlled by adjusting the value in the liquid outlet of the reactor. The dynamic model is expressed as following equations:

$$\frac{dn_i}{dt} = F_1 x_{1,i} - F_2 x_{2,i} + \gamma_i r - F_3 y_i \quad 3.26$$

$$F_3 y_i = F_{air} y_i - \vartheta_i^V F_{air} y_i + \vartheta_i^L n_i \quad 3.27$$

$$x_{1,i} = \frac{f_{1,i}}{F_1} \quad 3.28$$

$$x_{2,i} = \frac{n_i}{N} \quad 3.29$$

$$y_i = \frac{f_{3,i}}{F_3} \quad 3.30$$

$$F_1 = \sum_{i=1}^{NC} f_{1,i} \quad 3.31$$

$$F_2 = C_v h \quad 3.32$$

$$F_3 = \sum_{i=1}^{NC} f_{3,i} \quad 3.33$$

$$N = \sum_{i=1}^{NC} n_i \quad 3.34$$

$$\bar{\rho} = \sum_{i=1}^{NC} \rho_i n_i \quad 3.35$$

$$h = \frac{N}{\bar{\rho} A} \quad 3.36$$

$$V = h A \quad 3.37$$

$$C_i = \frac{n_i}{V} \quad 3.38$$

where the total number of moles (N) in the reactor is equal to the sum of the moles of each components i (n_i); the molar fraction of component i in the vapor phase (y_i) can be calculated by Eq.3.30, and the molar fraction of component i in the liquid inlet ($x_{1,i}$) and outlet ($x_{2,i}$) of the reactor can be calculated by Eq.3.28 and Eq.3.29, respectively. γ_i represents the stoichiometric coefficient of component i and C_v describes the value coefficient; ϑ_i^V is the coefficient for the reacted gases while ϑ_i^L is the removal coefficient of the moles of the liquid compounds. $f_{1,i}$, $f_{3,i}$ are the inlet molar flow rates of component i in the inlet stream and the vapor outlet, respectively. Based on the ideal mixing rule (Eq.3.35), the density of the liquid mixture ($\bar{\rho}$) can be calculated from the pure component density (ρ_i); the volume of the liquid (V) is calculated as the product of the cross-sectional area (A) times the level of the liquid (h). The concentrations of the enzyme (C_E) and the oxygen (C_O) are considered to be constant throughout the reaction, while the concentrations of the substrate (C_S) and the product (C_P) change with the time can be calculated by Eq.3.38.

The equations in this dynamic model are derived from the differential mass balance since the model parameters such as the concentrations of substrate and product are changing over the time. Different reaction systems have different reaction kinetic models and kinetic parameters. Generally, the kinetic model and its corresponding kinetic parameters are developed and regressed from experimental work. In this work, ICAS-MoT¹³¹ is applied as the process simulator for dynamic-state.

Table 3.1 summarizes the overall information of the proposed design method for hybrid processes. In the design stage of CAILD, besides the objective function and the constraints of the design problem, thermodynamic method (UNIFAC) and group parameters (e.g. group sets, boundaries of group number) are also included. The variables describing the IL structure are optimized by solving the formulated MINLP problem for CAILD. Subsequently, the optimal IL identified from CAILD and the information of its critical, physical and thermodynamic properties are used in the design stage of process simulation. Meanwhile, process parameters such as feed information, operating conditions are provided as well. The process variables (e.g. column configurations, solvent flowrate) are optimized by means of trade-off and sensitivity

analysis. On the other hand, when the IL is selected as the solvent for the liquid-liquid extraction, the LLE calculation of the IL containing system is performed aims to evaluate the possibility of the phase split. In the case of hybrid reaction-separation scheme, a dynamic-state simulation is also needed to evaluate the possibility of improving reaction performance (e.g. yield, reaction rate) by continuous product removal from reactor. As required, dynamic model describing the behavior of the reaction system, as well as kinetic parameters, reaction conditions etc., should be provided.

Table 3.1 Overall information of the proposed hybrid process design involving IL

CAILD (Stage 1)	
Objective function	e.g. $\max(\alpha_{1,2}^{\infty})$; $\max(\alpha_{1,2}^{S/F})$; $\min(\delta_{IL} - \delta_2)$; $\max(S)$; $\max(\{D \times S\})$ (Eqs.3.2-3.6)
IL structure constraints	Feasibility (Eqs.3.7-3.10), complexity (Eqs.3.12-3.13)
Thermodynamic property constraints	e.g. α (Eqs.3.2-3.3); S (Eq.3.5); D (Eq.3.6); Sl (Eq.3.14)
Physical property constraints	T_m, η (Eqs.3.15-3.16)
Thermodynamic method	UNIFAC (Eqs.2.21-2.32)
Fixed parameters	$C, A, S, n_S^L, n_{Sl}^L, n_S^U, n_{Sl}^U$
Optimization variables	$c_i, a_j, x_l, v_i, v_{kl}, n_{kl}$
Process design-simulation (Stage 2)	
Steady-state simulation	
Optimal IL (Identified from CAILD)	e.g. $[C_3mPy]^+ [BF_4]^-$; $[C_4mIm]^+ [Tf_2N]^-$
Critical properties	$T_b, T_c, P_c, V_c, \omega$ (Eqs.3.17-3.21)
Physical properties	$C_{pL}, \sigma, \eta, \lambda$ (Eqs.3.22-3.25)
Thermodynamic properties	$R_k, Q_k, \alpha_{mn}, \alpha_{nm}$ (UNIFAC-IL model)
Process parameters	Feed information (e.g. flowrate, composition), operating conditions (e.g. pressure, temperature)
Optimization variables	Number of stages, feed stage, reflux ratio, solvent flowrate
Dynamic-state simulation	
Dynamic model	Eqs.3.26-3.38
Fixed parameters	Kinetic parameters, reaction conditions
Performance indicator	Reaction rate, yield

3.1.3 Case studies

3.1.3.1 Separation process of aqueous solutions

Separation of aqueous solutions is widely encountered in process industries, such as in the separation process of the methanol-water mixture, where the energy requirement increases

significantly with respect to the recovery of methanol from 0.98 to 0.998 (mole-based). Likewise, acetone separation from aqueous solution has a similar energy consumption distribution, as shown in Figure 3.5, where data points of both examples come from the process simulation in Aspen Plus. For both cases, “hot-spots” can be identified based on their energy consumption distribution. Considering the significant energy savings potential of using energy efficient process to replace the energy intensive separation task (i.e. remove “hot-spots”), sustainable hybrid distillation designs proposed in this work are promising alternatives for these separation processes.

In the process of methanol separation from aqueous solution, the process task can be defined as follows: a 1000 kmol.h^{-1} liquid mixture consisting of 20 mol% methanol and 80 mol% water, to be separated by hybrid distillation with IL so that the methanol composition of distillate from extractive distillation column amounts to 99.8 mol%. For the case of acetone separation from aqueous solution, we consider a 1000 kmol.h^{-1} liquid mixture consisting of 20 mol% acetone and 80 mol% water which is separated by hybrid distillation with IL for meeting the acetone purification of 99.8 mol%. In this work, IL-based extractive distillation is considered to perform the energy intensive separation task of the process for both cases. Fixed process parameters for the proposed hybrid process are given in Table 3.2.

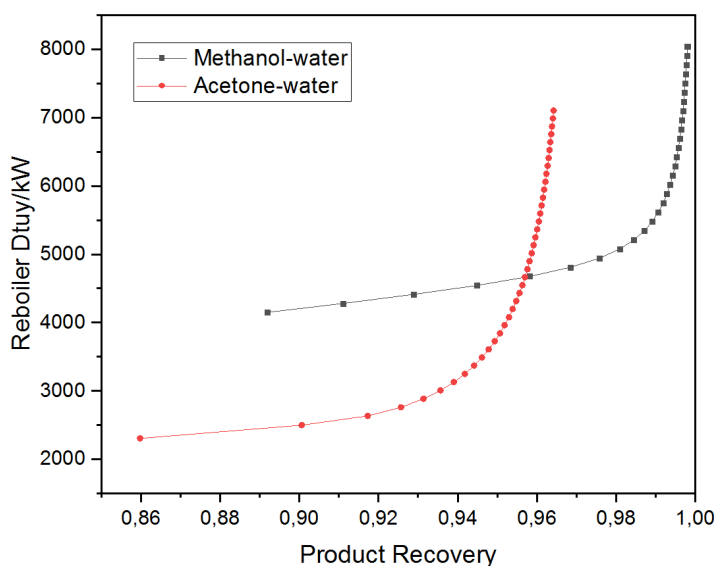


Figure 3.5 Energy consumption distribution in the separation process of aqueous solutions

As shown in Table 3.3, 2 widely studied 2 substituents, 2 cations and 7 anions were selected as building blocks for the IL design. Table 3.4 summaries the design information of the MINLP-based CAILD problem in these case studies. The formulated MINLP problem of both examples

are solved using deterministic global optimization solvers (LINDOGLOBAL) in the modelling system GAMS.

Table 3.2 Fixed parameters and simulation results of the conventional distillation for the separation process of aqueous solution

Fixed parameters	Methanol-water	Acetone-water
Feed		
Flow rate	1000 kmol/h	1000 kmol/h
Mole-based composition	0.2 CH ₃ OH, 0.8 H ₂ O	0.2 (CH ₃) ₂ CO, 0.8 H ₂ O
Methanol purity	99.8 mol % CH ₃ OH	99.8 mol % (CH ₃) ₂ CO
Distillation Column		
Pressure at the top	1 bar	1 bar
Pressure at the bottom	1.2 bar	1.2 bar
Number of stages	20	33
Feed stage	13	31
Reflux ratio	1.95	2.95
Reboiler heat duty	5987 kW	7022 kW
	(99.8 mol% CH ₃ OH)	(97 mol% (CH ₃) ₂ CO)

Table 3.3 Molecular building blocks for IL design in the case studies of aqueous separation

Type	Group	Subgroup	Type	Group	Subgroup
Substituents	CH ₃	CH ₃	Anions	[Tf ₂ N] ⁻	[Tf ₂ N] ⁻
		CH ₂		[BF ₄] ⁻	[BF ₄] ⁻
Cations	[Im] ⁺	[Im] ⁺		[PF ₆] ⁻	[PF ₆] ⁻
		[mIm] ⁺		[CF ₃ SO ₃] ⁻	[CF ₃ SO ₃] ⁻
	[Py] ⁺	[Py] ⁺		[CF ₃ COO] ^{-*}	[CF ₃ COO] ^{-*}
		[mPy] ⁺		[DMP] ⁻	[DMP] ⁻
				[SCN] ^{-*}	[SCN] ^{-*}

*NB: Groups only used in the case study of ethanol-water separation

Table 3.4 Design information of MINLP-based CAILD problem for the case studies of aqueous separation

Case	Number of continuous variables	Number of binary variables	Number of integer variables	Number of constraints		
				IL structure	Thermodynamic properties	Physical properties
Methanol-water	195	23	70	60	126	4
Acetone-water	195	21	70	60	126	4

By solving the MINLP-based CAILD optimization problem (see Equations 1-13) using γ^∞ based and S/F based relative volatility of methanol and water in the ternary system containing IL as objectives, 1-ethylpyridinium tetrafluoroborate ($[\text{C}_2\text{Py}]^+[\text{BF}_4]^-$) and 1-ethyl-3-methylpyridinium tetrafluoroborate ($[\text{C}_2\text{mPy}]^+[\text{BF}_4]^-$) are selected, respectively; meanwhile, 1-methylimidazolium tetrafluoroborate ($[\text{mIm}]^+[\text{BF}_4]^-$) is identified as entrainer while using the Hildebrand solubility parameter of ILs (δ_{IL}) as design target in the CAILD optimization problem. Similarly, for the separation process of acetone-water mixture, 3-methyl-1-propylpyridinium tetrafluoroborate ($[\text{C}_3\text{mPy}]^+[\text{BF}_4]^-$) and 1-methylpyridinium dimethylphosphate ($[\text{C}_1\text{Py}]^+[\text{DMP}]^-$) are identified, respectively, using γ^∞ based relative volatility (or δ_{IL}) and S/F based relative volatility as design targets. Table 3.5 provides the model statistics from GAMS solution of the MINLP-based CAILD problem and the structures of the generated IL candidates are given by Figure 3.6.

Table 3.5 Model statistics from GAMS solution for the case studies of aqueous separation

Case	Number of continuous variables	Number of binary variables	Number of equations	Number of constraints	Objective function	Number of iterations	CPU time (s)
Methanol-water	195	23	191	190	$\alpha_{1,2}^\infty$	210	4
					$\alpha_{1,2}^{S/F}$	203475	24
Acetone-water	195	21	191	190	$\alpha_{1,2}^\infty$	43048	21
					$\alpha_{1,2}^{S/F}$	159953	16

As shown in Figure 2b, two distillation columns and a flash unit are included in the proposed hybrid distillation with IL. Column 1 is used as traditional separation unit while Column 2 is considered to perform the energy intensive task of the separation processes. Subsequently, the flash unit is employed for the entrainer (IL) regeneration. The simulation of this hybrid distillation process is performed in Aspen Plus (V8.6), where distillation columns (Column 1, Column 2) are modelled by the RadFrac block and flash unit is modelled by the flash evaporation. As compared, conventional process simulation is also performed for the same separation task.

In the design step of process simulation, key operating variables like the number of stages, feed location in Column 2 and the corresponding flow rates of IL are optimized by trade-off and sensitivity analysis. As demonstrated, sensitivity analysis on feed location in Column 2 with certain number of stages ($N=12$) for the use of $[\text{C}_3\text{mPy}]^+[\text{BF}_4]^-$ as entrainer at different flow rates is shown in Figure 3.7. Based on the trade-off analysis, the columns with optimal feed location at different IL flow rates, the number of stages and flow rate yielding the minimum stages and energy requirements can be achieved (see Figure 3.8).

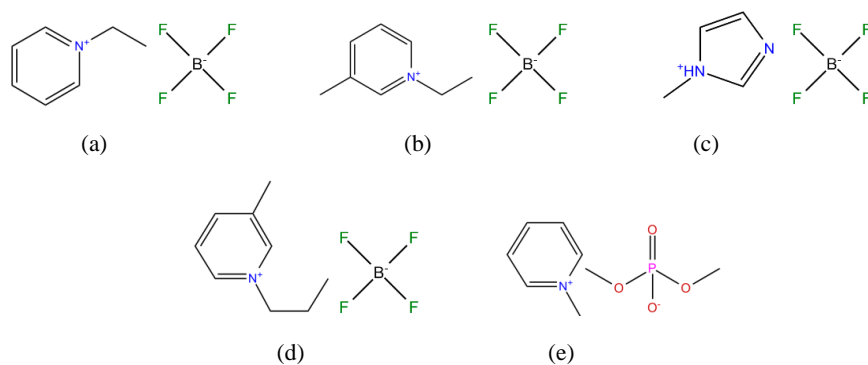


Figure 3.6 The structure of the designed ionic liquids for the hybrid distillation process:
 (a) $[C_2Py]^+[BF_4]^-$, (b) $[C_2mPy]^+[BF_4]^-$, (c) $[mIm]^+[BF_4]^-$, (d) $[C_3mPy]^+[BF_4]^-$, (e) $C_1Py^+[DMP]^-$

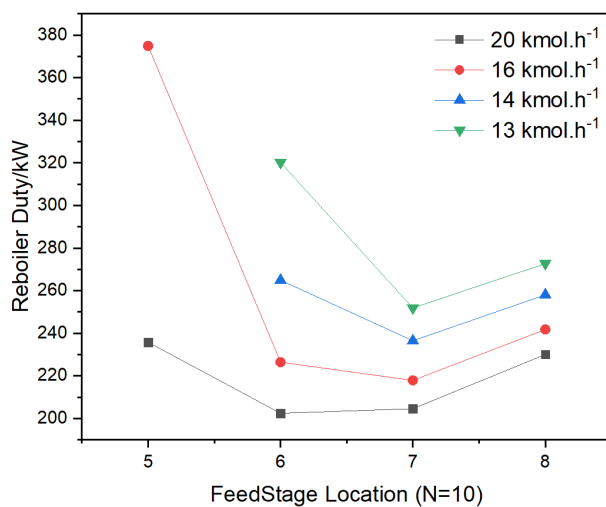


Figure 3.7 Reboiler heat duty plotted against feed stage location for meeting the separation task of acetone-water mixture using various amounts of $[C_3mPy]^+[BF_4]^-$ as entrainer

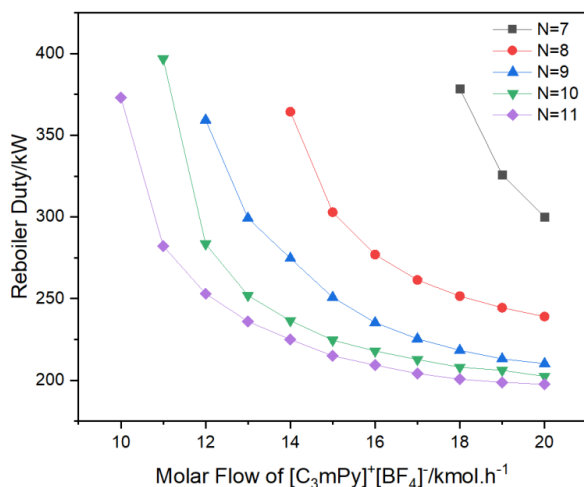


Figure 3.8 Reboiler heat duty plotted against the molar flow of $[\text{C}_3\text{mPy}]^+[\text{BF}_4]^-$ in the extraction distillation column with different number of column stages (N) for meeting the acetone purification requirement

For the purposes of comparison, the conventional distillation process of both systems is also simulated and optimized. The simulation results of hybrid separation scheme for both systems are summarized in Tables 3.6 and 3.7. The results indicate that hybrid distillation with all IL identified using different selection criteria have significant energy savings in comparison to the conventional distillation process, where 5987 kW is required for meeting the methanol purification of 99.8 mol% while 7022 kW is required to obtain the acetone recovery of 97 mol% (see Table 3.6).

Table 3.6 Simulation results for hybrid distillation with IL for methanol-water system

Design target	$\alpha_{1,2}^\infty$	$\alpha_{1,2}^{S/F}$	δ_{IL}
IL	$[\text{C}_2\text{Py}]^+[\text{BF}_4]^-$	$[\text{C}_2\text{mPy}]^+[\text{BF}_4]^-$	$[\text{mIm}]^+[\text{BF}_4]^-$
Entrainer flow rate, kmol/h	11	8	12
Column 1			
Number of stages	16	16	16
Feed stage	11	11	11
Reflux ratio	1.43	1.43	1.43
Reboiler heat duty, kW	4991	4991	4991
Column 2			
Number of stages	6	6	5
Entrainer stage	2	2	2
Feed stage	4	4	4
Reflux ratio	0.119	0.095	0.091
Reboiler heat duty, kW	186	141	124

Flash drum			
Operating pressure (bar)	0.1	0.1	0.1
Heat duty, kW	67	65	76
Overall heat duty, kW	5244	5197	5191

For methanol-water system, all three IL candidates have similar energy requirement. Among them, $[\text{mIm}]^+[\text{BF}_4]^-$ requires the least column stages and $[\text{C}_2\text{mPy}]^+[\text{BF}_4]^-$ is found to be the best selection in terms of the solvent consumption. For the separation of acetone-water mixture, all three selected ILs provide significant energy savings. Although $[\text{mIm}]^+[\text{BF}_4]^-$ requires the least number of column stages while, $[\text{C}_2\text{mPy}]^+[\text{BF}_4]^-$ shows the most attractive separation performance with lowest energy input and solvent consumption. Calculation results of both cases highlight the reliability and applicability of using $\alpha_{1,2}^{S/F}$ as design target to screen suitable ILs in the CAILD problem for separation processes of aqueous solution.

Although, only one main column is required for the conventional distillation process, hybrid scheme with IL can significantly reduce the energy consumption, especially for the acetone-water system where the purification would be very difficult after 96 mol% acetone. Additionally, the overall flow rate of ILs in the hybrid process is less than 20 kmol/h, which provides possibility of addressing the operational and economic constraints (e.g. high viscosity, high cost) in the use of ILs as solvents.

Table 3.7 Simulation results for hybrid distillation with IL for acetone-water system

Design target	$\alpha_{1,2}^\infty$	$\alpha_{1,2}^{S/F}$	δ_{IL}
IL	$[\text{C}_1\text{Py}]^+[\text{DMP}]^-$	$[\text{C}_3\text{mPy}]^+[\text{BF}_4]^-$	$[\text{mIm}]^+[\text{BF}_4]^-$
Entrainer flow rate, kmol/h	17	14	16
Column 1			
Number of stages	15	15	15
Feed stage	12	12	12
Reflux ratio	0.395	0.395	0.395
Reboiler heat duty, kW	3097	3097	3097
Column 2			
Number of stages	12	10	9
Entrainer stage	2	2	2
Feed stage	8	7	7
Reflux ratio	0.275	0.275	0.289
Reboiler heat duty, kW	241	233	230
Flash drum			
Operating pressure (bar)	0.1	0.1	0.1
Heat duty, kW	286	278	293
Overall heat duty, kW	3624	3608	3620

3.1.3.2 Bio-oxidation of alcohols

Aldehydes are important intermediates used in the manufacture of solvents, resins, plasticizers and pharmaceuticals because of their high chemical activity (<https://www.britannica.com/science/aldehyde>). Some sugars, hormones or vitamin derivatives are aldehydes.¹³² There are several methods for synthesizing aldehydes, and the method of alcohols dehydrogenation is widely used in industries. In this work, we select the oxidation of alcohols as the synthesis method to produce aldehydes and the bio-catalyst (galactose oxidase) is used in these bio-reactions (see Table 3.8). Galactose oxidase is a copper-dependent enzyme that has shown promising results for the bio-catalysis of the oxidation of primary alcohols to the corresponding aldehydes¹³³. Although this synthesis method has many advantages such as low environmental impact and high reaction specification, the limitations of enzymes associated with product and substrate inhibition result in highly diluted product, which leads to difficulties in downstream separations. For this reason, the proposed hybrid reaction-separation scheme (see Figure 3.3) is considered as the solution for such limitations, and the application is illustrated through the bio-oxidation of benzyl alcohol to produce benzaldehyde.

Experimental work regarding the bio-catalytic oxidation of primary alcohols to aldehydes has been carried out by Toftgaard Pedersen et al.¹³⁴ In their work, the oxidation of benzyl alcohol to benzaldehyde using enzyme Galactose oxidase was in focus and a reaction kinetic model, as expressed by Eq.3.39, was developed.

$$\frac{dC_S}{dt} = -r = -\frac{k_{cat}C_EC_SC_O}{C_SC_O + K_{MO}C_S + K_{MS}C_O\left(1 + \frac{C_P}{K_{IP}}\right)} \quad 3.39$$

Table 3.8 Information of the studied bio-oxidation of alcohols

Reaction scheme	A + B → C + D
Reaction class	Oxidation
Reactants	Primary alcohol, oxygen
Products	Aldehyde, water
Catalyst	Galactose oxidase
Reaction class form	

where r is the reaction rate (mmol/l·min) and k_{cat} is the rate constant ($\mu\text{mol}/\text{min}\cdot\text{mg}$ CFE (cell-free extract)). C_O , C_S , C_P are the concentrations of oxygen, substrate and product, respectively (mmol/l); C_E is the enzyme concentration in mg/l; K_{MO} , K_{MS} , K_{IP} are Michaelis constants for oxygen, benzyl alcohol and benzaldehyde, respectively (mmol/l). Table 3.9 summarizes the reactor conditions and the kinetic parameters for this bio-reaction process.

Table 3.9 Reactor conditions and kinetic parameters for alcohols dehydrogenation using galactose oxidase as biocatalysts

Kinetic parameters			
Parameters	value	Parameters	value
k_{cat} (kmol/kg CFE)	0.066	C_E (kg/m ³)	0.0011
K_{MS} (kmol/m ³)	0.051	C_O (kg/m ³)	0.5
K_{IP} (kmol/m ³)	0.0017	C_S (kg/m ³)	0.265
Reactor conditions			
T (°C)	25	$C_{alcohol}$ (kmol/m ³)	0.05
P (atm)	1	Aeration (vvm [*])	0.5

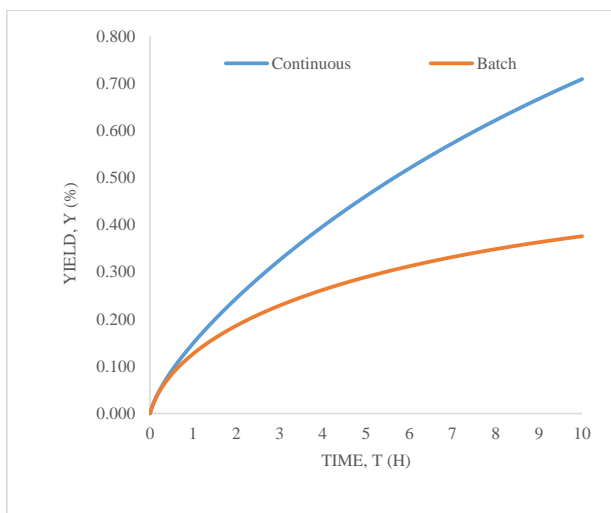
* vvm - volume of air (l) passing through a volume of medium (l) per unit time (min).

The performance of a reaction can be evaluated by the yield (Y), which is generally described as

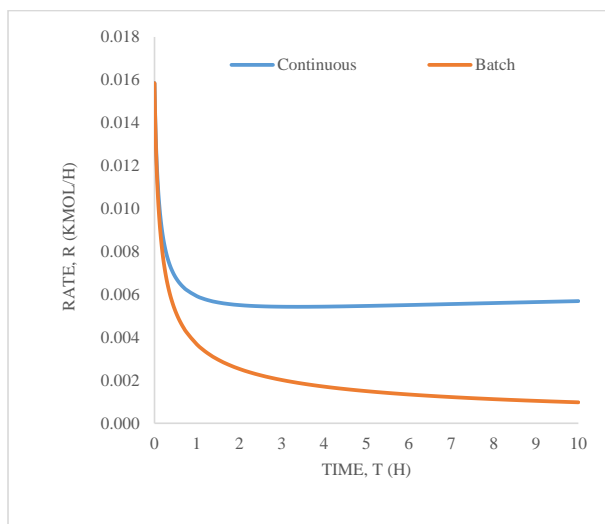
$$Y = \frac{n_p - n_{0,p}}{n_{0,r}} \quad 3.40$$

where, $n_{0,p}$ and n_p are the initial moles of product and the moles of product formed, respectively, while $n_{0,r}$ is the moles of the limiting reactant¹³⁵.

Based on the developed dynamic model (Eqs.3.26-3.38), the molar composition in the reactor with respect to time is calculated using the reaction conditions and the kinetic parameters presented in Table 3.9. For comparison purposes, the simulation of the batch operation is also performed. Figure 3.9 illustrates the product yield and reaction rate between batch operation and continuous product removal (hybrid reaction-separation scheme). Clearly the hybrid scheme involving continuous product removal has a better reaction and yield performance than the batch operation.



(a)



(b)

Figure 3.9 Comparison of product yield (a) and reaction rate (b) between batch operation and continuous product removal

In the downstream separation process, the solvent should be able to extract the product(s) from the aqueous phase and the reactant(s), and it should also be easily separated from the product(s). Since the separation technique of liquid-liquid extraction is considered, the separation

feasibility of the selected solvent can be evaluated by the ternary plot for system of water + aldehyde + solvent.

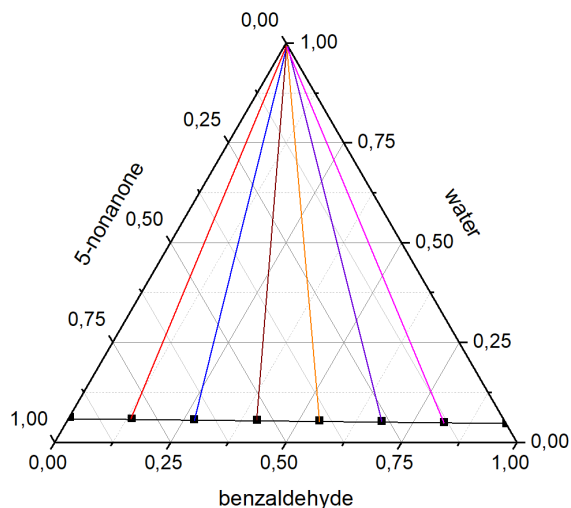


Figure 3.10 Ternary plot for system of water + benzaldehyde + 5-nonanone (calculated from UNIFAC model)

For bio-oxidation process of benzyl alcohol, an organic solvent, 5-nonanone (Figure 3.11(a)), is generated to separate benzaldehyde from water by using Pro-CAMD in ICAS (Gani et al., 1997) as organic solvent screening tool. Figure 3.10 presents the ternary plot for system of water + benzaldehyde + 5-nonanone. Although 5-nonanone is able to separate benzaldehyde from water, it is difficult to separate benzaldehyde from benzyl alcohol + water due to the similarities between benzaldehyde and benzyl alcohol. Moreover, the recovery of benzaldehyde from n-octane is also difficult. On the other hand, experimental data in some published works¹³⁶ shows that ILs might be the potential solvents to this separation task.

Table 3.10 Molecular building blocks for IL design in the bio-oxidation of benzyl alcohol

Type	Group	Subgroup	Type	Group	Subgroup
Cations	[Im] ⁺	[Im] ⁺	Anions	[Tf ₂ N] ⁻	[Tf ₂ N] ⁻
		[mIm] ⁺			[BF ₄] ⁻
	[N] ⁺	[CH ₃ N] ⁺	Substituents	CH ₃	CH ₃
		[C ₂ H ₅ N] ⁺			CH ₂
		[C ₃ H ₇ N] ⁺			
		[C ₄ H ₉ N] ⁺			

In this case, well-studied groups containing 2 cations, 2 anions and 2 substituents (see Table 3.10) were considered as molecular building blocks in CAILD. Table 11 summaries the design information of the MINLP-based CAILD problem for this case study. The formulated MINLP

problem is solved in the modelling system GAMS 24.4.6 on an Intel(R) Xeon(R) E5-1620 3.70 GHz PC running Windows 10 system, here we use a deterministic global optimization solver, LINDOGLOBAL.

Table 3.11 Design information of MINLP-based CAILD problem for the bio-oxidation of alcohols

Number of continuous variables	Number of binary variables	Number of integer variables	Number of constraints		
			IL structure	Thermodynamic properties	Physical properties
688	26	156	88	543	4

The same IL $[\text{C}_4\text{mIm}]^+[\text{Tf}_2\text{N}]^-$ is identified from the solution of the MINLP-based CAILD problem using different design targets (i.e. S and $\{D \times S\}$). Table 3.12 provides the model statistics from GAMS solution for this MINLP problem. The structure of $[\text{C}_4\text{mIm}]^+[\text{Tf}_2\text{N}]^-$ is given by Figure 3.11(b) and the UNIFAC-IL calculated LLE for system of water + benzaldehyde + $[\text{C}_4\text{mIm}]^+[\text{Tf}_2\text{N}]^-$ is presented in Figure 3.12. This results can also be partly verified by the experimental work from ¹³⁶, where the activity coefficients at infinite dilution of linear and branched C1-C6 alcohols and aldehydes in $[\text{C}_6\text{mIm}]^+[\text{Tf}_2\text{N}]^-$ shows its possibility to separate aldehydes from alcohols.

Table 3.12 Model statistics from GAMS solution for the bio-oxidation of alcohols

Number of continuous variables	Number of binary variables	Number of equations	Number of constraints	Objective function	Number of iterations	CPU time (s)
688	26	636	635	S	3000621	458
				$\{D \times S\}$	1854845	266

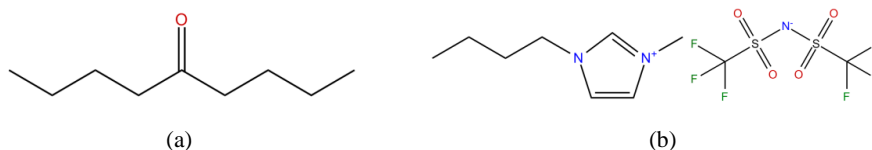


Figure 3.11 The structures of the selected organic and IL solvents: (a) 5-nonanone, (b) $[\text{C}_4\text{mIm}]^+[\text{Tf}_2\text{N}]^-$

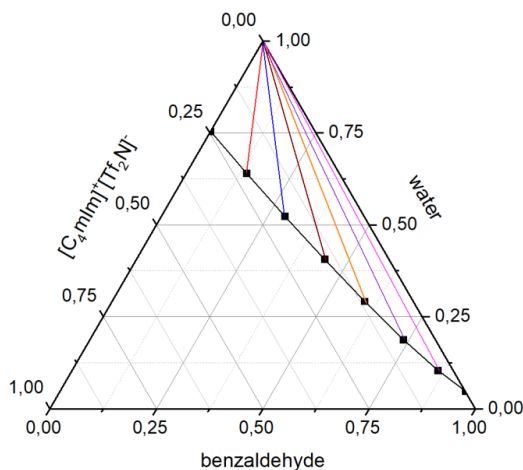


Figure 3.12 Ternary plot for system of water + benzaldehyde + $[C_4mIm]^+[Tf_2N]^-$ (calculated from UNIFAC-IL model)

3.1.4 Conclusions

This work presents a design method for hybrid process schemes that have the potential to satisfy the demands of lower energy consumption and reduced waste, as well as satisfying product specifications. The proposed IL-based hybrid schemes complement the ones using membranes (e.g. Figure 3.2a). Although both ILs and membranes have their regions of efficient operation, their potential for process improvements greatly depends on the studied system. In some cases, hybrid schemes involving ILs have guaranteed energy savings, but the ones using membranes have not, and vice versa. For some systems, if both ILs and membranes are available, the best scheme could be selected on the basis of an agreed set of performance criteria. For the purposes of process simulation, parameters of sub-models used to calculate four temperature-dependent properties of ILs were regressed based on a wide range of collected experimental data. By using this design method, optimal ILs are designed and further evaluated for case studies involving separation of aqueous solutions and bio-oxidation of alcohols. The identified ILs in both cases lead to process performance improvements and among the well-studied anions, $[BF_4]^-$ was found the most attractive for the extractive distillation of aqueous solutions.

In our present work, the design problem of hybrid process was addressed by a two-stage based solution strategy, although more reliable global optimization results consist of optimal IL solvent and corresponding process specifications can be simultaneous obtained by using an integrated solvent and process design method, computational efficiency remains a limiting factor with a significant increase in the complexity and the design space of the global-based MINLP problem. Since the limited property information of IL containing systems, only well-studied IL groups were considered as building blocks. However, more attractive IL candidates

may be generated once further IL groups are included where their property information is available. Additionally, verification by experiment will be necessary considering some designed IL(s) have never been studied or synthesized before. Future work will expand the specific design method into a generalized one that covers a wide range of processes with “hot-spots”, and improve the CAILD toolbox consisting of databases, models, and solution strategies for hybrid schemes.

3.2 INTEGRATED IONIC LIQUID AND PROCESS DESIGN

This chapter forms the basis of following publications:

Chen, Y.; Woodley, J.; Kontogeorgis, G.; Gani, R.: Integrated Ionic Liquid and Process Design involving Hybrid Separation Schemes. In Computer Aided Chemical Engineering; Elsevier, 2018; Vol. 44; pp 1045-1050.

Chen, Y.; Gani, R.; Kontogeorgis, G. M.; Woodley, J. M.: Integrated ionic liquid and process design involving azeotropic separation processes. Chemical Engineering Science 2019, 203, 402-414.

Abstract

In process industries, separation techniques need to be employed to match product quality and purity specifications. Most vapour-liquid based separation techniques involving the separation of close-boiling or azeotropic as well as gaseous mixtures are energy intensive. In this work, an integrated method that combines IL molecular structure optimisation and process design is presented for such separation processes. That is, the optimal IL molecular structure and the corresponding optimal flowsheet configuration for a specific IL-based separation process are simultaneously identified.

3.2.1 Introduction

Generally, the properties of ILs directly or indirectly impact the performance of the process in which the IL is employed as solvent. However, the classical two-stage design method (molecular design followed by process design) cannot fully represent the strong interdependencies between solvent properties and process performance. Thus, some trade-offs are necessary between tailor-made solvent properties in the design of whole chemical processes. For example, in the context of an extraction process, the selected solvent must offer both high capacity, selectivity and easy recovery for the species to be extracted. Alongside, properties such as viscosity and surface tension should also be considered because of their impact on the process operation and the size of processing units. Based on the reduced models of processing units (e.g. absorber, flash drum), integrated design method was used by ²⁷ and ²⁸ on CO₂ capture process with organic solvents. Similarly, ²⁹ optimized molecular structure (organic solvent) and process operations on the Diels-Alder reaction by using an integrated design method. In this

work, an integrated approach, where IL molecular design together with separation process synthesis-design is solved simultaneously, is presented. All groups (i.e. cations, anion, and substituents) are considered for IL molecular generation together with the cost of IL regeneration step. The application of the integrated IL and process synthesis-design method is highlighted through two case studies involving the separation of azeotropic mixtures.

3.2.2 Methodology

3.2.2.1 Framework

A framework for integrated IL and process design has been developed, as highlighted in Figure 3.13. It has five main sections: a) Property model library (GC-based property models, UNIFAC-IL model); b) IL structure (IL-groups set, IL structural parameters, CAILD); c) Process and cost models; d) Integrated IL and process design (MINLP problem formulation and solution); e) Solution and validation (use an appropriate solver and validate the solution through process analysis or experiments (if available)).

The work-flow employed by the methodology is as follows: First, retrieve the necessary GC-based property (e.g. density, viscosity, surface tension) models, the regressed UNIFAC-IL model parameters, and the collected group sets (i.e. cations, anions, substituents) from the model library contained in the IL database for the design of IL. Second, formulate the CAILD problem. Third, add the UNIFAC-IL model equations, the GC-based property models, the process and cost models, to formulate the integrated IL and process design problem as a MINLP model. Fourth, solve the MINLP problem with an appropriate solver to obtain, for example, the identified IL, process operating conditions, equipment sizing parameters and associated costs. Fifth, verify the optimal solution through analysis and/or experiment.

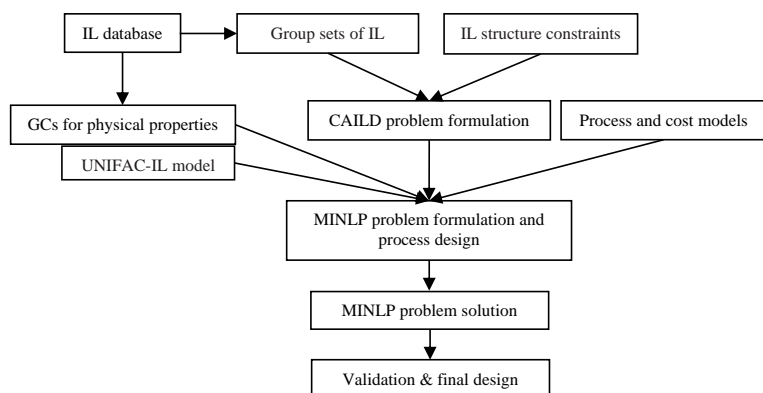


Figure 3.13 Framework of the integrated ionic liquid and process design

3.2.2.2 GC-based property models

As shown in Eq.3.41 and Eq.3.42, two types of property model, i.e. GC-based pure component property (θ_i) models and GC-based mixture property (θ_{mix}) models using the ideal mixing rule, are considered for the properties (e.g. density, heat capacity) involved in this method. All involved pure component property models are taken from Section 2.2.

$$\theta_i = \sum_{k=1}^N n_{k,i} \delta_k \quad 3.41$$

$$\theta_{mix} = \sum_{i=1}^M x_i \theta_i \quad 3.42$$

where N is the total number of groups representing the IL. δ_k represents the property contribution of group k for pure component property θ_i and $n_{k,i}$ denotes the number of group k in component i . M and x_i are the total number of components and the mole fraction of component i in mixture, respectively.

3.2.2.3 UNIFAC-IL model

The predictions of solubility and phase equilibria are essential for the design of ILs as solvents in separation processes. Due to the advantages of using UNIFAC as a thermodynamic model in the IL containing systems mentioned in Section 2.3, UNIFAC-IL model is used as the thermodynamic method in the integrated IL and process design.

3.2.2.4 Problem formulation

The integrated IL and process design problem is formulated as a mixed-integer non-linear programming (MINLP) optimization problem given by Eqs.3.43-3.48 In this work, the MINLP problem formulation from ²⁸ has been adopted.

$$\max/\min_{z,y} f(z,y) \quad 3.43$$

$$\text{s.t.} \quad g_p(z,y) = 0 \quad 3.44$$

$$g_t(z,y) \leq 0 \quad 3.45$$

$$g_m(y) \leq 0 \quad 3.46$$

$$z \in R^w \quad 3.47$$

$$y \in U^q \quad 3.48$$

where the m -dimensional vector z represents continuous variables involving mixture composition, physical properties, operating conditions, equipment sizes and process variables; the q -dimensional vector of integer and binary variables y denoting the molecular (IL) structure; f is the objective function, typically an economic performance metric (e.g. profit, capital investment), to be maximized or minimized subject to a set of constraints. g_p and g_t are sets of equality constraints and inequality constraints representing the process model and the thermodynamic model, respectively. Molecular (IL) structure feasibility and valency rules are represented by constraints g_m .

The design of ILs requires a systematic combination of various functional cations, anions and substituents based on certain structure constraints to generate feasible ILs of desired properties. A detailed set of constraints, as shown in Eqs.3.7–3.13 (see Section 3.1), is employed to ensure the feasibility and complexity of designed ILs.⁴⁴

3.2.3 Process and cost models

3.2.3.1 Process models

Although it is an energy intensive process, the separation of azeotropic mixtures is widely found in the chemical and petrochemical industries. In downstream separations of pharmaceuticals and in biochemical processes, azeotropes are also encountered and increase the difficulties in these industrial sectors^{137, 138}. Extractive distillation is an attractive technique for separating azeotropic mixtures since the selected entrainer can break the azeotrope by interacting with the components¹³⁹. The selection of the entrainer is a common concern in extractive distillation. Unlike VOCs that can escape into the atmosphere because of their high volatility, ILs possess attractive features, such as almost negligible vapor pressure and high thermal and chemical stability. IL based extractive distillation is a potential alternative to the extractive distillation using a volatile organic solvent as an entrainer^{12, 18, 140}.

To evaluate the potential of using ILs as non-volatile entrainers for the separation of the azeotropic mixtures by extractive distillation, a widely used process for extractive distillation using ILs as entrainers is employed, as shown in Figure 3.14. There the distillation column is used to separate the light key component, 1, from the heavy key component, 2, and the entrainer (IL); subsequently the IL is regenerated by combining a flash drum and an air-operated, atmospheric stripper.

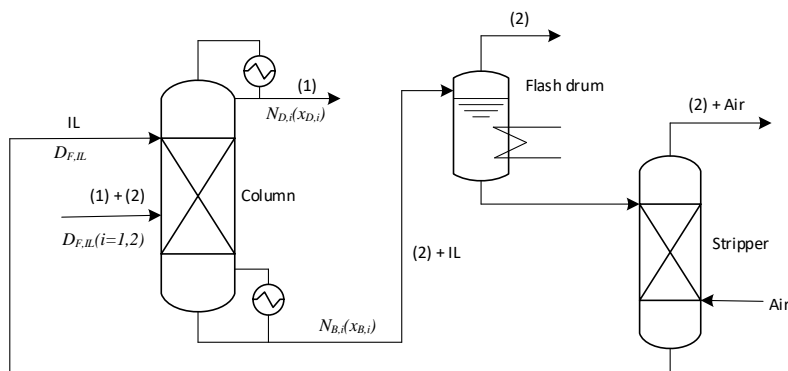


Figure 3.14 Ionic liquid-based extractive distillation process

Due to the large discrete IL molecular design space and the complex non-linear structure of the process design problem, shortcut models of processing units including a distillation column,²⁹ flash drum and stripper²⁷ are introduced.

Distillation column

A shortcut model of distillation column expressed as ideal vapor, equilibrium stages, and constant relative volatilities throughout the column is considered. The pressure at the top and bottom of the column is set to 1 bar and 1.2 bar, respectively.

The molar flowrates ($D_{F,i}$, $N_{D,i}$, $N_{B,i}$) and compositions ($x_{D,i}$, $x_{B,i}$) of the distillate and bottom streams for component i are expressed as

$$N_{D,i} = D_{F,i} \cdot \vartheta_i \quad 3.49$$

$$N_{B,i} = D_{F,i} - N_{D,i} \quad 3.50$$

$$x_{D,i} = \frac{N_{D,i}}{\sum_{i \in COM} N_{D,i}} \quad 3.51$$

$$x_{B,i} = \frac{N_{B,i}}{\sum_{i \in COM} N_{B,i}} \quad 3.52$$

where ϑ_i represents the recovery of the key component i in the distillate. COM is the set of all component i involved in the specified separation process. Due to no IL assumed to be present in the vapor phase ($N_{D,IL} = 0$) and the IL is fed at the top of the column, the molar flowrate of IL throughout the column is equal to the feed of IL ($N_{F,IL}$).

For the same reason of the negligible vapor pressure exhibited by ILs, only light key component (component 1) and heavy key component (component 2) are assumed to be present in the vapor phase, and then the VLE can be expressed as

$$P = x_1 \gamma_1 P_1^{sat} + x_2 \gamma_2 P_2^{sat} \quad 3.53$$

$$P y_i = x_i \gamma_i P_i^{sat} \quad i = 1, 2 \quad 3.54$$

where P_1^{sat} and P_2^{sat} , respectively, represent the saturated pressure of component 1 and 2. y_i are the vapor compositions for component i ($i = 1, 2$).

The Antoine equation is used to predict the saturated pressure, as shown in Eq.3.55

$$\ln P_i^{sat} = A_i - \frac{B_i}{T + C_i} \quad i = 1, 2 \quad 3.55$$

Relative volatilities at the top ($\alpha_{1,2}^D$) and bottom ($\alpha_{1,2}^B$) of the column are represented as

$$\alpha_{1,2}^D = \frac{\gamma_1^D P_1^{sat,D}}{\gamma_2^D P_2^{sat,D}} \quad 3.56$$

$$\alpha_{1,2}^B = \frac{\gamma_1^B P_1^{sat,B}}{\gamma_2^B P_2^{sat,B}} \quad 3.57$$

where γ_1^D, γ_2^D are the activity coefficient of component 1 and component 2 at the top of the column while γ_1^B, γ_2^B are the activity coefficient of component 1 and component 2 at the bottom of the column, respectively. Similarly, $P_1^{sat,D}, P_2^{sat,D}$ are the saturated pressure of component 1 and component 2 at the top of the column while $P_1^{sat,B}, P_2^{sat,B}$ are the saturated pressure of component 1 and component 2 at the bottom of the column, respectively. Since the IL is fed at the top of the column and therefore the relative volatility calculation at the top, i.e. $\alpha_{1,2}^D$, in Eq.3.56 also includes the IL.

The average relative volatility of the component 1 and component 2 throughout the column is defined as

$$\alpha_{1,2} = \sqrt{\alpha_{1,2}^D \cdot \alpha_{1,2}^B} \quad 3.58$$

In order to estimate the column size (N_t) and reflux ratio (R), the Westerberg method ²⁷ is employed in this work and the value of arbitrary weights φ_N and φ_R are set as 0.8

$$N_{lk} = 12.3 / \left((\alpha_{1,2} - 1)^{2/3} \cdot (1 - \vartheta_1)^{1/6} \right) \quad 3.59$$

$$N_{hk} = 12.3 / \left((\alpha_{1,2} - 1)^{2/3} \cdot \vartheta_2^{1/6} \right) \quad 3.60$$

$$R_{lk} = 1.38 / \left((\alpha_{1,2} - 1)^{0.9} \cdot (1 - \vartheta_1)^{0.1} \right) \quad 3.61$$

$$R_{hk} = 1.38 / \left((\alpha_{1,2} - 1)^{0.9} \cdot \vartheta_2^{0.1} \right) \quad 3.62$$

$$N_t = \varphi_N \max\{N_{lk}, N_{hk}\} + (1 - \varphi_N) \min\{N_{lk}, N_{hk}\} \quad 3.63$$

$$R = \varphi_R \max\{R_{lk}, R_{hk}\} + (1 - \varphi_R) \min\{R_{lk}, R_{hk}\} \quad 3.64$$

In Eqs.3.59-3.64, indices lk, hk represent the key component with low volatility and high volatility, respectively. For the ternary system containing IL, compound 1 is lk , compound 2 is hk and compound 3 is the IL. In this design method, the arbitrary weights were introduced to describe the non-ideality of the distillation.

Due to the extremely low vapor pressure exhibited by ILs as aforementioned, the saturation pressure for the ILs was assumed to be zero. As a result, no IL was assumed to be present in the vapor phase. Therefore, the enthalpy of vaporization of the stream in the condenser and reboiler are calculated as molar weight sum of the enthalpies of vaporization of compound 1 and 2

$$\Delta H_{vap}^B = x_{B,i} \sum_{i=1,2} \Delta H_{vap}^{B,i} \quad 3.65$$

$$\Delta H_{vap}^D = x_{D,i} \sum_{i=1,2} \Delta H_{vap}^{D,i} \quad 3.66$$

where the temperature dependence of the enthalpy of vaporization can be obtained by Eq.3.67 proposed by Poling et al.¹⁴¹

$$\Delta H_{vap}^i = \Delta H_{vap,298.15}^i \left(\frac{1-T/T_c^i}{1-298.15/T_c^i} \right)^{0.375} \quad i = 1, 2 \quad 3.67$$

As a result, the heat duties of the condenser and the reboiler is determined

$$Q_{reb} = \Delta H_{vap}^B (R + 1) \sum_{i=1,2} N_{D,i} \quad 3.68$$

$$Q_{cond} = \Delta H_{vap}^D (R + 1) \sum_{i=1,2} N_{D,i} \quad 3.69$$

Flash drum¹⁴²

The size of the flash drum can be determined by

$$V_{vessel} = 2F_{liquid}\epsilon V_{liquid} \quad 3.70$$

Where, F_{liquid} is the liquid molar flowrate (mol.s^{-1}) and V_{liquid} is the molar volume of liquid (m^3) and a residence time ϵ of 300 (s) is considered.

Stripper

The stripper is represented by a shortcut model containing several assumptions such as complete mixing, thermodynamic equilibrium and constant tray efficiency throughout the column.

The number of theoretical stages of the stripper for a given separation can be estimated as follows¹⁴³

$$N_e = \left((S/(S-1)) \ln(1-1/S) x_{IN,2}/x_{OUT,2} + 1/S \right) \quad 3.71$$

Where, $S = mG/L$ (G : molar flowrate of gas; L : molar flowrate of liquid) is the stripping factor, $x_{IN,2}$ = inlet concentration of compound 2, $x_{OUT,2}$ = outlet concentration of compound 2; $m = \gamma P^{sat}/P$ is the phase equilibrium constant.

An overall tray efficiency factor E_0 defined as Eq.48 is used to express the tray efficiency throughout the column

$$E_0 = N_e/N_a \quad 3.72$$

N_a is the actual number of trays, based on which the tray stack height h and the column height H can be determined

$$h = N_a TS \quad 3.73$$

$$H = 1.15 N_a TS \quad 3.74$$

Where, the tray spacing TS is set to 0.6096 m and the overall tray efficiency E_0 is assumed to be 0.2.

The column diameter of the stripper can be calculated as follows

$$D = 2 \sqrt{\frac{A_t}{\pi}} \quad 3.75$$

$$A_t = 1.2A_n \quad 3.76$$

$$A_n = q_V / U_n \quad 3.77$$

$$U_n = 0.8U_{n,flood} \quad 3.78$$

Where, A_t and A_n represent the total cross section and the net area of the column (m^2), respectively. q_V is the volume flowrate of air ($\text{m}^3 \cdot \text{s}^{-1}$) fed at the bottom of the column, and the $U_{n,flood}$ is obtained using Eq.3.79 proposed by Perry et al.¹⁴⁴

$$U_{n,flood} = C_{sb,flood} \cdot \left(\frac{\sigma_L}{20}\right)^{0.2} \cdot \sqrt{\frac{\rho_L - \rho_V}{\rho_V}} \quad 3.79$$

In Eq.3.79, σ_L is the liquid surface tension (mNm^{-1}) that can be calculated by Eq.2.7; ρ_L , ρ_V are the densities of liquid and gas ($\text{kg} \cdot \text{m}^{-3}$). $C_{sb,flood}$ is obtained from a correlation established by¹⁴⁵, and is expressed as a function of the tray spacing TS (inches) and a ratio of liquid to vapor kinetic energy through F_{LV}

$$C_{sb,flood} = 0.0105 + 8.127 \times 10^{-4} (25.4TS)^{0.755} e^{(-1.463F_{LV}^{0.842})} \quad 3.80$$

$$F_{LV} = \sqrt{\frac{\rho_L q_L}{\rho_V q_V}} \quad 3.81$$

In Eq.3.81, q_L represents the volumetric liquid flowrate ($\text{m}^3 \cdot \text{s}^{-1}$). It can be calculated based on the information of liquid molar flowrate, density and molar weight.

3.2.3.2 Cost models

To evaluate the economic performance of the IL-based extractive distillation process, the annual cost of processing units including distillation column (AC_{dis}), flash drum (AC_{drum}), and stripper ($AC_{stripper}$) needs be calculated. Cost models used in²⁹ and²⁷ are adopted in this work. The total annual cost (TAC) of the separation process is applied as our performance objective in this integrated design method. In order to obtain a practical and applicable process design, the boundaries of some variables are introduced. For example, the boundary of the solvent flowrate ($D_{F,IL}$) is intended to be economically considered and an upper bound of the operating temperature in the flash drum (T_{drum}) is introduced to avoid decomposition of the IL. Similarly, considering the processing operations, reasonable constraints on some properties of IL (e.g. T_m , η) are included as well. The units of cost, utility and temperature are US \$/year, J and K, respectively, in the following calculation.

The capital investment of the distillation column (CI_{col}) contributed by the cost of trays and the cost of the column vessel

$$CI_{col} = \left((N_t / 0.8) \times 500 + ((N_t / 0.8 - 1) \times 0.6 + 6) \times 2500 \right) / 3 \quad 3.82$$

The heat transfer areas of the heat exchanger (S_{heater}), condenser (S_{cond}) and reboiler (S_{reb}) can be calculated by

$$S_{heater} = Q_H / \left(\frac{T_F - T_0}{\ln((423 - T_0)/(423 - T_F))} \times 1420 \right) \quad 3.83$$

$$S_{reb} = Q_{reb} / ((493 - T_{bub}) \times 1420) \quad 3.84$$

$$S_{cond} = Q_{cond} / (567.8 \times 20 / \ln((T_{dew} - 300) / (T_{dew} - 320))) \quad 3.85$$

where T_{bub} and T_{dew} are the bubble and dew temperatures at reboiler and condenser.

The capital cost of heat exchange units (CI_u) can be calculated by their corresponding base cost (BC_u), where u represents heat exchanger, reboiler and condenser.

$$BC_u = 300 \times (S_u / 0.51)^{0.024} \quad 3.86$$

$$CI_u = BC_u \times 3.12 \times (1.83 + 1.35 - 1) / 3 \quad 3.87$$

$$CI_{dis} = CI_{col} + \sum_u CI_u \quad 3.88$$

The utility cost of the heat exchanger (UC_{heater}), condenser (UC_{cond}), reboiler (UC_{reb}) and distillation column (UC_{dis}) are given by

$$UC_{cond} = 330 \times 24 \times 60 \times 60 \times Q_{cond} \cdot \tau_{CW} / (75.33 \times 20) \quad 3.89$$

$$UC_{heater} = 330 \times 24 \times 60 \times 60 \times Q_H \cdot \tau_{HS} / 38012.4 \quad 3.90$$

$$UC_{reb} = 330 \times 24 \times 60 \times 60 \times Q_{cond} \cdot \tau_{HS} / 33303.6 \quad 3.91$$

$$UC_{dis} = UC_{cond} + UC_{heater} + UC_{reb} \quad 3.92$$

$$AC_{dis} = CI_{dis} + UC_{dis} \quad 3.93$$

where the price of hot steam (τ_{HS}) and the price of cooling water (τ_{CW}) are set to 0.00012 (US \$/mol) and 2.47E-7 (US \$/mol), respectively.

The purchase cost of the flash drum, CI_{drum} is a function of the volume of the flash drum V_{drum} (m³) and the pressure factor, F_p determined by the pressure of flash drum, P_{drum} (MPa); The utility cost of the flash drum (UC_{drum}) depends on its heat duty (Q_{drum}) and τ_{HS}

$$AC_{drum} = CI_{drum} + UC_{drum} \quad 3.94$$

$$CI_{drum} = 4832.42 F_p V_{drum}^{0.6287} \quad 3.95$$

$$F_p = 0.057375 P_{drum}^2 + 0.05805 P_{drum} + 1.0136 \quad 3.96$$

$$UC_{drum} = 330 \times 24 \times 60 \times 60 \times Q_{drum} \cdot \tau_{HS} / 33303.6 \quad 3.97$$

The annual cost of stripper is:

$$AC_{stripper} = CI_{shell} + CI_{trays} \quad 3.98$$

The cost of the shell (CI_{shell}) is calculated as:

$$CI_{shell} = 3185 F_p D^{1.066} H^{0.82} \quad 3.99$$

where D is the column diameter in m, H is the column height in m, and F_p is the pressure factor; the cost of the trays (CI_{trays}) is a function of the tray stack height h (m), the diameter D (m), and factor F_c (is set to 1 in this work):

$$CI_{trays} = 323.3F_pD^{1.55}hF_c \quad 3.100$$

3.2.4 Application examples

The objective of this work is to simultaneously identify optimal IL and the corresponding separation process design corresponding to the best economic performance, subjecting to a list of constraints involving molecular structure, IL properties, process model and operating conditions.

Problem details

The integrated IL and process design involving extractive distillation schemes can be formulated as an MINLP optimization problem summarized in Table 3.13:

Table 3.13 Integrated design (MINLP) problem formulation

Minimize:	$TAC = AC_{dis} + AC_{drum} + AC_{stripper}$
Variables:	Binary: vectors c_i ($i \in C$), a_j ($j \in A$), x_l ($1 \leq l \leq N$) Integer: vectors n_{kl} , v_{kl} ($1 \leq l \leq N$; $k \in S$), v_i ($i \in C$) Continuous: temperature, flowrate, composition, equipment sizes....
s.t.	Variable boundaries: $0 < D_{F,IL} < 100$ (kmol/h), $T_{drum} < 500$ (K) <hr/> IL structure constraints: Chemical feasibility: Eqs.3.7–3.11 Chemical complexity: Eqs.3.12–3.13 <hr/> IL property constraints: Physical property estimation: Eqs.2.1–2.8, 11, 3.41-3.42 Property boundary: Eqs.3.15-3.16 <hr/> Thermodynamic model: UNIFAC-IL: Eqs.2.21-2.32 <hr/> Process models: Distillation column: Eqs.3.49–3.69 Flash Drum: Eq.3.70 Stripper: Eqs.3.71-3.81 <hr/> Economic models: AC_{dis} : Eqs.3.82–3.93 AC_{drum} : Eqs.3.94–3.97 $AC_{stripper}$: Eqs.3.98–3.100

In this work, case studies including ethanol-water separation (Case 1) and acetone-methanol separation (Case 2) are performed to demonstrate the proposed methodology. For both cases, deterministic global optimization solver, LINDOGLOBAL, is used to solve the formulated MINLP problems in the modelling system GAMS 24.4.6 on an Intel(R) Xeon(R) E5-1620 3.70 GHz PC running Windows 10 system. The same optimization solution was observed for each case by using many initializations. Additionally, different well-known MINLP solvers (e.g. BARON, CONOPT) have been tried to solve the formulated problems but without success due to convergence problems. Table 3.14 gives information on the number of variables and constraints of the formulated MINLP problems and Table 3.15 provides the model statistics from GAMS solution for Case 1 and Case 2. Detailed results of the case studies are given in the following sections.

Table 3.14 Information of the formulated MINLP problems in terms of size of each vector of variables and constraints

	Size of the vectors						
	z	y		$g_p(z, g_t(z, y))$		$g_m(y)$	Nonlinear constraints
		Binary	Integer				
Case 1	568	15	62	137	404	10	472
Case 2	569	13	62	138	404	10	472

Table 3.15: Model statistics from GAMS solution for Case 1 and Case 2

	Number of continuous variables	Number of binary variables	Number of equations	Number of constraints	Number of iterations	CPU time (s)
Case 1	568	15	551	551	938401	349
Case 2	569	13	552	552	17811	64

Property model parameters

For these two case studies, group volume (R_k) and surface area (Q_k) parameters, and interaction parameters (a_{nm} , a_{mn}) between IL groups and conventional groups are taken from the original UNIFAC model.^{79, 91} In their work, the R_k and Q_k are estimated based on the rules of Bondi¹³⁰ while the a_{nm} and a_{mn} are obtained based on a wide range of available experimental data on activity coefficients of various solutes at infinite dilution in ILs by minimizing the objective function (Eq.3.101)

$$OF = \sum_i^N \left| \frac{\gamma_i^{\infty, exp} - \gamma_i^{\infty, calc}}{\gamma_i^{\infty, exp}} \right| \quad 3.101$$

where $\gamma_i^{\infty, exp}$ and $\gamma_i^{\infty, calc}$ represent the experimental and calculated infinite dilution activity coefficients of the solutes (i) in ILs, respectively. N is the total number of infinite dilution activity coefficients (γ^∞) data points. Meanwhile, comparisons between the UNIFAC-IL predictions and experimental ternary VLE data of several binary azeotropes (ethanol–water,

acetone–methanol, ethyl acetate–ethanol, 1-propanol–water and 2-propanol–water) with some ILs have been presented to validate the performance of the UNIFAC-IL model.⁷⁹

In order to compare economic performance of the whole extractive distillation process using the optimal IL identified in this work and previous works, fixed process parameters including column operating pressure, composition of feed and distillate used by⁷⁹ were applied. Well-studied groups containing 2 substituents, 2 cations and 7 anions were selected as molecular building blocks for the IL design, as shown in Table 3.16.

Table 3.16 Molecular building blocks selected for IL design

Type	Groups	Type	Groups
Substituents	CH ₃	Anions	[Tf ₂ N] ⁻
	CH ₂		[BF ₄] ⁻
Cation cores	[Im] ⁺		[PF ₆] ⁻
	[Py] ⁺		[CF ₃ SO ₃] ⁻
			[CF ₃ COO] ^{-*}
			[DMP] ⁻
			[SCN] ^{-*}

*NB: Groups only used in the case study of ethanol-water separation

3.2.4.1 Ethanol –water separation

The task of the ethanol-water separation process can be expressed as a 200 kmol.h⁻¹ liquid mixture consisting of 70 mol% ethanol and 30 mol% water, to be separated by extractive distillation that the ethanol composition of distillate (140 kmol.h⁻¹) amounts to 99.8 mol%. Fixed process parameters (i.e., column operating pressure, flowrate and composition of feed and distillate....) are given in Table 3.17.

Table 3.17 Fixed parameters of the ethanol-water separation process

Fixed parameters	Value
Distillation column	
Pressure at the top	1 atm
Pressure at the bottom	1.2 atm
Feed rate and composition	200 kmol/h, (0.7 C ₂ H ₅ OH, 0.3 H ₂ O)
Distillate flowrate	140 kmol/h
Molar composition of distillate	0.998 C ₂ H ₅ OH
Flash drum	
Operating pressure	0.1 atm
Stripper	
Air temperature	298.15 K
Molar composition of IL at the bottom	0.999

For the case study of ethanol-water separation process, free variables such as: (1) IL structure, (2) IL flowrate, (3) reflux ratio, (4) size of the processing units (e.g. number of column trays, volume of flash drum), (5) temperature of the flash drum, and (6) air flow in the stripping column should be optimized to achieve the best economic performance of the overall extractive distillation process. A set of constraints of these variables are introduced to make sure the designed ILs and the process operations are feasible for industrial applications. Optimization results, including the best IL molecular structure and the corresponding optimal distillation column design variables are simultaneously obtained by solving the formulated MINLP problem (given in Table 3.18). Meanwhile, two nonlinear programming (NLP) problems of reference design are also formulated and solved as comparisons.

In this case, 1-methylpyridinium hexafluorophosphate ($[\text{mPy}]^+[\text{PF}_6]^-$) is found to be the best IL as a solvent with an economically attractive TAC of 719 733 US \$/year. For the same ethanol-water separation task, Seiler et al.¹² used experimentally selected IL, 1-ethyl-3-methylimidazolium tetrafluoroborate ($[\text{emIm}]^+[\text{BF}_4]^-$) as an entrainer and ⁷⁹ determined 1, 3-dimethylimidazolium dimethylphosphate ($[\text{mmIm}]^+[\text{DMP}]^-$) as an entrainer based on the CAMD method using the Hildebrand solubility parameter of azeotropic mixtures as a target. For comparing the economic performance of this ethanol-water separation process using ILs identified through different methods, integrated these two fixed ILs and the same process models used in this work, optimization results (see Table 3.18) give TAC values of 916 144 US\$, and 1 073 665 US\$, respectively, also achieved by solving their corresponding NLP problems.

Table 3.18 Optimization results of the proposed integrated design and the reference design problems for the ethanol-water separation process

Optimization Variable	This work	Solvent1 ¹²	Solvent2 ⁷⁹
Ionic liquid			
Molecule	$[\text{mPy}]^+[\text{PF}_6]^-$	$[\text{emIm}]^+[\text{BF}_4]^-$	$[\text{mmIm}]^+[\text{DMP}]^-$
Cation	$[\text{Py}]^+$	$[\text{Im}]^+$	$[\text{Im}]^+$
Anion	$[\text{PF}_6]^-$	$[\text{BF}_4]^-$	$[\text{DMP}]^-$
Valence of the cation base	1	2	2
Number of CH ₃ in side 1	1	1	1
Number of CH ₃ in side 3	0	1	1
Number of CH ₂ in side 3	0	1	0
Flowrate (kmol/h)	67.0	73.1	65.4
Distillation column			
Number of trays N_t	9	13	14
Reflux ratio R	0.442	0.714	0.789
AC_{column} (US \$/year)	431 008	525 801	550 459
Flash drum			

T_{drum} (K)	444.8	446.0	471.3
AC_{drum} (US \$/year)	142 682	150 951	216 058
Stripper			
Number of stages N_a	17	18	22
Air flowrate q_V (kmol/h)	463.6	521.0	559.5
$AC_{stripper}$ (US \$/year)	146 043	239 392	307 158
TAC (US \$/year)	719 733	916 144	1 073 665

As shown in Table 3.18, AC_{drum} contributes major cost to TAC when using all three ILs as solvents, indicating that the economic performance of this separation process mainly depends on the relative volatility of the components to be separated, which indirectly reflects the importance of their activity coefficients in the IL containing system. In this case, all contributions (i.e. AC_{drum} , AC_{drum} , $AC_{stripper}$) of the TAC using $[mPy]^+ [PF_6]^-$ are the lowest compared to the other two referenced ILs. Despite the fact that both the experimentally selected $[emIm]^+ [BF_4]^-$ and the CAMD-based designed $[mmIm]^+ [DMP]^-$ have better performance of the minimum concentration to break azeotrope (ethanol-water), nevertheless, $[mPy]^+ [PF_6]^-$ identified in this work, is considered the best one with the highest economic performance (TAC). This result highlights the necessity of investigating trade-offs among different solvent properties to obtain the best overall process performance. It also indicates that the proposed integrated IL and process design method allow the identification of the best IL and the corresponding optimal process conditions which would lead to a considerable decrease in TAC. The structures of ILs involved in this case study are given in Figure 3.15.

Table 3.19 Fixed parameters of the acetone-methanol separation process

Fixed parameters	Value
Distillation column	
Pressure at the top	1 atm
Pressure at the bottom	1.2 atm
Feed rate and composition	200 kmol/h, (0.5 (CH ₃) ₂ CO, 0.5 CH ₃ OH)
Distillate flowrate	100 kmol/h
Molar composition of distillate	0.995 (CH ₃) ₂ CO
Flash drum	
Operating pressure	0.1 atm
Stripper	
Air temperature	298.15 K
Molar composition of IL at the bottom	0.999

3.2.4.2 Acetone-methanol separation

The separation task of acetone-water can be represented as follows: 200 kmol.h⁻¹ liquid mixture consisting of 50 mol% acetone and 50 mol% methanol, to be separated by extractive distillation, such that the acetone purity of the distillate (100 kmol.h⁻¹) amounts to 99.5 mol%. Fixed process

parameters (i.e., column operating pressure, flowrate and composition of feed and distillate....) are given in Table 3.19.

As well as the separation of ethanol-water, to determine the minimum TAC of the overall extractive distillation process, the following variables: (1) IL structure, (2) IL flowrate, (3) reflux ratio, (4) size of the processing units, (5) temperature of the flash drum, and (6) air flow in the stripping column should be optimized. The best IL molecular structure and the optimal flowsheet configurations are simultaneously identified by solving the formulated MINLP problem. A selected optimisation results of the integrated IL and process design, and two reference design problems for the acetone-methanol separation are given in Table 8.

In this case, 1, 2, 3-trimethylimidazolium dimethylphosphate ($[C_{1mm}Im]^+[DMP]^-$) is found to be the best IL as a solvent with a minimum TAC of 775 216 US \$/year. Two solvents, 3-methyl-1-octylpyridinium trifluoromethanesulfonate ($[omPy]^+[CF_3SO_3]^-$) and 1-ethyl-3-methylimidazolium trifluoromethanesulfonate ($[emIm]^+[CF_3SO_3]^-$) investigated by Roughton et al.⁷⁹ are considered for comparison. In their work, $[omPy]^+[CF_3SO_3]^-$ was experimentally selected while $[emIm]^+[CF_3SO_3]^-$ was identified based on the CAMD method using the Hildebrand solubility parameter of the azeotropic mixture, as a target. For using these two fixed ILs and the same process and economic models as integrated design cases, optimization results are also obtained by solving their corresponding NLP problems in this work. As shown in Table 8, the total costs of the optimization process using these two ILs as solvents are 959 870 US \$/year and 1 019 379 US \$/year, respectively.

Table 3.20 Optimization results of the proposed integrated design and the reference design problems for the acetone-methanol separation process

Optimization Variable	This work	Solvent1 ⁷⁹	Solvent2 ⁷⁹
Ionic liquid			
Molecule	$[C_{1mm}Im]^+[DMP]^-$	$[emIm]^+[CF_3SO_3]^-$	$[omPy]^+[CF_3SO_3]^-$
Cation	$[Im]^+$	$[Im]^+$	$[Py]^+$
Anion	$[DMP]^-$	$[CF_3SO_3]^-$	$[CF_3SO_3]^-$
Valence of the cation base	3	2	2
Number of CH ₃ in side 1	1	1	1
Number of CH ₃ in side 2	1	0	0
Number of CH ₃ in side 3	1	1	1
Number of CH ₂ in side 3	0	1	7
Flowrate (kmol/h)	56.1	38.1	56.3
Distillation column			
Number of trays N_t	20	32	27
Reflux ratio R	1.309	2.474	1.999
AC_{column} (US \$/year)	592 620	884 003	768 664

Flash drum			
T_{drum} (K)	366.8	364.7	369.0
AC_{drum} (US \$/year)	67 670	64 590	84 154
Stripper			
Number of stages N_a	22	21	22
Air flowrate q_V (kmol/h)	366.8	177.6	298.6
$AC_{stripper}$ (US \$/year)	114 927	70 786	107 052
TAC (US \$/year)	775 216	1 019 379	959 870

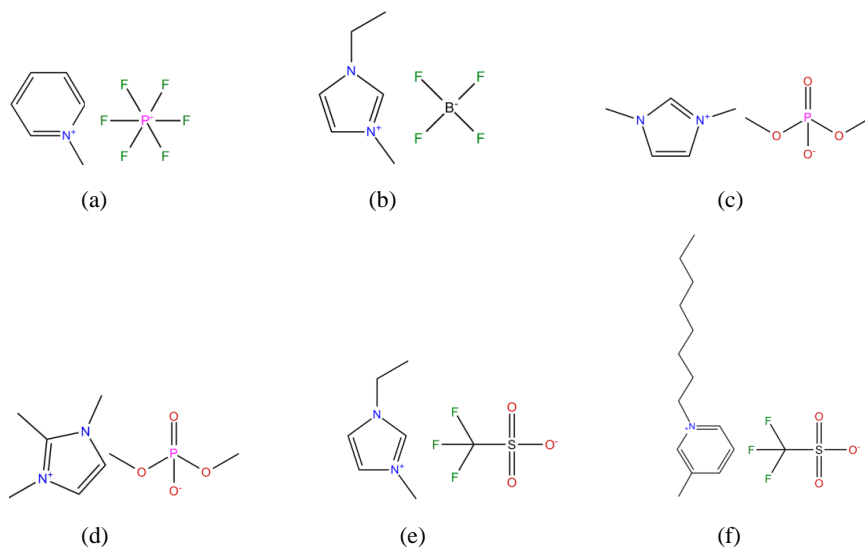


Figure 3.15 The structure of six ionic liquids involved in case studies:

(a) $[mPy]^+[PF_6]^-$, (b) $[emIm]^+[BF_4]^-$, (c) $[mmIm]^+[DMP]^-$, (d) $[C_1mmIm]^+[DMP]^-$
(e): $[emIm]^+[CF_3SO_3]^-$, (f) $[omPy]^+[CF_3SO_3]^-$

Same as the separation of ethanol-water mixture, AC_{drum} also provides major contribution to the TAC in this case (see Table 3.20). The results reinforce the effect of the relative volatility of components to be separated on the economic performance of the separation process. Since the relative volatility of the components to be separated depends on their activity coefficients in the IL containing system, therefore, the thermodynamic property of IL plays the main role in the separation process. Unlike the first case, contributions of AC_{drum} and $AC_{stripper}$ using referenced IL, $[emIm]^+[CF_3SO_3]^-$, are the lowest among all three IL solvents in this case, this is mainly because of its lowest flowrate. However, compared to the two reference cases, the integrated design method proposed in the present work is capable of simultaneously identifying the optimal IL and the corresponding optimal process configurations which can significantly improve the overall economic performance (lower TAC). Although the separation process

using $[\text{C}_{1\text{mmIm}}]^+[\text{DMP}]^-$ as an entrainer has the best economic performance, both the CAMD-based determined $[\text{omPy}]^+[\text{CF}_3\text{SO}_3]^-$ and the experimentally selected $[\text{emIm}]^+[\text{CF}_3\text{SO}_3]^-$ can break this azeotrope at a lower concentration, especially the process using $[\text{emIm}]^+[\text{CF}_3\text{SO}_3]^-$ has the lowest AC_{drum} , AC_{stripper} and the flowrate of IL, which indicates the importance of investigating trade-offs among different IL properties for process design. The structures of ILs involved in this case study are also given in Figure 3.15.

3.2.5 Conclusions

A systematic method combining GC-based property models, UNIFAC-IL models, CAMD and process design, representing CAILD, to simultaneously determine the optimal IL as a separating agent and the corresponding optimal process design has been developed. In this method, all groups (i.e. cations, anion, substituents) contained in IL molecular are treated separately and the cost of IL regeneration is also included. Case studies involving separation of azeotropic mixtures such as ethanol-water and acetone-methanol have been presented to evaluate the performance of this integrated design method. A set of constraints on rules of combination and properties of ILs are introduced to ensure the designed ILs are chemically feasible. The IL molecular structure and the process variables are optimized simultaneously by the formulation and solution of MINLP problems using economic performance (TAC) as the objective function. Comparisons between the achieved economic performance of the whole extractive distillation process using optimal IL identified in this work and previous work(s) highlights the importance of investigating trade-offs among different properties of ILs to obtain the best overall process performance, and also verify the proposed integrated design method. The optimization results of the MINLP problems are further evaluated by detailed process analysis. We should note that the applicability and reliability of the calculation results would be improved if experimental validation is available.

Because of the limited group parameters for IL containing systems, only well-studied groups of ILs are considered as building blocks in this work. However, the developed methodology can easily be extended to other ILs, once their group parameters are available. We are currently extending the model library for IL properties as well as a wide range of IL-based separation processes.

3.3 IONIC LIQUID-BASED *IN-SITU* PRODUCT REMOVAL DESIGN

This chapter forms the basis of following unpublished work:

Chen, Y.; Garg, N.; Luo, H.; Kontogeorgis, G. M.; Woodley, J. M.: Ionic liquid-based in-situ product removal (ISPR) design for small molecule fermentation. (Biotechnology Progress). In preparation.

Abstract

Limitations of fermentation processes mostly related with product inhibition results in highly diluted product leading to difficult downstream separations. In the past few decades, in-situ product removal (ISPR) technology has been introduced as one possible tool for relieving the inhibition on cells. In these ISPR-integrated fermentation processes, selecting an appropriate separation method that is capable to remove inhibitory product from the fermentation broth is of great importance. In this regard, ionic liquid (IL)-based liquid-liquid extraction (LLE) that allows efficient bioproducts recovery from dilute aqueous solutions may bring the potential and are worth investigating. Nevertheless, it is still very challenging to apply this new separation technique in ISPR since the process performance of an IL-based ISPR varies drastically from one processing scheme to another, and from one IL solvent to another. Therefore, the processing scheme and the used IL solvent need to be carefully design and selected for achieving an industrially available IL-based ISPR process. In this work, a three-stage systematic design method that combines ISPR processing schemes selection, IL-based LLE systems design and process evaluation is proposed as a guidance for such purposes. This design method of IL-based in-situ product removal mainly focuses on the small molecule fermentation process. As a proof of the concept, results of acetone-butanol-ethanol (ABE) fermentation and its separation process by using this design method are presented.

3.3.1 Introduction

Many chemical transformation processes used in various industries have inherent drawbacks from a commercial and environmental point of view. Undesired reactions may result in poor product yields. High temperatures and/or high pressures needed to drive reactions lead to high utility consumption and increased energy costs in the downstream processing. Harsh and hazardous processes involving high temperatures, pressures, acidity, or alkalinity need high capital investment, specially designed equipment and control systems. Unwanted by-products may also prove difficult to separate or costly to dispose of. High chemicals and energy consumption as well as harmful by-products also pose negative impact on the environment. On the other hand, bioprocesses involving the use of living microorganisms (i.e. fermentation) for the production of chemical and biochemical products have received considerable attention. This

is due to their reactions that are often carried out under mild conditions, and particularly they have the option of using sustainable feedstocks. It is therefore they are regarded as potentially sustainable alternatives for conventional synthesis routes. However, limitations of bioprocesses mostly related with product inhibition results in low productivity and highly diluted product leading to difficult downstream separations.^{7, 8, 30} In all cases, improved reaction conditions¹⁴⁶ as well as rapid inhibitory product removal from the fermentation broth may bring potential to overcome these constraints.

In the past few decades, *in-situ* product removal (ISPR) that integrates the conversion step with the first product recovery step has been introduced as one possible tool for bioprocess intensification.^{7, 8, 30, 146-148} By far, various ISPR-integrated fermentation processes have been studied to produce a wide range of biochemical products.³⁰ In general, different forms of ISPR depending on the location (internally or externally) of the product removal (directly or indirectly) can be applied. Among all ISPR processing schemes, the internal product removal has lower equipment costs due to both reaction and product removal taking place in the same vessel, while the external product removal allows easier process control and reduces the contact time between the biocatalyst and the organic solvent. In addition, the direct product removal does not need physical barrier such as membrane, while the indirect product removal reduces the solvent standards such as biocompatibility and toxicity. More discussions on different ISPR schemes using IL solvents are provided in Section 3.3.2.1. Currently, ISPR technologies are being used for the recovery of industrial chemicals, pharmaceuticals, fuels and food ingredients such as propionic acid (PA). In ISPR, both product capacity and product removal rate of the separation method are critical because they directly and greatly affect the process operations and equipment costs. Therefore, the selection of an appropriate ISPR separation method is of great importance.⁷ To date, various separation methods (e.g. membrane methods, crystallization, chromatographic methods)^{4, 149-151} have been studied and applied according to the nature of the reactant and product to be removed. Organic solvents (e.g. hexane, toluene) are typically used for the recovery of small molecules from aqueous media because of their immiscibility with aqueous media¹⁵². However, most conventional organic solvents are volatile and toxic that may denature the enzymes and proteins to be recovered, and environmental impact is another industrial concern. Unlike most commonly used organic solvents, ionic liquids (ILs) are non-volatile and non-flammable, providing alternatives in chemical, biochemical and other industrial processes.¹¹ To date, ILs have been widely studied as solvents for separation processes involving gas separation (e.g. CO₂ capture, shale gas purification)¹⁵³⁻¹⁵⁵ and liquid-liquid separation (e.g. extraction, extractive distillation).^{45, 80, 156} Additionally, ILs have also been reported as enhanced extraction solvents that can improve the activity and stability of biomolecules, such as proteins and enzymes, in aqueous solutions.¹⁵⁷⁻¹⁶⁴ For example, Du et al.¹⁶⁵ used aqueous biphasic system (ABS) formed by 1-butyl-3-methylimidazolium chloride ([C₄mim][Cl]) and K₂HPO₄ to extract proteins and it was found that the proteins maintain their structural integrity and biological properties when concentrated in the IL-rich phase. Ventura et al.¹⁶⁶ reported that the activity of the commercial enzyme *Candida antarctica* lipase B (CaLB)

increases greatly by using aqueous solutions of 1-decyl-3-methylimidazolium chloride ([C₁₀mim][Cl]), at pH 7.0. More applications of aqueous solutions containing ILs for the extraction and separation of bioactive compounds have been summarized in a critical review completed by Ventura et al.¹⁴ In bioprocesses, IL-based separation method, especially its liquid-liquid extraction (LLE) techniques have been widely studied for the separation and/or purification of target bioproducts produced via fermentation or by biosynthetic routes.^{14, 167}

Since most bioreactions are carried out in dilute aqueous conditions and this typically leads to a water-rich feed to the downstream process. Therefore, hydrophobic water-immiscible ILs are initially preferred considering their applications may allow the combination of extraction, purification, and concentration in a single step. Meanwhile, the use of water-miscible ILs is presented as IL-based aqueous biphasic systems (ABS) by adding a salting-out agent to create a second liquid phase.¹⁶⁸ It is already well accepted that the toxicity of ILs mainly depends on their hydrophobicity, and therefore hydrophilic water-miscible ILs generally exhibit low toxicities. In addition, since ABS are mainly composed of water they are recognized as biocompatible, non-denaturing and benign media for cells, cell organelles and biologically active substances. Therefore, IL-based ABS recently have been in focus as novel extraction method for bioproduct recovery.^{168, 169}

One of the main advantages of using ILs as solvents is that their polarities and affinities can be tailored by a proper combination of cation/anion and substituents. This contributes to a better application of IL-based LLE approaches. So far, most of previous studies on bioproduct recovery by using IL-based LLE techniques have focused on the downstream separation process only, but few of them have considered the possibility of including IL-based LLE techniques and their applications in ISPR. It is therefore a three-stage systematic design method for such purposes is presented in this work. Generally, the processing operations of bioprocesses vary greatly from one bioproduct to another, the proposed design method of IL-based *in-situ* product removal mainly focuses on the small molecule fermentation process. This design method is demonstrated through its application on the acetone-butanol-ethanol (ABE) fermentation process, considering the IL systems with water and ABE compounds have been widely experimentally studied and the UNIFAC-IL model has also been extended to these systems.

3.3.2 Design Methodology

The proposed design method includes three design stages (Figure 3.16). First, a suitable ISPR processing scheme is selected according to the properties of the product and reactant. Afterwards, ILs are optimally design/screening due to their properties significantly affect the process performance. In this design stage, both experimental data-based screening method and CAILD are considered for its design and screening. Meanwhile, thermodynamic models such as COSMO-RS and UNIFAC-IL models are employed for the thermodynamic calculation of

the studied LLE systems. Finally, the identified IL-based ISPR scheme is validated in the design stage of process evaluation.

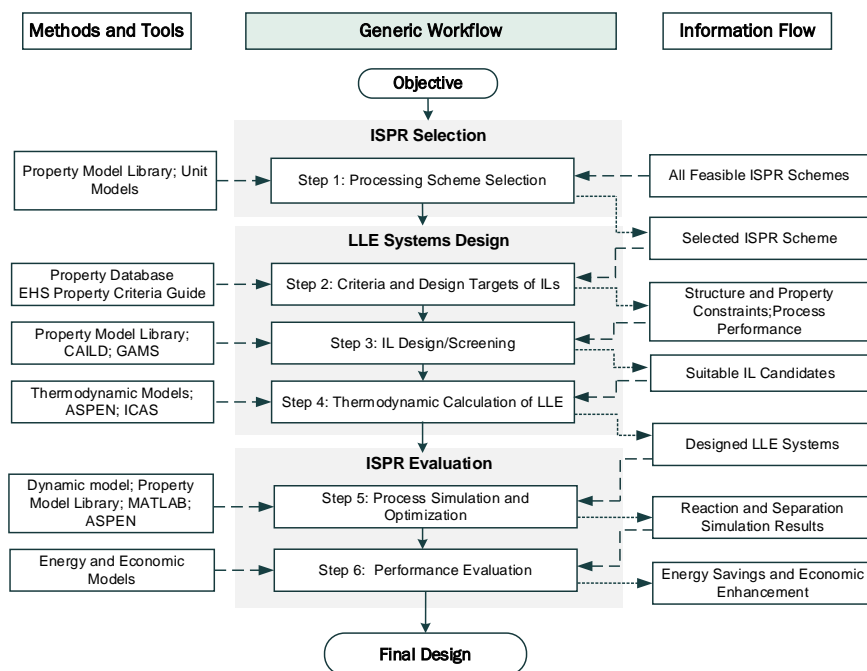
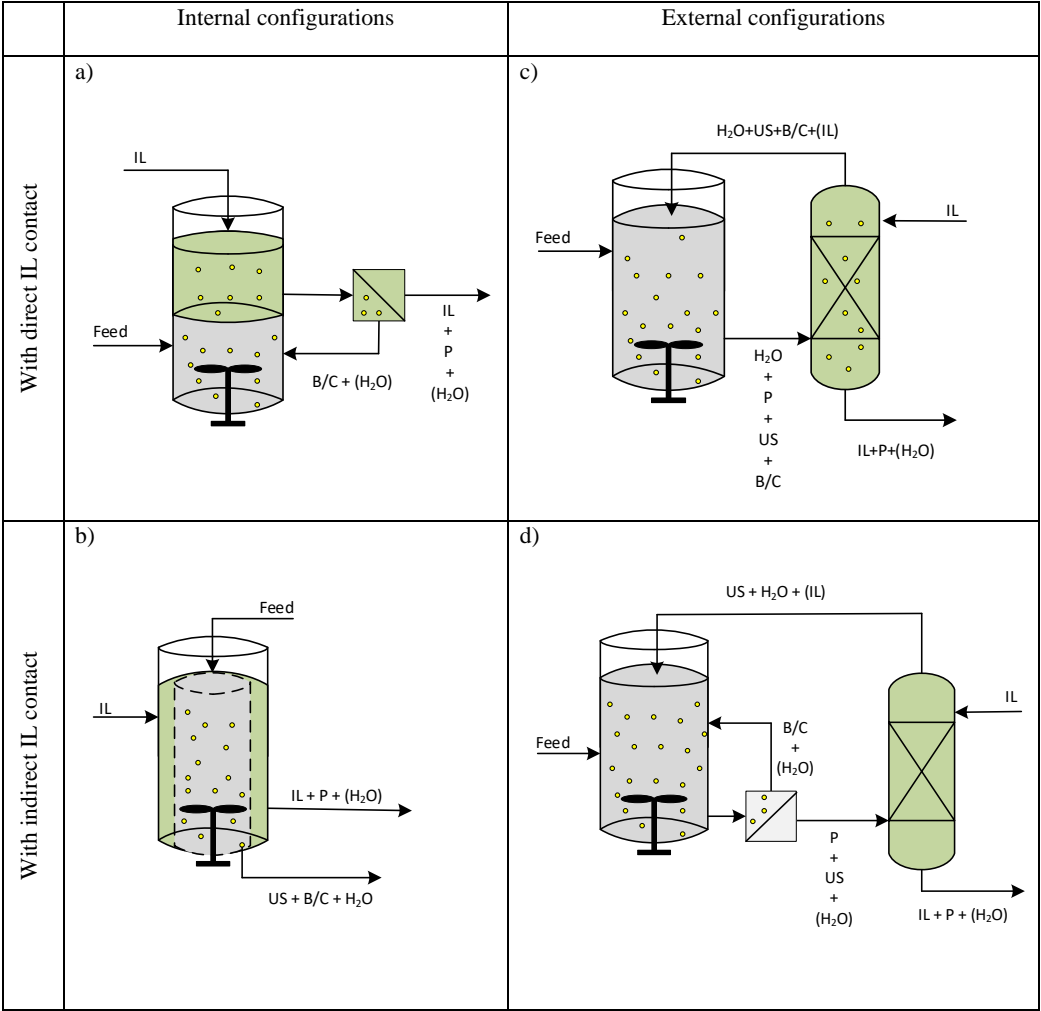


Figure 3.16 Design methodology of IL-based *in-situ* product removal for small molecule fermentation

3.3.2.1 ISPR Selection

Step 1. ISPR Schemes Selection. Similar to conventional organic solvents, ILs can also be classified as water-miscible (where IL-based ABS can be formed), and water-immiscible. Using either water-miscible or water-immiscible ILs as solvents, different forms of ISPR schemes depending on the location (internally or externally) of the product removal (directly or indirectly) can be considered (see Figure 3.17). Scheme-1, corresponds to the internal product removal with the direct IL contact, where both reaction and product removal are completed in the same vessel and therefore the number of processing units can be reduced. Scheme-2, corresponds to the external product removal with direct IL contact, where contact time between the solvent and the biocatalyst/cells is decreased as the product removal take place in the external separation unit. On the other hand, Scheme-3, corresponds to the internal product removal with indirect IL contact, where biocatalyst/cells are generally isolated from the solvent by physical barrier such as membrane.¹⁷⁰ Scheme-4, corresponds to external product removal with indirect IL contact, where the biocatalyst/cells are separated from product before feeding to downstream separation unit. In all these cases, two-liquid phase systems containing

ILs will improve the reaction yield/productivity as well as the bioproduct concentration fed to the downstream processing unit. Generally, ABS that mainly composed of water are more attractive in bioreaction systems because of their biocompatibility as media for cells, biologically active products and substances, and therefore has been widely studied for the purification and recovery of bioproducts.^{14, 168}



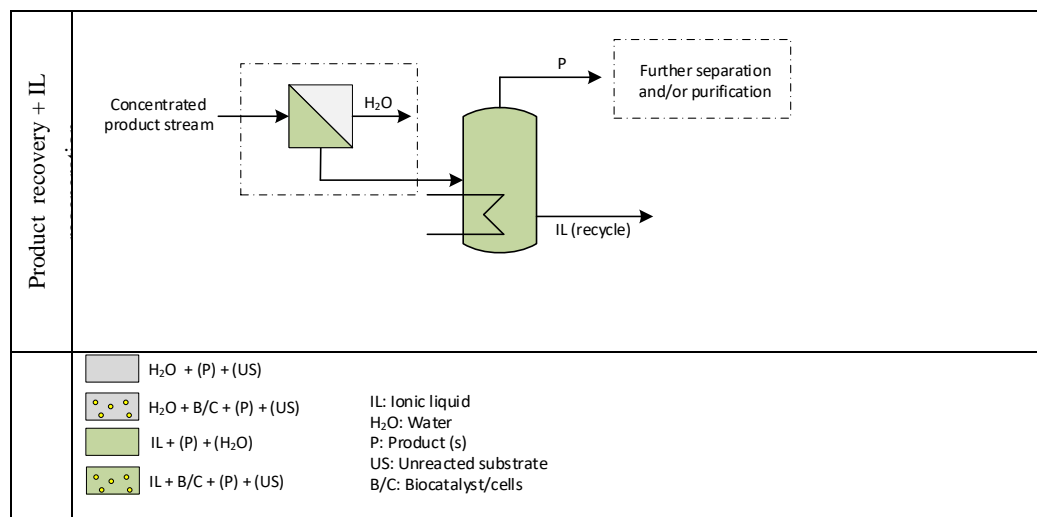


Figure 3.17 Conceptual design of IL-based *in-situ* product removal for microbe-derived small molecules

When water-immiscible ILs are used as solvents in the ISPR design, the concentrated product stream fed to the downstream separation unit(s) generally contains no water and therefore both product(s) recovery and IL regeneration can be completed by evaporation in a flash unit. On the other hand, in the ISPR schemes using water-miscible ILs as solvents, where the product is concentrated in IL-rich aqueous phase and therefore the water should be removed from the concentrated product stream followed by product recovery operation. For the water removal process, reverse osmosis (RO) using a partially permeable membrane to remove ions, molecules and larger particles from water can be considered as dehydration unit. In RO, an applied pressure is used to overcome osmotic pressure, a colligative property that is driven by chemical potential differences of the solvent, and a thermodynamic parameter. RO can remove many types of dissolved and suspended chemical species as well as biological ones (principally bacteria) from water, and is used in both industrial processes and the production of potable water. The result is that the solute is retained on the pressurized side of the membrane and the pure solvent is allowed to pass to the other side. To be "selective", this membrane should not allow large molecules or ions through the pores (holes) but water to pass freely.

For both internal and external ISPR schemes with direct solvent contact, the biocatalyst/cells are directly in contact with the IL (see Figure 3.17a and c). Conversely, in both internal and external ISPR schemes with indirect solvent contact, the biocatalyst/cells are prevented from the contact with IL (see Figure 3.17b and d). For this reason, the selection of IL for a two liquid-phase system with direct contact is more difficult compared to those indirect contact schemes. Also, it must not be toxic and deactivate the biocatalyst/cells. Additionally, in the internal configurations (Figure 3.17a and b), both reaction and product removal are carried out in the

same processing unit which can lower the investment cost, while in the external configurations, the contact time between the solvent and the biocatalyst/cells is reduced by introducing a separate loop containing an external unit.^{7, 170} Suitable ISPR scheme can be selected according to the properties of the product and reactant.

3.3.2.2 IL-based LLE systems design

Step 2. Criteria and Design Targets of ILs. Considering the numerous applicable ILs to industrial processes, it is necessary to narrow the list of potential ILs by evaluating their suitability in practical industry application. Therefore, a reasonable criteria of IL selection need to be considered at the design stage of IL-based LLE systems. In comparison to organic solvents, the selected ILs should fulfil the requirements of environmental sustainability, health and safety concerns. Although ILs typically present high thermal and chemical stability, systematic understanding of their toxicity and biodegradability is still limited; thus, a better structure-based knowledge of these properties is critical. The toxicity of ILs is an important property that directly relates to health and safety concerns. For the purpose of advanced design of ‘green’ ILs, numerous studies regarding the toxicity of IL principle groups have been performed. As reported,¹⁷¹⁻¹⁷³ the antimicrobial properties of ILs (defined as minimal inhibitory and bactericidal concentrations against microbial strains) relevant for human health is observed to increase with the length of the side alkoxy chain (from 2 to 12 carbon atoms), and the anions effect on the toxicity was observed secondary to the cations effect. Together with these observations, the non-aromatic head groups were generally found less toxic than their corresponding aromatic analogues.¹⁷⁴ For the major property associated to the evaluation of environmental impact, biodegradability of ILs has also been studied and discussed recently.¹⁷⁵⁻¹⁷⁹ It is observed that the presence of groups (e.g. amides, esters, hydroxyls) in the side chain of some cations such as imidazolium,¹⁸⁰ pyridinium^{181, 182} can significantly enhance the biodegradability of their corresponding ILs. Meanwhile, some studies show that ILs having alkyl chains containing four carbon atoms are poorly biodegradable but those cholinium (cation)-based ILs are observed to be readily biodegradable. Nonetheless, the knowledge of their modes of toxicity, and biodegradation pathways is still limited. Therefore, further experimental investigation is necessary for the specific system under study.

When choosing an IL as solvent for bioproduct recovery, it should be easy to separate it from the dilute aqueous phase as well as remove the desired products from IL rich phase. Their separation performance is generally described by solvent properties at infinite dilution such as infinite dilution distribution coefficient (D), selectivity (S), solvent loss (Sl) and solute loss (Ul), defined as:

$$D = \frac{\gamma_{i,Aq}^{\infty} M_{w,H_2O}}{\gamma_{i,IL}^{\infty} M_{w,IL}} \quad 3.102$$

$$S = \frac{\gamma_{H_2O,IL}^{\infty}}{\gamma_{i,IL}^{\infty}} \quad 3.103$$

$$Sl = \frac{1}{\gamma_{iL,Aq}^{\infty}} \quad 3.104$$

$$Ul = \frac{1}{\gamma_{i,Aq}^{\infty}} \quad 3.105$$

where $\gamma_{i,Aq}^{\infty}$, $\gamma_{iL,Aq}^{\infty}$ are the infinite dilution activity coefficient of solute i and solvent (IL) in aqueous raffinate phase, while $\gamma_{i,IL}^{\infty}$, $\gamma_{j,IL}^{\infty}$ are the infinite dilution activity coefficient of solute i in IL-rich extract phase, respectively. In Eq.1, M_{w,H_2O} and $M_{w,IL}$ denote the molecular weights of water and IL, respectively.

For a given IL-water-solute system, the distribution coefficient of solute i (D_i) and water (D_{H_2O}) are expressed by their equilibrium weight fraction in IL-rich extract phase ($x_{iL}^i, x_{iL}^{H_2O}$) and aqueous raffinate phase ($x_{iAq}^i, x_{Aq}^{H_2O}$), respectively. The selectivity is given as the ratio of the distribution coefficient, D_i and D_{H_2O} .

$$D_i = \frac{x_{iL}^i}{x_{Aq}^i} \quad 3.106$$

$$D_{H_2O} = \frac{x_{iL}^{H_2O}}{x_{Aq}^{H_2O}} \quad 3.107$$

$$S_i = \frac{D_i}{D_{H_2O}} \quad 3.108$$

Distribution coefficient is a measure of the difference in solubility of the solute (desired product) in two split phases at equilibrium and the product is usually supposed to be concentrated in water-immiscible phase. Selectivity is the ratio of the infinite dilution activity coefficients of solute i and water in the hydrophobic solvent phase. Most commonly, the selectivity must exceed unity for a possible separation. Solvent loss is the amount of solvent in aqueous raffinate phase. It is desired for this amount to be almost zero, in order for less solvent to be used. Likewise, solute loss is the amount of solute i that remains dissolved in aqueous raffinate phase. In order to obtain a successful extraction, the value of this parameter should be as small as possible. For water-miscible ILs, the IL-based ABS is formed by adding a salting-out agent as second phase is created. When using water-immiscible ILs, two phases already exists before the addition of any salts, and one of the phases is far from being aqueous-rich due to the low solubility of these ILs in water. In addition to the properties associated to biocompatibility and separation performance, thermophysical and physical properties such as viscosity and melting point are also needed to be taken into account considering their significant impact on the industrial operations.

Step 3. IL Design/Selection. As successful IL-based LLE systems largely depend on the selection of suitable ILs, here both conventional selection method (i.e. experimental data-based method) and systematic screening method (i.e. CAILD) are considered. With sufficient experimental data for a certain case under study, the conventional method is more attractive as

it can provide more reliable results. Compared to conventional selection methods that are usually cost intensive and time consuming, CAILD is more systematic and effective. In all possible cases of IL-based ISPR, the solvent loss should be as low as possible. Generally, the selectivity of ILs is employed as design target and the other thermodynamic associated properties such as solubility, distribution coefficient and solute loss are used as design constraints.

Step 4. Thermodynamic Calculation of LLE.

It has been shown that, in most cases, UNIFAC-IL model can provide reliable thermodynamic predictions and also has good group extendibility. The activity coefficient calculation in UNIFAC is based on the functional group information of involved components and therefore proper decomposition of IL molecule is needed for use of this thermodynamic method. Among commonly used decomposition approaches,^{58, 95} the manner in which IL is decomposed separately into cation, anion and substituents is preferred because of its improved design space and flexibility.⁹⁴ It should be noted that the salting-out agent should also be included in the thermodynamic calculation when using IL-based ABS as extraction system.

3.3.2.3 ISPR Evaluation

Step 5. Process Simulation and optimization. From the practical and economic point of view, process simulation is a good manner to evaluate the process performance as desired. Generally, the optimal IL for a specific design should be identified based on the best process performance. However, it is unrealistic to simulate the process considering all possible ILs as solvents and therefore only the optimal ILs designed/selected in the Step 2 are simulated. In this design stage, both dynamic-state simulation of upstream reaction process and steady-state simulation of downstream separation process are performed. Meanwhile, in order to obtain optimal processing configurations, process optimization is also included.

In the steady-state simulation, no variations of temperature, pressure, composition and reaction rate with respect to time is considered. On the other hand, the dynamic-state that describes the reaction behavior is simulated with ISPR, where the model equation is generally derived from the differential mass balance since the composition and reaction rate vary with respect to time in the reactor. To date, the simulation of processes involving ILs is still a challenging task since ILs are still not included in the component database of common process simulators (e.g. Aspen Plus, PRO/II) and the required information of IL-containing systems for calculating their thermodynamic behaviors are also limited. Nonetheless, works regarding process simulation of IL-containing systems have been studied recently. Among these works, Aspen Plus is the most widely used simulation tool, where ILs are introduced as pseudo-components by specifying their physical and critical properties. Physical properties can be calculated by group GC-based models developed in Section 2.2, while critical properties can be predicted from the fragment contribution-corresponding states method presented by.¹²⁹

Step 6. Performance Evaluation. Finally, based on the reaction and separation simulation results from Step 6, the process performance of the ISPR schemes can be evaluated with the applicable energy and economic models. In the ISPR schemes with IL-based ABS, the product concentrated in IL-rich aqueous phase and therefore the water should be removed from the concentrated product stream prior to the product recovery operation. For the water removal process, reverse osmosis (RO) that uses a partially permeable membrane to remove ions, molecules and larger particles from water can be considered as dehydration unit. Therefore, the cost model of the membrane unit may also be considered in some cases.

3.3.3 Applied IL-based ISPR in ABE fermentation

Butanol has been identified as an important biofuel since it offers several advantages (e.g. high energy content, lower hygroscopic nature and volatility) over ethanol and other fermentation derived fuels.¹⁸³ Butanol can be produced via acetone–butanol–ethanol (ABE) fermentation from a wide variety of cellulosic biomass using various strains of *Clostridium acetobutylicum* or *Clostridium beijerinckii* in anaerobic conditions. However, large-scale production of butanol from ABE fermentation is still economically limited due to its low yield and productivity. The inhibitory effect associated with this fermentation process mainly comes from the butanol toxicity to the culture. As reported, only 22 g/L of total fermentation products with a butanol concentration below 13 g/L are typically obtained during a batch process,¹⁸⁴ which results in a high process cost including large fermentation volumes required and high energy demand in downstream product recovery. For this reason, separation methods that enable effective and rapid removal of toxic components (especially butanol) from the fermentation broth is essential for improving the economic competitiveness of bio-butanol production from ABE fermentation.

By far, separation techniques such as adsorption, gas stripping, solvent extraction and pervaporation have been used for the product recovery in ABE fermentation process¹⁸⁵. Meanwhile, *in-situ* product recovery strategies that remove product from broth during ABE fermentation have also been studied, demonstrating the reduction of process inhibition and the improvement of butanol productivity.¹⁸⁶ Table 3.21 summarizes the recent experimental work regarding the application of *in-situ* product recovery strategy with different separation methods in ABE fermentation. Results show that *in-situ* product recovery process has higher productivity and yield compared to the batch process. Nevertheless, problems of *in-situ* product recovery strategies with conventional separation methods also exist. For example, when combining gas stripping with *in-situ* product recovery strategy, the energy demand of the whole process will increase due to the duty required at the condenser for products recovery from the gas stream.¹⁸⁷ As mentioned above, ISPR with IL-based LLE has potential to improve the productivity, as well as lower the energy consumption in downstream product recovery process. In this work, we are trying to use this process strategy for the butanol production via ABE fermentation, and the proposed three-stage systematic design method is applied.

Table 3.21 Review of experimental work of using *In-situ* product recovery strategy with different separation methods in ABE fermentation

Microorganism	Substrate	Productivity increase (vs. batch process)	Yield increase (vs. batch process)	Separation method	Ref.
Clostridium beijerinckii BA101	Glucose	229%	5%	Gas stripping	188
Clostridium acetobutylicum JB200	Glucose	33%	25%	Two-stage gas stripping	189
Clostridium acetobutylicum ATCC 824	Glucose	28%	10%	Extraction	190
Clostridium acetobutylicum ATCC 824	Glucose	56%	8%	Extraction-gas stripping	190
Clostridium beijerinckii CC101	Glucose	32%	15%	Adsorption	191
Clostridium acetobutylicum B3	Glucose	40%	15%	Permeating–heating–gas stripping	191
Clostridium acetobutylicum ATCC 55025	Glucose	15%	3%	Pervaporation	192
Clostridium acetobutylicum ATCC824	Glucose/ xlycose	126%	67%	Pervaporation	193

3.3.3.1 ISPR scheme selection

As stated in section 3.3.2.2, different schemes of IL-based ISPR can be generated for using water-immiscible ILs. Extractive fermentation with *in-situ* product removal may not be suitable for large-scale production due to various reasons: slow mass transfer into solvent, phase cell inhibition by solvent (interface toxicity) and loss of cells at interface, difficult process control to mention few. In contrast, these shortcomings can be avoided by using an external product removal scheme. Therefore, product removal in an external extraction column with a recycle of water back to the fermenter has been preferred for large-scale production of bio-butanol.^{194, 195}

Figure 3.18 shows the proposed IL-based ISPR scheme for the production of bio-butanol from ABE fermentation. The fermentation broth is withdrawn from the fermenter and fed to the extractive column (E-C1) at a time when the fermentation products start to inhibit microorganism, and then the product lean broth are recycled to the fermenter. It should be noted

that a membrane unit (M-U1) is required between the fermenter and extractive column in order to retain the microorganisms and/or some intermediates inside the fermenter. After leaving the extractive column, the product rich phase is sent to a flash unit (F-U1), where the most of fermentation products together with the extracted water are evaporated and then separated from IL solvent, which is recycled back to the extractive column after being cooled to the fermentation temperature. Afterwards, light products acetone and ethanol are separated from water and butanol in a distillation column (D-C1). Next, the butanol-water mixture, which can form a heterogeneous azeotrope, is further separated by using a two-column distillation system with a decanter (D-U1). In this system, almost pure water obtained in the bottom of the distillation column (D-C1) is cooled to the fermentation temperature before being recycled to the fermenter. Meanwhile, a high purity butanol product can be obtained in the bottom of the second distillation column (D-C2) in this two-column distillation system. A solvent make-up stream is also considered for the IL losses occurring in the whole process. Together with process optimization, heat integration that allows energy savings is also considered in this process. The detailed information of these designs is given in Section 3.3.3.3

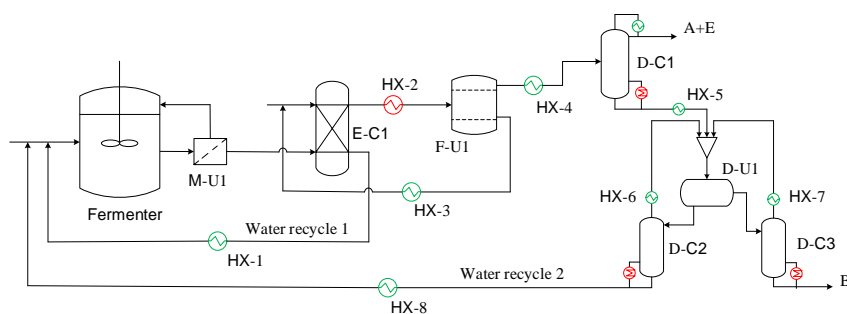


Figure 3.18 IL-based ISPR scheme for continuous production of bio-butanol from ABE fermentation

3.3.3.2 Screening IL for LLE systems design

Solvent plays an important role as removal and concentrating agent for biomolecule compounds from dilute aqueous solutions. In order to obtain an effective recovery of butanol from dilute broth, a good solvent with a high affinity for butanol combined with low water co-extraction is highly desired. Several organic solvents,¹⁹⁶⁻¹⁹⁸ especially oleyl alcohol (OA) have been studied as extractive solvent in ABE fermentation process due to their high selectivity and/or high capacity for butanol-water system. Recently, some water-immiscible ILs with high distribution coefficient and selectivity for this binary mixture also been reported.¹⁹⁹ These studied solvents with their experimental distribution coefficient and selectivity for butanol-water system are summarized in Figure 3.19. By far, tetraoctylammonium 2-methyl-1-naphthoate ([TOA] [MNaph]) reported has the best separation performance due to its high selectivity and D_{butanol} for butanol-water system. Figure 3.20 gives the structures of OA and [TOA] [MNaph].

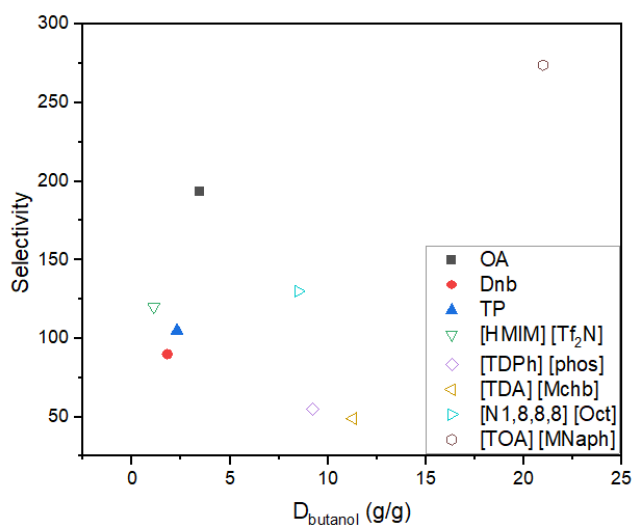
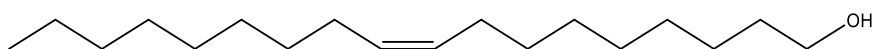
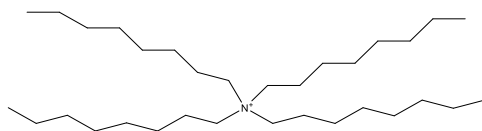


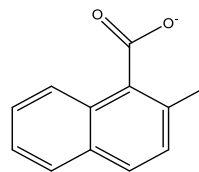
Figure 3.19 Experimental selectivities (Eq.3.108) and distribution coefficients (Eq.3.106) of some reported solvents in butanol-water system (Dnb: Di-n-butylphthalate, TP: Tricresyl phosphate, [HMIM][Tf₂N]: 1-hexyl-3-methylimidazolium bis(trifluoromethylsulfonyl)imide, [TDPH][phos]: Tetradecyl(trihexyl)-phosphonium bis-2,4,4-trimethylpentyl-phosphinate, [TDA][Mchb]: Tetrakis(decyl)-ammonium 1-methyl-1-cyclohexanoate, [N1,8,8,8][Oct]: 1-methyltrioctylammonium octanoate)



OA



[TOA]



[MNaph]

Figure 3.20 Structures of oleyl alcohol (OA) and tetraoctylammonium 2-methyl-1-naphthoate ([TOA] [MNaph])

Besides the IL selection from experimental data involving distribution and selectivity, CAILD is also used to find suitable ILs for the butanol recovery in ABE fermentation process. In this

work, an optimal IL, trihexyltetradecylphosphonium tetracyanoborate ([TDPh][TCB]), is identified by solving a formulated mixed-integer non-linear programming (MINLP) problem, where the maximization of selectivity is set as the objective function and multi design constraints are imposed on the IL structure, thermodynamic properties (i.e. distribution, solvent power and solvent loss) and physical properties (i.e. melting point temperature, viscosity). In this work, a complex CAILD-based MINLP problem is solved in the modelling system GAMS by using a deterministic global optimization solver, LINDOGLOBAL.

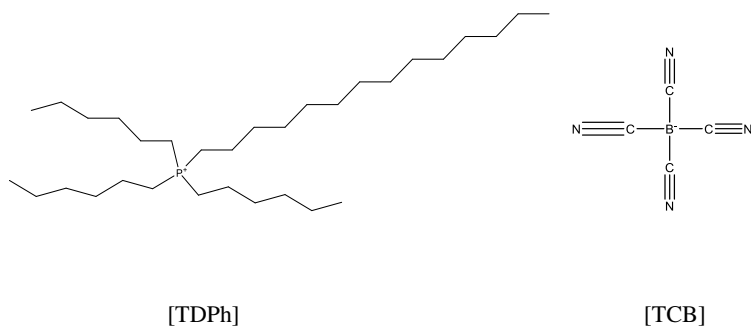


Figure 3.21 Structure of trihexyltetradecylphosphonium tetracyanoborate ([TDPh][TCB])

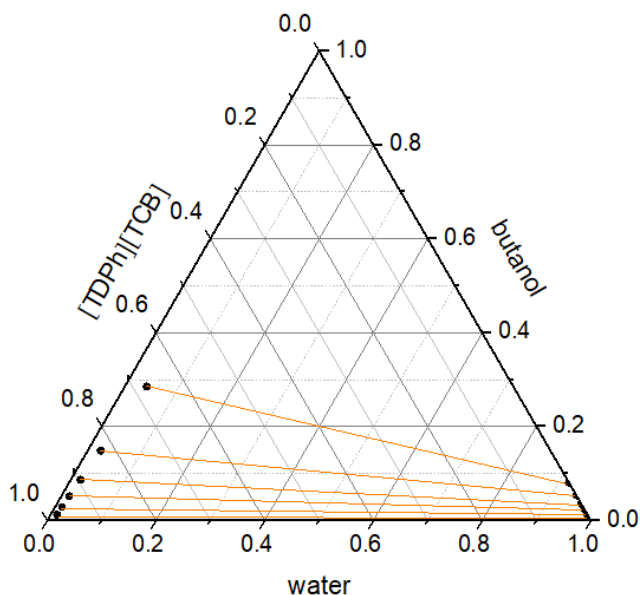


Figure 3.22 UNIFAC-IL calculated liquid-liquid equilibria for the ternary system of [TDPh][TCB]-water-butanol (mass fraction)

The structure of [TDPH][TCB] is given in Figure 3.21 and the UNIFAC-IL calculated liquid-liquid equilibria for the ternary system of [TDPH][TCB]-water-butanol is presented in Figure 3.22. It is to be noted experimental correction of these phase equilibria calculations is not available due to the fact that no experimental work of [TDPH][TCB] have been reported so far. Nonetheless, the reliability of these calculations can be evaluated from the accuracy of the UNIFAC-IL model. In this work, the used UNIFAC-IL model was extended from a wide range of experimental infinite dilution activity coefficient data and have been verified by a large experimental liquid-liquid and vapor-liquid equilibria.⁷⁷ The MAPE (mean absolute percentage error) of the predictions for IL-alcohol-water systems (893 data points) is about 5.7%. Therefore, the phase equilibria calculated from this UNIFAC-IL model is reliable.

3.3.3.3 Process simulation and performance evaluation

In this work, water-immiscible ILs, [TOA] [MNaph] and [TDPH] [TCB], are finally selected as the extractive solvents for the studied ABE fermentation process. In order to evaluate the proposed IL-based ISPR scheme for ABE fermentation, process simulations including dynamic simulation of fermentation process and steady-state simulation of downstream separation process are performed and illustrated. In this work, a kinetic model developed by Mulchandani and Volesky²⁰⁰ (see Appendix D) is employed for simulating the reactor (fermenter), where the accumulation of butanol (B) and butyric acid (BA) accounts for the process inhibition, as shown in Eqs.3.109 and 3.110.

$$f(I) = \exp(-0.01BBA) \quad BBA \leq 8.0 \text{ g/L} \quad 3.109$$

$$f(I) = -0.153BBA + 2.16 \quad 8.0 \leq BBA \leq 13.9 \text{ g/L} \quad 3.110$$

$$BBA = C_B + C_{BA} \quad 3.111$$

where concentration of butanol (C_B) and butyric acid (C_{BA}) as well as other involved components (i.e. substrate, microorganism, acetic acid, acetone, ethanol and water) can be calculated from the reactor model, as expressed in Eq.3.112.

$$\frac{dC_i}{dt} = r_i - \vartheta(C_i - C_{i,IN}) \quad 3.112$$

Here, r_i is the rate of reaction and ϑ is the dilution factor that corresponds to the ratio between the volumetric flow rate withdrawn from the reactor and the reactor volume. C_i and $C_{i,IN}$ denote the concentration of the component i of the recycled stream and inside the fermenter, respectively. Clearly, the reactor model of a typical batch process can be expressed by Eq.3.112 with no product removal (i.e. $\vartheta = 0$), while Eq.3.112 with no substrate make-up stream ($C_{S,IN} = 0$) representing another special reactor model of the fermentation process. Here, we are studying and comparing the dynamic behaviors of three different processing schemes, i.e., batch process (Scheme-1), ISPR with no substrate make-up stream (Scheme-2) and ISPR with substrate make-up stream (Scheme-3). The ordinary differential equation (ODE) system from

Eq.11 is solved in MATLAB by using ODE45 algorithm. The dynamic simulation results of all three processing schemes are given in Figures 3.23, 3.24 and 3.25, respectively.

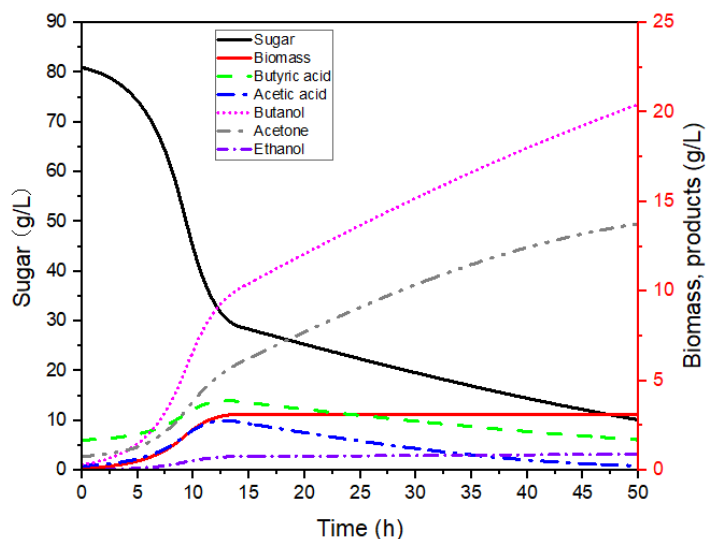


Figure 3.23 Component concentration tracking for batch fermentation process

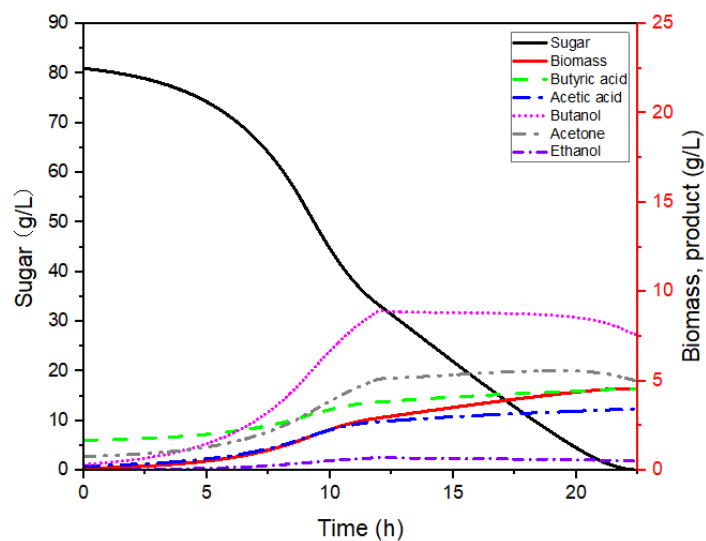


Figure 3.24 Component concentration tracking of the ISPR fermentation process with no substrate make-up steam

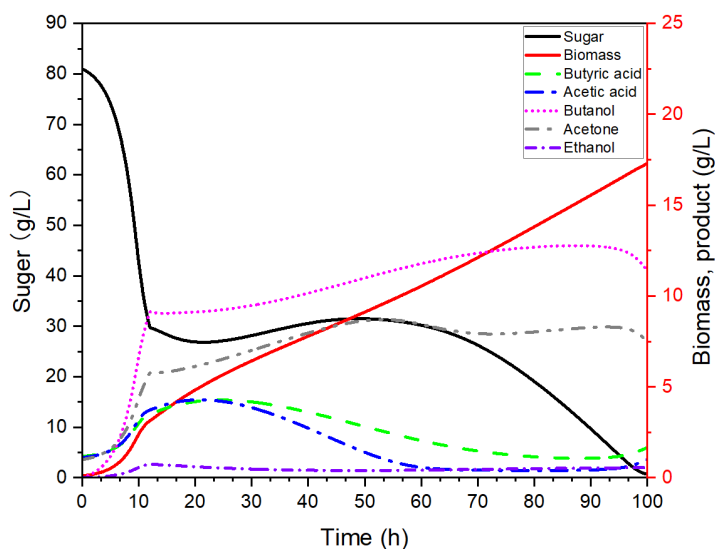


Figure 3.25 Component concentration tracking of the ISPR fermentation process with substrate make-up steam

As shown in Figure 8, the growth of microorganism significantly inhibited after 13 h due to the accumulation of butanol and butyric acid, resulting in a reduction in the rate of sugar consumption. After 50h, the fermentation is almost ceased when the concentration of ABE reaches 38.5 g/L with a butanol concentration of 20.4 g/L. In Scheme-2, the ABE products are removed (after 12 h) through filtrate stream from the fermenter thereby reducing the inhibition of the fermentation process. The rate of product removal can be controlled by changing the flowrate of recycled and filtrate stream. In order to obtain a stable butanol concentration in the reactor during the whole fermentation process, a dilution ratio of 0.1 h^{-1} is used. Unlike the situation of Scheme-1, sugar can be fully converted to the products in this scheme. Moreover, less than 23 h is needed to achieve a 100% sugar conversion (see Figure 3.24), which means that more than 54% of the fermentation time can be saved as compared to the batch fermentation process. Therefore, based on the same fermenter volume, the butanol productivity of Scheme-2 is around 1.8 times greater than that of Scheme-1.

For Scheme-1 and Scheme-2, the fermentation process will be ceased either after a time due to the toxic effect of products or the full consumption of the substrate. In order to achieve a stable butanol production in the fermenter, a processing scheme of ISPR with substrate make-up stream (Scheme-3) can be used. In this scheme, the ABE products are removed through the filtrate stream after 12 h, while a substrate make-up stream is added to the product lean broth before it is recycled to the fermenter. By varying the dilution ratio, it was found that the butanol concentration is kept around 10 g/L with a dilution ratio of 0.11 h^{-1} , which allows a stable butanol production between 12 and 100 h (see Figure 3.25) and the butanol productivity of this

scheme is around 2.7 times greater than that of the batch processing scheme. The composition of the broth sent to the downstream separation for all three processing schemes is given in Table 3.22. It is to be noted that we treat the filtrate fermentation broth and fermentation broth remained in the fermenter as a whole in Scheme-2, while the average composition of the filtrate stream between 12 and 100 (h) is applied in Scheme-3.

Table 3.22: Composition of the broth sent to the downstream separation for all three processing schemes.

	Scheme-1	Scheme-2	Scheme-3
Component	Mass fraction	Mass fraction	Mass fraction
Butanol	2.04E-02	8.10E-03	1.02E-03
Acetone	1.38E-02	5.19E-03	8.0E-04
Ethanol	8.92E-04	5.61E-04	4.41E-05
Water	0.9649	0.9862	0.9813

In this work, the downstream separation process including products recovery and purification is simulated in Aspen Plus (V8.6). The missing thermodynamic parameters of UNIFAC-IL model for the studied system are calculated from COSMO-RS. As reported,⁷⁷ the MAPE of COSMO-RS for the IL-ketone systems is about 30%. Although such prediction performance is not good enough, the concentration of acetone has relatively small inhibition impact on the studied ABE fermentation process. For this reason, using thermodynamic parameters calculated from COSMO-RS for [TOA][MNaph]-acetone system is acceptable.

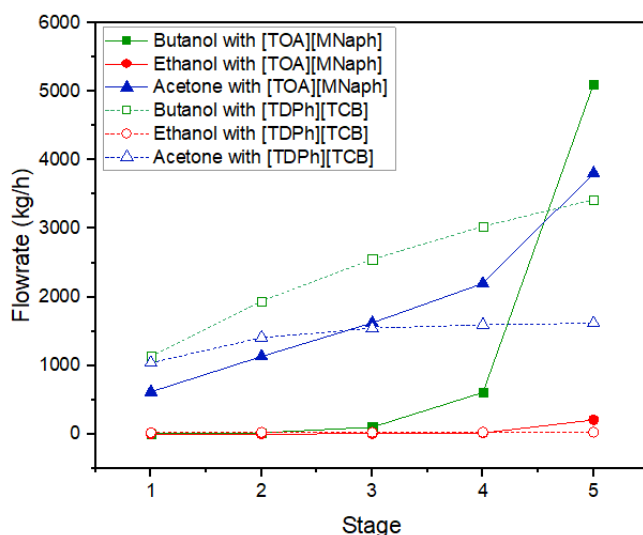


Figure 3.26 Separation performance of [TOA][MNaph] and [TDPH][MNaph] for ABE fermentation broth (simulated in a five-stage extract column)

Table 3.23 Optimized simulation results of the ABE downstream separation for all processing schemes

Units	Variables	Scheme-1	Scheme-2	Scheme-3
E-C1	Pressure (bar)	1.0	1.0	1.0
	Number of stages	32	32	36
F-U1	Pressure (bar)	0.5	0.5	0.5
	Temperature (°C)	120	135	135
	Energy input (MW)	3.02	5.98	5.09
D-C1	Pressure (bar)	0.5	0.5	0.5
	Number of stages	72	66	56
	Feed location	17	13	17
	Reboiler duty (MW)	5.61	7.51	7.11
D-C2	Pressure (bar)	0.5	0.5	0.5
	Number of stages	6	6	6
	Feed location	1	1	1
	Reboiler duty (MW)	1.48	2.50	2.23
D-C3	Pressure (bar)	0.5	0.5	0.5
	Number of stages	7	7	8
	Feed location	1	1	1
	Reboiler duty (MW)	1.19	1.21	1.20
HX-1	Energy demand (MW)	-1.69	-4.41	-3.51
HX-2	Energy demand (MW)	23.45	58.79	46.65
HX-3	Energy demand (MW)	-14.96	-45.45	-34.54
HX-4	Energy demand (MW)	-7.04	-12.28	-10.39
HX-5	Energy demand (MW)	-0.08	-0.11	-0.10
HX-6	Energy demand (MW)	-1.24	-2.10	-1.87
HX-7	Energy demand (MW)	-1.12	-1.13	-1.13
HX-8	Energy demand (MW)	-0.71	-1.16	-1.04
Total energy demand (MW)		11.30	17.20	15.63
Energy demand (MJ/kg of butanol produced)		8.14	12.38	11.25
Solvent flowrate (t/h)		60	155	124

As shown in Figure 3.18, E-C1 is modelled by the Extract column block, while F-U1 and D-U1 are modelled by Flash and Decanter separator block, respectively. Meanwhile, all distillation columns (i.e. D-C1, D-C2, and D-C3) are modelled by the RadFrac block. As shown in Figure 3.26, [TOA][MNaph] has better performance of separating ABE from dilute aqueous solution than [TDPH][TCB], especially for butanol. For this reason, only processes using [TOA][MNaph] are further simulated and demonstrated for the studied ABE downstream separation. The optimized simulation results to recover 5t/h butanol (99.8% mass purity) from the fermentation broth of all three processing schemes are given in Table 3.23. Meanwhile, a

all discussed and investigated. The conceptual design of IL-based ISPR that is able to reduce the inhibition on cells and increase the volumetric productivity is exemplified for butanol production from ABE fermentation. In this case, [TOA][MNaph] is finally identified as the best extraction solvent in the design of LLE systems for the product removal. The dynamic simulation results of the fermentation process show that, compared with the batch fermentation process, the ISPR processing scheme can significantly improve the process productivity. However, the optimized simulation results of the downstream separation process reveal that butanol recovery from batch fermentation broth demands lowest energy and solvent input due to its highest product concentration. Nonetheless, the application of IL-based ISPR processing schemes can have at least 27% energy savings compared to the conventional downstream distillation process. In addition, in the case of using internal IL-based ISPR processing schemes, a reduced energy consumption is achievable since they generally have enriched product stream. Particularly, a significant increase in process productivity by using IL-based ISPR processing schemes offers great advantage for the production of high-value bioproducts.

The results of the studied ABE fermentation process demonstrate that, if properly designed, IL-based ISPR is able to afford higher productivity and energy performance of bioprocesses when compared to batch processing operation. This work mainly focuses on the bioprocess of microbe-derived small molecules, but it can potentially be a guidance to the other bioprocesses. Nevertheless, some issues need to be addressed for its widespread use in bioprocesses. Firstly, current experimental database is still limited to some well-known ILs and small molecules. Therefore, more experimental work covering new IL-bioprocess systems is necessary. Secondly, the separation method of IL-based ABS has many advantages, but its optimal design is very difficult due to the limitation of the thermodynamic models. For this reason, current thermodynamic models such as UNIFAC and NRTL need to be extended to the IL-based aqueous biphasic systems. In addition, although the major properties associated to the evaluation of environmental impact and biodegradability of ILs have been recently studied, the knowledge of their modes of toxicity, and biodegradation pathways is still limited. Therefore, further experimental investigation and theoretical study are essential and should be the focus of attention in the coming years. Finally, in terms of the ISPR technology itself, the robustness of the design to industrial conditions is critical. Controlling the conditions is more difficult for an ISPR process than for a non-integrated process and thereby any efforts for improving the robustness of the design is highly desirable when ISPR is applied.

3.4 CHAPTER SUMMARY

ILs are introduced to the intensified process designs and three design methodologies are proposed, respectively. (1) A hybrid process design method allowing units operating at their highest process efficiencies to perform one (or more) process tasks is proposed to obtain optimal process operations with better energy (and reaction) performance. (2) An integrated design method combining GC-based property models, UNIFAC-IL models, computer-aided

molecular design (CAMD) and process design is proposed to simultaneously optimize the IL structure and process operations. (3) A three-stage design method that combines ISPR processing schemes selection, IL-based liquid-liquid extraction systems design and process evaluation is proposed for the small molecule fermentation process.

4 GAS SEPARATIONS

In this chapter, gas separations including shale gas purification and natural gas sweetening are presented.

Chapter structure and contents:

4.1 Shale gas purification

4.2 Natural gas sweetening

4.1 SHALE GAS PURIFICATION

This chapter forms the basis of following publication:

Liu, X.; Chen, Y.; Zeng, S.; Zhang, X.; Zhang, S.; Liang, X.; Gani, R.; Kontogeorgis, G. M.: Structure optimization of tailored ionic liquids and process simulation for shale gas separation. AIChE Journal 2020, 66, e16794.

Abstract

Shale gas, as a potential substitute of energy source, requires important processing steps before utilization. The most common separation technology applied is distillation, which is energy-intensive. In this chapter, a strategy for hybrid shale gas separation processing, where IL-based absorption together with distillation are employed for energy efficient and cost economic gas processing, is developed.

4.1.1 Introduction

Coal has been a primary energy source since the industrial revolution. With increasing environmental pollution and decreasing energy sources, finding alternative energy sources is very important. With a large potential amount available for utilization, shale gas, as a kind of natural gas trapped within shale formations, has been receiving much attention. In addition to its important role as a fuel, shale gas is also a source of hydrocarbons for petrochemical feed stocks to produce value-added chemicals. Due to the presence of large amounts of CH_4 and reasonable amounts of C_2H_6 , many studies have been undertaken on natural gas and shale gas related to the production of potential products such as syngas, methanol and ethylene.^{201, 202} Although it is usually regarded as a “clean” fuel compared to other fossil fuels, the shale gas found in reservoir deposits is not strictly “clean” and free from impurities. It is primarily composed of CH_4 , considerable amounts of light and heavier hydrocarbons as well as contaminating compounds such as CO_2 , H_2 , H_2S , etc.²⁰³ Thus, the impurities must be removed before their utilization to meet strict pipe-line quality standards specifications for a consumer fuel to avoid pipeline and equipment corrosion as well as to enhance its calorific value. Therefore, different technologies need to be employed for separation of the unwanted gases. The most common separation technology applied is distillation, which consumes large amounts of energy to give the desired high purity products.²⁰⁴⁻²⁰⁶ These distillation columns operate at low temperatures and high pressures and have high energy demands. In this chapter, a hybrid IL-based gas separation scheme to separate a model shale gas mixture is developed and evaluated, with extended databases and property prediction models.

4.1.2 Methodology

In this work, a three-stage methodology is proposed (Figure 4.1) in order to synthesize and design IL-based shale gas separation processes. The first stage involves IL screening where the gas to be separated is selected through analysis of the specific gas mixture and the associated IL-gas properties. The appropriate IL is selected based on available and predicted solubility and selectivity for specific gas separation problems. The screening method has two options: a) selects the IL based on its availability and already known properties; b) generates and selects IL candidates through computer-aided molecular design techniques that best match the desired target properties. In option b, appropriate thermodynamic models for the prediction of properties need to be employed. The UNIFAC model is used to predict solubility of gas in ILs, while COSMO-RS model is employed as a backup model when parameters of UNIFAC model are unavailable. Also, group contribution models for prediction of pure properties prediction are needed. These models constitute a model library through which not only potentially better ILs could be designed but also existing ILs not selected in option-a could now be considered based on available data as well as estimated missing properties, thereby, extending the application range of the IL screening method. The second stage involves process design and simulation for the gas separation problem for both selected ILs. The gas separation sequence is decided for each IL and the corresponding separation schemes are generated. The required thermodynamic models for the simulation of the selected gas-IL systems are established through fitting of needed model parameters from experimental data or predicted data. Then, the whole process is simulated. The important design parameters such as the amount of solvent needed, operating conditions (temperature and pressure), are determined through sensitivity analysis on the separation performance. The third stage involves process evaluation, where the total energy consumption and selected economic performance indicators are calculated. The results obtained for different IL-based processes with selected ILs from the first stage are compared. As a case study, in this work, two ILs are selected as candidates, one is selected from option-a employing database search to identify the most appropriate IL (for immediate application as the IL already exists), while, a second IL is generated and selected through option-b, having better selectivity and other missing properties. Note that this second IL could be an existing IL that could not be selected previously because of missing properties, or, a potentially attractive candidate for possible future synthesis as it is not currently available. The comparison indicates whether the potential improvements are sufficient to invest in the development of the new IL.

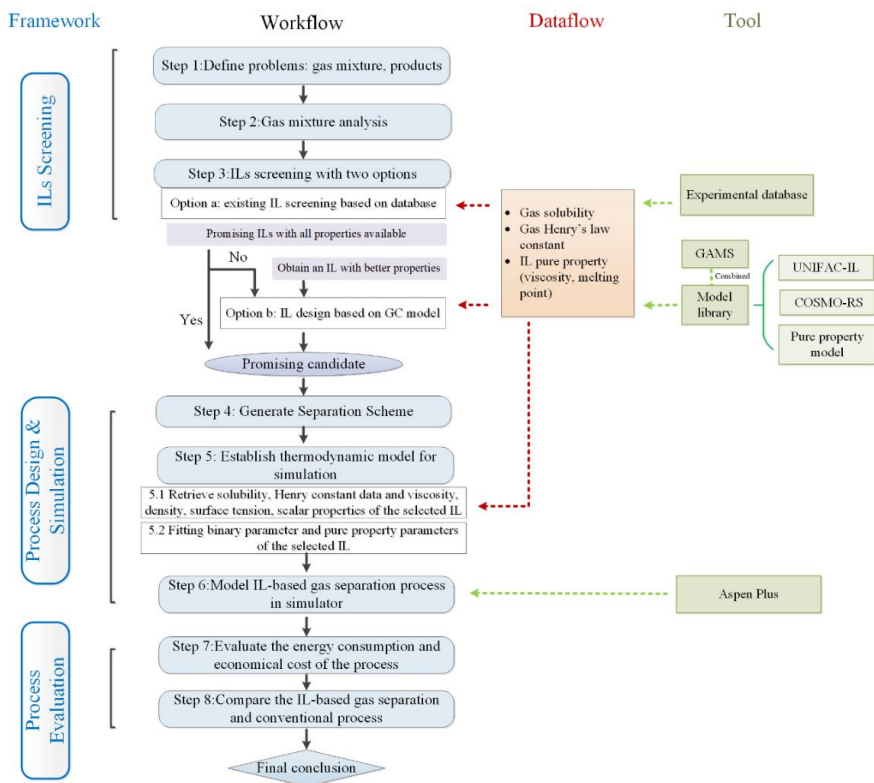


Figure 4.1 The whole workflow for hybrid IL-based gas separation process

4.1.3 ILs Screening

4.1.3.1 Problem definition and gas mixture analysis

For a given gas mixture separation problem, the absorbed gas and products are first defined. In this work, based on the reported raw shale gas²⁰³, a model with 5 gases is considered, as given in Table 4.1. We assume that 2000 kmol/h of raw shale gas is available at 30 bar and 20°C²⁰². In order to have low solvent consumption, the gas present in the largest amount (methane, CH₄, whose concentration is 80%) is not absorbed and the other gases are removed, if necessary. For example, if the processed shale gas is to be used as fuel, it is necessary to remove CO₂, which is present in the raw shale gas, giving a gas mixture of H₂ and CH₄, which can be utilized as a high-quality fuel. Note that economically feasible separation of high purity C₂H₄ and C₂H₆, which are regarded as common building blocks for the production of thousands of chemical products²⁰⁷, could also be considered.

Based on the solubility database established in Section 2.1, the solubility of each gas in ILs is checked. If the IL does not absorb CH₄, then all other gases could be potentially removed and

the method needs to identify which gas to remove first. In this case, the solubility of the gas in IL and the selectivity of the IL solubility compared to CH₄ needs to be checked. Also, the boiling points of the gases compared to CH₄ needs to be checked. The first gas to be removed should have the highest solubility and selectivity compared to CH₄ in IL. For the other gases that could not be absorbed by IL, they can be separated through a series of distillation steps, whose sequence is based on a ranking beginning from the gas with lowest boiling point and going to the highest.

Table 4.1 Raw shale gas component

Component	Percent (%)	Boiling point (°C)
H ₂	3	-252.8
CH ₄	80	-161.4
C ₂ H ₄	3	-103.7
C ₂ H ₆	7	-88.6
CO ₂	7	-78.5

4.1.3.2 IL screening method

The gas solubility and selectivity are quantified through the Henry's law constant. However, as the reported Henry's law constant is usually mole-based and the solvent is usually measured on a mass basis, therefore, in this work, the mass-based Henry's law constant, which is the mole-based Henry's law constant multiplied by the molecular mass of IL (kg/mol), is considered. The most suitable IL is the one, which has the minimum mass-based Henry's law constant of gas and a high selectivity of gas/CH₄. In addition, judging a solvent's potential for industrial application, the following pure component properties are also considered: viscosity, which affects the absorption capacity of solvent as well as the fluidity in process, normal melting point, making sure that the solvent is liquid at the operation condition.²⁰⁸ It should be noted, however, these pure component properties may not be available for the selected IL based on solubility and selectivity alone. Therefore, it is useful to also have an option for model-based IL screening.

The IL screening method has two options; a) practical IL screening based on the experimental database to identify any IL for which the needed gas solubility data and experimental pure property of the IL are available; b) computer-aided IL design option using a predictive thermodynamic model (UNIFAC-IL), together with a suite of verified GC-based pure component property models. These models are required such that unavailable pure properties of ILs with good separation potential could be further considered in the next stages. The objective of the model-based option-b is to systematically design a potentially superior IL that may provide the incentive for further studies on its future synthesis, development and application. In option-a, trihexyltetradecylphosphonium bis(2,4,4-trimethylpentyl)phosphinate) ([thtdp][phos]) is selected as the best IL solvent for the studied shale gas separation task. Similar with option-a, no solvent could be found with acceptable solubility and selectivity for absorbing C₂H₄ and C₂H₆. Then minimization of mass-based H_{CO_2} (Eq.4.1)

with a higher selectivity (Eq.4.2) than IL-a is considered as the optimal target in this computer-aided IL design problem. Meanwhile, we also specify stricter constraints on the pure component properties (Eqs.4.3-4.4) and IL molecular structure (Eqs.3.7-3.13). A pyridinium based IL ([MMpy][eFAP] (IL-b): 1,3-dimethylpyridinium tris(pentafluoroethyl) trifluorophosphate) is identified as the best IL solvent by solving the formulated MINLP-based CAILD problem. This IL-b, has almost three times higher selectivity than IL-a. The structures of [thtdp][phos] and [MMpy][eFAP] are given in Figure 4.2 and 4.3, respectively.

$$H_i = M_{IL} P_i^{sat} \gamma_i^{\infty} \quad 4.1$$

$$H_{CH_4}/H_{CO_2} \geq 15 \quad 4.2$$

$$T_m < 298.5 \text{ (K)} \quad 4.3$$

$$\eta < 0.1 \text{ (Pa} \cdot \text{s)} \quad 4.4$$

Where, M_{IL} is the molar mass of ionic liquid, γ_i^{∞} is the infinite dilution activity coefficient of component i , obtained from UNIFAC-IL model, P_i^{sat} is the saturated pressure of component i . T_m is the melting point of IL and η is the viscosity of IL.

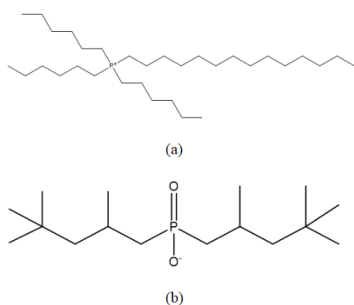


Figure 4.2 Structure of [thtdp][phos]

($C_{48}H_{100}O_2P_2$); (a) cation, (b) anion

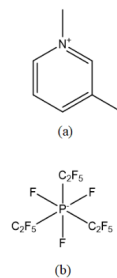


Figure 4.3 Structure of [MMpy][eFAP]

($C_{13}H_{10}F_{18}NP$); (a) cation , (b)anion

4.1.4 Process design and simulation

4.1.4.1 Process design

As stated in Section 4.1, the gas separation process consists of an absorption step followed by two distillation (or hybrid distillation-membrane) steps. Thus, the total gas separation process consists of two main parts; CO_2 removal and light hydrocarbon gas separation. As illustrated in Figure4.4, the CO_2 removal section consists of an absorption column followed by a series of depressurised flash vessels. To ensure a high CO_2 recovery rate, a vacuum pressure (around 0.5 bar) is fixed for the last flash vessel, from which, the recovered IL solvent is recycled to the top of the absorber.

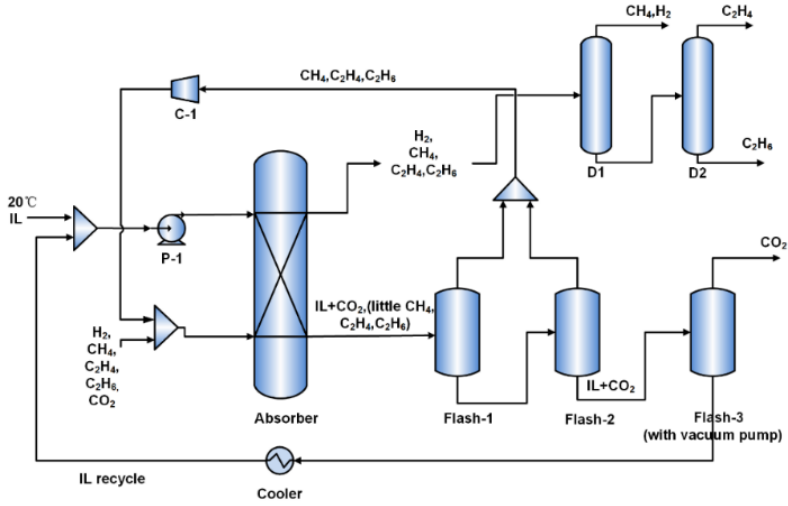


Figure 4.4 Hybrid IL-based shale gas separation process.

4.1.4.2 Process simulation

Gas separation measurement

The process simulation for the shale gas separation is divided into two main parts: CO₂ removal and light hydrocarbon gas separation. In order to evaluate the process separation performance, the CO₂ removal rate in absorber, gas purification (Vol%) of each gas stream and the gas recovery rate are considered using the following equations.

$$Removal_{gas} = 1 - \frac{\text{mole/mass flow of } X \text{ in gasout stream top in absorber}}{\text{mole/mass flow of } X \text{ in feedgas stream}} \times 100\% \quad 4.5$$

$$Recovery_{gas} = \frac{\text{mole/mass flow of } X \text{ out of related } X \text{ stream}}{\text{mole/mass flow of } X \text{ in feedgas stream}} \times 100\% \quad 4.6$$

Sensitivity analysis of key operation parameters

Consumption of IL and stage numbers in absorber: The influence of solvent consumption on the absorbed rate of CO₂ is shown in Figure 4.5. In order to evaluate the separation capacity under different stages of absorber, the CO₂ absorbed rate at each different stage number in absorber is calculated based on Eq.4.5. As seen from Figure 4.5, with increasing IL amount and stage number, more CO₂ can be absorbed, but the IL amount plays a more important role by removing most of CO₂. As a result, the stage number of absorber is set to 10. The remaining shale gas can fulfill requirement (<Vol3%) of CO₂ content in commercial gas. The comparison of the two IL-based absorption processes shows that the IL amount required for a 100% removal

is different. Less amount of IL-a ([thtdp][phos]) is needed under the same CO₂ removal rate because of a 0.25-times-higher solubility than that in IL-b. However, in addition of the selectivity, IL-b shows better performance on other pure component properties for application, such as a much lower value in viscosity and heat capacity. Considering that more than 95% CO₂ has been absorbed, the solvent amount is determined to be 630 ton/h for [thtdp][phos] and 750 ton/h for [MMpy][eFAP]. According to another research for IL-based CO₂ removal work²¹⁸ (72 ton/h IL used to purify the biogas containing 390kg/h CO₂ in the feed gas), the amount of IL used in this work is reasonable.

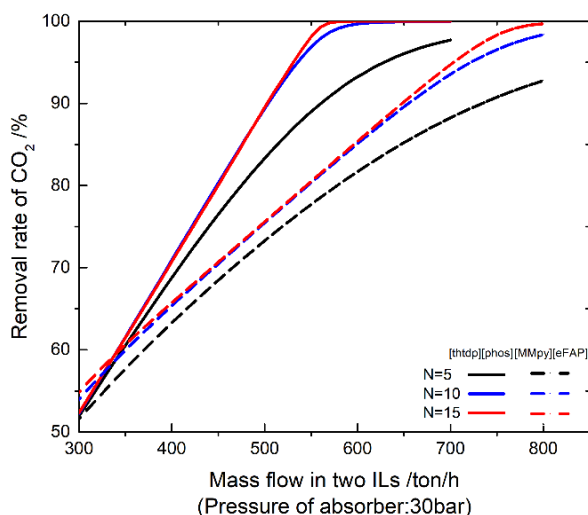


Figure 4.5 CO₂ removal rate versus IL amount in two IL-based processes. N means stage number

Desorption pressure of flash: Being a physical solvent-based process, the CO₂ is usually desorbed through a series of 3 flashes with decreasing pressures. The pressure is determined based on the mass flow of CO₂ coming out of the last flash. Figure 4.6 shows the influence of the pressure of first flash (flash-1) on the mass flow of CO₂ out of the system for the two different IL-based processes. The stream coming out of the absorber has a high pressure which is 30 bar. It is found that the CO₂ recovery out of the last flash decreases rapidly when the pressure decreases to around 8 bar. This implies that a large decrease of the pressure in the first flash would lead to a lower CO₂ recovery rate with large amount of gas going back to the absorber. Then, the pressure of flash-1 for [thtdp][phos] and [MMpy][eFAP] is set to 20 bar and 14 bar, respectively. Similarly, for flash-2, to keep a high recovery rate of CO₂, the pressure is determined to be 8 bar, 12 bar, respectively for the [thtdp][phos] and [MMpy][eFAP] based processes.

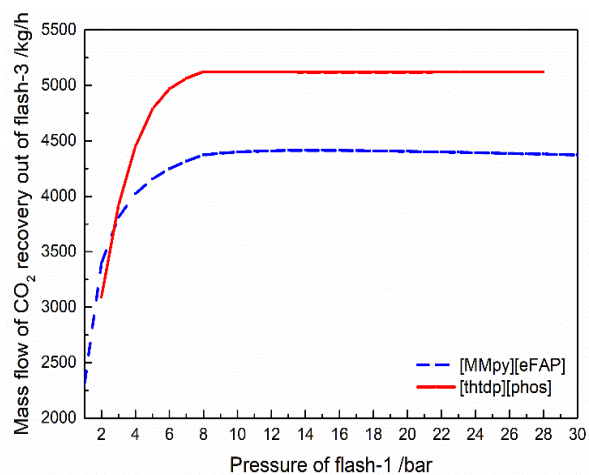


Figure 4.6 Pressure of flash-1 versus mass flow of CO₂ out of last flash for the two ILs considered in this work

For the last flash-3, vacuum pressure is employed to obtain a high recovery rate of CO₂. As seen in Figure 4.7, when the pressure is set to 0.5 bar, for the [thtdp][phos] based process, 90% recovery rate of CO₂ could be achieved, but for the [MMpy][eFAP] based process, a lower pressure is needed (0.25 bar).

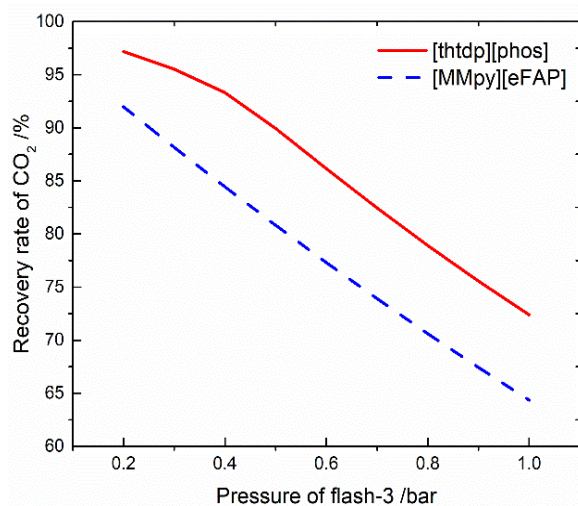


Figure 4.7 Temperature of flash-3 versus recovery rate of CO₂ for the two ILs considered in this work

Key parameters of the distillation columns: Due to the close boiling points of C₂H₄ and C₂H₆ (see data given in Table 4.1), more stages and also higher reflux ratio are needed in D2. Besides,

as other hybrid process schemes for these gas separation have been reported,^{26, 219} they are not investigated in detail here. The important issue here is how much C₂H₄ and C₂H₆ are available and whether an economically feasible scheme for their separation is necessary. Also, it could be that C₂H₄, C₂H₆ with a small amount of CO₂ could be directly used in synthesis of other higher value chemicals.²²⁰ Note that the main fuel product is obtained from the first distillation column quite easily.

4.1.5 Process Evaluation

4.1.5.1 Energy and cost estimation methodology

Energy consumption evaluation

Energy consumption is regarded as a key indicator for any process evaluation, especially for CO₂ separation processes. Usually, the total energy consumption (TEC) for a process includes the thermal energy and the electricity. Then, the total energy is expressed by an equivalent energy penalty,²²¹ but in the IL-based processes of this work, only electricity is consumed in the three-stage flash vessels (not considering the two distillation steps, but they are not affected by the IL). As a result, the total energy consumption is, in our case, equal to the electricity consumption. To compare with other processes with different raw gas and with other technologies, the specific energy consumption (SEC) is a useful indicator:

$$SEC = \frac{TEC}{m_{out}} \quad 4.7$$

where the units of TEC and SEC are MJ/h, MJ/kg gas, respectively, m_{out} is the mass flow of the gas out of the system.

Economic evaluation

The purpose with the economic analysis of the process is to calculate the total removal cost (TRC) which is used to evaluate and compare the two processes. TRC is calculated from the sum of the annualized capital cost (ACC) and total operating expense (OPEX) both of which are computed based on other types of costs, as shown in Table 4.2.²²²⁻²²⁴

The annualized capital cost (ACC) can be calculated from translating the total capital expense (CAPEX) into annualized capital investment of the whole project, as in Eq.4.8. CAPEX is then computed according to Abu-Zahra et al.²²³ and Schach et al.²²⁵ The purchased equipment cost (PEC) is obtained according to Walas.²²⁶ The size of the equipment is obtained from the simulation in Aspen Plus. All the equipment costs are updated to the year 2018 with the Chemical Engineering Cost Index.²²⁷

The ACC equation is:

$$ACC = \frac{TCI}{((1 + ir)^n - 1)/ir(1 + ir)^n} \quad 4.8$$

Where ir denotes the annual interest rate, assuming 8% in this work, n denotes project lifetime, assuming 25 years.²²²

Table 4.2 Calculation measures of total removal cost (TRC)

Cost item	Calculation basis
TRC	Total operating expense (OPEX), annualized capital cost (ACC)
OPEX	Variable operating cost (VOC), fixed operating cost (FOC)
ACC	Total capital expense (CAPEX)
CAPEX	Fixed capital investment (FCI), working capital, startup cost, initial solvent cost
FCI	Direct cost (DC), indirect cost (IC)
DC, IC	Purchased equipment cost (PEC) with a coefficient of the percentage

The total operating expense (OPEX) includes two parts: one is the variable operating cost (VOC) which contains the solvent make-up and the public utilities such as heat steam, cooling water and electricity. The other part is the fixed operating cost (FOC), including the operating labor, maintenance, R & D cost, etc. The price of utilities is obtained from literature.²²⁸⁻²³¹ The price of both ILs is estimated to be 100k\$/ton under the assumption of industrial production in the future based on the estimation by Linzhou Keneng Materials Technology Co., Ltd. China²²² Due to the non-volatility of IL, most of IL is recycled during the process and a little of fresh IL is needed. We have assumed 0.35g/ton CO₂ in this work.²³² As a result, the two processes could be compared under the condition of same unit price in solvent.

4.1.5.2 Process evaluation results

Energy consumption

For the IL-based CO₂ removal process in this work, the total energy consumption (TEC) is only consumed through electricity. It is generated from pump, vacuum pump and compressor for solvent recycle and gas recovery. To make a better comparison, we simulate the two processes under same CO₂ recovery rate (90%), as seen in Table 4.3. The TEC for CO₂ removal in the two processes are shown in Figure 4.8. It is found that the IL-b process could achieve a 54% reduction in TEC compared with the IL-a process. As a result, we can conclude that even though the designed IL-b has somewhat lower solubility than IL-a (leading a high solvent consumption, given in Table 4.3), the high CO₂/CH₄ selectivity results in less gas to be recycled and thus the electricity consumed in compressor (given in Table 4.3) can be much reduced. The specific energy consumption (SEC) in these two processes are 0.71 MJ/kg CO₂, 0.33 MJ/kg CO₂,

respectively for processes using IL-a and IL-b as given in Table 4.3, indicating a better improvement of using the designed ILb. In addition, compared with the SEC in the MDEA process (1.56MJ/kgCO₂) and also in another IL ([bmim][NTf₂]) based process (0.86MJ/kgCO₂) reported in our previous work,²²¹ the IL-based process gives an improved energy-based technology.

Table 4.3 Process evaluation results in the two IL-based processes

	IL-a process	IL-b process
CO ₂ recovered from last flash (CO ₂ stream), kg/h	5541.6	5548.5
CO ₂ recovery rate, %	90.0	90.1
CO ₂ purity in CO ₂ stream, %	50.0	61.0
Solvent needed, kg/kg CO ₂	81.5	131.3
Total equivalent energy penalty, GJ/ton CO ₂	0.7	0.3
Electricity cost for CO ₂ removal process, \$/ton CO ₂	19.8	9.1
Total cost for CO ₂ removal process, \$/ton CO ₂	54.0	37.8
CH ₄ purity in CH ₄ stream, Vol%	96.1	96.1
CH ₄ recovery rate, %	95.5	97.2
Utility cost to produce CH ₄ in D1, \$/ton CH ₄	12.0	12.0
Total cost to produce CH ₄ in whole shale gas separation process, \$/ton CH ₄	29.8	26.3
C ₂ H ₆ purity in C ₂ H ₆ stream, Vol%	96.0	97.5
C ₂ H ₆ recovery rate, %	65.8	74.7
Utility cost to produce C ₂ H ₆ in D2, \$/ton C ₂ H ₆	30.2	29.1
Total cost to produce C ₂ H ₆ in whole shale gas separation process, \$/ton C ₂ H ₆	263.8	208.5

Note: D1, D2 denote the two distillation columns.

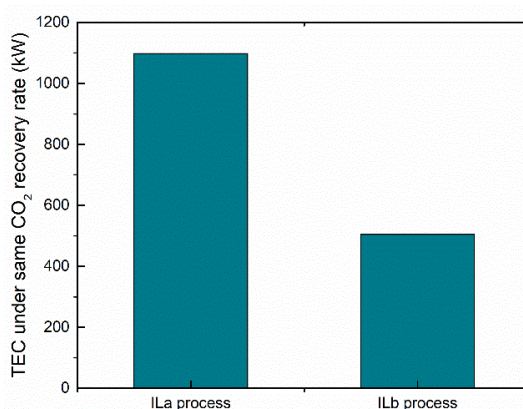


Figure 4.8 The total energy consumption (TEC) for the CO₂ removal process in the two IL-based processes

Economic analysis

For CO₂ removal process, the distribution of total removal cost (TRC) per ton CO₂ is shown in Figure 4.9. It can be observed that the total operating expense (OPEX) occupies more than 90% of the annualized total removal cost. Even though the high price of IL, the solvent make-up per year is around 1560\$/year which occupies little of the OPEX. The main utility cost is electricity consumed by compressor and pumps due to gas and solvent recovery. Besides the fixed operating cost (FOC), the variable operating cost (VOC) is the second dominating contributor to the OPEX. This illustrates the importance of reducing the total energy consumption. Compared with the IL-a process, the higher selectivity of CO₂/CH₄ in IL-b process gives a reduction of 54% and 30%, respectively for electricity cost and TRC of per ton CO₂ removal. Additionally, compared with the conventional amine-based processes reported by other researchers in total cost (for instance, 55\$/ton CO₂ by Hassan et al.²³³ 74€/ton CO₂ by Raynal et al.²³⁴ 112\$/ton CO₂ by Mores et al.²²⁹ and 70\$/ton CO₂ by Huang et al.²²²), the designed IL-b process cost (38\$/ton CO₂) is lower, demonstrating the important effect of the selectivity property of a solvent on the whole process. The cost for IL-a process (54\$/ton CO₂) is similar to the above reported costs for traditional technology. Both these two processes indicate a promising cost-efficient technology for IL-based CO₂ removal.

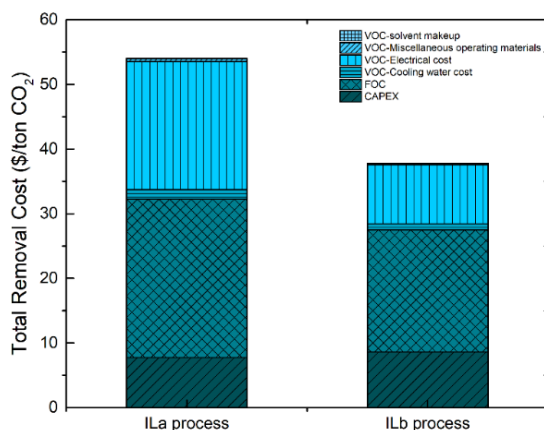


Figure 4.9 Comparison of total cost for CO₂ removal in the two IL-based processes

For the light hydrocarbon gas separation, as given in Table 4.3, two high-purity streams (CH₄ and C₂H₆ gas streams with more than Vol 96%) could be obtained as two commercial products in both the IL-based processes. Some performance criteria are compared under the same gas purity rate.

The utility applied in distillation column to produce each gas and the total cost of the whole separation process to produce per ton gas are calculated and shown in Table 4.3. It is found that

the utility cost to produce light hydrocarbon gases in the two distillation columns in IL-b process is slightly lower than that in IL-a process. This is because the higher selectivity of CO₂ to other gases in IL-b, leading much more light hydrocarbon gases that come out from top of the absorber in the IL-b process than that in IL-a process. Similarly, combined with the lower cost in CO₂ removal process, the total cost for these two gases production processes could be reduced much more in IL-b process than in IL-a process, especially for C₂H₆. However, considering the higher recovery rate of CH₄, C₂H₆ and lower total cost for CO₂ removal, the designed IL-b process points to a better choice than the IL-a process. According to the price of commercial CH₄ (~2400\$/tonCH₄²³⁵), this further light hydrocarbon gas separation has the potential to achieve a good profit. Note also that additional energy could be reduced through the use of other hybrid technologies for the light hydrocarbon gases separation such as combined with membrane²⁶ or adsorption processes, which is a topic for future consideration.

4.1.6 Conclusion

This chapter proposes a hybrid IL-based technology for gas separation process where the IL is used to remove the gas in small amount to obtain the desired final products. A three-stage methodology, in which systematic IL screening, process design and simulation, and process evaluation, is established. For the model shale gas considered, two ILs are selected through the two options: IL-a ([thtdp][phos]) is identified through an experimental database while IL-b, ([MMpy][eFAP]) is obtained using a model-based option to find additional IL based on the design method of CAILD.

The two IL-based CO₂ removal processes followed by distillation for hydrocarbon gas separation are simulated and evaluated in terms of energy consumption and economics. Even though larger amount of IL-b is needed, the higher selectivity of CO₂/CH₄ helps to not only obtain a higher purity CO₂ gas under the same gas recovery rate, but also achieve a 54% lower total energy demand, compared with IL-a process, resulting in a lower total removal cost per ton CO₂ to around 30%. Economic analysis shows that the operation expense (OPEX) is one of the main contributors to the total removal cost of per ton CO₂ separation, showing an importance of reducing the total energy demand. High purity (>Vol96%) of CH₄ and C₂H₆ gas streams could be obtained as products with a good profit in both IL-based separation processes, with much better results for IL-b process. As a result, IL-b with its good separation results, designed through option-b, provides a promising recommendation for future solvent development of gas separation process.

4.2 NATURAL GAS SWEETENING

This chapter forms the basis of following unpublished work:

Chen, Y.; Meng, X.; Cai, Y.; Kontogeorgis, G. M.; Woodley, J. M.: Natural gas sweetening using tailored ionic liquid-methanol mixture solvent with selective removal of H₂S and CO₂. (Energy and Environmental Science). In preparation.

Abstract

The removal of contaminants especially hydrogen sulfide (H₂S) and carbon dioxide (CO₂) from natural gas often requires complex processing strategies and therefore significantly influences the cost of the natural gas production. Natural gas has different range of composition depending on type, depth and location of the underground reservoirs and its composition from a given reservoir may even differs with time, which makes the purification process more challenging. In this regard, we present an ionic liquid (IL)-methanol mixture solvent that allows concurrent and selective removal of H₂S and CO₂ by tailoring the IL structure and its ratio in the mixture solvent.

4.2.1 Introduction

Natural gas, mostly identified as a clean energy source, has become one of the most attractive fuels in the world's supply of energy. Besides its primary use as a fuel, natural gas is also an important source of hydrocarbons for petrochemical feed stocks.¹ Nature gas has diverse energy-related applications from industrial use to the production of electricity.² In contrast to conventional fuels such as gasoline and diesel, natural gas produces much less CO₂, SO₂ and NO_x, with no particulate matter emissions and thereby has reduced adverse impact on the climate and the environment.³ The increase in natural gas supply provides a prospect for meeting the world's growing demand for clean energy in the future. However, raw natural gas usually contains many impurities (e.g. CO₂, H₂S, C₂₊) and the presence of these impurities often associated with severe corrosion problems that can damage the equipment system and even lead to pipe rupture.⁴ H₂S with the characteristic foul odor of rotten eggs is very poisonous, corrosive, and flammable. It is must be noted that H₂S presents odorless when its concentration in the air exceeds a certain value. CO₂ is another major acid gas contaminant and its presence contribute to a major cause of the corrosion problems. Therefore, these impurities especially H₂S and CO₂ need to be removed from natural gas to meet the criteria of the pipeline transportation and the quality standards of the gas products.⁵ The removal of such impurities remains one of the most critical concerns in the natural gas industry.

To date, various separation methods have been studied for the upgrade of natural gas and each of them have their own advantages and limitations relative to others. Among them, adsorption process is a major commercial technology that has been widely used to process natural gas in industry. Generally, absorption process using chemical solvent such as monoethanolamine

(MEA), diethanolamine (DEA), triethanolamine (TEA), diisopropylamine (DIPA) or methyl diethanolamine (MDEA) has high absorption capacity but also demands high energy for the solvent regeneration, while physical solvent process is preferred for feed gas with low temperature and high acid gas concentrations.⁶ The Selexol process using a physical solvent made of dimethyl ethers of polyethylene glycol (DEPG),¹³ is selective toward removing sulfur compounds but not typically remove enough CO₂ to meet the pipeline gas requirements. Glycerol carbonate is another physical solvent that has high selectivity of removing CO₂, but the capacity is relatively low. The Rectisol process using methanol as a solvent has been widely used in industry due to it has some advantages (e.g. noncorrosivity, low viscosity, availability) over other physical solvents. However, Rectisol process must be operated at very low temperature due to the high vapor pressure of methanol, which can result in substantial solvent loss and enormous elevation of power consumption.⁶

In the purification process of natural gas, H₂S and CO₂ need to be optimally removed due to they can cause serious equipment corrosion, environmental and/or health problems. The concentration of CO₂ and H₂S in natural gas varies drastically from one gas well to another, and from region to region, and even differs with time in a given reservoir.⁶ It is very challenging to have concurrent removal of H₂S and CO₂ since they are competitively captured at the same adsorption position in almost all the commercially and benchmark available adsorbents. Mostly, chemical and physical solvents such as MEA, MDEA and DEPG are selective toward removing H₂S or CO₂ and therefore it is very difficult to meet the pipeline specifications for both H₂S and CO₂. In addition, the problem of solvent's loss due to their high volatilities and the high energy requirement for their regeneration is also encountered in the natural gas purification process while using these organic solvents. In industrial operations, qualified natural gas can be achieved at the expenses of using large amount of solvent. Nevertheless, such a gas processing scheme would significantly increase the equipment size and the energy consumption. Therefore, an adsorbent that is capable to simultaneously control the removal of H₂S and CO₂ is highly desired as it can provide a universal alternative for processing the natural gas with different concentrations of H₂S and CO₂.

By far, ILs have been widely studied as solvents for gas separations.^{7, 8} However, these gas separation processes are often limited to the high viscosity and high cost of ILs. On the other hand, the use of methanol with low viscosity and high availability is usually limited to its high vapor pressure. Conceivably, a mixture solvent combining IL and menthol that has both advantages of IL and methanol may provide a potential alternative in the gas separation process. To date, only a few studies on the use of IL-methanol mixture solvent in the separation process can be found in the literature² and investigations regarding its application for the concurrent removal of H₂S can CO₂ have never been reported.

Although the use of IL-methanol mixture solvents offers unexpected opportunities for the upgrade of natural gas, there are still some challenging issues that need to be addressed before its practical application. Firstly, it is very essential to find a suitable IL due to different ILs

generally present with very distinct properties and separation performances, however, the very limited experimental data of the IL-natural gas system is a major challenge in this regard. Secondly, how to effectively control the H₂S/CO₂ selectivity of the mixture solvent in correspond to nature gas with different H₂S and CO₂ concentrations also challenges the upgrading process. The uncertainty of the process operation is another challenging problem need to be dealt with accordingly, otherwise deterioration of performance and production losses may occur. Herein this chapter aims to explore the possibility of using IL-menthol mixture solvent for concurrent and selective removal of H₂S and CO₂ by trying to solve the challenging problems described above. In addition, experimental studies are also carried out to elucidate the mechanism governing the selective adsorption of H₂S and CO₂.

4.2.2 Tailor-made IL-methanol mixture solvent

Currently, experimental data and computational models are the two major approaches used for solvent screening. The experimental based method is usually preferred since it can provide more reliable results. However, due to lack of sufficient experimental data of IL-natural gas systems especially IL-H₂S system, it is very limited to select suitable ILs to process natural gas containing H₂S. On the other hand, predictive property models such as GC-based and UNIFAC-IL-Gas models have been developed in Section 2. This make it possible of using computer-aided design method to find suitable IL-methanol mixture solvents for processing natural gas.

4.2.2.1 Formulation of the design problem

In the design problem of IL-methanol mixture solvent, the objective is to maximize the solvent separation performance of the designed IL-methanol mixture solvent, which is a function of the binary, integer and continuous variables subject to a series of structural (IL molecule), property (pure & mixture) and process model constraints (composition). This can be formulated as a MINLP optimization problem described as:

$$\max/\min_{z,y} f(z,y)$$

s. t. IL structural constraints: Eqs.3.7-3.13

IL pure property constraints: Eqs.4.1-4.2

IL – methanol mixture property constraints:

$$\frac{1}{x_{IL}} + \frac{\partial \ln \gamma_{IL}}{\partial x_{IL}} \geq 0 \quad 4.9$$

process model constraints:

$$x_{IL} + x_{methanol} = 1 \quad 4.10$$

Eq.4.9 is used to fulfil the necessary and sufficient condition for the phase stability of IL-methanol mixture. In this equation, x_{IL} denotes the mole fraction of IL in this binary mixture and the activity coefficient of IL, γ_{IL} , can be calculated from UNIFAC-IL model. Eqs.4.10 gives a process model constraint describing the composition of a binary mixture in terms of the mole fraction of IL and methanol ($x_{methanol}$).

4.2.2.2 Solvent targeted removal of H₂S

While searching for mixture solvent is selective toward removing H₂S, the objective function of the design problem can be described as following:

$$\max_{z,y} f(z,y) = \frac{\gamma_{CH_4}^{\infty} \gamma_{MeOH, CH_4}^{\infty}}{M_{IL} \gamma_{H_2S}^{\infty} \gamma_{MeOH, H_2S}^{\infty}} \quad 4.11$$

where $\gamma_{MeOH, CH_4}^{\infty}$ and $\gamma_{MeOH, H_2S}^{\infty}$ are the infinite dilute activity coefficient of CH₄ and H₂S in methanol, respectively. The molar weight (M_{IL}) of different ILs varies a lot but their cost are mostly based on the weight consumption. For this reason, M_{IL} is also included in the objective function.

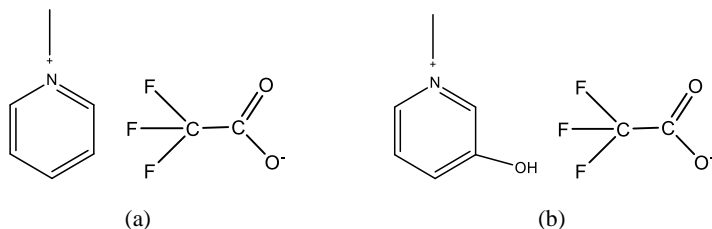


Figure 4.10 The structure of [C₁Py][TFA] (a) and [C₁OHPy][TFA] (b)

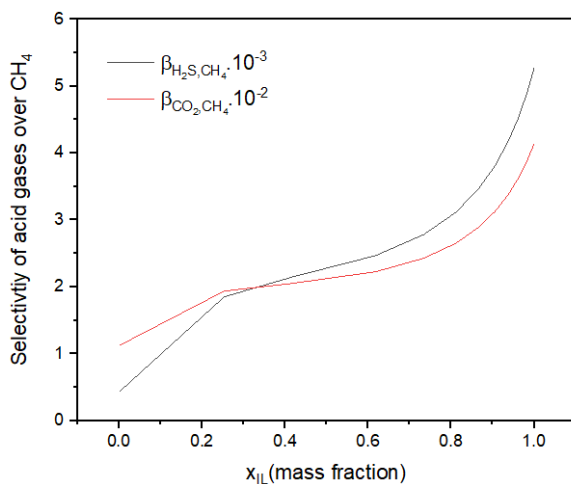


Figure 4.11 Removal selectivity of H₂S and CO₂ over CH₄ in [C₁Py][TFA]–methanol mixture solvent with different compositions

By solving the formulated MINLP problem with the objective function of Eq.4.11, ionic liquid 1-methylpyridinium trifluoroacetate ([C₁Py][TFA]) with the highest affinity towards H₂S is identified for use in IL-methanol mixture solvent. Figure 4.10 (a) gives the structure of [C₁Py][TFA] and Figure 4.11 presents the removal selectivity of H₂S and CO₂ over CH₄ in [C₁Py][TFA]–methanol mixture solvent with different compositions.

4.2.2.3 Solvent targeted removal of CO₂

While searching for mixture solvent is selective toward removing CO₂, the objective function of the design problem can be described as following:

$$\max_{z,y} f(z,y) = \frac{\gamma_{CH_4}^{\infty} \gamma_{MeOH, CH_4}^{\infty}}{MIL \gamma_{CO_2}^{\infty} \gamma_{MeOH, CO_2}^{\infty}} \quad 4.12$$

where $\gamma_{MeOH, CO_2}^{\infty}$ is the infinite dilute activity coefficient of CO₂ in methanol.

By solving the formulated MINLP problem with the objective function of Eq.12, ionic liquid 3-hydroxy-1-methylpyridinium trifluoroacetate ([C₁OHPy][TFA]) with the highest affinity towards CO₂ is identified for use in IL-methanol mixture solvent. Figure 4.10 (b) gives the structure of [C₁OHPy][TFA] and Figure 4.12 presents the removal selectivity of H₂S and CO₂ over CH₄ in [C₁OHPy][TFA]–methanol mixture solvent with different compositions.

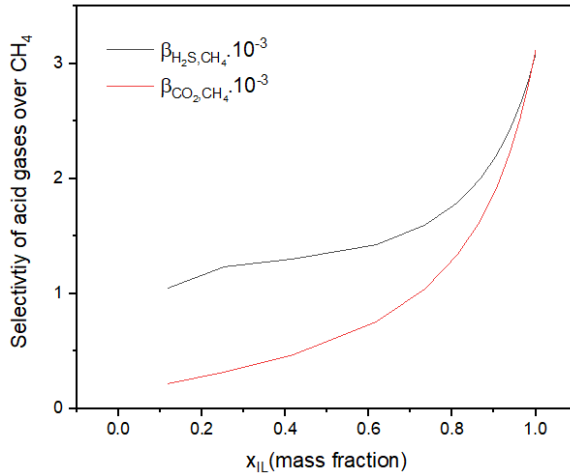


Figure 4.12 Removal selectivity of H₂S and CO₂ over CH₄ in [C₁OHPy][TFA]–methanol mixture solvent with different compositions

4.2.3 Case study on industrial-scale natural gas upgrading

In this section, case study on natural gas upgrading process is carried out to investigate the potential of using IL-methanol mixture solvents. One of the world's largest natural gas purification plants in China is taken as the case. The annual processing capacity of raw natural gas (high-sulfur) in this plant is 12 billion cubic meters. The purification standards for the two main acid gases are H₂S content ≤6mg/m³ and CO₂ ≤3 mass%. Table 4.4 gives the mole composition of raw gas detected in three different time periods. Obviously, the concentration of CO₂ and H₂S differs with time from the same production well.

Table 4.4 Composition of raw natural gas in three different time periods

Components	Composition 1, mole%	Composition 2, mole%	Composition 3, mole%
CH ₄	77.53	70.61	74.49
C ₂ H ₆	0.01	0.01	0.02
C ₃ H ₈	0.00	0.00	0.00
H ₂ S	14.90	20.27	16.51
CO ₂	7.14	70.61	8.49
H ₂	0.01	0.01	0.01
N ₂	0.41	0.57	0.48

4.2.3.1 Process design and simulation

In this work, a natural gas upgrading process using IL-methanol mixture solvent is proposed (see Figure 4.13). After mixing with the retrieved gas (compressed from the top of Flash unit) in mixer 2 (MIX2), the high-pressure raw gas is cooled down in HE1 and then fed to the bottom of absorption column (Column 1). Meanwhile, make-up IL and methanol are added to the recycled mixture solvent pumped from the bottom of distillation column (Column 2), and then fed to the top of absorption column after being cooled in Cooler 1. Afterwards, the purified gas is obtained from the top of Column 1 and the impurity gases retained in the mixture solvent are sent to the flash unit. By controlling the pressure and temperature, the retrieved gas containing most absorbed CH₄ escapes from the top of the flash unit is recycled back to the absorption column, while the acid gas-rich solvent is withdrawn from the bottom and then sent to the distillation column to desorb the remaining dissolved gases. In Column 2, the mixture solvent from the bottom is recycled back to the absorption column and the removed gas (e.g. H₂S, CO₂) from the top enters the next processing unit.

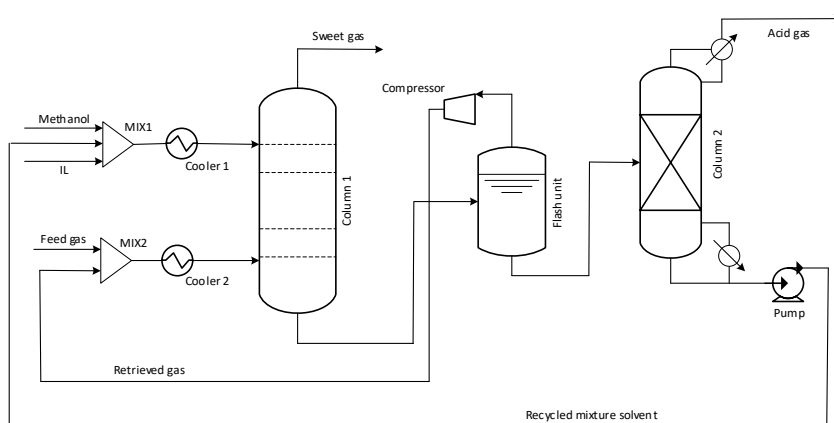


Figure 4.13 Natural gas upgrading process using IL-methanol mixture solvent

As a model-based representation of chemical and other technical processes in software, process simulation typically provides informative knowledge for a particular process prior to its industrial application. In this work, a commercial software, Aspen Plus, is used to simulate the natural gas sweetening process as described by Figure 4.13. To date, ILs are not included to the component database in Aspen Plus and therefore they are generally introduced as pseudo-components by specifying their molecular information such as molar weight, physical and critical properties. Besides this information, a suitable thermodynamic model is also necessary to predict the thermodynamic behaviors of the studied IL containing systems. In this case, physical properties of ILs are calculated from GC-based property models develop in Section 2.2 and their critical properties are estimated from the fragment contribution-corresponding states method developed by Huang et al.⁹ Meanwhile, the UNIFAC-IL-Gas model proposed in Section 2.3 is used for the thermodynamic calculations of the studied separation systems.

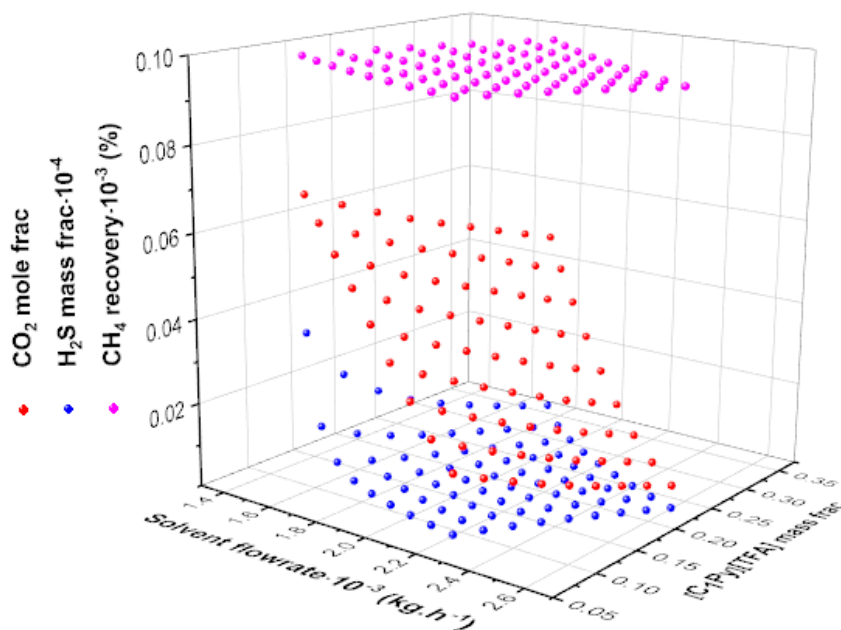


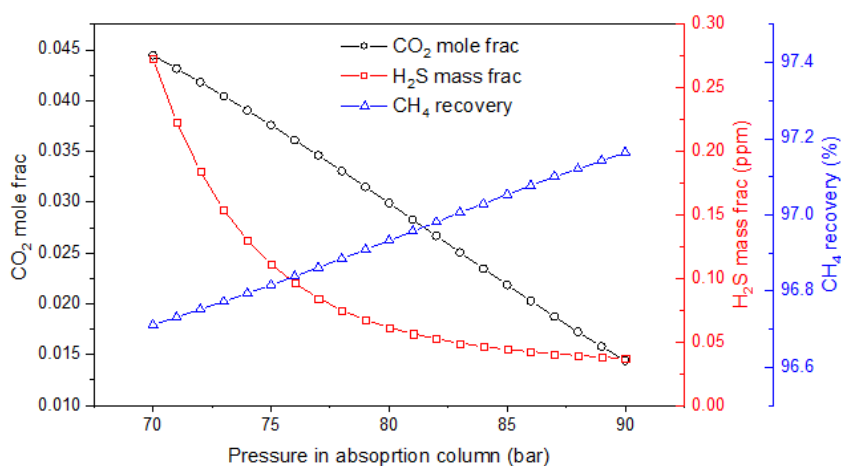
Figure 4.14 Influence of solvent flowrate and solvent composition on the recovery of CH₄ and the purity of sweet gas

4.2.3.2 Results and discussion

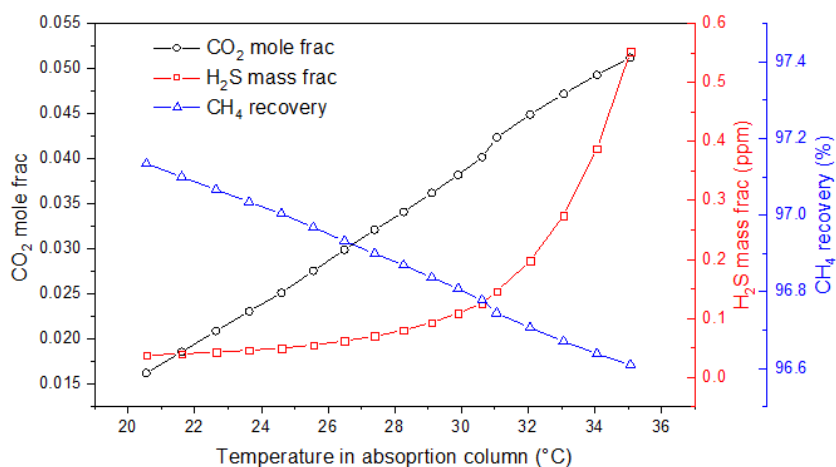
In this case, the raw natural gas has high H₂S content and therefore [C₁Py][TFA] towards removing H₂S is selected for use in the IL-methanol mixture solvent. In order to obtain an optimal process satisfying all process constraints especially the quality standards specified on H₂S and CO₂, influence of each process variable on the process performance need to be carefully investigated. By varying the solvent flow rates and the ratio of [C₁Py][TFA] in the mixture solvent, the recovery of CH₄ and the purify of sweet gas mainly expressed by the H₂S

and CO₂ content are obtained and provided in Figure 4.14. As expected, the remained H₂S and CO₂ in sweet gas decrease with the increase of solvent flowrate. Meanwhile, these two acid gases in sweet gas increase while the ratio of [C₁Py][TFA] increases in the mixture solvent but the increase of CO₂ shows larger than H₂S, this can be explained by that the soluble capacity of H₂S and CO₂ in methanol (mass-based) is higher than that of [C₁Py][TFA] but such difference on H₂S is smaller than CO₂. In contrast, both the solvent flowrate and the ratio of [C₁Py][TFA] in the mixture solvent have limited impact on the recovery of CH₄ due to the solvent components, i.e. methanol and [C₁Py][TFA], have very low solubility of CH₄.

Besides the solvent flowrate and its composition, operating variables such as pressure and temperature are also worth investigating since they directly impact the process operations. Figures 4.15 presents the recovery of CH₄ and the purity of sweet gas influenced by the pressure and temperature in absorption column. Clearly, the concentration of H₂S and CO₂ in sweet gas decreases with the increase of pressure in the absorption column, but the recovery of CH₄ increases with these changes. In contrast, the concentration of H₂S and CO₂ in sweet gas increases with increasing the temperature in this column, but the recovery of CH₄ decreases under the same condition. Obviously, the influence of both pressure and temperature on the concentration of H₂S in sweet gas is very limited when the concentration less than 0.05ppm. It was found that the recovery of CH₄ increases while the concentration of H₂S and CO₂ in sweet gas decreases, and vice versa. This can be explained as that H₂S and CO₂ are more competitive than CH₄ in occupying the solvent space for gas molecules and therefore less CH₄ is detained by the solvent when more H₂S and CO₂ dissolved.



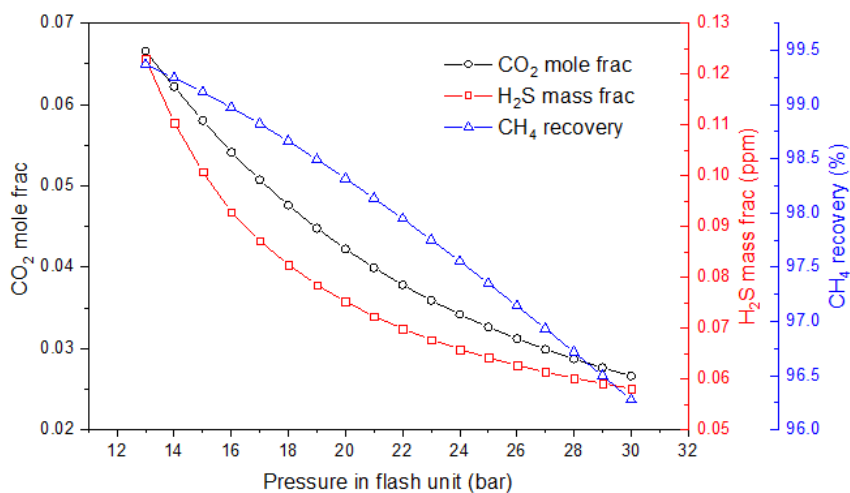
(a)



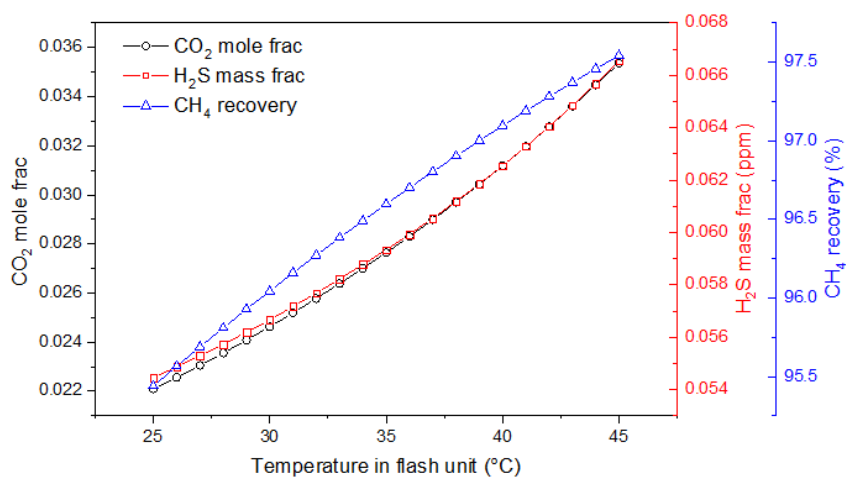
(b)

Figure 4.15 Influence of pressure (a) and temperature (b) in absorption column on the recovery of CH₄ and the purity of sweet gas

As shown in Figure 4.16, the concentration of H₂S and CO₂ in sweet gas as well as the recovery of CH₄ increase with the decrease of pressure or the increase of temperature in the flash unit. This is because more H₂S, CO₂ and CH₄ as retrieved gas are recycled back to the absorption column while decreasing the pressure or increasing the temperature in the flash unit. Nevertheless, the influence of pressure on the purity of sweet gas and the recovery of CH₄ are much bigger than the influence of temperature in this operating unit. For the distillation column, the concentration of H₂S in sweet gas increases greatly with the increase of pressure or decrease of reflux ration, as shown in Figure 4.17. This can be explained by the fact that more H₂S retained in mixture solvent is recycled back to the absorption column while increasing the pressure or decreasing the reflux ratio in the distillation column. On the other hand, these two operating variables show few influences on the concentration of CO₂ in sweet gas and the recovery of CH₄.

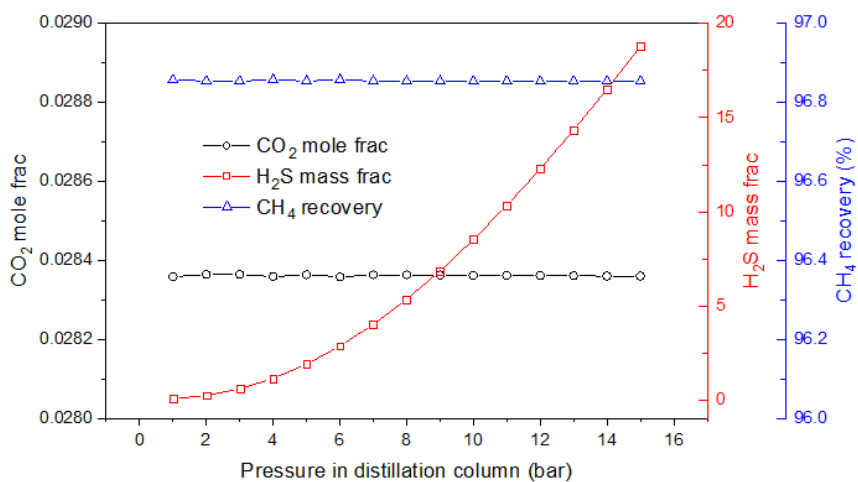


(a)

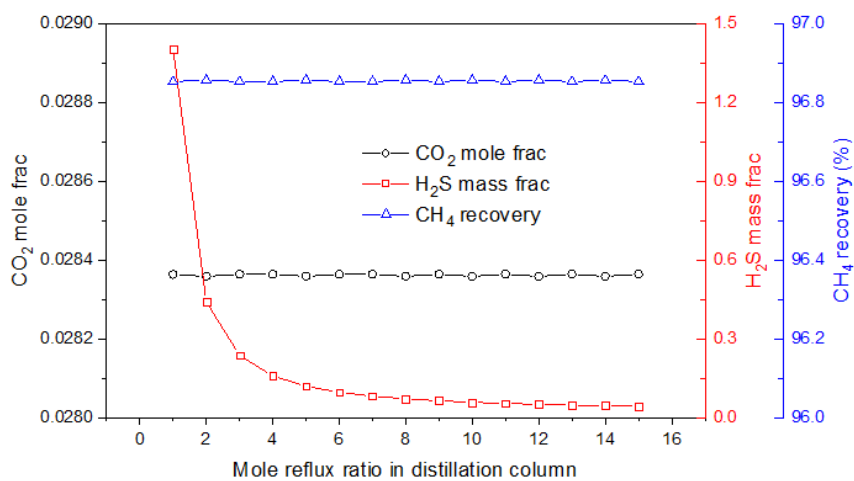


(b)

Figure 4.16 Influence of pressure (a) and temperature (b) in flash unit on the recovery of CH_4 and the purity of sweet gas



(a)



(b)

Figure 4.17 Influence of pressure (a) and reflux ration (b) in distillation column on the recovery of CH_4 and the purity of sweet gas

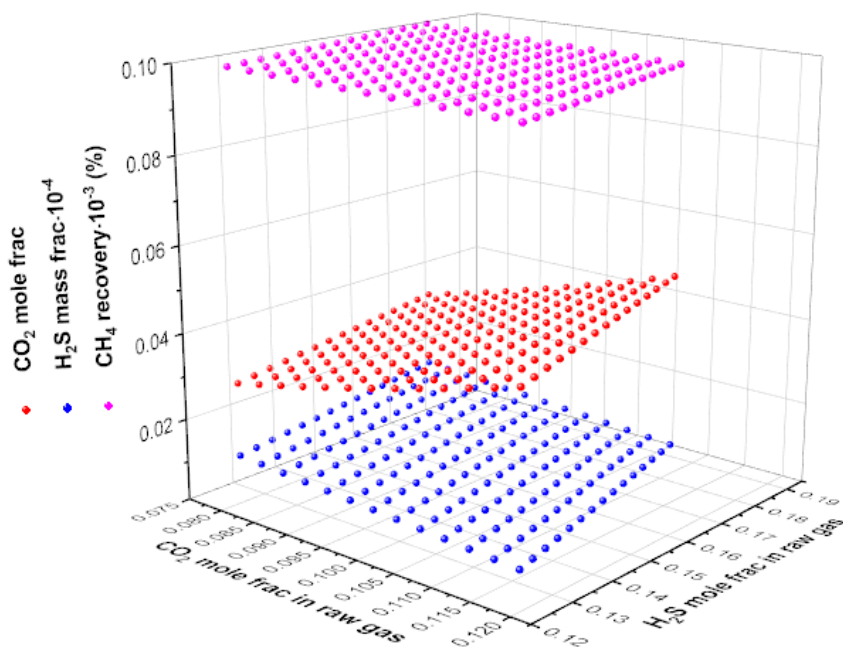


Figure 4.18 Influence of H₂S and CO₂ concentrations in raw natural gas on the recovery of CH₄ and the purity of sweet gas

The robustness of a design to industrial conditions is critical. In natural gas industry, the concentration of CO₂ and H₂S in raw natural gas varies drastically from one gas well to another, and from region to region, and even differs with time in a given reservoir. Therefore, it is of great importance to know the influence of CO₂ and H₂S concentrations in raw natural gas on the process operations. As shown in Figure 4.18, CO₂ and H₂S concentrations in raw natural gas have little impact on the recovery of CH₄. As expected, the concentration of CO₂ in sweet gas increases with the increase of CO₂ or H₂S concentration in raw natural gas and the concentration of H₂S in sweet gas increases with the increase of H₂S concentration in raw natural gas. However, the concentration of H₂S in sweet gas decreases while increasing the concentration of CO₂ in raw natural gas.

Simulation results show that natural gas upgrading process using IL-methanol mixture solvent has two main advantages over the MDEA-based process which is currently applied in the studied natural gas purification plant: 1. The proposed process demands much less solvent due to IL-methanol mixture solvent has higher solubility and selectivity of H₂S and CO₂ over CH₄ than MDEA-based solvent; 2. The regeneration of IL-methanol mixture solvent is achievable by using low-temperature waste heat while a large amount of heating utilities are required to regenerate MDEA-based solvent, which means that the proposed process has much energy

performance than the current commercial (MDEA-based) process. Detailed energy and economic evaluations will be provided in the near future.

4.2.4 Experimental section

Experimental work is going on.

4.2.5 Conclusions

This chapter presents an IL-methanol mixture solvent that allows concurrent and selective removal of H_2S and CO_2 by tailoring the IL structure and its ratio in the mixture solvent. Purification process using such a mixture solvent is capable to process natural gas with a wide range of H_2S and CO_2 concentrations. Afterwards, an industrial-scale natural gas upgrading process using IL-methanol mixture solvents is further simulated and evaluated. Computer-aided design methods are used to identify the optimal IL towards removing H_2S or CO_2 . The results indicate that CO_2 and H_2S can be effectively removed by the designed IL-methanol mixture solvent and the removal selectivity of these two acid gases can be easily tuned by adjusting the ratio of IL and methanol, in response to the gas feed with different CO_2 and H_2S concentrations. Remarkably, the natural gas upgrading process using IL-mixture solvent has much better process performance than the current commercial (MDEA-based) natural gas upgrading process. The proposed mixture solvent offers the prospect of lowering the purification cost in the production of natural gas. This IL-methanol mixture solvent can also be used in the oil and petroleum refining industries, where CO_2 and H_2S are also one of the main impurities in refinery-off-gas (ROG) and syngas. It to be noted that experimental studies of this case are going on. Experimental results as well as the detailed energy and economic evaluation on the proposed natural gas upgrading process will be provided in the near future.

5 BIO-ISOPRENE RECOVERY

In this chapter, an IL-based bio-isoprene recovery process is presented.

Chapter structure and contents:

5.1 Bio-isoprene recovery

5.1 BIO-ISOPRENE RECOVERY

This chapter forms the basis of following publication:

Chen, Y.; Liu, X.; Kontogeorgis, G. M.; Woodley, J. M.: Ionic-Liquid-Based Bioisoprene Recovery Process Design. Industrial & Engineering Chemistry Research 2020, 59, 7355-7366.

Abstract

Bioisoprene, which can be produced from renewable feedstocks through fermentation, is a promising alternative to petroleum-derived isoprene. However, challenges including selection of feasible recovery techniques for bioisoprene should be addressed to achieve economic and technical competitiveness. In this work, ionic liquids (ILs) are first introduced as solvents for the recovery of bioisoprene. To describe the thermodynamic behavior, the UNIFAC-IL model is first extended to the bioisoprene systems as it combines gas-organic chemicals in IL containing systems. By using a computer-aided IL design (CAILD) method, 6 out of 248742 structurally constrained ILs are screened as optimal candidates for their further performance evaluation. Simulation results indicate that all 6 ILs have much better process performance than the alternative, isopropyl myristate. Moreover, $[N_{1,1,3,0}][DMP]$ is identified as the best IL with the lowest solvent flowrate and the highest recovery ratio of isoprene. This work shows the potential of using ILs for the recovery of bioisoprene from fermentation off-gas.

5.1.1 Introduction

Isoprene (2-methyl-1, 3-butadiene) is an important commodity chemical for producing a wide variety of industrial products including cis-polyisoprene or synthetic rubber used in tire manufacture, as well as elastomers used in surgical gloves, motor mounts, fittings, rubber bands, and shoes. Isoprene was first produced synthetically in 1860 by the pyrolysis of natural rubber.²³⁶ Since the 1970s, most isoprene production at an industrial scale comes from petrochemical resources and was first commercialized by a company now known as Nippon Zeon (Tokyo, Japan).²³⁷ In the process of petroleum steam-cracking, isoprene can be selectively and efficiently extracted from complex mixtures of hydrocarbons by extractive distillation using polar organic solvents.²³⁸ Therefore, at large scale isoprene with a competitive price can be produced from fossil feedstocks. Nonetheless, the current supply and demand balance as well as the demand for processes based on sustainable feedstocks within the global isoprene industry is at risk in the coming years. Furthermore, isoprene supply is further limited as availability of crude C5 feed streams for isoprene extraction is declining since the trend of using light hydrocarbons or natural gas as feedstock in the refining industry.²³⁶

With a growing industrial demand for isoprene and a simultaneous environmental imperative to reduce greenhouse gases, bioisoprene produced from renewable sources (e.g. glucose, sucrose) through fermentation is being considered as a potential alternative to petroleum-derived isoprene. To improve the yield of diene products, Abdelrahman and co-workers proposed a hybrid process of combining fermentation and thermochemical catalysis for reviewable isoprene produce.²³⁹ Most recent work shows that fermentation via mesaconic acid is also possible but provides few extra benefits over the *E.coli* process.²⁴⁰ Compared to the isoprene production from petrochemical resources, the biological process is more sustainable and environmentally friendly. Nevertheless, the costs of bioisoprene are slightly higher than the actual market price of its fossil counterpart and its global contribution is still small. Results obtained by Morais and co-workers reveal that the isoprene production by bacteria is able to substitute the petroleum-based process, with reasonable energy and material efficiency, but improvements are still required.²⁴¹ Current state-of-the-art technology has led to an improved sugar conversion in the fermentation process of isoprene and since the product has a boiling point of 34 °C, it can be recovered from the fermentation off-gas in a continuous process.²³⁶ Nonetheless, an advanced bioprocess that is capable of lowering the unit cost of bioisoprene is essential for its further commercial production.

The fermentation process to produce bioisoprene is aerobic and the oxygen continuously supplied by air while generated isoprene is released into the vapor phase (off-gas) together with water vapor, residual air gases (i.e. N₂, O₂) and produced gas (i.e. CO₂). This is unusual for fermentation processes, since the product usually resides in the liquid water phase. In principle when the product is found in the vapour phase it leads to a particularly attractive downstream process (as the product is separated from liquid by-product, water and cells merely by phase separation). However, the concentration of bioisoprene (vapor phase) in the off-gas is very low under aerobic conditions, while the concentration of isoprene (liquid phase) from the petrochemical source for extractive distillation is 10–20%.²³⁷ Therefore, the recovery efficiency of bioisoprene from off-gas in the downstream process is essential for its replacement of petroleum-derived isoprene.

Various methods^{242, 243} have been proposed for the recovery of bioisoprene from off-gas and among them, separation techniques of activated carbon absorption and solvent extraction have been mainly studied. McAuliffe's work shows that >80% bioisoprene can be recovered from the off-gas by using activated carbon absorption method²⁴⁴ and its separation performance also verified in Zou's work.²³⁷ This method is attractive to recover bioisoprene with low concentration at laboratory level, however, its application for large-scale isoprene recovery is still limited.²³⁷ For the recovery technique of solvent extraction, unlike the polar solvents such as acetonitrile, N-methylpyrrolidone, dimethylformamide used in the extraction process of isoprene from petrochemical feed streams, isopropyl myristate and isoparaffin are suggested for the recovery process of bioisoprene since both of them can extract isoprene from off-gas

efficiently. Recent work shows that the mixture of methyl carbitol and sulfolane is also capable of extracting isoprene.²³⁷

As most separation processes, the problem of solvent's escape into the atmosphere because of their high volatilities and the high energy requirement for their regeneration is also encountered in the bioisoprene recovery using conventional organic chemicals as solvents. On the other hand, ionic liquids (ILs) are being considered as potential alternatives for organic solvents in many separation processes (e.g. CO₂ capture, azeotropic separation).¹¹ To date, the cost of ILs is one of the main impediments to IL utilization. The current expense of IL is suggested as 30\$/kg by BASF from IL bulk production,²⁴⁵ while the market price of benchmark organic solvent (i.e. isopropyl myristate) is 2-3 \$/kg. However, the cost of IL is decreasing with the development of the cost-effective synthetic methods and the application of inexpensive raw materials.^{246, 247} As reported, large scale production of triethylammonium hydrogen sulfate ([HNEt₃][HSO₄]) will be as low as 1.24 \$/kg,²⁴⁸ which shows that ILs have potential to compete with conventional organic chemicals in terms of solvent cost.

In biotechnology, the application of ILs has been studied in various fields, ranging from solvents for extraction to reaction media for biotransformation.^{14, 138, 156, 168, 249-251} Additionally, the toxicity mechanism of ILs has been investigated for their environmental and health concerns,^{171-173, 252, 253} and a new synthesis of ILs completely derived from nature are being emerged since they are inexpensive, biocompatible, and biodegradable with low toxicity.²⁴⁷ Although the use of ILs offers unexpected opportunities in biotechnology, investigations regarding their application in the process of bioisoprene production have never been reported so far. This work aims to investigate the possibility of using ILs for the recovery of isoprene from fermentation off-gas.

5.1.2 ILs screening

Under aerobic fermentation conditions, bioisoprene is produced as a vapor-phase product released into the off-gas together with normal air components (e.g. N₂, CO₂, O₂) and water vapor. Generally, water is removed by using a dehumidifier unit before the further separation and recovery of isoprene. Therefore, the selected solvents should be able to extract bioisoprene efficiently and selectively from the air components remained in the fermentation off-gas. To find suitable ILs for this bioseparation task, the design method of CAILD is considered.

5.1.2.1 Specific extension of UNIFAC-IL model

13 gases are included in the UNIFAC-IL-Gas model developed in Section 2.3. In order to improve the model performance to the bio-isoprene recovery system, we specifically extend the UNIFAC-IL model to IL-gas systems only covering N₂, CO₂, O₂. As presented in Figure 5.1, 3 gases (N₂, O₂, CO₂), 4 conventional main groups and 20 IL main ionic groups are involved in this UNIFAC-IL model extension. The AARD (%) between experimental and calculated activity coefficient of N₂, O₂ and CO₂ are 10.2%, 9.2% and 12.1%, respectively,

showing the reliability of this extended UNIFAC-IL model. Comparisons between the experimental and calculated activity coefficients are presented in Figure 5.2. Comparisons of some experimental data that are not used in the regression and their corresponding predicted values from extended UNIFAC-IL model, as presented in Figure 5.3, illustrate the good predictive performance of this extended model.

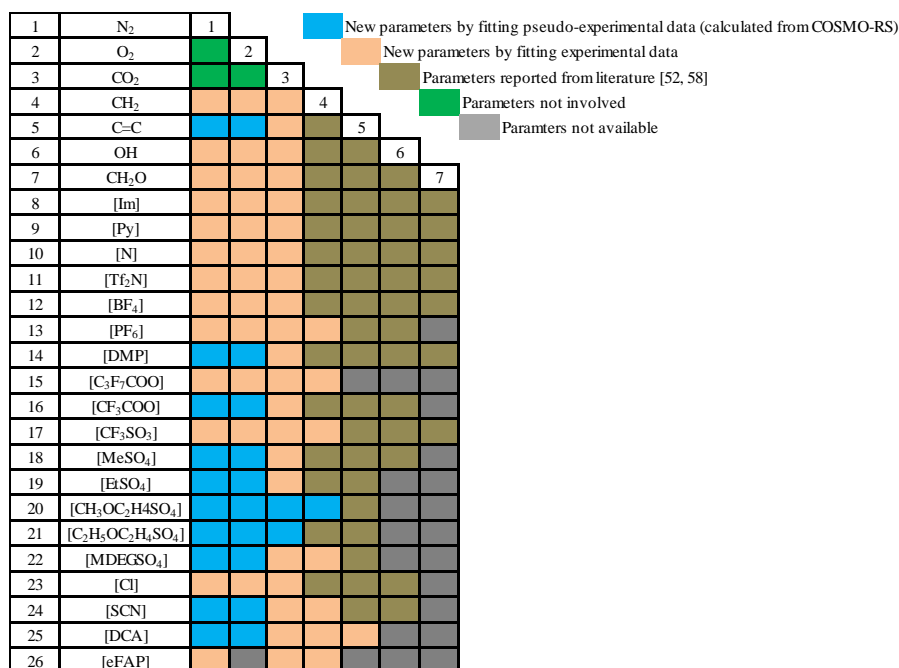


Figure 5.1 The extended UNIFAC-IL-Gas group interaction parameter matrix

5.1.2.2 Computer-aided optimal ILs design

Generally, normal air component gases (e.g. N₂, O₂) in the bioisoprene system have very low solubility in ILs under atmospheric pressure at room temperature from the published experimental works, and another air component gas, CO₂, is soluble in some ILs under high pressure at room temperature. Since the operation of isoprene recovery process is under atmospheric pressure in this case, it would be reasonable to set the infinite dilution solubility coefficient of isoprene as the objective function and set the infinite dilution selectivity coefficients as thermodynamic property constraints in the IL design stage. Based on the design objective function and the constraints on the IL structure and properties, the CAILD can be formulated as a MINLP problem (which is summarized in Table 5.1).

By solving the formulated MINLP problem, we find that all top optimal ILs from 248742 structural constrained ILs are the combinations of cation subgroup [C₃H₇N] and anion group [DMP] which can be explained based on the desired interactions between them and the groups

of isoprene and the other gas components (i.e. N₂, O₂, CO₂) for the separation purpose. Although more identified optimal ILs (e.g. 7ILs, 10ILs) can be evaluated by the process simulation method, only top 6 optimal ILs are selected as solvent candidates for their further performance evaluation as this is enough to demonstrate the performance of the identified ILs, as well as the reliability of the CAILD solution. The detailed information of the identified optimum ILs from CAILD solution are presented in Table 5.2. Their melting points and viscosities are less than 295 (K) and 50 (cP), respectively, as expected from the imposed constraints. The designed targets (i.e. infinite dilution solubility coefficients) of the ILs are ranked as follows: [N_{1,1,3,0}][DMP] > [N_{1,3,0,0-C=C}][DMP] > [N_{1,2,3,0}][DMP] > [N_{2,3,0,0-C=C}][DMP] = [N_{1,3,0,1-C=C}][DMP] > [N_{1,3,3,0}][DMP]. Moreover, ammonium-based cations generally have lower toxicity compared to the aromatic cations such as imidazolium and pyridinium rings²⁵³, which could improve the availability of these designed ILs in terms of environmental and health concerns.

Table 5.1 CAILD-based MINLP problem formulation

Objective function (maximization)	$S_{iso} = \frac{1}{M_{IL}\gamma_{iso}^{\infty}}$	S_{iso} : infinite dilution solubility coefficient of isoprene M_{IL} : molar mass of IL γ_{iso}^{∞} : infinite dilution activity coefficient of isoprene
molecular structural constraints	Eqs.3.7-3.13	
Physical property constraints	Eq.3.16 Eq.4.1	
Thermodynamic property constraints	$\beta_{iso,z} = \frac{P_z^s \gamma_z^{\infty}}{P_{iso}^s \gamma_{iso}^{\infty}} > 150$	$\beta_{iso,z}$: infinite dilution selectivity coefficient z: air component (i.e. N ₂ , O ₂ , CO ₂) γ_z^{∞} : infinite dilution activity coefficient of air component z P_z^s : vapor pressure of air component z P_{iso}^s : vapor pressure of isoprene

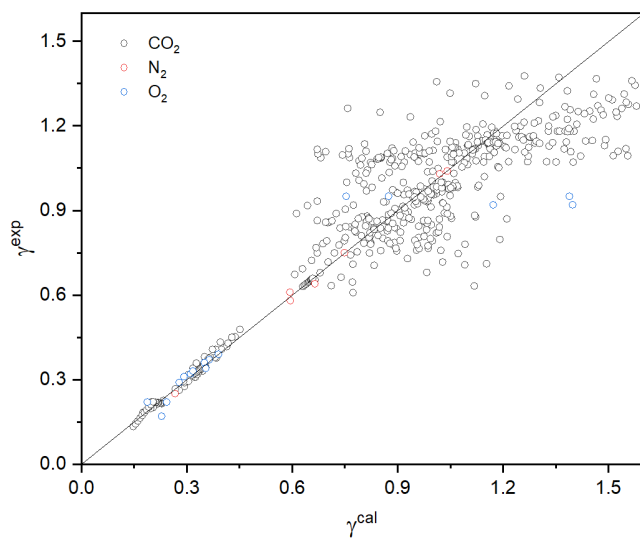


Figure 5.2 Comparison between experimental and calculated activity coefficient of N_2 , O_2 and CO_2 using extended UNIFAC-IL model

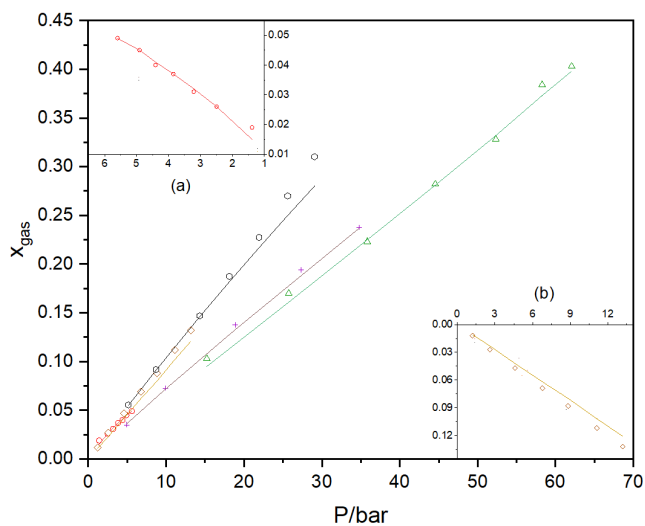
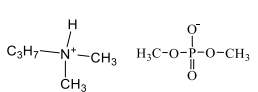
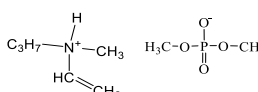
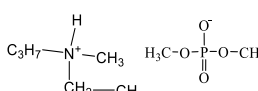
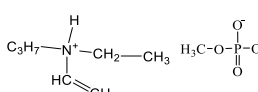
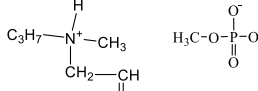
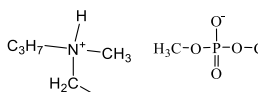


Figure 5.3 Comparisons of experimental data²⁵⁴⁻²⁵⁷ and predicted values for x_{gas} - P covering $[CH_3OC_2mIm][Tf_2N]-N_2$ at 303.15K (\circ) in (a), $[emIm][EtSO_4]-CO_2$ at 303.15K (\diamond) in (b) and 323.15K (Δ), $[emIm][BF_4]-CO_2$ at 298.2K (\circ) and 313.2K ($+$). Lines are predicted results using the UNIFAC-IL model extended in this work

Table 5.2 Detailed information of identified optimum ILs from CAILD method

ILs	Structure	MW (g.mol ⁻¹)	$S_{iso} * 10^2$	T_m (K)	η (cP)	$\beta_{iso,z}$	
[N _{1,1,3,0}][DMP]		213.22	7.700	233.0	42.67	N ₂	258.8
						O ₂	373.9
						CO ₂	200.2
[N _{1,3,0,0-C=C}][DMP]		225.23	6.993	227.4	42.76	N ₂	252.7
						O ₂	329.0
						CO ₂	204.4
[N _{1,2,3,0}][DMP]		227.25	6.559	229.2	41.88	N ₂	259.7
						O ₂	341.9
						CO ₂	175.0
[N _{2,3,0,0-C=C}][DMP]		239.26	6.000	223.7	41.86	N ₂	230.7
						O ₂	302.1
						CO ₂	179.3
[N _{1,3,0,1-C=C}][DMP]		239.26	6.000	223.7	41.86	N ₂	230.7
						O ₂	302.1
						CO ₂	179.3
[N _{1,3,3,0}][DMP]		241.27	5.672	225.5	43.32	N ₂	238.5
						O ₂	315.6
						CO ₂	154.8

5.1.3 Process design and simulation

Two metabolic pathways, i.e. the 2C-methyl-D-erythritol 4-phosphate (MEP) pathway and the mevalonic acid (MVA) pathway, are known to synthesize isoprene.²⁵⁸⁻²⁶⁰ By far, the MVA pathway is the best characterized one as it has been exploited industrially for the production of isoprenoids in both yeast and bacteria.²⁶¹ The production of bioisoprene from glucose in presence of oxygen via *E. coli* engineered with MVA pathway can be expressed as in Figure 5.4, where the mass yield of isoprene on glucose is 25.2%.

As presented in Figure 5.4, *E. coli* engineered with MVA pathway to isoprene requires two O₂ per isoprene produced, while four CO₂ and 5 H₂O are generated as well. For this reason, most

produced H_2O should be discharged from the fermentor while isoprene, CO_2 and small amount of H_2O are removed as fermentation off-gas. Depending on the components in the off-gas of the bioisoprene system, a bioisoprene production process involving IL-based extraction recovery technique is proposed, as shown in Figure 5.5. In addition to recovery techniques for organic solvent based extraction and activated carbon, a dehumidifier unit is required before the contact of the steam with IL solvents since moisture may affect their absorption capacity. After removing the water from the fermentation off-gas, the remaining vapor components are sent to the absorption column, where the normal air components (i.e. N_2 , O_2 and CO_2) escape from the top of the column and isoprene is retained by the IL solvent. Due to the big volatility difference of isoprene and IL solvent, isoprene can be easily recovered from the IL solvent by using a simple flash unit. However, the operating temperature of the flash unit is limited since isoprene decompose at 120°C (<https://pubchem.ncbi.nlm.nih.gov/compound/Isoprene>). For this reason, here a vacuum flash evaporation is considered to recover the product from solvent as much as possible. Finally, a liquid isoprene product can be obtained after the condensation of the vapor isoprene from the top of the flash unit.

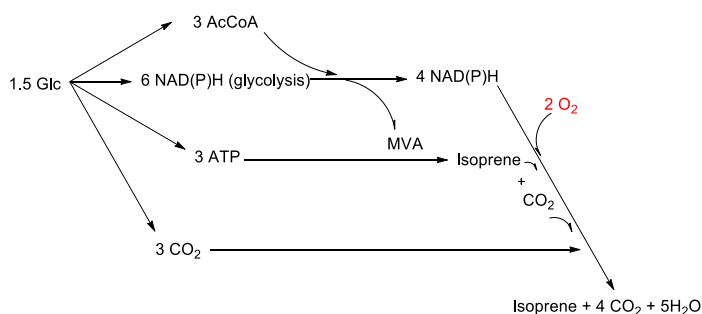


Figure 5.4 MVA pathway for producing isoprene from glucose in presence of oxygen (Glc, glucose; AcCoA, acetyl-coenzyme A; NADPH, nicotinamide adenine dinucleotide phosphate/reduced form; ATP, adenosine triphosphate)

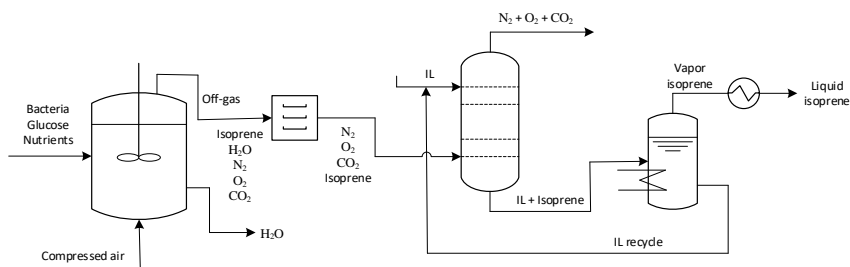


Figure 5.5 Bioisoprene production process by using IL-based recovery technique

Process simulation as discipline uses mathematical models as basis for analysis, prediction, testing, detection of a process behavior unrelated to whether the process is existing in reality or not. Process simulation is there to increase the level of knowledge for a particular process and chemical engineering in general (<https://simulatelive.com/simulate/steady-state/process-simulation-as-the-key-discipline-of-chemical-engineering>). In this work, Aspen Plus is employed as simulator for the detailed process simulation, where all 6 optimum IL candidates identified from the CAILD method are considered.

In this work, the task of the bioisoprene recovery process is to separate isoprene from N_2 , O_2 , and CO_2 in dehumidified off-gas by using IL solvent, and then recover isoprene from the IL solvent. In this process, isoprene should be recovered as much as possible while the other air components (i.e. N_2 , O_2 and CO_2) should be less retained. So far, isopropyl myristate is studied as the most promising organic solvent for the recovery of isoprene. Therefore, it is very important to compare the performance of the identified optimal ILs with the performance of this benchmark organic solvent. For the purposes of comparison, the bioisoprene recovery process of using isopropyl myristate as solvent is also simulated and optimized. The simulation of this recovery process is performed in Aspen Plus (V8.6), where absorption column is modeled by the RadFrac block and IL regeneration unit is modeled by the flash evaporation.

5.1.4 Results and discussions

In the design step of process simulation, key operating variables such as the number of stages and the flow rates of solvent are optimized by sensitivity and trade-off analysis. As demonstrated, sensitivity analysis on flow rates of solvent with the different number of stages (N) for using $[N_{1,3,3,0}][DMP]$ and isopropyl myristate as solvents are provided in Figures 5.6 and 5.7, respectively. As expected, the retained isoprene (%) increases with increasing solvent flowrate and the number of column stages. As shown in Figure 5.6, IL-based process has large difference of retained isoprene (%) with different number of stages at the region of low solvent flowrate. In contrast, this happens at the region of high solvent flowrate by using isopropyl myristate (see Figure 5.7). Nonetheless, $N=4$ is the optimal number of stages for both processes since the difference of retained isoprene (%) is very small at high product recovery region between $N=4$ and $N=5$. The simulation results with IL ($[N_{1,3,3,0}][DMP]$) show much better process performance than isopropyl myristate in terms of solvent flowrate and the percentage of product recovery.

To evaluate the influence of the solvent flowrate on the other containing gas components in off-gas, analysis on recovery percentage of isoprene and retained air gas components ($N_2+O_2+CO_2$) with certain number of stages ($N=4$) are also provided. As shown in Figures 5.8 and 5.9, air gas components exhibit a linear relationship with the flowrate of both $[N_{1,3,3,0}][DMP]$ and isopropyl myristate. The simulation results indicate that these gas components are generally more easily to be retained in isopropyl myristate than in $[N_{1,3,3,0}][DMP]$ with the same isoprene recovery, showing the better selectivity of $[N_{1,3,3,0}][DMP]$ for isoprene over the other air gas

components. Based on the trade-off analysis, the number of stages and the flow rate of solvent yielding the best performance of isoprene recovery and retained air components can be achieved for certain cases.

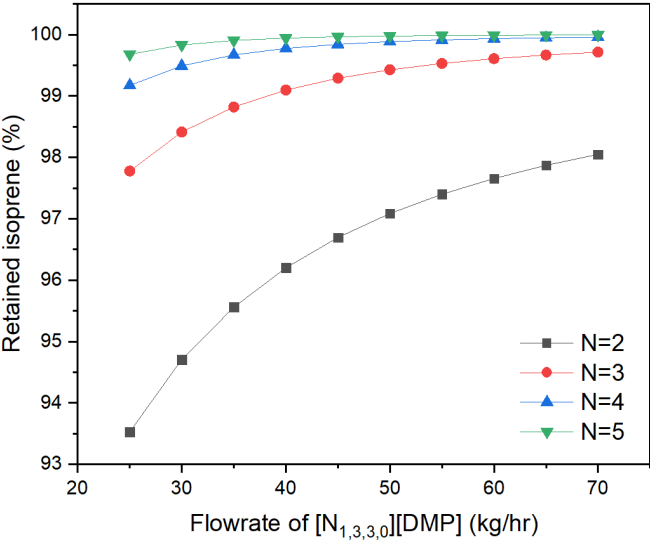


Figure 5.6 Retained isoprene (%) against the mass flowrate of $[N_{1,3,3,0}][DMP]$ in the absorption column with different number of column stages (N)

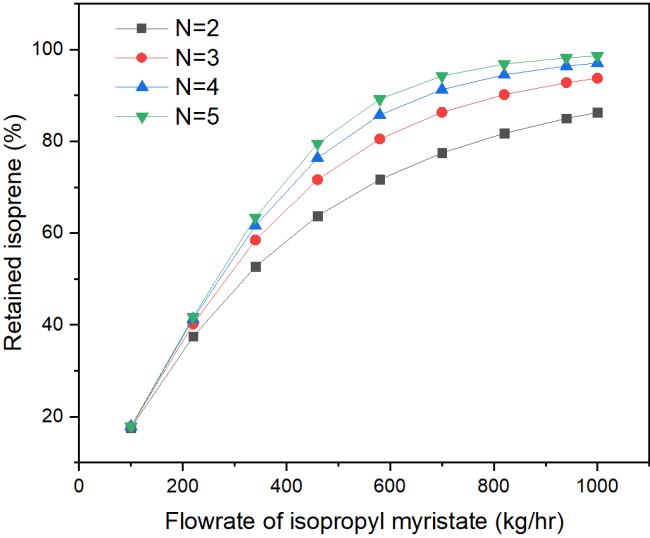


Figure 5.7 Retained isoprene (%) against the mass flowrate of isopropyl myristate in the absorption column with different number of column stages (N)

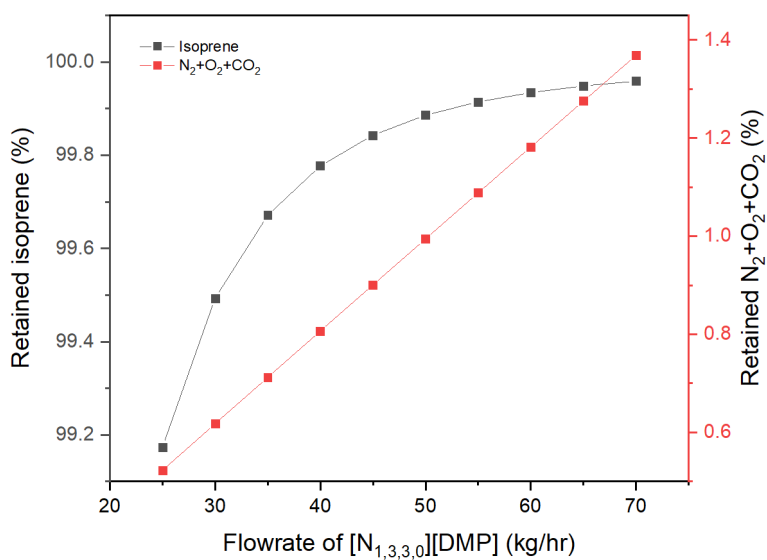


Figure 5.8 Retained isoprene and $N_2+O_2+CO_2$ (%) against the mass flowrate of $[N_{1,3,3,0}][DMP]$ in the absorption column with the number of column stages $N=4$

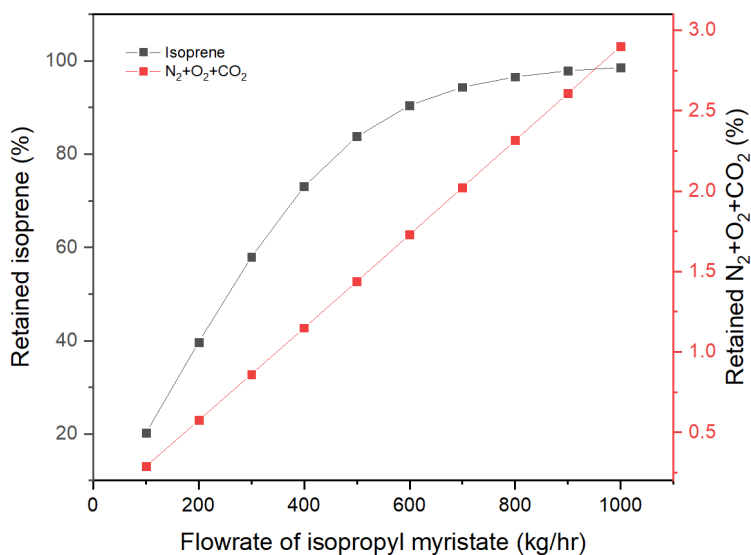


Figure 5.9 Retained isoprene and $N_2+O_2+CO_2$ (%) against the mass flowrate of isopropyl myristate in the absorption column with the number of column stages $N=4$

Table 5.3 Compositions of studied off-gas systems for sensitivity analysis

Off-gas	Isoprene (% v/v)	N ₂ (% v/v)	O ₂ (% v/v)	CO ₂ (% v/v)
Composition of system 1	1.89	75.47	15.09	7.55
Composition of system 2	2.75	73.40	12.84	11.01
Composition of system 3	3.57	71.43	10.71	14.29
Composition of system 4	4.35	69.56	8.70	17.39
Composition of system 5	5.08	67.80	6.78	20.34

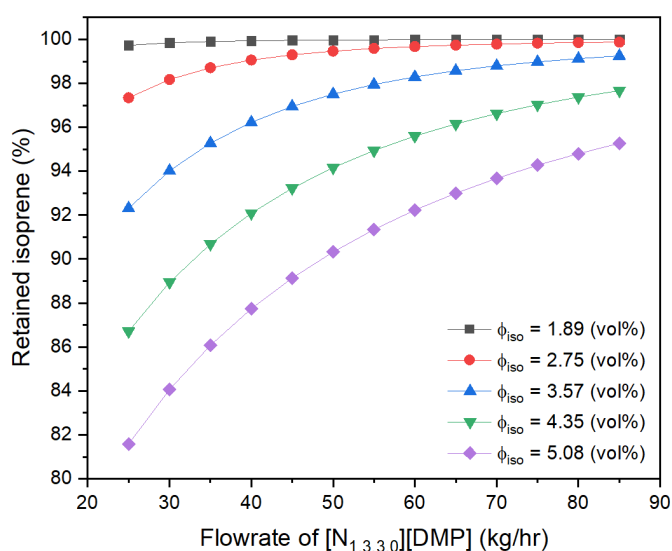


Figure 5.10 Retained isoprene (%) against the mass flowrate of [N_{1,3,3,0}][DMP] in the absorption column with different percent isoprene in off-gas (N=4)

Considering that the percent isoprene (ϕ_{iso}) and the levels of other gases such as CO₂ and O₂ in the off-gas has significant impact on its separation process, a sensitivity analysis on the composition of off-gas is also necessary. According to the MVA pathway to produce isoprene, the composition of the dehumidified off-gas can be calculated from the flowrate of compressed air and the volumetric productivity of isoprene. By using deep-tank culture conditions, a volumetric productivity of 2g/L/hr with a yield of 11% isoprene from glucose have been obtained in Cervin's work.²⁶² Based on this condition, the 5 bioisoprene systems with different percent isoprene are studied in this work, as shown in Table 5.3. Sensitivity analysis on different volume percent isoprene by using IL ([N_{1,3,3,0}][DMP]) and isopropyl myristate are presented in Figures 5.10 and 5.11, respectively. The simulation results show that the solvent flowrate in IL-based process is more sensitive to the composition of bioisoprene system than isopropyl

myristate -based process. This can be explained by the much lower flowrate of IL which is required in order to achieve the same recovery of isoprene. The simulation information of the recovery process for bioisoprene system using all identified ILs and isopropyl myristate are summarized in Table 5.4. The simulation results show that all 6 ILs have much better process performance than isopropyl myristate and $[N_{1,1,3,0}][DMP]$ is identified as the best IL with the lowest solvent flowrate and the highest recovery ratio of isoprene. We should note that the lower and upper explosion limits of isoprene in air are 1% (v/v) and 9.7% (v/v), respectively. But based on literature search performed, studies on the explosion limits in bioisoprene system have not yet been reported and this must be investigated before any practical implementation.

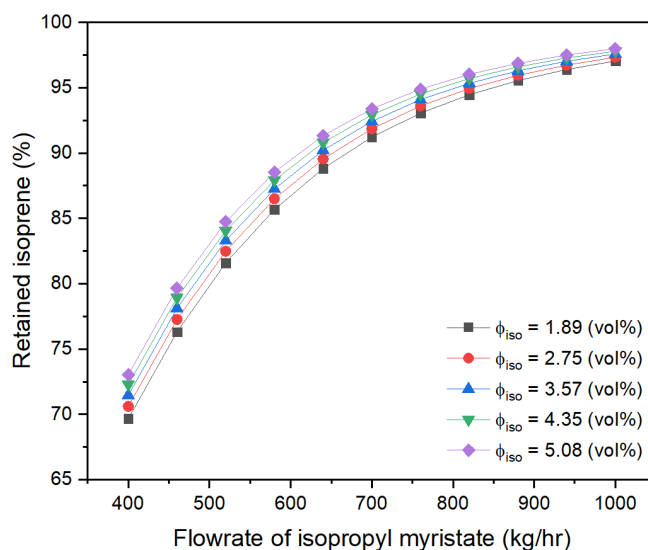


Figure 5.11 Retained isoprene and CO_2 (%) against the mass flowrate of isopropyl myristate in the absorption column with different percent isoprene in off-gas ($N=4$)

Table 5 Simulation results of the bioisoprene recovery process using different solvents

Solvents	Flowrate of solvent (kg/hr)	Recovery Ratio (%)	Purity of product (%)
$[N_{1,1,3,0}][DMP]$	48	85.05	99.50
$[N_{1,3,0,0-C=C}][DMP]$	56	84.73	99.50
$[N_{1,2,3,0}][DMP]$	53	84.28	99.50
$[N_{2,3,0,0-C=C}][DMP]$	57	83.17	99.50
$[N_{1,3,0,1-C=C}][DMP]$	57	83.17	99.50
$[N_{1,3,3,0}][DMP]$	63	82.84	99.50

Isopropyl myristate	340	76.77	87.15
---------------------	-----	-------	-------

Flowrate of dehumidified off-gas: 100 (kg/hr)

Composition of dehumidified off-gas (% v/v): Isoprene 4.35, N₂ 69.56, O₂ 8.70, CO₂ 17.39

Unit operating conditions: Absorption column (P=1 bar, N=4); Flash unit (P=0.01 bar, T=100 °C)

5.1.5 5. Conclusions

In summary, we have investigated the possibility of using ILs as solvents for the recovery of isoprene from fermentation off-gas. To describe the thermodynamic behavior of bioisoprene systems involved ILs, the UNIFAC-IL model that combines gases-organic chemicals is extended by using a wide range of experimental data from published works and a certain number of pseudo-experimental data from COSMO calculations. Based on this extended thermodynamic model, a CAILD-MINLP problem is formulated and solved, from where 6 out of 248742 structural constrained ILs are selected and further evaluated by means of process simulations in Aspen Plus. For comparison purposes, the isoprene recovery process using the typically used isopropyl myristate is also simulated and optimized. Simulation results show that all 6 ILs have much better process performance than isopropyl myristate and [N_{1,1,3,0}][DMP] is identified as the best IL with the lowest solvent flowrate and the highest recovery ratio of isoprene.

Although experimental verification of these ILs is required for their further industrial application, the process simulation results indicate that IL-based recovery technique has the potential to improve the economic and technical competitive of bioisoprene production process. In this work, we find that all identified ILs are the combinations of cation subgroup [C₃H₇N] and anion group [DMP] because of their interactions with the groups of isoprene and other gas components in the off-gas, which could be a guidance for the experiment works in the future. We hope that the promising performance of the identified ILs will invite more systematic experimental validations.

6 APPLICATIONS IN ELECTROCHEMISTRY

In this chapter, using ILs as multi-functional additives in lithium titanate (LTO) batteries is presented.

Chapter structure and contents:

6.1 Additives in LTO batteries

6.1 ADDITIVES IN LTO BATTERIES

This chapter forms the basis of following unpublished work:

Cai, Y.; Chen, Y.; Xu, T.; Solms, N.; Kontogeorgis, G. M.; Woodley, J. M.; Zhang, S.; Thomsen, K.: Computer-aided multifunctional ionic liquid design for electrolyte in LTO rechargeable batteries. (Advanced Functional Materials). In preparation.

ABSTRACT

Functional additives that can suppress the water and HF content are highly desired as their presence in the electrolyte can significantly improve the performance of lithium titanate (LTO) rechargeable batteries. In this chapter, we explore the possibility of using multifunctional ionic liquids (ILs) for such a purpose.

6.1.1 Introduction

Lithium titanate $\text{Li}_4\text{Ti}_5\text{O}_{12}$ (LTO) anode with many attractive features such as stable voltage plateau of 1.5 V vs. Li/Li^+ high safety and better cycling performance has been proposed for rechargeable lithium-ion batteries. However, the intrinsic lithium ion diffusion coefficient and electronic conductivity of LTO are very low, which may deteriorate its high rate performance.^{1, 2} In addition, the swelling problem caused by the catalytic decomposition of electrolyte on the surface of the LTO electrode and the presence of water in the electrolyte also limits its application in lithium ion batteries. Still, the formation of solid electrolyte interphase (SEI) film on the surface of the LTO electrode is very slow, resulting in an increase in HF (a destructive compound in the electrode) generated from the reaction of LiPF_6 with H_2O . This reaction is assumed to take place in two stages as follows:³



A solution would be to use an additive to promote the film formation.⁴ Liu et al.⁵ reported that carbonate-based electrolytes can form a SEI layer to depress the swelling problem of LTO-based batteries. Vinylene Carbonate (VC) has been also tested as an SEI film-forming electrolyte additive in LTO batteries. Published works reveal that the VC additive can contribute to a protective layer formation on the LTO electrode, thereby improving the battery's rate and cycling performance.^{6, 7} Although these additives can promote film formation to a certain extent, more efficient, green and safe electrolyte additives are still highly desirable from a sustainable point of view and with regards to the environment and safety. Ionic liquids (ILs), regarded as green and safe chemical compounds, have attracted attention in electrochemistry due to their outstanding properties.^{8, 9} In this chapter, we explore the possibility of using multifunctional ILs for such a purpose. Similar to chemical and biochemical separation processes, finding optimal ILs with good performance is essential for using them as additives

in LTO batteries. In this regard, we use CAILD as a non-experimental design method for selecting IL additives prior to the corresponding experimental work.

6.1.2 Computer-aided IL Additives Design

6.1.2.1 CAILD-based Problem Formulation

Electrical conductivity is the measure of a material's ability to allow the transport of an electric charge and is a critical property in electronic applications.^{10, 11} For this reason, we set the electrical conductivity as the objective function in CAILD. Based on the design objective function of maximizing electrical conductivity and the constraints on the molecular structure and properties, the CAILD can be formulated as a mixed-integer non-linear programming (MINLP) problem, as follows:

Objective function $f_{obj} = \max(\varepsilon)$ ε : electrical conductivity

Molecular structural constraints Eqs.3.7-3.13

Property constraints Eqs.4.3-4.4

6.1.2.2 Solution and Analysis

It has been shown that organic additives with unsaturated bonds (e.g. C=C, C=O)¹²⁻¹⁵ generally decompose prior to other main solvents to form stable SEI films on anode surfaces, which can effectively suppress the electrolyte decomposition on graphitic carbon and therefore improve the anodic cyclability.^{12, 16} Meanwhile, it is well known that trace impurities of water can initiate the thermal decomposition of carbonate electrolytes containing LiPF₆, which results in the generation of hydrofluoric acid (HF).¹⁷⁻¹⁹ Consequently, the LiMn₂O₄ electrode is easily eroded by HF generating electrolytes at different states of charge. These HF attacks will further destabilize the SEI film.²⁰ For this reason, great efforts have been made for improving the cyclability of LiMn₂O₄-based batteries by inhibiting HF production or by removing water and neutralizing acids.²¹⁻²⁸ Among those strategies, the application of functional additives is widely being investigated and it has been accepted that both H₂O and HF can possibly be stabilized by ethanolamine through hydrogen bonds of N...H-F(O) and F(O)...H-N.

Based on the understanding of organic additives in electrolytes mentioned above, two functional groups, vinyl and amide are included as cation substituents for the IL molecular design. As shown in Table 6.1, 4 substituents, 6 cations and 15 anions were selected as molecular building blocks in CAILD.

The formulated CAILD-based MINLP problem was solved by Python programming, from where a set of 100 ILs were selected from 1,089,450 candidates. The ILs were selected on the basis of their electrical conductivity and their structure. By comparing the electrical conductivities of all 100 IL candidates, it is found that ILs with imidazolium-based cations or

[Tf₂N]⁻ anions have higher electrical conductivity than their counterparts. In addition, the electrical conductivity of IL decreases with the increasing number of alkyl groups on the cation side chain. Among the 100 screened IL candidates, only 7 ILs containing both vinyl and amide functional groups remained, as presented in Table 6.2. Based on the current conditions in our laboratory, one of these 7 ILs, [VAIM][TFSI] was synthesized for further experimental validation as additive in LIB electrolyte.

Table 6.1 Group building blocks involved in the molecular design of IL

Type	Groups	Type	Groups
Substituents	CH ₃	Anions	[Tf ₂ N] ⁻
	CH ₂		[BF ₄] ⁻
	CH ₂ =CH		[PF ₆] ⁻
	O=C-NH ₂		[CH ₃ COO] ⁻
Cation cores	[Im] ⁺		[MeSO ₄] ⁻
	[Py] ⁺		[EtSO ₄] ⁻
	[Pyr] ⁺		[CF ₃ SO ₃] ⁻
	[N] ⁺		[CH ₃ SO ₃] ⁻
	[Pip] ⁺		[N(CN) ₂] ⁻
	[Morp] ⁺		[B(CN) ₄] ⁻
			[EtPO ₃] ⁻
			[BuPO ₃] ⁻
			[HePO ₃] ⁻
			[Pf ₂ N] ⁻
			[eFAP] ⁻

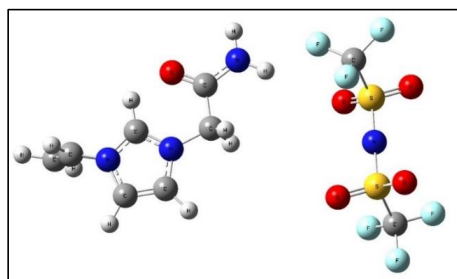
Table 6.2 Top 7 IL candidates containing both vinyl and amide functional groups with their predicted properties

No. of IL additives	Group combination	MW(g.mol ⁻¹)	Tm/K	η /Pa.s	ε / S.m ⁻¹
IL33	1 [Im], 1 [Tf2N], 1 CH2=CH, 1 O=C-NH2	674,98	283,132	0,0638	1,639
IL48	1 [Im], 1 [Tf2N], 2 CH2, 1 CH2=CH, 1 O=C-NH2	714,016	294,964	0,0617	1,291
IL56	1 [Im], 1 [Tf2N], 1 CH2, 1 CH2=CH, 1 O=C-NH2	719,014	279,373	0,0736	1,179
IL80	1 [Py], 1 [Tf2N], 1 CH2=CH, 1 O=C-NH2	683,987	287,701	0,0801	0,955
IL83	1 [N], 1 [Tf2N], 3 CH2, 1 CH2=CH, 1 O=C-NH2	758,05	291,205	0,0711	0,928
IL93	1 [Im], 1 [Tf2N], 2 CH2, 1 CH2=CH, 1 O=C-NH2	763,048	275,614	0,0849	0,847
IL98	1 [Im], 1 [Tf2N], 1 CH3, 1 CH2, 1 CH2=CH, 1 O=C-NH2	733,041	295,969	0,0770	0,809

6.1.3 Experimental Section

The molecular structure of ionic liquid [VAIM][TFSI] is illustrated in Figure 6.1(a). It was synthesized employing a two-step method in our lab. The final IL product is a little bit yellow as shown in Figure 6.1(b). Its purity IL was more than 99 %, and there was no impurity peak in the ¹H NMR spectrum of this synthesized IL. After drying for 48 hours, the IL was mixed with the base electrolyte.

The base electrolyte used in this work was an ethylene carbonate (EC)-ethyl carbonate (EMC) solvent mixture (with a mass ratio of 3:7) containing 1M (M: mol/L) LiPF₆. The purities of both solvents (EC, MEC) were more than 99.95 %, and the lithium salt was more than 99.5 % pure. The chemicals were supplied from Linzhou Keneng Materials Technology Co. The IL additive was added to the base electrolyte with stirring for 10 minutes. The added amounts corresponded to 0.5 wt %, 1.0 wt % and 3.0 wt %. Target electrolytes were stored in a glove box filled with argon for more than 24 hours. The water content of the electrolytes was less than 10 ppm, while the water and oxygen contents of the glove box were less than 1 ppm as measured by Karl Fischer titration.



(a)



(b)

Figure 6.1 Molecular structure of ionic liquid [VAIM][TFSI] (a) and macroscopic appearance of synthesized ionic liquid [VAIM][TFSI] (b)

Table 6.3 Water content (ppm) of electrolytes with and without ionic liquid [VAIM][TFSI] at different standing time

IL content				
Standing Time	0 %	0.5 wt %	1.0 wt %	3.0 wt %
Beginning	8.98	8.56	8.43	8.38
7days	9.50	9.11	9.07	9.01
1 month	17.56	13.56	12.21	11.18

Table 6.4 Hydrogen fluoride content (ppm) of electrolytes with and without ionic liquid [VAIM][TFSI] at different standing time

IL content				
Standing Time	0 %	0.5 wt %	1.0 wt %	3.0 wt %
Beginning	41	32	27	25
7days	45	36	31	29
1 month	61	42	35	31

6.1.4 Experimental Results and Discussion

6.1.4.1 Physicochemical Properties

Water and HF are two important indicators for evaluating the quality of electrolyte. The use of high quality battery grade electrolytes, in which the water content is less than 15 ppm and the hydrogen fluoride content less than 50 ppm,^{29,30} is critical for high electrochemical performance. Due to the special surface characteristics of LTO materials, nanoscale particles have high affinity for water which is difficult to remove. The water and HF contents of electrolytes with

different content of [VAIM][TFSI] (0%, 0.5 wt %, 1.0 wt %, 3.0 wt %) were measured at different standing times, as presented in Table 6.3 and Table 6.4. In the beginning, the water content of base electrolyte is 8.98 ppm, which gets lower after adding some [VAIM][TFSI] into the base electrolyte. The water content decreases as the ionic liquid content increases. The water content increases with increasing of standing time in all the prepared samples. The growth rate decreases with the increase of the IL content. After one month standing time, the electrolyte without IL additive, had a water content of 25.56 ppm which is more than 15 ppm, and can therefore not be used in the commercial market. However, the electrolytes with IL contained less than 15 ppm water. Similar results were obtained in terms of HF. In this study, the [VAIM][TFSI] effectively inhibits the generation of HF and water, as well as guarantees the quality of the electrolyte.

6.1.4.2 Cycling Performance Analyses

The LTO/Li coin cells were charged and discharged at the first ten cycles with a rate of 0.1 C, then they cycled at higher rate with 0.5 C. Figure 6.2 shows the cycle performances of LTO/Li coin cells using electrolytes with different content of [VAIM][TFSI]. In the beginning, the specific capacity of LTO/Li coin cell in the base electrolyte with 0.5 wt % IL additive is highest, up to 158.0 mAhg⁻¹. The following value is for the electrolyte without using IL additive. It has higher specific capacity than the electrolytes with 1 wt % and 3.0 %. From the curves, it is seen that the capacity in LTO/Li coin half-cell without IL decays faster, and the value becomes the lowest after 200 cycles with 149.8 mAhg⁻¹. The value for the electrolyte with 0.5 wt % is 156.8 mAhg⁻¹. The capacity retention in the electrolytes with 0 wt %, 0.5 wt %, 1.0 wt % and 3.0 wt % IL additive is 96.03%, 99.24 %, 98.71 % and 98.82%, respectively, after 200 cycles at a rate 0.5 C shown in Figure 6.2.

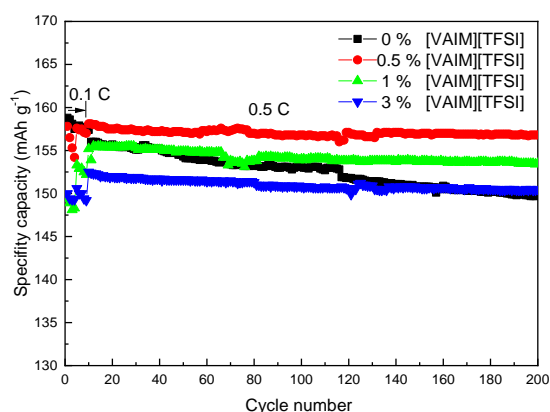


Figure 6.2 Cycle performance of LTO/Li batteries in different electrolytes at 0.5 C rate

The cycle performances of LTO/Li coin half-cells at a rate of 1.0 C are given in Figure 6.3 The half-cell with 0.5 wt % [VAIM][TFSI] possess the highest specific capacity, up to 155.7 mAhg⁻¹ and the lowest impedance. The half-cell without IL has the lowest specific capacity (145.3 mAhg⁻¹) and the highest impedance. The specific capacity of a half-cell with 1.0 wt % IL additive is 153.1 mAhg⁻¹, and with 3.0 wt % IL additive is 149.7 mAhg⁻¹, at 1.0 C rate. Due to the large current change from 0.5 C to 1.0 C, a relatively large polarization results in the loss of capacity of half-cells at 1.0 C. As presented in Table .5, the capacity retention of LTO/Li half-cells in the electrolytes with 0 wt %, 0.5 wt %, 1.0 wt % and 3.0 wt % IL additive after 100 cycles at a rate of 1.0 C is 98.35%, 99.61 %, 99.48 % and 99.33 %, respectively. . It was found that the specific capacity of half-cells without [VAIM][TFSI] faded faster. All half-cells with [VAIM][TFSI] showed good cycling performance at 0.5 C and 1.0 C rates.

Table 6.5 Capacity retention in LTO/Li half-cells with different electrolytes at different rate

Rate	0 wt % IL	0.5 wt % IL	1.0 wt % IL	3.0 wt % IL
Capacity retention after 200 cycles at 0.5 C (%)	96.03	99.24	98.71	98.82
Capacity retention after 100 cycles at 1.0 C (%)	98.35	99.61	99.48	99.33

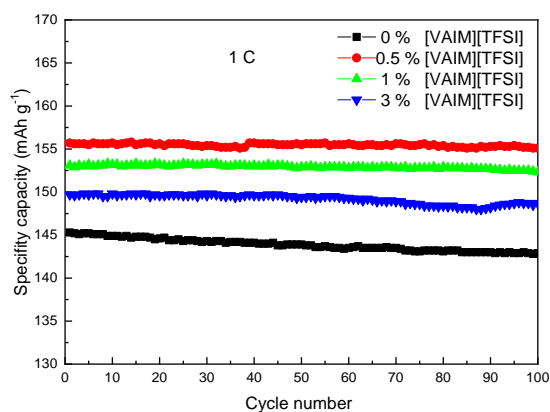


Figure 6.3 Cycle performance of LTO/Li batteries in different electrolytes at 1 C rate

6.1.4.3 Rate Performance Analysis

C-rate is an important basis for evaluating the electrochemical performance of lithium batteries. Figure 6.4 gives the C-rate performance of the LTO/Li battery with different content of [VAIM][TFSI]. All coin cells were cycled at various rates, including 0.1 C, 0.5 C, 1 C, 2 C, 5 C, 10 C, 15 C, and 20 C. The initial specific capacity of the half-cell in the electrolytes with 0 wt %, 0.5 wt %, 3.0 wt % is similar at the low rate while the initial specific capacity for the battery with 1.0 wt % IL is a little higher (Figure 6.4). With increasing C-rate, the capacity of the cell without IL declines rapidly from 0.1 C to 20 C. The capacity retention (compared with the last loop of 0.1 C) from 0.1 C to 20 C is 40.88 %. The cell in the electrolyte with 0.5 wt % [VAIM][TFSI] has the best C-rate performance. As shown in Table 6.6, the capacity retentions in the cells with 0.5 wt %, 1.0 wt % and 3.0 wt % IL additive is 87.50 %, 74.13 % and 68.86 %, respectively.

The charge and discharge profiles of LTO electrodes in different electrolytes and at different rates are plotted in Figure 6.5. The discharge voltage plateau is similar for the four IL contents and is about 1.55 V at low rate. The distinct discharge voltage plateau is evident at higher rates, and the values with IL additive are higher than those without additive. The discharge voltage plateau decreases with the increase of the rate, due to the fact that the polarization increases as the current increases, and it descends sharply in the electrolyte without IL.

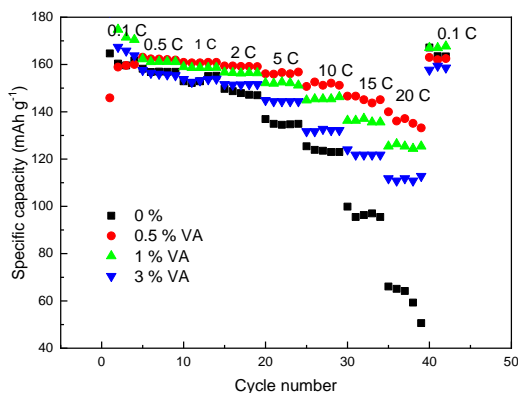


Figure 6.4 Rate performance of LTO batteries in different electrolytes

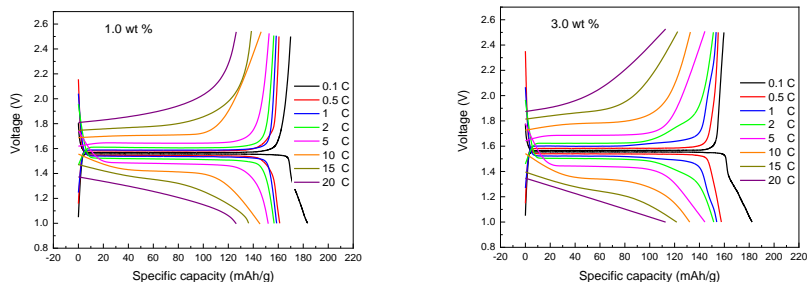


Figure 1.5 Charge and discharge curves of LTO/Li batteries in the electrolytes with different content of ionic liquid, at different rates

Table 6.6 Capacity retentions (compared with the last loop of 0.1 C) of LTO/Li battery with different content of ionic liquid at different rates compared to the retention at 0.1 C

	0 %		0.5 wt %		1.0 wt %		3.0 wt %	
Rate	Specific capacity	Capacity retention	Specific capacity	Capacity retention	Specific capacity	Capacity retention	Specific capacity	Capacity retention
C	mAhg ⁻¹	%	mAhg ⁻¹	%	mAhg ⁻¹	%	mAhg ⁻¹	%
0.1	161.7	100.00	160.0	100.00	170.5	100.00	163.8	100.00
0.5	158.2	97.84	163.1	101.94	162.3	95.19	157.6	96.21
1	155.2	95.98	160.9	100.56	159	93.26	153.9	93.96
2	149.7	92.58	159.4	99.63	156.7	91.91	151.6	92.55
5	136.9	84.66	156.8	98.00	152.5	89.44	144.9	88.46
10	125.4	77.55	152.6	95.38	146.3	85.81	132.7	81.01
15	99.9	61.78	146.6	91.63	136.3	79.94	124	75.70
20	66.1	40.88	140	87.50	126.4	74.13	112.8	68.86
0.1	167.2	-	163	-	167.8	-	159.4	-

6.1.4.4 Impedance Analysis

Electrochemical impedance spectroscopy (EIS) is a very powerful way to get electrochemical information of a battery. EIS can not only offer detailed kinetic information but can also be used to monitor changes in battery properties under different conditions. In our work, EIS is used to investigate the kinetics of the electrochemical process at the LTO electrode. Figure 6.6 shows the electrochemical impedance spectra of LTO/Li half-cells using the electrolytes with

0%, 0.5 wt %, 1.0 wt %, 3.0 wt % [VAIM][TFSI] after 200 cycles, the frequency range is from 0.01Hz to 10^5 Hz. The half circle in the high frequency range represents the charge transfer resistance of the LTO/Li battery, and the half circle in the low frequency range denotes its diffusive resistance. It can be found that the electrolyte with 0.5 wt % [VAIM][TFSI] has the lowest impedance. It indicates that the Li^+ movement through the surface of the electrode is positive, the half cell in the electrolyte with 0.5 wt % [VAIM][TFSI] has the largest specific capacity and the lowest resistance. By contrast, the cell without IL shows the highest charge transfer resistance among all studied electrolytes after 200 cycles, which results in capacity loss.

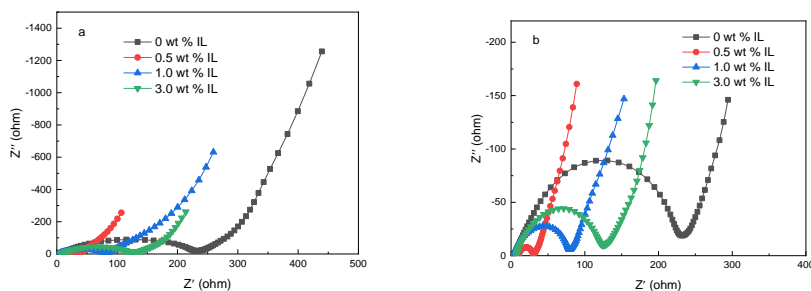


Figure 6.6 Impedance spectra of LTO batteries in different electrolytes after 200 cycles, (b) is an enlarged image of (a) at high frequency

6.1.4.5 SEM Analyses

Figure 6.7 (a), (b), (c) and (d) shows the surface morphology of the LTO electrode after full discharge in different electrolytes with 0 %, 0.5 wt %, 1.0 wt % and 3.0 wt % [VAIM][TFSI], using Scanning Electron Microscopy (SEM). It can be seen from Figure 6.7 (a) that lithium titanate particles are more distinct, and there is no apparent passive film formation. After the addition of IL, there is also no obvious passive film on the electrode surface. However, the boundary of lithium titanate particles becomes fuzzy, which can be seen from Figure 6.7 (b). It indicates that some decomposition of electrolyte with IL additive during the charge process is covered on the LTO electrode by the influence of IL. For the electrolyte with 3% IL additive, particle clusters appear on the surface of the electrode.

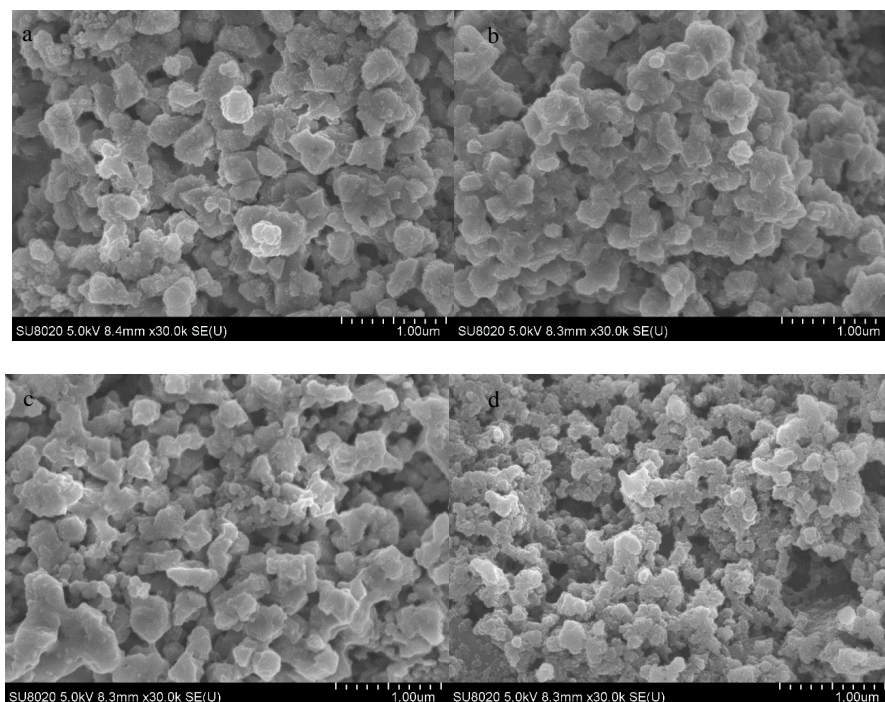


Figure 6.7 SEM images of LTO electrode after fully discharge in the base electrolyte with 0 % (a), 0.5 wt % (b), 1.0 wt %, 3.0 wt % (d) ionic liquid [VAIM][TFSI]

6.1.4.6 XPS Analysis

X-ray photoelectron spectroscopy (XPS) has been widely used to verify the specific elements of the electrode surface.³¹ The XPS spectra of the surface at the electrodes in the base electrolytes with different content of [VAIM][TFSI] (0 %, 0.5 wt %, 1.0 wt % and 3.0 wt %) were, respectively, plotted in Figure 6.8, Figure 6.9, Figure 6.10 and Figure 6.11. In the C 1s spectra, the peak at 284.1 eV is attributed to the C-C bond from the carbon black, 286.0 eV is attributed to PVDF, 287.6 eV is attributed to the C=O bond from lithium alkyl carbonates (R-CH₂OCO₂-Li) and polycarbonates, and 290.9 eV is attributed to Li₂CO₃.³² As illustrated in these figures, the intensity of the Li₂CO₃ peak for the electrode with no IL component is the strongest. The value decreases with the increase of IL content. This indicates that the used IL additive can suppress electrolyte decomposition. In the O 1s spectra, 531.1 eV is attributed to the C=O bond from lithium alkyl carbonates (R-CH₂OCO₂-Li).³³ In addition, the intensity of the C=O peak in electrolyte without IL is higher than all electrolytes with IL additive, indicating the inhibitory effect of IL on electrolyte decomposition. In the F 1s spectra, the peak at 684.5-685.8 eV is attributed to LiF, the peak at ~686.1 eV is attributed to LiP_xO_yF_z, the peak at 687 eV - 689 eV is attributed to PVDF.³³ The strength of LiF in all electrolytes with IL additive is

higher than that of LiF in the electrolyte without IL. LiF covers the surface of the LTO anode as a barrier layer to prevent the reductive electrolyte decomposition, and to reduce the gas swelling of LTO battery. This is beneficial to the cycling performance. The N 1s peak is clearly detected at about ~401 eV which is attributed to CN, and the S 2p peak can also be found at about 170.5 eV in the electrolyte with IL additive, but not in the electrolyte without IL. Both N and S elements come from the [VAIM][TFSI]. It is indicated that more and more decomposition of IL appears on the surface of LTO electrode as the IL content increases.

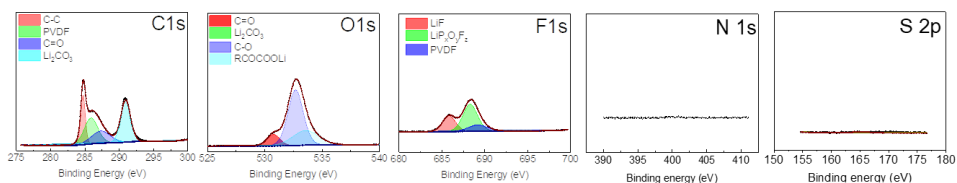


Figure 6.8 XPS spectra for the surface of LTO in electrolyte without ionic liquid [VAIM][TFSI]

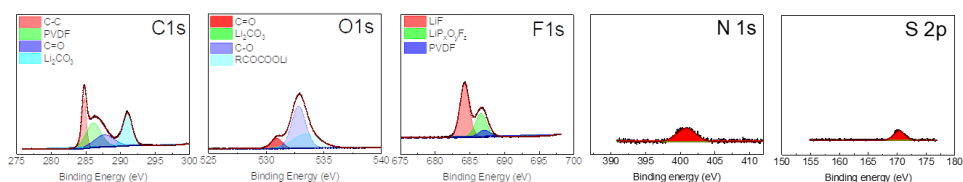


Figure 6.9 XPS spectra for the surface of LTO in electrolyte with 0.5 wt % ionic liquid [VAIM][TFSI]

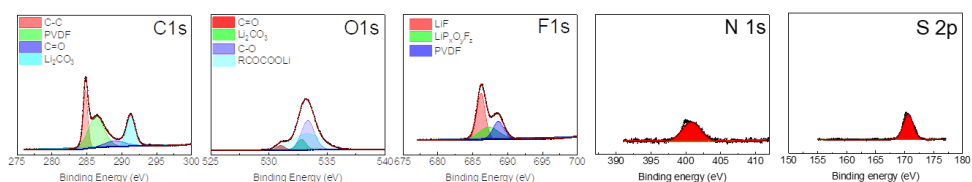


Figure 6.10 XPS spectra for the surface of LTO in electrolyte with 1.0 wt % ionic liquid [VAIM][TFSI]

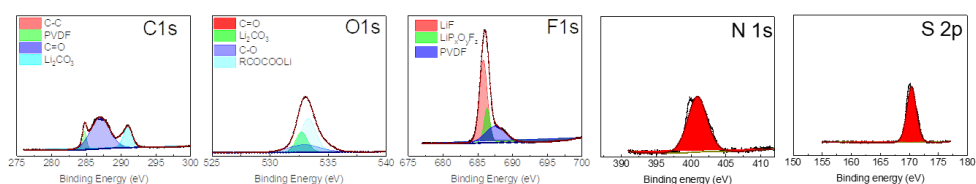


Figure 6.11 XPS spectra for the surface of LTO in electrolyte with 0.5 wt % ionic liquid [VAIM][TFSI]

6.1.5 Conclusions

By formulating and solving a complex CAILD-based MINLP problem, a new type of ionic liquid 3-(2-amino-2-oxoethyl)-1-vinylimidazolium bis(trifluoromethylsulfonyl)amide ([VAIM][TFSI]) was intentionally designed for use as a multifunctional additive in the electrolyte. This IL was synthesized for the first time through a two-step method, and then electrolytes with 0%, 0.5 wt%, 1.0 wt%, and 3.0 wt% [VAIM][TFSI] were individually investigated in LTO/Li batteries. As expected, the presence of [VAIM][TFSI] in the electrolyte can concurrently suppress the system's water and HF content, which leads to good durability performance. Meanwhile, the gas generated from the catalytic decomposition of organic solvents on the LTO electrode is also reduced. This can largely prevent the battery from swelling and rapid breakdown, thereby improving its safety. Among all studied LTO/Li batteries, the battery with 0.5 wt % [VAIM][TFSI] exhibits the best cycle and rate performance, and its capacity retention is 99.43 % at 5 C and 89.41 % at 20 C under the condition of high current discharge, but only 85.37 % and 42.94 % are remained in the case of LTO/Li battery without using [VAIM][TFSI]. In addition, the EIS spectra reveals that the electrolyte with 0.5 wt % IL additive has the lowest charge transfer resistance. The experimental results verify the possibility of using computer-aided design methods in battery chemistry and highlight the excellent potential of using multifunctional ILs as electrolyte additives. This work provides guidance for further efforts to design suitable ILs in electrochemistry.

7 CONCLUSIONS

In this chapter, conclusions and main achievements of this work are provided.

Chapter contents:

7.1 Conclusions

7.1 CONCLUSIONS

Developing new sustainable and innovative industrial technologies is still a critical task to address the increasing energy and environmental challenges. Technologies using ionic liquids (ILs) have been widely studied, and it was demonstrated that ILs have significant potential to replace the conventional organic solvents in many separation processes. However, some challenges need to be addressed before taking their place in industrial applications, such as how to lower the price of ILs and reduce their viscosities, particularly how to efficiently design/screen suitable ILs for different separation systems. Thus, this work presents a systematic computer-aided design method that is able to rapidly screen suitable ILs with desired properties as well as meet desired specific-task standards. Unlike experimental-based or other trial-and-error solvent screening methods that are usually time consuming and expensive, this non-experimental based design method is both cost- and time-efficient due to its dependence on predictive property models. One of the key novelties of this design method is that it not only screens suitable ILs from current existing IL database but also can find new high-performance ILs that have not been synthesized yet.

In this design method, group contribution (GC)-based property models are developed for estimating various properties of ILs including density, viscosity, heat capacity, surface tension, thermal conductivity, melting point and electrical conductivity. More than 15000 experimental data points in a wide range of temperature (and pressure) covering nearly 300 ILs stem from 8 cation families, 34 anion families and 4 substituents are used. All property models are validated by using 20-30% of data points as test datasets. These GC-based property models can be easily integrated in the computer-aided design method of ILs, and they can also be easily extended to new IL groups when experimental data of those ILs is available. Alongside, a comprehensive UNIFAC-IL-Gas model consisting of two sub-models, i.e. UNIFAC-IL-Gas (Exp.) model and UNIFAC-IL-Gas (Pseudo-Exp.) model, is also developed for the thermodynamic calculations of systems containing ILs. A large number of experimental data collected from literature and a certain number of pseudo-experimental data generated from a calibrated COSMO-RS model are involved in this model's development. Similarly, this model is tested by using 20-30% of experimental data points for each IL-gas system. Overall, 7 cation groups, 24 anion groups, and 3 substituent groups decomposed from 100 ILs as well as 13 gases including CO₂, SO₂, H₂S, NH₃, N₂O, CO, N₂, O₂, H₂, CH₄, C₂H₄, C₂H₆, C₃H₈ are covered in this thermodynamic model. In addition, as UNIFAC-IL-Gas model combines IL-gas and other IL-solute systems, it can be applied for the design of IL-based mixture solvents, which could give significant opportunity to potentially expand the use of ILs. Furthermore, this model can be updated, or further extended, to new gas-IL systems that are currently not included in this study, once their experimental data becomes available.

Together with the development of property models, ILs are also introduced to the intensified process designs in this work. Based on the conceptual design of hybrid process schemes,

integrated solvent and process design and *in situ* product removal (ISPR), three design methodologies are, respectively, proposed for each of the process intensification method and their applications are illustrated by different case studies. (1) Separation of aqueous solutions using hybrid separation schemes with ILs demands much less energy inputs as compared to conventional separation process. Also, bio-oxidation of alcohols using hybrid reaction-separation schemes has better reaction and yield performance than conventional processing operation. (2) The proposed integrated IL and process design method is used to simultaneously optimize IL molecular structure and process operations for three separation processes, i.e. separation of ethanol-water, separation of acetone-methanol, and CO₂ capture process. In all three cases, this integrated design method provides the best energy and economic performance among all design methods published in literature.^{27, 28, 79} (3) IL-based ISPR design is applied to the case study of acetone-butanol-ethanol (ABE) fermentation process and the results show that the productivity of IL-based ISPR processing scheme with or without substrate make-up stream is around 3 and 1.8 times greater than that of the batch processing scheme. Meanwhile, they also induce at least 27% energy savings as compared to the conventional downstream distillation process.

Besides all the case studies described above, the proposed computer-aided design method of ILs is also used to design optimal ILs for some other applications: for removing acid gas (e.g. CO₂, H₂S) from shale/natural gas, for recovering bio-isoprene from fermentation off-gas, and as electrolyte additives in lithium titanate (LTO) batteries. In all studied cases, the designed ILs provide better process performance when compared to their corresponding benchmark solvents or additives. In addition, we are currently working on the design of IL-based mixture solvents that are capable to selectively remove H₂S and CO₂ from raw natural gas.

The main achievements of this work are summarized as following:

- An IL database covering a large number of experimental data collected from literature and a number of pseudo-experimental data generated from COSMO-RS model is developed.
- A systematic computer-aided design method that is able to rapidly and reliably screen suitable ILs with desired properties as well as meet specific-task standards is developed.
- GC-based property models are developed for estimating various properties of ILs including density, viscosity, heat capacity, surface tension, thermal conductivity melting point and electrical conductivity.
- A comprehensive UNIFAC-IL-Gas model consisting of two sub-models, i.e. UNIFAC-IL-Gas (Exp.) model and UNIFAC-IL-Gas (Pseudo-Exp.) model, is developed for the thermodynamic calculations of systems containing ILs.
- A hybrid process design method allowing units operating at their highest process efficiencies to perform one (or more) process tasks is proposed to obtain optimal process operations with better energy (and reaction) performance.

- An integrated design method combining GC-based property models, UNIFAC-IL models, computer-aided molecular design (CAMD) and process design is proposed to simultaneously optimize the IL structure and process operations.
- A three-stage design method that combines ISPR processing schemes selection, IL-based liquid-liquid extraction systems design and process evaluation is proposed for the recovery of microbe-derived small molecules in bioprocesses.
- A design method of IL-based mixture solvents is being studied.

8 FUTURE PERSPECTIVES

In this last part of the thesis, future perspectives and directions of taking ILs to industrial applications covering property models, process design, and molecular simulation are presented.

Chapter contents:

8.1 Future perspectives

8.1 FUTURE PERSPECTIVES

The challenges of expanding the use of ILs and taking their place to industrial applications need to be addressed in the future research are as follows:

Database and property models

- Current experimental database is still limited to well-known ILs and their systems. Therefore, more experimental work covering new ILs and their systems especially IL-bioprocess systems is necessary.
- GC-based property models and UNIFAC-IL-Gas model need to be updated, or extended to new IL groups and IL containing systems once their experimental data become available in the future. Particularly, aqueous biphasic system (ABS) has many advantages in bio-separations, but its optimal design is very difficult due to the limitation of the thermodynamic models. For this reason, thermodynamic models such as UNIFAC and NRTL need to be extended to such systems.
- Although the major properties associated to the evaluation of environmental impact and biodegradability of ILs has been recently studied, the knowledge of their modes of toxicity, and biodegradation pathways is still limited. Therefore, further experimental investigation and theoretical study are essential and should be the focus of attention in the coming years.

Process design and evaluation

- For the integrated IL and process design, we need more efficient problem solution algorithms and more powerful computer systems to perform detailed modelling, which would increase the reliability and applicability of design results.
- Controlling the conditions is more difficult for an ISPR process than for a non-integrated process and thereby more efforts (e.g. uncertainty quantification) need to be made in the future to improve the robustness of IL-based ISPR design.
- Challenges such as life cycle analysis, scale-up and economic analyses of IL-based processes need to be addressed before its implementation in industrial applications.

Methods/tools

- At present, thermodynamic methods such as COSMO and UNIFAC are often used to predict thermodynamic behavior of systems containing ILs. However, predictions from COSMO-based models are generally not good enough, while UNIFAC-IL models are mostly limited to IL-small molecule systems due to insufficient experimental data. Therefore, an experiment-independent thermodynamic method with good predictive capability for IL containing systems with large molecules is highly desirable. In this regard, molecular simulation is a potential alternative as the behavior of ILs can be

predicted at conditions inaccessible to experiment and a fundamental understanding of the microscopic basis for the observed macroscopic properties can be obtained as well. For this reason, a molecular force field that is able to predict thermodynamic behavior and other properties of IL containing systems is necessary.

- In many cases, computer-aided design methods based on the property estimation models has their own computational limitations. In this regard, the application of deep learning methods in the optimal design of ILs is worth investigating as they are able to navigate uncharted territories of the chemical space.

REFERENCES

1. Sholl, D. S.; Lively, R. P., Seven chemical separations: to change the world: purifying mixtures without using heat would lower global energy use, emissions and pollution--and open up new routes to resources. *Nature* **2016**, 532, (7600), 435-438.
2. Lutze, P.; Gani, R.; Woodley, J. M., Process intensification: a perspective on process synthesis. *Chem. Eng. Process.* **2010**, 49, (6), 547-558.
3. Babi, D. K.; Holtbruegge, J.; Lutze, P.; Górak, A.; Woodley, J. M.; Gani, R., Sustainable process synthesis--intensification. *Comput. Chem. Eng.* **2015**, 81, 218-244.
4. Garg, N.; Woodley, J. M.; Gani, R.; Kontogeorgis, G. M., Sustainable solutions by integrating process synthesis-intensification. *Comput. Chem. Eng.* **2019**, 126, 499-519.
5. Garg, N.; Kontogeorgis, G. M.; Gani, R.; Woodley, J. M., A process synthesis-intensification method for generation of novel and intensified solutions. *Chem. Eng. Process.* **2020**, 108103.
6. Vooradi, R.; Bertran, M.-O.; Frauzem, R.; Anne, S. B.; Gani, R., Sustainable chemical processing and energy-carbon dioxide management: review of challenges and opportunities. *Chem. Eng. Res. Des.* **2017**.
7. Woodley, J. M.; Bisschops, M.; Straathof, A. J.; Ottens, M., Future directions for in situ product removal (ISPR). *J. Chem. Technol. Biotechnol.* **2008**, 83, (2), 121-123.
8. Woodley, J. M., Bioprocess intensification for the effective production of chemical products. *Comput. Chem. Eng.* **2017**.
9. Wankat, P. C., *Separation process engineering*. Pearson Education: 2006.
10. Garg, N., Phenomena-based Process Synthesis-Intensification. **2019**.
11. Rogers, R. D.; Seddon, K. R., Ionic liquids--solvents of the future? *Science* **2003**, 302, (5646), 792-793.
12. Seiler, M.; Jork, C.; Kavarnou, A.; Arlt, W.; Hirsch, R., Separation of azeotropic mixtures using hyperbranched polymers or ionic liquids. *AIChE J.* **2004**, 50, (10), 2439-2454.
13. Welton, T., Room-temperature ionic liquids. Solvents for synthesis and catalysis. *Chem. Rev.* **1999**, 99, (8), 2071-2084.
14. Ventura, S. P.; e Silva, F. A.; Quental, M. V.; Mondal, D.; Freire, M. G.; Coutinho, J. A., Ionic-liquid-mediated extraction and separation processes for bioactive compounds: past, present, and future trends. *Chem. Rev.* **2017**, 117, (10), 6984-7052.
15. Vekariya, R. L., A review of ionic liquids: Applications towards catalytic organic transformations. *J. Mol. Liq.* **2017**, 227, 44-60.
16. Liu, B.; Jin, N., The applications of ionic liquid as functional material: a review. *Curr. Org. Chem.* **2016**, 20, (20), 2109-2116.
17. Shang, D.; Liu, X.; Bai, L.; Zeng, S.; Xu, Q.; Gao, H.; Zhang, X., Ionic liquids in gas separation processing. *Current Opinion in Green and Sustainable Chemistry* **2017**, 5, 74-81.
18. Lei, Z.; Dai, C.; Zhu, J.; Chen, B., Extractive distillation with ionic liquids: a review. *AIChE J.* **2014**, 60, (9), 3312-3329.
19. Rautenbach, R.; Albrecht, R., The separation potential of pervaporation: Part 2. Process design and economics. *J. Membr. Sci.* **1985**, 25, (1), 25-54.
20. Goldblatt, M.; Gooding, C. In *An engineering analysis of membrane-aided distillation*, AIChE Symp. Ser, 1986; 1986; pp 51-69.
21. Davis, J. C.; Valus, R. J.; Eshraghi, R.; Velikoff, A. E., Facilitated transport membrane hybrid systems for olefin purification. *Sep. Sci. Technol.* **1993**, 28, (1-3), 463-476.
22. Moganti, S.; Noble, R. D.; Koval, C. A., Analysis of a membrane/distillation column hybrid process. *J. Membr. Sci.* **1994**, 93, (1), 31-44.

23. Stephan, W.; Noble, R. D.; Koval, C. A., Design methodology for a membrane/distillation column hybrid process. *J. Membr. Sci.* **1995**, 99, (3), 259-272.
24. Pettersen, T.; Argo, A.; Noble, R. D.; Koval, C. A., Design of combined membrane and distillation processes. *Sep. Technol.* **1996**, 6, (3), 175-187.
25. Caballero, J. A.; Grossmann, I. E.; Keyvani, M.; Lenz, E. S., Design of hybrid distillation–vapor membrane separation systems. *Ind. Eng. Chem. Res.* **2009**, 48, (20), 9151-9162.
26. Tula, A. K.; Befort, B.; Garg, N.; Camarda, K. V.; Gani, R., Sustainable process design & analysis of hybrid separations. *Computers & Chemical Engineering* **2017**, 105, 96-104.
27. Pereira, F. E.; Keskes, E.; Galindo, A.; Jackson, G.; Adjiman, C. S., Integrated solvent and process design using a SAFT-VR thermodynamic description: High-pressure separation of carbon dioxide and methane. *Comput. Chem. Eng.* **2011**, 35, (3), 474-491.
28. Burger, J.; Papaioannou, V.; Gopinath, S.; Jackson, G.; Galindo, A.; Adjiman, C. S., A hierarchical method to integrated solvent and process design of physical CO₂ absorption using the SAFT - γ Mie approach. *AIChE J.* **2015**, 61, (10), 3249-3269.
29. Zhou, T.; McBride, K.; Zhang, X.; Qi, Z.; Sundmacher, K., Integrated solvent and process design exemplified for a Diels–Alder reaction. *AIChE J.* **2015**, 61, (1), 147-158.
30. Van Hecke, W.; Kaur, G.; De Wever, H., Advances in in-situ product recovery (ISPR) in whole cell biotechnology during the last decade. *Biotechnol. Adv.* **2014**, 32, (7), 1245-1255.
31. Valencia-Marquez, D.; Flores-Tlacuahuac, A.; Vasquez-Medrano, R., Simultaneous optimal design of an extractive column and ionic liquid for the separation of bioethanol–water mixtures. *Ind. Eng. Chem. Res.* **2012**, 51, (17), 5866-5880.
32. Jacquemin, J.; Ge, R.; Nancarrow, P.; Rooney, D. W.; Costa Gomes, M. F.; Pádua, A. A.; Hardacre, C., Prediction of ionic liquid properties. I. Volumetric properties as a function of temperature at 0.1 MPa. *J. Chem. Eng. Data* **2008**, 53, (3), 716-726.
33. Jacquemin, J.; Nancarrow, P.; Rooney, D. W.; Costa Gomes, M. F.; Husson, P.; Majer, V.; Pádua, A. A.; Hardacre, C., Prediction of ionic liquid properties. II. Volumetric properties as a function of temperature and pressure. *J. Chem. Eng. Data* **2008**, 53, (9), 2133-2143.
34. Qiao, Y.; Ma, Y.; Huo, Y.; Ma, P.; Xia, S., A group contribution method to estimate the densities of ionic liquids. *J. Chem. Thermodyn.* **2010**, 42, (7), 852-855.
35. Gardas, R. L.; Coutinho, J. A., Extension of the Ye and Shreeve group contribution method for density estimation of ionic liquids in a wide range of temperatures and pressures. *Fluid Phase Equilib.* **2008**, 263, (1), 26-32.
36. Lazzús, J. A., ρ –T–P prediction for ionic liquids using neural networks. *J. Taiwan Inst. Chem. Eng.* **2009**, 40, (2), 213-232.
37. Shen, C.; Li, C.-x.; Li, X.-m.; Lu, Y.-z.; Muhammad, Y., Estimation of densities of ionic liquids using Patel–Teja equation of state and critical properties determined from group contribution method. *Chem. Eng. Sci.* **2011**, 66, (12), 2690-2698.
38. Valderrama, J. O.; Zarricueta, K., A simple and generalized model for predicting the density of ionic liquids. *Fluid Phase Equilib.* **2009**, 275, (2), 145-151.
39. Abildskov, J.; Ellegaard, M. D.; O’Connell, J. P., Densities and isothermal compressibilities of ionic liquids—modeling and application. *Fluid Phase Equilib.* **2010**, 295, (2), 215-229.
40. Ji, X.; Adidharma, H., Thermodynamic modeling of ionic liquid density with heterosegmented statistical associating fluid theory. *Chem. Eng. Sci.* **2009**, 64, (9), 1985-1992.
41. Wang, J.; Li, Z.; Li, C.; Wang, Z., Density prediction of ionic liquids at different temperatures and pressures using a group contribution equation of state based on electrolyte perturbation theory. *Ind. Eng. Chem. Res.* **2010**, 49, (9), 4420-4425.
42. Gani, R.; Nielsen, B.; Fredenslund, A., A group contribution approach to computer - aided molecular design. *AIChE J.* **1991**, 37, (9), 1318-1332.

43. Harper, P. M.; Gani, R.; Kolar, P.; Ishikawa, T., Computer-aided molecular design with combined molecular modeling and group contribution. *Fluid Phase Equilib.* **1999**, 158, 337-347.
44. Karunanithi, A.; Mehrkesh, A., *Computer-Aided Design of Tailor-Made Ionic Liquids*. 2013; Vol. 59, p 4627-4640.
45. Chen, Y.; Gani, R.; Kontogeorgis, G. M.; Woodley, J. M., Integrated ionic liquid and process design involving azeotropic separation processes. *Chem. Eng. Sci.* **2019**, 203, 402-414.
46. Paduszynski, K.; Domanska, U., A new group contribution method for prediction of density of pure ionic liquids over a wide range of temperature and pressure. *Ind. Eng. Chem. Res.* **2011**, 51, (1), 591-604.
47. Gardas, R. L.; Coutinho, J. A., A group contribution method for heat capacity estimation of ionic liquids. *Ind. Eng. Chem. Res.* **2008**, 47, (15), 5751-5757.
48. Gardas, R. L.; Coutinho, J. A., Group contribution methods for the prediction of thermophysical and transport properties of ionic liquids. *AIChE J.* **2009**, 55, (5), 1274-1290.
49. Gardas, R. L.; Coutinho, J. A., Applying a QSPR correlation to the prediction of surface tensions of ionic liquids. *Fluid Phase Equilib.* **2008**, 265, (1), 57-65.
50. Lazzús, J. A., A group contribution method to predict the melting point of ionic liquids. *Fluid Phase Equilib.* **2012**, 313, 1-6.
51. Simoni, L. D.; Lin, Y.; Brennecke, J. F.; Stadtherr, M. A., Modeling liquid-liquid equilibrium of ionic liquid systems with NRTL, electrolyte-NRTL, and UNIQUAC. *Ind. Eng. Chem. Res.* **2008**, 47, (1), 256-272.
52. Lei, Z.; Zhang, J.; Li, Q.; Chen, B., UNIFAC model for ionic liquids. *Ind. Eng. Chem. Res.* **2009**, 48, (5), 2697-2704.
53. Kato, R.; Gmehling, J., Systems with ionic liquids: Measurement of VLE and $\gamma \infty$ data and prediction of their thermodynamic behavior using original UNIFAC, mod. UNIFAC (Do) and COSMO-RS (Ol). *J. Chem. Thermodyn.* **2005**, 37, (6), 603-619.
54. Lei, Z.; Dai, C.; Wang, W.; Chen, B., UNIFAC model for ionic liquid - CO₂ systems. *AIChE J.* **2014**, 60, (2), 716-729.
55. Haghtalab, A.; Paraj, A., Computation of liquid-liquid equilibrium of organic-ionic liquid systems using NRTL, UNIQUAC and NRTL-NRF models. *J. Mol. Liq.* **2012**, 171, 43-49.
56. Nebig, S.; Gmehling, J., Prediction of phase equilibria and excess properties for systems with ionic liquids using modified UNIFAC: Typical results and present status of the modified UNIFAC matrix for ionic liquids. *Fluid Phase Equilib.* **2011**, 302, (1-2), 220-225.
57. Hector, T.; Gmehling, J., Present status of the modified UNIFAC model for the prediction of phase equilibria and excess enthalpies for systems with ionic liquids. *Fluid Phase Equilib.* **2014**, 371, 82-92.
58. Lei, Z.; Dai, C.; Liu, X.; Xiao, L.; Chen, B., Extension of the UNIFAC model for ionic liquids. *Ind. Eng. Chem. Res.* **2012**, 51, (37), 12135-12144.
59. Lei, Z.; Dai, C.; Yang, Q.; Zhu, J.; Chen, B., UNIFAC model for ionic liquid - CO (H₂) systems: an experimental and modeling study on gas solubility. *AIChE J.* **2014**, 60, (12), 4222-4231.
60. Pereda, S.; Raeissi, S.; Andreatta, A. E.; Bottini, S. B.; Kroon, M.; Peters, C. J., Modeling gas solubilities in imidazolium based ionic liquids with the [Tf₂N] anion using the GC-EoS. *Fluid Phase Equilib.* **2016**, 409, 408-416.
61. Chen, Y.; Mutelet, F.; Jaubert, J.-N. I., Modeling the solubility of carbon dioxide in imidazolium-based ionic liquids with the PC-SAFT equation of state. *J. Phys. Chem. B* **2012**, 116, (49), 14375-14388.
62. Navarro, P.; Ayuso, M.; Palma, A. M.; Larriba, M.; Delgado-Mellado, N.; García, J. n.; Rodríguez, F.; Coutinho, J. o. A.; Carvalho, P. J., Toluene/n-heptane separation by

extractive distillation with tricyanomethanide-based ionic liquids: experimental and CPA EoS modeling. *Ind. Eng. Chem. Res.* **2018**, 57, (42), 14242-14253.

63. Diedenhofen, M.; Eckert, F.; Klamt, A., Prediction of infinite dilution activity coefficients of organic compounds in ionic liquids using COSMO-RS. *J. Chem. Eng. Data* **2003**, 48, (3), 475-479.

64. Gutiérrez, J. P.; Meindersma, G. W.; de Haan, A. B., COSMO-RS-based ionic-liquid selection for extractive distillation processes. *Ind. Eng. Chem. Res.* **2012**, 51, (35), 11518-11529.

65. Fang, J.; Zhao, R.; Su, W.; Li, C.; Liu, J.; Li, B., A molecular design method based on the COSMO - SAC model for solvent selection in ionic liquid extractive distillation. *AIChE J.* **2016**, 62, (8), 2853-2869.

66. Dong, Y.; Huang, S.; Guo, Y.; Lei, Z., COSMO - UNIFAC model for ionic liquids. *AIChE J.* **2020**, 66, (1), e16787.

67. Zhu, R.; Taheri, M.; Zhang, J.; Lei, Z., Extension of the COSMO-UNIFAC Thermodynamic Model. *Ind. Eng. Chem. Res.* **2020**.

68. Klamt, A.; Eckert, F., COSMO-RS: a novel and efficient method for the a priori prediction of thermophysical data of liquids. *Fluid Phase Equilib.* **2000**, 172, (1), 43-72.

69. Banerjee, T.; Singh, M. K.; Khanna, A., Prediction of binary VLE for imidazolium based ionic liquid systems using COSMO-RS. *Ind. Eng. Chem. Res.* **2006**, 45, (9), 3207-3219.

70. Zhang, X.; Liu, Z.; Wang, W., Screening of ionic liquids to capture CO₂ by COSMO - RS and experiments. *AIChE J.* **2008**, 54, (10), 2717-2728.

71. Zhou, T.; Chen, L.; Ye, Y.; Chen, L.; Qi, Z.; Freund, H. r.; Sundmacher, K., An overview of mutual solubility of ionic liquids and water predicted by COSMO-RS. *Ind. Eng. Chem. Res.* **2012**, 51, (17), 6256-6264.

72. Manan, N. A.; Hardacre, C.; Jacquemin, J.; Rooney, D. W.; Youngs, T. G., Evaluation of gas solubility prediction in ionic liquids using COSMOthermX. *J. Chem. Eng. Data* **2009**, 54, (7), 2005-2022.

73. Zhao, X.; Yang, Q.; Xu, D.; Bao, Z.; Zhang, Y.; Su, B.; Ren, Q.; Xing, H., Design and screening of ionic liquids for C₂H₂/C₂H₄ separation by COSMO - RS and experiments. *AIChE J.* **2015**, 61, (6), 2016-2027.

74. Farahipour, R.; Mehrkesh, A.; Karunanithi, A. T., A systematic screening methodology towards exploration of ionic liquids for CO₂ capture processes. *Chem. Eng. Sci.* **2016**, 145, 126-132.

75. Zhao, Y.; Gani, R.; Afzal, R. M.; Zhang, X.; Zhang, S., Ionic liquids for absorption and separation of gases: An extensive database and a systematic screening method. *AIChE J.* **2017**, 63, (4), 1353-1367.

76. Liu, X.; Zhou, T.; Zhang, X.; Zhang, S.; Liang, X.; Gani, R.; Kontogeorgis, G. M., Application of COSMO-RS and UNIFAC for ionic liquids based gas separation. *Chemical Engineering Science* **2018**, 192, 816-828.

77. Song, Z.; Zhou, T.; Qi, Z.; Sundmacher, K., Extending the UNIFAC model for ionic liquid-solute systems by combining experimental and computational databases. *AIChE J.* **2020**, 66, (2), e16821.

78. Brignole, E. A.; Bottini, S.; Gani, R., A strategy for the design and selection of solvents for separation processes. *Fluid Phase Equilib.* **1986**, 29, 125-132.

79. Roughton, B. C.; Christian, B.; White, J.; Camarda, K. V.; Gani, R., Simultaneous design of ionic liquid entrainers and energy efficient azeotropic separation processes. *Comput. Chem. Eng.* **2012**, 42, 248-262.

80. Song, Z.; Li, X.; Chao, H.; Mo, F.; Zhou, T.; Cheng, H.; Chen, L.; Qi, Z., Computer-aided ionic liquid design for alkane/cycloalkane extractive distillation process. *Green Energy Environ.* **2019**, 4, (2), 154-165.

81. Song, Z.; Zhang, C.; Qi, Z.; Zhou, T.; Sundmacher, K., Computer - aided design of ionic liquids as solvents for extractive desulfurization. *AIChE J.* **2018**, 64, (3), 1013-1025.
82. Nebig, S.; Gmehling, J., Measurements of different thermodynamic properties of systems containing ionic liquids and correlation of these properties using modified UNIFAC (Dortmund). *Fluid Phase Equilib.* **2010**, 294, (1), 206-212.
83. Dai, C.; Lei, Z.; Chen, B., Predictive thermodynamic models for ionic liquid-SO₂ systems. *Ind. Eng. Chem. Res.* **2015**, 54, (43), 10910-10917.
84. Yu, G.; Dai, C.; Lei, Z., Modified UNIFAC-Lei Model for Ionic Liquid-CH₄ Systems. *Ind. Eng. Chem. Res.* **2018**, 57, (20), 7064-7076.
85. Chen, Y.; Liu, X.; Kontogeorgis, G. M.; Woodley, J. M., Ionic-Liquid-Based Bioisoprene Recovery Process Design. *Ind. Eng. Chem. Res.* **2020**.
86. Lei, Z.; Dai, C.; Chen, B., Gas solubility in ionic liquids. *Chem. Rev.* **2014**, 114, (2), 1289-1326.
87. Fredenslund, A.; Jones, R. L.; Prausnitz, J. M., Group - contribution estimation of activity coefficients in nonideal liquid mixtures. *AIChE J.* **1975**, 21, (6), 1086-1099.
88. Constantinescu, D.; Gmehling, J. r., Further development of modified UNIFAC (Dortmund): revision and extension 6. *J. Chem. Eng. Data* **2016**, 61, (8), 2738-2748.
89. Weidlich, U.; Gmehling, J., A modified UNIFAC model. 1. Prediction of VLE, hE, and gamma_∞. *Ind. Eng. Chem. Res.* **1987**, 26, (7), 1372-1381.
90. Hansen, H. K.; Rasmussen, P.; Fredenslund, A.; Schiller, M.; Gmehling, J., Vapor-liquid equilibria by UNIFAC group contribution. 5. Revision and extension. *Ind. Eng. Chem. Res.* **1991**, 30, (10), 2352-2355.
91. Wittig, R.; Lohmann, J.; Gmehling, J., Vapor- liquid equilibria by UNIFAC group contribution. 6. Revision and extension. *Ind. Eng. Chem. Res.* **2003**, 42, (1), 183-188.
92. Nocon, G.; Weidlich, U.; Gmehling, J.; Onken, U., Prediction of Gas Solubilities by a Modified UNIFAC - Equation. *Berichte der Bunsengesellschaft für physikalische Chemie* **1983**, 87, (1), 17-23.
93. Dahl, S.; Fredenslund, A.; Rasmussen, P., The MHV2 model: a UNIFAC-based equation of state model for prediction of gas solubility and vapor-liquid equilibria at low and high pressures. *Ind. Eng. Chem. Res.* **1991**, 30, (8), 1936-1945.
94. Song, Z.; Zhang, C.; Qi, Z.; Zhou, T.; Sundmacher, K., Computer - aided design of ionic liquids as solvents for extractive desulfurization. *AIChE J.* **2018**.
95. Lei, Z.; Dai, C.; Chen, B., Gas solubility in ionic liquids. *Chem. Rev.* **2013**, 114, (2), 1289-1326.
96. Papadakis, E.; Tula, A. K.; Gani, R., Solvent selection methodology for pharmaceutical processes: Solvent swap. *Chem. Eng. Res. Des.* **2016**, 115, 443-461.
97. Tula, A. K.; Befort, B.; Garg, N.; Camarda, K. V.; Gani, R., Sustainable process design & analysis of hybrid separations. *Comput. Chem. Eng.* **2016**.
98. Martínez-Aragón, M.; Burghoff, S.; Goetheer, E.; de Haan, A., Guidelines for solvent selection for carrier mediated extraction of proteins. *Sep. Purif. Technol.* **2009**, 65, (1), 65-72.
99. Drioli, E.; Stankiewicz, A. I.; Macedonio, F., Membrane engineering in process intensification—An overview. *J. Membr. Sci.* **2011**, 380, (1), 1-8.
100. Holbrey, J.; Seddon, K., Ionic liquids. *Clean Technol. Environ. Policy* **1999**, 1, (4), 223-236.
101. Valencia-Marquez, D.; Flores-Tlacuahuac, A.; Vasquez-Medrano, R., Simultaneous optimal design of an extractive column and ionic liquid for the separation of bioethanol–water mixtures. *Ind. Eng. Chem. Res.* **2011**, 51, (17), 5866-5880.
102. Karunanithi, A. T.; Mehrkesh, A., Computer - aided design of tailor - made ionic liquids. *AIChE J.* **2013**, 59, (12), 4627-4640.

103. Chong, F. K.; Foo, D. C.; Eljack, F. T.; Atilhan, M.; Chemmangattuvalappil, N. G., Ionic liquid design for enhanced carbon dioxide capture by computer-aided molecular design approach. *Clean Technol. Environ. Policy* **2015**, 17, (5), 1301-1312.
104. Chong, F. K.; Eljack, F. T.; Atilhan, M.; Foo, D. C.; Chemmangattuvalappil, N. G., A systematic visual methodology to design ionic liquids and ionic liquid mixtures: Green solvent alternative for carbon capture. *Comput. Chem. Eng.* **2016**, 91, 219-232.
105. Farahipour, R.; Mehrkesh, A.; Karunanithi, A. T., A systematic screening methodology towards exploration of ionic liquids for CO₂ capture processes. *Chem. Eng. Sci.* **2016**, 145, 126-132.
106. Barton, A. F., *CRC handbook of solubility parameters and other cohesion parameters*. Routledge: 2017.
107. Kumar, A. A. P.; Banerjee, T., Thiophene separation with ionic liquids for desulphurization: A quantum chemical approach. *Fluid Phase Equilib.* **2009**, 278, (1-2), 1-8.
108. Anantharaj, R.; Banerjee, T., COSMO-RS-based screening of ionic liquids as green solvents in denitrification studies. *Ind. Eng. Chem. Res.* **2010**, 49, (18), 8705-8725.
109. Klamt, A., Conductor-like screening model for real solvents: a new approach to the quantitative calculation of solvation phenomena. *J. Phys. Chem.* **1995**, 99, (7), 2224-2235.
110. Klamt, A.; Jonas, V.; Bürger, T.; Lohrenz, J. C., Refinement and parametrization of COSMO-RS. *J. Phys. Chem. A* **1998**, 102, (26), 5074-5085.
111. Eike, D. M.; Brennecke, J. F.; Maginn, E. J., Predicting infinite-dilution activity coefficients of organic solutes in ionic liquids. *Ind. Eng. Chem. Res.* **2004**, 43, (4), 1039-1048.
112. Lee, B.-S.; Lin, S.-T., Screening of ionic liquids for CO₂ capture using the COSMO-SAC model. *Chem. Eng. Sci.* **2015**, 121, 157-168.
113. Lin, S.-T.; Sandler, S. I., A priori phase equilibrium prediction from a segment contribution solvation model. *Ind. Eng. Chem. Res.* **2002**, 41, (5), 899-913.
114. Lin, S.-T.; Chang, J.; Wang, S.; Goddard, W. A.; Sandler, S. I., Prediction of vapor pressures and enthalpies of vaporization using a COSMO solvation model. *J. Phys. Chem. A* **2004**, 108, (36), 7429-7439.
115. Lei, Z.; Xiao, L.; Dai, C.; Chen, B., Group contribution lattice fluid equation of state (GCLF EOS) for ionic liquids. *Chem. Eng. Sci.* **2012**, 75, 1-13.
116. Dai, C.; Lei, Z.; Wang, W.; Xiao, L.; Chen, B., Group contribution lattice fluid equation of state for CO₂-ionic liquid systems: an experimental and modeling study. *AIChE J.* **2013**, 59, (11), 4399-4412.
117. Paduszynski, K.; Lukoshko, E. V.; Królikowski, M.; Domanska, U.; Szydlowski, J., Thermodynamic study of binary mixtures of 1-butyl-1-methylpyrrolidinium dicyanamide ionic liquid with molecular solvents: new experimental data and modeling with PC-SAFT equation of state. *J. Phys. Chem. B* **2015**, 119, (2), 543-551.
118. Santiago, R. S.; Santos, G. R.; Aznar, M., UNIQUAC correlation of liquid-liquid equilibrium in systems involving ionic liquids: The DFT-PCM approach. *Fluid Phase Equilib.* **2009**, 278, (1-2), 54-61.
119. Trohalaki, S.; Pachter, R.; Drake, G. W.; Hawkins, T., Quantitative structure- property relationships for melting points and densities of ionic liquids. *Energy Fuels* **2005**, 19, (1), 279-284.
120. Sun, N.; He, X.; Dong, K.; Zhang, X.; Lu, X.; He, H.; Zhang, S., Prediction of the melting points for two kinds of room temperature ionic liquids. *Fluid Phase Equilib.* **2006**, 246, (1-2), 137-142.
121. Palomar, J.; Ferro, V. R.; Torrecilla, J. S.; Rodríguez, F., Density and molar volume predictions using COSMO-RS for ionic liquids. An approach to solvent design. *Ind. Eng. Chem. Res.* **2007**, 46, (18), 6041-6048.
122. Torrecilla, J. S.; Palomar, J.; García, J. n.; Rodríguez, F., Effect of cationic and anionic chain lengths on volumetric, transport, and surface properties of 1-alkyl-3-methylimidazolium

- alkylsulfate ionic liquids at (298.15 and 313.15) K. *J. Chem. Eng. Data* **2009**, 54, (4), 1297-1301.
123. Diedenhofen, M.; Klamt, A.; Marsh, K.; Schäfer, A., Prediction of the vapor pressure and vaporization enthalpy of 1-n-alkyl-3-methylimidazolium-bis-(trifluoromethanesulfonyl) amide ionic liquids. *PCCP* **2007**, 9, (33), 4653-4656.
124. Jacquemin, J.; Husson, P.; Padua, A. A.; Majer, V., Density and viscosity of several pure and water-saturated ionic liquids. *Green Chem.* **2006**, 8, (2), 172-180.
125. Guerrero, H.; Martín, S.; Pérez-Gregorio, V.; Lafuente, C.; Bandrés, I., Volumetric characterization of pyridinium-based ionic liquids. *Fluid Phase Equilib.* **2012**, 317, 102-109.
126. Fröba, A.; Rausch, M.; Krzeminski, K.; Assenbaum, D.; Wasserscheid, P.; Leipertz, A., Thermal conductivity of ionic liquids: measurement and prediction. *Int. J. Thermophys.* **2010**, 31, (11-12), 2059-2077.
127. Chen, Y.; Kontogeorgis, G. M.; Woodley, J. M., Group Contribution-based estimation method for properties of ionic liquids. *Ind. Eng. Chem. Res.* **2019**.
128. Mousazadeh, M.; Faramarzi, E., Corresponding states theory for the prediction of surface tension of ionic liquids. *Ionics* **2011**, 17, (3), 217-222.
129. Huang, Y.; Dong, H.; Zhang, X.; Li, C.; Zhang, S., A new fragment contribution - corresponding states method for physicochemical properties prediction of ionic liquids. *AIChE J.* **2013**, 59, (4), 1348-1359.
130. Bondi, A., van der Waals volumes and radii. *J. Phys. Chem.* **1964**, 68, (3), 441-451.
131. Fedorova, M.; Sin, G.; Gani, R., Computer-aided modelling template: Concept and application. *Comput. Chem. Eng.* **2015**, 83, 232-247.
132. Smith, M. B., *March's advanced organic chemistry: reactions, mechanisms, and structure*. John Wiley & Sons: 2020.
133. Whittaker, J. W., Free radical catalysis by galactose oxidase. *Chem. Rev.* **2003**, 103, (6), 2347-2364.
134. Toftgaard Pedersen, A.; Birmingham, W. R.; Rehn, G.; Charnock, S. J.; Turner, N. J.; Woodley, J. M., Process requirements of galactose oxidase catalyzed oxidation of alcohols. *Org. Process Res. Dev.* **2015**, 19, (11), 1580-1589.
135. Liese, A.; Seelbach, K.; Wandrey, C., *Industrial biotransformations*. John Wiley & Sons: 2006.
136. Heintz, A.; Verevkin, S. P.; Ondo, D., Thermodynamic properties of mixtures containing ionic liquids. 8. Activity coefficients at infinite dilution of hydrocarbons, alcohols, esters, and aldehydes in 1-hexyl-3-methylimidazolium bis (trifluoromethylsulfonyl) imide using gas-liquid chromatography. *J. Chem. Eng. Data* **2006**, 51, (2), 434-437.
137. Barton, P., Solvent recovery opportunities in the pharmaceutical industry. *Curr. Opin. Drug Discovery Dev.* **2000**, 3, (6), 707-713.
138. Simoni, L. D.; Chapeaux, A.; Brennecke, J. F.; Stadtherr, M. A., Extraction of biofuels and biofeedstocks from aqueous solutions using ionic liquids. *Comput. Chem. Eng.* **2010**, 34, (9), 1406-1412.
139. Benedict, M.; Rubin, L. C., Extractive and azeotropic distillation. *Theoretical Aspects. Trans. Am. Inst. Chem. Eng.* **1945**, 41, 353-370.
140. Corderí, S.; González, B.; Calvar, N.; Gómez, E., Ionic liquids as solvents to separate the azeotropic mixture hexane/ethanol. *Fluid Phase Equilib.* **2013**, 337, 11-17.
141. Poling, B. E.; Prausnitz, J. M.; O'Connell, J. P., *The properties of gases and liquids*. McGraw-hill New York: 2001; Vol. 5.
142. Douglas, J. M., *Conceptual design of chemical processes*. McGraw-Hill New York: 1988; Vol. 1110.
143. Kohl, A. L.; Nielsen, R., *Gas purification*. Elsevier: 1997.
144. Perry, R. H.; Green, D.; Maloney, J., Chemical Engineers Handbook. 6th. In New York: McGraw-Hill: 1997.

145. Lygeros, A.; Magoulas, K., Column flooding and entrainment. *Hydrocarbon Process.* **1986**, 65, (12), 43-44.
146. Kragl, U., The Role of Reaction Engineering in Bioprocess Development. *CHIMIA Int. J. Chem.* **2020**, 74, (5), 378-381.
147. Freeman, A.; Woodley, J. M.; Lilly, M. D., In situ product removal as a tool for bioprocessing. *Bio/technol.* **1993**, 11, (9), 1007-1012.
148. Lye, G. J.; Woodley, J. M., Application of in situ product-removal techniques to biocatalytic processes. *Trends Biotechnol.* **1999**, 17, (10), 395-402.
149. Rype, J.-U.; Garde, A.; Vrang, A.; Madsen, S.; Jonsson, G., Integrated membrane-process boosting productivity and product yield of pharmaceutical protein production. *Desalination* **2006**, 199, (1-3), 403-404.
150. Bechtold, M.; Makart, S.; Heinemann, M.; Panke, S., Integrated operation of continuous chromatography and biotransformations for the generic high yield production of fine chemicals. *J. Biotechnol.* **2006**, 124, (1), 146-162.
151. Buque - Taboada, E. M.; Straathof, A. J.; Heijnen, J. J.; Van der Wielen, L. A., In situ product removal using a crystallization loop in asymmetric reduction of 4 - oxoisophorone by *Saccharomyces cerevisiae*. *Biotechnol. Bioeng.* **2004**, 86, (7), 795-800.
152. Grundtvig, I. P. R.; Heintz, S.; Krühne, U.; Gernaey, K. V.; Adlercreutz, P.; Hayler, J. D.; Wells, A. S.; Woodley, J. M., Screening of organic solvents for bioprocesses using aqueous-organic two-phase systems. *Biotechnol. Adv.* **2018**, 36, (7), 1801-1814.
153. Zhang, X.; Zhang, X.; Dong, H.; Zhao, Z.; Zhang, S.; Huang, Y., Carbon capture with ionic liquids: overview and progress. *Energy Environ. Sci.* **2012**, 5, (5), 6668-6681.
154. Chen, Y.; Woodley, J.; Kontogeorgis, G.; Gani, R., Integrated Ionic Liquid and Process Design involving Hybrid Separation Schemes. In *Comput. Aided Chem. Eng.*, Elsevier: 2018; Vol. 44, pp 1045-1050.
155. Liu, X.; Chen, Y.; Zeng, S.; Zhang, X.; Zhang, S.; Liang, X.; Gani, R.; Kontogeorgis, G. M., Structure optimization of tailored ionic liquids and process simulation for shale gas separation. *AIChE J.* **2020**, 66, (2), e16794.
156. Chen, Y.; Koumaditi, E.; Gani, R.; Kontogeorgis, G. M.; Woodley, J. M., Computer-Aided Design of Ionic Liquids for Hybrid Process Schemes. *Comput. Chem. Eng.* **2019**, 106556.
157. Passos, H.; Freire, M. G.; Coutinho, J. A., Ionic liquid solutions as extractive solvents for value-added compounds from biomass. *Green Chem.* **2014**, 16, (12), 4786-4815.
158. Tang, B.; Bi, W.; Tian, M.; Row, K. H., Application of ionic liquid for extraction and separation of bioactive compounds from plants. *J. Chromatogr. B* **2012**, 904, 1-21.
159. Afonso, C. A.; Singh, S.; Mikkola, J.-P.; Palou, R.; Bogel-Lukasik, R.; Gathergood, N.; Jang, G.-W. B.; Freire, M.; Sheldon, R.; Stark, A., *Ionic liquids in the biorefinery concept: challenges and perspectives*. Royal Society of Chemistry: 2015.
160. Bogdanov, M. G., Ionic liquids as alternative solvents for extraction of natural products. In *alternative solvents for natural products extraction*, Springer: 2014; pp 127-166.
161. Dreyer, S.; Kragl, U., Ionic liquids for aqueous two - phase extraction and stabilization of enzymes. *Biotechnol. Bioeng.* **2008**, 99, (6), 1416-1424.
162. Bisht, M.; Kumar, A.; Venkatesu, P., Analysis of the driving force that rule the stability of lysozyme in alkylammonium-based ionic liquids. *Int. J. Biol. Macromol.* **2015**, 81, 1074-1081.
163. Desai, R. K.; Streefland, M.; Wijffels, R. H.; Eppink, M. H., Extraction and stability of selected proteins in ionic liquid based aqueous two phase systems. *Green Chem.* **2014**, 16, (5), 2670-2679.
164. Cao, Q.; Quan, L.; He, C.; Li, N.; Li, K.; Liu, F., Partition of horseradish peroxidase with maintained activity in aqueous biphasic system based on ionic liquid. *Talanta* **2008**, 77, (1), 160-165.

165. Du, Z.; Yu, Y. L.; Wang, J. H., Extraction of proteins from biological fluids by use of an ionic liquid/aqueous two - phase system. *Chem. Eur. J.* **2007**, 13, (7), 2130-2137.
166. Ventura, S. P.; Santos, L. D.; Saraiva, J. A.; Coutinho, J. A., Ionic liquids microemulsions: the key to Candida antarctica lipase B superactivity. *Green Chem.* **2012**, 14, (6), 1620-1625.
167. Chen, Y.; Liu, X.; Kontogeorgis, G. M.; Woodley, J. M., Ionic-Liquid-Based Bioisoprene Recovery Process Design. *Ind. Eng. Chem. Res.* **2020**, 59, (16), 7355-7366.
168. Freire, M. G.; Claudio, A. F. M.; Araujo, J. M.; Coutinho, J. A.; Marrucho, I. M.; Lopes, J. N. C.; Rebelo, L. P. N., Aqueous biphasic systems: a boost brought about by using ionic liquids. *Chem. Soc. Rev.* **2012**, 41, (14), 4966-4995.
169. Cláudio, A. F. M.; Marques, C. F.; Boal-Palheiros, I.; Freire, M. G.; Coutinho, J. A., Development of back-extraction and recyclability routes for ionic-liquid-based aqueous two-phase systems. *Green Chem.* **2014**, 16, (1), 259-268.
170. Stark, D.; von Stockar, U., In situ product removal (ISPR) in whole cell biotechnology during the last twenty years. In *Process integration in biochemical engineering*, Springer: 2003; pp 149-175.
171. Zhao, D.; Liao, Y.; Zhang, Z., Toxicity of ionic liquids. *Clean-soil, air, water* **2007**, 35, (1), 42-48.
172. Pham, T. P. T.; Cho, C.-W.; Yun, Y.-S., Environmental fate and toxicity of ionic liquids: a review. *Water Res.* **2010**, 44, (2), 352-372.
173. Petkovic, M.; Seddon, K. R.; Rebelo, L. P. N.; Pereira, C. S., Ionic liquids: a pathway to environmental acceptability. *Chem. Soc. Rev.* **2011**, 40, (3), 1383-1403.
174. Stolte, S.; Arning, J.; Bottin-Weber, U.; Müller, A.; Pitner, W.-R.; Welz-Biermann, U.; Jastorff, B.; Ranke, J., Effects of different head groups and functionalised side chains on the cytotoxicity of ionic liquids. *Green Chem.* **2007**, 9, (7), 760-767.
175. Petkovic, M.; Ferguson, J. L.; Gunaratne, H. N.; Ferreira, R.; Leitao, M. C.; Seddon, K. R.; Rebelo, L. P. N.; Pereira, C. S., Novel biocompatible cholinium-based ionic liquids— toxicity and biodegradability. *Green Chem.* **2010**, 12, (4), 643-649.
176. Romero, A.; Santos, A.; Tojo, J.; Rodriguez, A., Toxicity and biodegradability of imidazolium ionic liquids. *J. Hazard. Mater.* **2008**, 151, (1), 268-273.
177. Neumann, J.; Steudte, S.; Cho, C.-W.; Thöming, J.; Stolte, S., Biodegradability of 27 pyrrolidinium, morpholinium, piperidinium, imidazolium and pyridinium ionic liquid cations under aerobic conditions. *Green Chem.* **2014**, 16, (4), 2174-2184.
178. Peric, B.; Sierra, J.; Martí, E.; Cruañas, R.; Garau, M. A.; Arning, J.; Bottin-Weber, U.; Stolte, S., (Eco) toxicity and biodegradability of selected protic and aprotic ionic liquids. *J. Hazard. Mater.* **2013**, 261, 99-105.
179. Hou, X.-D.; Liu, Q.-P.; Smith, T. J.; Li, N.; Zong, M.-H., Evaluation of toxicity and biodegradability of cholinium amino acids ionic liquids. *PloS one* **2013**, 8, (3), e59145.
180. Garcia, M. T.; Gathergood, N.; Scammells, P. J., Biodegradable ionic liquids Part II. Effect of the anion and toxicology. *Green Chem.* **2005**, 7, (1), 9-14.
181. Gathergood, N.; Garcia, M. T.; Scammells, P. J., Biodegradable ionic liquids: Part I. Concept, preliminary targets and evaluation. *Green Chem.* **2004**, 6, (3), 166-175.
182. Harjani, J. R.; Singer, R. D.; Garcia, M. T.; Scammells, P. J., Biodegradable pyridinium ionic liquids: design, synthesis and evaluation. *Green Chem.* **2009**, 11, (1), 83-90.
183. Qureshi, N.; Ezeji, T. C., Butanol, 'a superior biofuel' production from agricultural residues (renewable biomass): recent progress in technology. *Biofuels, Bioprod. Biorefin.* **2008**, 2, (4), 319-330.
184. Green, E. M., Fermentative production of butanol—the industrial perspective. *Curr. Opin. Biotechnol.* **2011**, 22, (3), 337-343.
185. Staggs, K. W.; Nielsen, D. R., Improving n-butanol production in batch and semi-continuous processes through integrated product recovery. *Process Biochem.* **2015**, 50, (10), 1487-1498.

186. Outram, V.; Lalander, C. A.; Lee, J. G.; Davies, E. T.; Harvey, A. P., Applied in situ product recovery in ABE fermentation. *Biotechnol. Progr.* **2017**, 33, (3), 563-579.
187. Lodi, G.; De Guido, G.; Pellegrini, L. A., Simulation and energy analysis of the ABE fermentation integrated with gas stripping. *Biomass Bioenergy* **2018**, 116, 227-235.
188. Ezeji, T. C.; Qureshi, N.; Blaschek, H. P., Microbial production of a biofuel (acetone–butanol–ethanol) in a continuous bioreactor: impact of bleed and simultaneous product removal. *Bioprocess. Biosyst. Eng.* **2013**, 36, (1), 109-116.
189. Xue, C.; Zhao, J.; Liu, F.; Lu, C.; Yang, S.-T.; Bai, F.-W., Two-stage in situ gas stripping for enhanced butanol fermentation and energy-saving product recovery. *Bioresour. Technol.* **2013**, 135, 396-402.
190. Lu, K.-M.; Li, S.-Y., An integrated in situ extraction-gas stripping process for Acetone–Butanol–Ethanol (ABE) fermentation. *J. Taiwan Inst. Chem. Eng.* **2014**, 45, (5), 2106-2110.
191. Xue, C.; Liu, F.; Xu, M.; Tang, I.-C.; Zhao, J.; Bai, F.; Yang, S.-T., Butanol production in acetone–butanol–ethanol fermentation with in situ product recovery by adsorption. *Bioresour. Technol.* **2016**, 219, 158-168.
192. Xue, C.; Yang, D.; Du, G.; Chen, L.; Ren, J.; Bai, F., Evaluation of hydrophobic microzeolite-mixed matrix membrane and integrated with acetone–butanol–ethanol fermentation for enhanced butanol production. *Biotechnol. Biofuels* **2015**, 8, (1), 1-9.
193. Van Hecke, W.; Vandezande, P.; Dubreuil, M.; Uyttebroek, M.; Beckers, H.; De Wever, H., Biobutanol production from C5/C6 carbohydrates integrated with pervaporation: experimental results and conceptual plant design. *J. Ind. Microbiol. Biotechnol.* **2016**, 43, (1), 25-36.
194. Roffler, S.; Blanch, H. W.; Wilke, C. R., Extractive fermentation of acetone and butanol: process design and economic evaluation. *Biotechnol. Progr.* **1987**, 3, (3), 131-140.
195. Oudshoorn, A.; Van Der Wielen, L. A.; Straathof, A. J., Assessment of options for selective 1-butanol recovery from aqueous solution. *Ind. Eng. Chem. Res.* **2009**, 48, (15), 7325-7336.
196. Matsumura, M.; Kataoka, H., Separation of dilute aqueous butanol and acetone solutions by pervaporation through liquid membranes. *Biotechnol. Bioeng.* **1987**, 30, (7), 887-895.
197. Groot, W.; Soedjak, H.; Donck, P.; Van der Lans, R.; Luyben, K. C. A.; Timmer, J., Butanol recovery from fermentations by liquid-liquid extraction and membrane solvent extraction. *Bioprocess. Eng.* **1990**, 5, (5), 203-216.
198. Kraemer, K.; Harwardt, A.; Bronneberg, R.; Marquardt, W., Separation of butanol from acetone–butanol–ethanol fermentation by a hybrid extraction–distillation process. *Comput. Chem. Eng.* **2011**, 35, (5), 949-963.
199. Garcia-Chavez, L. Y.; Garsia, C. M.; Schuur, B.; de Haan, A. B., Biobutanol recovery using nonfluorinated task-specific ionic liquids. *Ind. Eng. Chem. Res.* **2012**, 51, (24), 8293-8301.
200. Mulchandani, A.; Volesky, B., Modelling of the acetone - butanol fermentation with cell retention. *Can. J. Chem. Eng.* **1986**, 64, (4), 625-631.
201. Ehlinger, V. M.; Gabriel, K. J.; Noureldin, M. M. B.; El-Halwagi, M. M., Process Design and Integration of Shale Gas to Methanol. *ACS Sustainable Chemistry & Engineering* **2014**, 2, (1), 30-37.
202. He, C.; You, F., Shale Gas Processing Integrated with Ethylene Production: Novel Process Designs, Exergy Analysis, and Techno-Economic Analysis. *Industrial & Engineering Chemistry Research* **2014**, 53, (28), 11442-11459.
203. Hill, R. J.; M.Jarvie, D.; Zumberge, J.; Henry, M.; Pollastro, R. M., Oil and Gas Geochemistry and Petroleum Systems of the Fort Worth Basin. *AAPG Bulletin* **2007**, 91, (4), 445-473.

204. Chen, Z.; Henson, M. A.; Belanger, P.; Megan, L., Nonlinear Model Predictive Control of High Purity Distillation Columns for Cryogenic Air Separation. *IEEE Transactions on Control Systems Technology* **2010**, 18, (4), 811-821.
205. Maqsood, K.; Ali, A.; Shariff, A. B. M.; Ganguly, S., Synthesis of conventional and hybrid cryogenic distillation sequence for purification of natural gas. *Journal of Applied Sciences* **2014**, 21, 2722-2729.
206. Maqsood, K.; Ali, A.; Shariff, A. B. M.; Ganguly, S., Process intensification using mixed sequential and integrated hybrid cryogenic distillation network for purification of high CO₂ natural gas. *Chemical Engineering Research and Design* **2017**, 117, 414-438.
207. Sirola, J. J., The impact of shale gas in the chemical industry. *AIChE Journal* **2014**, 60, (3), 810-819.
208. Chen, Y.; Kontogeorgis, G. M.; Woodley, J. M., Integrated ionic liquid and process design involving azeotropic separation processes. *Chemical Engineering Science* **2019**, Revised.
209. Kumelan, J.; Pérez-Salado Kamps, Á.; Tuma, D.; Maurer, G., Solubility of H₂ in the ionic liquid [hmim][Tf₂N]. *Journal of Chemical & Engineering Data* **2006**, 51, (4), 1364-1367.
210. Ramdin, M.; Olasagasti, T. Z.; Vlugt, T. J. H.; de Loos, T. W., High pressure solubility of CO₂ in non-fluorinated phosphonium-based ionic liquids. *The Journal of Supercritical Fluids* **2013**, 82, 41-49.
211. Chen, Y.; Kontogeorgis, G. M.; Woodley, J. M., Group-contributed estimation method for properties of ionic liquids. *Ind. Eng. Chem. Res.* **2019**, 58, (10), 4277-4292.
212. Valderamma, J. O.; Sanga, W. W.; Lazzus, J. A., Critical Properties, Normal Boiling Temperature, and Acentric Factor of Another 200 Ionic Liquids. *Ind. Eng. Chem. Res.* **2008**, 47, 1318-1330.
213. Campbell, S. W.; Thodos, G., Rackett model-Saturated Liquid Densities of Polar and Nonpolar Pure Substances. *Ind. Eng. Chem. Fundam.* **1984**, 23, 500-510.
214. Ferreira, A. G. M.; Simões, P. N.; Ferreira, A. F.; Fonseca, M. A.; Oliveira, M. S. A.; Trino, A. S. M., Transport and thermal properties of quaternary phosphonium ionic liquids and IoNanofluids. *The Journal of Chemical Thermodynamics* **2013**, 64, 80-92.
215. Neves, C. M. S. S.; Carvalho, P. J.; Freire, M. G.; Coutinho, J. A. P., Thermophysical properties of pure and water-saturated tetradecyltriethylphosphonium-based ionic liquids. *The Journal of Chemical Thermodynamics* **2011**, 43, (6), 948-957.
216. Almeida, H. F. D.; Lopes-da-Silva, J. A.; Freire, M. G.; Coutinho, J. A. P., Surface tension and refractive index of pure and water-saturated tetradecyltriethylphosphonium-based ionic liquids. *The Journal of Chemical Thermodynamics* **2013**, 57, 372-379.
217. Ramdin, M.; Amphianitis, A.; Bazhenov, S.; Volkov, A.; Volkov, V.; Vlugt, T. J. H.; Loos, T. W. d., Solubility of CO₂ and CH₄ in Ionic Liquids: Ideal CO₂/CH₄ Selectivity. *Ind. Eng. Chem. Res.* **2014**, 53, (40), 15427-15435.
218. Xu, Y.; Huang, Y.; Wu, B.; Zhang, X.; Zhang, S., Biogas upgrading technologies: Energetic analysis and environmental impact assessment. *Chinese J. Chem. Eng.* **2015**, 23, (1), 247-254.
219. Hosseinpour, S.; Fatemi, S.; Mortazavi, Y.; Gholamhoseini, M.; Ravanchi, M. T., Performance of CaX Zeolite for Separation of C₂H₆, C₂H₄, and CH₄ by Adsorption Process; Capacity, Selectivity, and Dynamic Adsorption Measurements. *Separation Science and Technology* **2010**, 46, (2), 349-355.
220. Shen, Z.; Liu, J.; Xu, H.; Yue, Y.; Hua, W.; Shen, W., Dehydrogenation of ethane to ethylene over a highly efficient Ga₂O₃/HZSM-5 catalyst in the presence of CO₂. *Applied Catalysis A: General* **2009**, 356, (2), 148-153.
221. Liu, X.; Huang, Y.; Zhao, Y.; Gani, R.; Zhang, X.; Zhang, S., Ionic Liquid Design and Process Simulation for Decarbonization of Shale Gas. *Industrial & Engineering Chemistry Research* **2016**, 55, (20), 5931-5944.

222. Huang, Y.; Zhang, X.; Zhang, X.; Dong, H.; Zhang, S., Thermodynamic Modeling and Assessment of Ionic Liquid-Based CO₂Capture Processes. *Ind. Eng. Chem. Res.* **2014**, 53, (29), 11805-11817.
223. Abu-Zahra, M. R. M.; Niederer, J. P. M.; Feron, P. H. M.; Versteeg, G. F., CO₂ capture from power plants: Part II. A parametric study of the economical performance based on mono-ethanolamine. *International Journal of Greenhouse Gas Control* **2007**, 1, (2), 135-142.
224. Schach, M. O.; Schneider, R. D.; Schramm, H.; Repke, J. U., Techno-Economic Analysis of Postcombustion Processes for the Capture of Carbon Dioxide from Power Plant Flue Gas. *Ind.eng.chem.res* **2015**, 49, (5), 532-539.
225. Schach, M.-O.; Schneider, R.; Schramm, H.; Repke, J.-U., Techno-Economic Analysis of Postcombustion Processes for the Capture of Carbon Dioxide from Power Plant Flue Gas. *Industrial & Engineering Chemistry Research* **2010**, 49, (5), 2363-2370.
226. Walas, S. M., 20 - COSTS OF INDIVIDUAL EQUIPMENT. In *Chemical Process Equipment*, Walas, S. M., Ed. Butterworth-Heinemann: Boston, 1990; pp 663-669.
227. Mignard, D., Correlating the chemical engineering plant cost index with macro-economic indicators. *Chemical Engineering Research and Design* **2014**, 92, (2), 285-294.
228. Karimi, M.; Hillestad, M.; Svendsen, H. F., Capital costs and energy considerations of different alternative stripper configurations for post combustion CO₂ capture. *Chemical Engineering Research and Design* **2011**, 89, (8), 1229-1236.
229. Mores, P.; Rodríguez, N.; Scenna, N.; Mussati, S., CO₂ capture in power plants: Minimization of the investment and operating cost of the post-combustion process using MEA aqueous solution. *International Journal of Greenhouse Gas Control* **2012**, 10, 148-163.
230. Peters, L.; Hussain, A.; Follmann, M.; Melin, T.; Hägg, M. B., CO₂ removal from natural gas by employing amine absorption and membrane technology—A technical and economical analysis. *Chemical Engineering Journal* **2011**, 172, (2-3), 952-960.
231. Luyben, W. L., *Distillation Design and Control Using Aspen™ Simulation*. 2013.
232. Ma, T.; Wang, J.; Du, Z.; Abdeltawab, A. A.; Al-Enizi, A. M.; Chen, X.; Yu, G., A process simulation study of CO₂ capture by ionic liquids. *International Journal of Greenhouse Gas Control* **2017**, 58, 223-231.
233. Hassan, S. M. N.; Douglas, P. L.; Croiset, E., Techno-Economic Study of CO₂ Capture from an Existing Cement Plant Using MEA Scrubbing. *International Journal of Green Energy* **2007**, 4, (2), 197-220.
234. Raynal, L.; Bouillon, P.-A.; Gomez, A.; Broutin, P., From MEA to demixing solvents and future steps, a roadmap for lowering the cost of post-combustion carbon capture. *Chemical Engineering Journal* **2011**, 171, (3), 742-752.
235. Shindell, D. T.; Fuglestad, J. S.; Collins, W. J., The social cost of methane: theory and applications. *Faraday Discuss* **2017**, 200, 429-451.
236. Whited, G. M.; Feher, F. J.; Benko, D. A.; Cervin, M. A.; Chotani, G. K.; McAuliffe, J. C.; LaDuca, R. J.; Ben-Shoshan, E. A.; Sanford, K. J., Technology update: development of a gas-phase bioprocess for isoprene-monomer production using metabolic pathway engineering. *Ind. Biotechnol.* **2010**, 6, (3), 152-163.
237. Huibin, Z.; Liu, H.; Aboulnga, E.; Liu, H.; Cheng, T.; Xian, M., Microbial Production of Isoprene: Opportunities and Challenges. *Ind. Biotechnol.* **2017**, 473-504.
238. Ushio, S., Extract isoprene with DMF. *Chem. Eng.* **1972**, 79, (5), 82-83.
239. Abdelrahman, O. A.; Park, D. S.; Vinter, K. P.; Spanjers, C. S.; Ren, L.; Cho, H. J.; Zhang, K.; Fan, W.; Tsapatsis, M.; Dauenhauer, P. J., Renewable isoprene by sequential hydrogenation of itaconic acid and dehydra-decyclization of 3-methyl-tetrahydrofuran. *ACS Catal.* **2017**, 7, (2), 1428-1431.
240. Lundberg, D. J.; Lundberg, D. J.; Zhang, K.; Dauenhauer, P. J., Process Design and Economic Analysis of Renewable Isoprene from Biomass via Mesaconic Acid. *ACS Sustainable Chem. Eng.* **2019**, 7, (5), 5576-5586.

241. Morais, A. R.; Dworakowska, S.; Reis, A.; Gouveia, L.; Matos, C. T.; Bogdał, D.; Bogel-Lukasik, R., Chemical and biological-based isoprene production: Green metrics. *Catal. Today* **2015**, 239, 38-43.
242. King, C. J. In *Separations in the production of high-volume fuels and chemicals by biological processing*, Proceedings of the 25th Intersociety Energy Conversion Engineering Conference, 1990; IEEE: 1990; pp 509-513.
243. Ruhl, M. J., Recover VOCs via adsorption on activated carbon. *Chem. Eng. Prog. (United States)* **1993**, 89, (7).
244. McAuliffe, J. C.; Paramonov, S. E.; Sanford, K. J., Fuel compositions comprising isoprene derivatives. US8450549B2: 2013.
245. Hansmeier, A. R.; Meindersma, G. W.; de Haan, A. B., Desulfurization and denitrogenation of gasoline and diesel fuels by means of ionic liquids. *Green Chem.* **2011**, 13, (7), 1907-1913.
246. George, A.; Brandt, A.; Tran, K.; Zahari, S. M. N. S.; Klein-Marcuschamer, D.; Sun, N.; Sathitsuksanoh, N.; Shi, J.; Stavila, V.; Parthasarathi, R., Design of low-cost ionic liquids for lignocellulosic biomass pretreatment. *Green Chem.* **2015**, 17, (3), 1728-1734.
247. Gomes, J. M.; Silva, S. S.; Reis, R. L., Biocompatible ionic liquids: fundamental behaviours and applications. *Chem. Soc. Rev.* **2019**.
248. Chen, L.; Sharifzadeh, M.; Mac Dowell, N.; Welton, T.; Shah, N.; Hallett, J., Inexpensive ionic liquids:[HSO₄]⁻-based solvent production at bulk scale.
249. Plechkova, N. V.; Seddon, K. R., Applications of ionic liquids in the chemical industry. *Chem. Soc. Rev.* **2008**, 37, (1), 123-150.
250. Fadeev, A. G.; Meagher, M. M., Opportunities for ionic liquids in recovery of biofuels. *Chem. Commun.* **2001**, (3), 295-296.
251. Brandt-Talbot, A.; Gschwend, F. J.; Fennell, P. S.; Lammens, T. M.; Tan, B.; Weale, J.; Hallett, J. P., An economically viable ionic liquid for the fractionation of lignocellulosic biomass. *Green Chem.* **2017**, 19, (13), 3078-3102.
252. Coleman, D.; Gathergood, N., Biodegradation studies of ionic liquids. *Chem. Soc. Rev.* **2010**, 39, (2), 600-637.
253. Stolte, S.; Matzke, M.; Arning, J.; Bösch, A.; Pitner, W.-R.; Welz-Biermann, U.; Jastorff, B.; Ranke, J., Effects of different head groups and functionalised side chains on the aquatic toxicity of ionic liquids. *Green Chem.* **2007**, 9, (11), 1170-1179.
254. Zhou, L.; Shang, X.; Fan, J.; Wang, J., Solubility and selectivity of CO₂ in ether-functionalized imidazolium ionic liquids. *J. Chem. Thermodyn.* **2016**, 103, 292-298.
255. Blanchard, L. A.; Gu, Z.; Brennecke, J. F., High-pressure phase behavior of ionic liquid/CO₂ systems. *J. Phys. Chem. B* **2001**, 105, (12), 2437-2444.
256. Soriano, A. N.; Doma Jr, B. T.; Li, M.-H., Solubility of carbon dioxide in 1-ethyl-3-methylimidazolium tetrafluoroborate. *J. Chem. Eng. Data* **2008**, 53, (11), 2550-2555.
257. Lei, Z.; Yuan, J.; Zhu, J., Solubility of CO₂ in propanone, 1-ethyl-3-methylimidazolium tetrafluoroborate, and their mixtures. *J. Chem. Eng. Data* **2010**, 55, (10), 4190-4194.
258. Zhao, Y.; Yang, J.; Qin, B.; Li, Y.; Sun, Y.; Su, S.; Xian, M., Biosynthesis of isoprene in *Escherichia coli* via methylerythritol phosphate (MEP) pathway. *Appl. Microbiol. Biotechnol.* **2011**, 90, (6), 1915.
259. Liu, C.-L.; Bi, H.-R.; Bai, Z.; Fan, L.-H.; Tan, T.-W., Engineering and manipulation of a mevalonate pathway in *Escherichia coli* for isoprene production. *Appl. Microbiol. Biotechnol.* **2019**, 103, (1), 239-250.
260. Tian, H.; Zada, B.; Singh, B. H.; Wang, C.; Kim, S.-W., Synthetic Biology Approaches for the Production of Isoprenoids in *Escherichia coli*. In *Curr. Dev. Biotechnol. Bioeng.*, Elsevier: 2019; pp 311-329.
261. Anthony, J. R.; Anthony, L. C.; Nowroozi, F.; Kwon, G.; Newman, J. D.; Keasling, J. D., Optimization of the mevalonate-based isoprenoid biosynthetic pathway in *Escherichia coli*

for production of the anti-malarial drug precursor amorpha-4, 11-diene. *Metab. Eng.* **2009**, 11, (1), 13-19.

262. Cervin, M. A.; Chotani, G. K.; Feher, F. J.; La Duca, R.; McAuliffe, J. C.; Miasnikov, A.; Peres, C. M.; Puhala, A. S.; Sanford, K. J.; Valle, F., Compositions and methods for producing isoprene. US8288148B2: 2012.

APPENDIX A

GROUP CONTRIBUTION PARAMETERS FOR GC-BASED PROPERTY MODELS

Table A.1 Group contribution parameters for density

	$a_{i,\rho}$ (kg.m ⁻³)	$b_{i,\rho}$ (kg.m ⁻³ .K ⁻¹)	$c_{i,\rho}$ (kg.m ⁻³ .MPa ⁻¹)
Substituents			
-CH ₃	-66.767	0.163	-0.274
-CH ₂ -	-40.521	0.030	-0.020
-dmN	-69.079	0.086	10.161
Cations			
1,3-dimethylimidazolium (+)	1,099 x 10 ³	3.956	6.687
1,1-dimethylpyridinium (+)	1,147 x 10 ³	3.810	6.714
1,1-dimethylpyrrolidinium (+)	1,094 x 10 ³	3.885	6.543
Tetramethyl ammonium (+)	1,106 x 10 ³	3.952	19.553
Tetramethyl phosphonium (+)	1,693 x 10 ³	3.361	7.144
1,1-dimethylpiperidinium (+)	1,043 x 10 ³	3.956	6.608
Anions			
[Tf ₂ N]-	724.274	-4.933	-5.969
[BF ₄]-	395.546	-4.594	-6.219
[PF ₆]-	649.046	-4.932	-5.879
[Cl]-	335.520	-4.745	-6.368
[Ac]-	241.839	-4.613	-6.178
[MeSO ₄]-	353.840	-4.439	-6.258
[EtSO ₄]-	377.558	-4.665	37.100
[CF ₃ SO ₃]-	598.051	-4.938	-6.057
[Br]-	560.637	-4.763	-6.051
[CF ₃ COO]-	453.169	-4.787	36.623
[N(CN) ₂]-	261.113	-4.659	35.582
[C(CN) ₃]-	259.203	-4.687	-6.181
[AlCl ₄]-	295.949	-4.155	49.891
[InCl ₄]-	861.751	-5.046	138.233
[(CH ₃) ₂ PO ₄]-	373.126	-4.680	-6.251
[FeCl ₄]-	609.170	-4.827	54.561
[GaCl ₄]-	161.394	-3.189	25.417
[Tf ₂ N]-	116.042	-2.676	-7.299

Table D.2 Group contribution parameters for heat capacity

	$a_{i,C_{pL}}$	$b_{i,C_{pL}} \text{ (K}^{-1}\text{)}$	$d_{i,C_{pL}} \text{ (K}^{-2}\text{)}$
Substituents			
-CH ₃	156.63	-112.01	19.28
-CH ₂ -	5.35	-1.36	0.30
-dmN	26.73	-13.61	2.42
Cations			
1,3-dimethylimidazolium (+)	22.45	-22.59	-2.59
1-methylpyridinium (+)	2.98	-6.39	-5.48
1,1-dimethylpyrrolidinium (+)	19.49	-20.52	-2.75
Tetramethyl ammonium (+)	106.57	-71.42	4.06
Trihexyl tetradecyl phosphonium (+)	-45.85	41.35	-9.45
1,1-dimethylpiperidinium (+)	23.98	-19.57	-2.87
Anions			
[Tf ₂ N]-	13.80	30.68	2.23
[BF ₄]-	-25.69	25.09	2.86
[PF ₆]-	0.00	42.57	0.43
[Cl]-	2.82	19.25	3.80
[Ac]-	8.11	19.50	4.02
[MeSO ₄]-	-54.86	59.36	-2.41
[EtSO ₄]-	16.92	20.05	3.75
[CF ₃ SO ₃]-	-7.10	36.11	1.09
[Br]-	-0.17	21.96	3.16
[CF ₃ COO]-	2.36	26.69	2.61
[N(CN) ₂]-	5.94	22.35	3.24
[C(CN) ₃]-	45.52	0.00	6.75
[(CH ₃) ₂ PO ₄]-	-444.63	299.91	-39.11
[FeCl ₄]-	-16.99	42.17	0.00

Table D.3 Group contribution parameters for viscosity ($R_{0\eta}$ =14.877 Pa.s)

	$a_{i,\eta}$	$b_{i,\eta} \text{ (K)}$	$d_{i,\eta} \text{ (K}^2\text{)}$
Substituents			
-CH ₃	0.933	-7.113	13.456
-CH ₂ -	-0.346	1.460	0.076
-dmN	5.319	-35.574	61.498
Cations			
1,3-dimethylimidazolium (+)	1.811	-12.885	68.642
1,2,3-trimethylimidazolium (+)	-1.260	3.516	53.002
1-methylpyridinium (+)	3.710	-26.702	94.864
1,1-dimethylpyrrolidinium (+)	0.106	0.605	45.537
Tetramethyl ammonium (+)	6.829	-48.328	134.296
Tetramethyl phosphonium (+)	-0.650	4.068	38.609

Trihexyl tetradecyl phosphonium (+)	0.275	-9.725	94.069
1,1-dimethylpiperidinium (+)	7.069	-52.878	152.840
Anions			
[Tf ₂ N]-	-8.316	-16.355	21.492
[BF ₄]-	-5.882	-36.536	67.261
[PF ₆]-	-15.446	22.093	-12.529
[Cl]-	-95.536	507.333	-750.412
[Ac]-	7.889	-141.685	261.178
[MeSO ₄]-	-8.035	-20.293	37.956
[EtSO ₄]-	-6.103	-34.046	63.386
[CF ₃ SO ₃]-	-4.313	-38.135	52.575
[Br]-	-8.849	-16.287	45.433
[CF ₃ COO]-	-2.852	-50.171	72.712
[N(CN) ₂]-	-7.697	-20.126	22.490
[C(CN) ₃]-	-5.616	-36.359	52.103
[AlCl ₄]-	-9.494	-5.058	-7.965
[(CH ₃) ₂ PO ₄]-	-6.464	-32.730	71.381
[FeCl ₄]-	-6.766	-25.374	33.078
[Tf ₂ N]-	-6.092	-35.181	65.466

Table D.4 Group contribution parameters for surface tension

	$a_{i,\sigma}$ (N.m ⁻¹)	$b_{i,\sigma}$ (N.m ⁻¹ .K ⁻¹)	$d_{i,\sigma}$ (N.m ⁻¹ .K ⁻²)
Substituents			
-CH ₃	2.583	-1.734	0.286
-CH ₂ -	-0.195	0.079	-0.010
Cations			
1,3-dimethylimidazolium (+)	-2.431	0.280	-0.257
1-methylpyridinium (+)	-4.906	1.928	-0.525
1,1-dimethylpyrrolidinium (+)	-1.882	-0.092	-0.190
Tetramethyl ammonium (+)	-1.672	0.096	-0.249
Trihexyl tetradecyl phosphonium (+)	10.822	-8.234	1.061
1,1-dimethylpiperidinium (+)	-2.199	0.186	-0.247
Anions			
[Tf ₂ N]-	-0.247	-0.511	0.268
[BF ₄]-	-1.161	0.327	0.127
[PF ₆]-	0.340	-0.683	0.291
[Cl]-	0.704	-0.838	0.310
[Ac]-	5.260	-3.763	0.752
[MeSO ₄]-	-4.272	2.336	-0.198
[EtSO ₄]-	1.762	-1.692	0.463
[CF ₃ SO ₃]-	0.818	-1.087	0.352
[Br]-	-12.018	7.002	-0.905
[CF ₃ COO]-	-0.049	-0.568	0.269

[N(CN) ₂]-	-0.793	0.089	0.177
[C(CN) ₃]-	0.060	-0.385	0.235
[AlCl ₄]-	0.202	-0.561	0.270
[InCl ₄]-	1.211	-1.207	0.375
[(CH ₃) ₂ PO ₄]-	-0.396	-0.128	0.181
[FeCl ₄]-	1.340	-1.320	0.390
[GaCl ₂]-	0.349	-0.667	0.290
[Tf ₂ N]-	-0.005	-0.015	0.066

Table D.5 Group contribution parameters for thermal conductivity

	$c_{i,1\lambda}$ (W.m ⁻¹ .K ⁻¹)	$c_{i,2\lambda}$ (W.m ⁻¹ .K ⁻²)	$c_{i,3\lambda}$ (W.m ⁻¹ .K ⁻³)
Substituents			
CH ₃	-0.047	3.50E-04	-6.24E-07
CH ₂	-0.035	2.12E-04	-3.37E-07
dmN	-0.090	3.75E-04	-1.92E-07
Cations			
1,3-dmim (+)	0.195	-3.82E-04	3.78E-05
1-mpy (+)	0.347	-0.001	3.85E-05
1,1-dmpyr (+)	0.506	-0.002	4.10E-05
Am1,1,1,1 (+)	0.845	-0.004	4.38E-05
Ph1,1,1,1 (+)	0.627	-0.003	4.40E-06
TDph (+)	0.340	-0.001	3.92E-05
Anions			
[Tf ₂ N] ⁻	0.108	-6.74E-04	-3.61E-05
[BF ₄] ⁻	-0.171	0.001	-3.86E-05
[PF ₆] ⁻	0.149	-7.86E-04	-3.60E-05
[Cl] ⁻	-0.150	0.001	-3.92E-05
[Ac] ⁻	-0.122	0.002	-4.00E-05
[MeSO ₄] ⁻	0.119	-3.83E-04	-3.66E-05
[EtSO ₄] ⁻	0.763	-0.005	-3.01E-05
[CF ₃ SO ₃] ⁻	-0.020	5.87E-04	-3.80E-05
[CF ₃ COO] ⁻	-0.020	3.47E-04	-3.77E-05
[N(CN) ₂] ⁻	1.191	-0.007	-2.69E-05
[C(CN) ₃] ⁻	0.166	-5.67E-04	-3.65E-05
[B(CN) ₄] ⁻	0.017	3.96E-04	-3.81E-05
[DMP] ⁻	-0.172	-0.013	-1.30E-05
[DEP] ⁻	2.174	0.000	-1.84E-05
[SCN] ⁻	-0.020	5.87E-04	-3.80E-05
[eFAP] ⁻	-0.172	0.001	-3.89E-05

Table D.6 Group contribution parameters for melting point

	t_c (K)		t_a (K)		t_g (K)
Cations		Anions		Anions	
Imidazolium (+)	249.704	[BF ₄]-	40.001	[N(CN) ₂]-	21.607
Pyridinium (+)	279.704	[PF ₆]-	66.454	[C(CN) ₃]-	14.151
Pyrrolidinium (+)	260.259	[Cl]-	94.707	[AlCl ₄]-	31.601
Tetramethyl ammonium (+)	289.007	[Ac]-	6.707	[Tf ₂ N]-	24.101
Tetramethyl phosphonium (+)	297.262	[MeSO ₄]-	20.901	Substituents	
Piperidinium (+)	364.333	[CF ₃ SO ₃]-	22.651	-CH ₃	-27.747
Anions		[Br]-	105.407	-CH ₂ -	-1.303
[Tf ₂ N]-	22.757	[CF ₃ COO]-	23.969	-dmN	27.345

Table D.7 Group contribution parameters for electrical conductivity ($R_{0e}=7.175 \text{ S}\cdot\text{m}^{-1}$)

	$a_{i,\varepsilon}$	$b_{i,\varepsilon}$ (K)	$c_{i,\varepsilon}$ (K ²)
Cation cores			
Im (+)	-3.395	-2.203	-20.040
Py (+)	-8.186	27.411	-75.921
Pyr (+)	-11.433	22.238	-53.087
N (+)	-6.350	18.130	-47.838
P (+)	-2.374	-8.287	2.510
S (+)	0.217	-20.101	19.628
Pip (+)	-10.215	0.634	-9.746
Morp (+)	-7.063	-8.805	-3.713
Substituents			
(ring)-H	0.768	0.239	-1.863
-CH ₃	-0.916	14.681	-32.162
-CH ₂ -	-0.261	0.818	-2.914
-OH	-15.037	113.352	-219.442
-CH ₂ OCH ₃	-14.857	87.076	-129.174
Anions			
[Tf ₂ N] ⁻	2.434	-4.774	8.068
[BF ₄] ⁻	1.004	12.416	-35.592
[PF ₆] ⁻	-0.712	26.779	-71.130
[Cl] ⁻	-5.238	61.590	-138.793
[Br] ⁻	9.181	-58.797	81.002
[I] ⁻	-4.199	0.039	14.055
[COO] ⁻	4.746	-16.881	16.851
[C ₁ COO] ⁻	-18.287	137.632	-250.943
[C ₂ COO] ⁻	2.586	1.629	-30.423
[C ₃ COO] ⁻	2.232	6.316	-46.319
[C ₅ COO] ⁻	7.528	-30.348	62.526

[C ₇ COO] ⁻	6.315	-24.051	52.043
[C ₉ COO] ⁻	8.680	-42.717	83.824
[MeSO ₄] ⁻	0.663	5.064	-14.378
[EtSO ₄] ⁻	-0.901	19.849	-42.019
[C ₈ SO ₄] ⁻	-2.117	24.723	-64.297
[CF ₃ SO ₃] ⁻	1.935	-0.173	-4.067
[CF ₃ COO] ⁻	1.445	1.756	-1.403
[CH ₃ SO ₃] ⁻	-9.465	77.852	-141.887
[N(CN) ₂] ⁻	0.384	10.832	-10.825
[C(CN) ₃] ⁻	1.209	2.114	-1.333
[B(CN) ₄] ⁻	-0.526	12.808	-11.593
[C ₂ PO ₃] ⁻	1.020	-5.226	14.679
[C ₄ PO ₃] ⁻	0.433	-3.128	0.337
[C ₆ PO ₃] ⁻	19.378	-137.830	241.937
[C ₈ PO ₃] ⁻	1.111	-23.714	68.857
[Pf ₂ N] ⁻	1.179	3.507	-14.629
[eFAP] ⁻	2.392	-8.346	16.376
[OHCO ₂] ⁻	-1.491	8.359	3.457
[(OH) ₂ PO ₂] ⁻	3.303	-19.117	43.664
[NO ₃] ⁻	3.193	-2.012	0.138
[TS ₂ N] ⁻	-0.920	16.681	-17.053
[Tos] ⁻	-10.515	83.229	-158.476
[SCN] ⁻	2.298	1.030	-7.327

APPENDIX B

GROUP INTERACTION PARAMETERS FOR UNIFAC-IL-GAS MODEL

Group i	Group j	a_{ij} /K	a_{ji} /K
1	14	345.666	8263.447
1	15	2756.331	-861.127
1	16	-526.94	-185.923
1	17	369.609	3.574
1	18	35.985	273.466
1	19	-266.717	348.868
1	20	328.338	-885.129
1	21	178.074	8.483
1	22	183.335	84.429
1	23	4290.779	-186.683
1	24	91.512	-94.301
1	25	-109.387	3.117
1	26	90.297	175.978
1	27	105.069	217.517
1	28	-267.962	15845.413
1	29	70.406	2.901
1	30	-313.276	5210.923
1	31	-117.32	557123.353
1	32	612.287	-194.366
1	33	263.737	108.455
1	34	-211.101	5835.258
1	35	4501.104	-65.587
1	36	-71	308.979
1	37	4361.815	5848.482
1	38	-270.548	4040.883
1	39	-216.611	5356.545
1	40	-46.832	-36.672

1	41	0.769	-37.589
1	42	4290.779	8199.819
1	43	-112.511	24603.541
1	44	48.071	307.36
1	45	-134.384	-114.697
1	46	-183.244	4921.637
1	47	72.859	-37.024
2	14	1006.93	828.764
2	15	352.749	9382.033
2	16	-6.168	-714.615
2	17	548.31	0.278
2	18	77.794	10000.000
2	19	4069.937	-430.448
2	20	182.4	10000.000
2	21	0.008	844.586
2	22	-244.414	451.838
2	23	-1663.373	434.671
2	24	-214.779	1.174
2	25	4001.684	-702.854
2	26	4069.937	-281.085
2	27	-248.768	-62.22
2	28	-198.964	1.05
2	29	-311.209	-52.319
2	30	-279.509	1.985
2	31	0.672	-446.314
2	32	-706.601	5027.576
2	33	-199.336	51.463
2	34	-14.803	-572.429
2	35	1200.926	-521.128
2	36	-277.841	300.62
2	37	94.909	-998.496
2	38	-655.175	-628.769
2	39	-5.901	-515.59
2	40	895.546	-574.093

2	41	-389.795	965.606
2	42	2872.276	10000
2	43	-181.983	1.73
2	44	316.496	-329.336
2	45	-4663.975	-335.882
2	46	4069.252	-525.497
2	47	3688.11	72758.31
3	14	129.83	146.594
3	15	2759.662	176.319
3	16	-49.9	-209.873
3	17	73.712	38.785
3	18	-159.661	582.119
3	19	2924.126	-63.677
3	20	-52.769	-269.23
3	21	-187.633	-24.753
3	22	915.532	-44.491
3	23	153.403	-149.928
3	24	-5.775	53.718
3	25	9.344	39.328
3	26	-152.839	10993.582
3	27	69.911	-59.478
3	28	1120.308	-188.564
3	29	134.38	-71.021
3	30	-55.587	130.724
3	31	1111.876	-292.912
3	32	-338.249	12181.45
3	33	520.64	381.463
3	34	4240.421	-362.914
3	35	-234.218	-10.632
3	36	13.523	39.945
3	37	-654.318	-269.229
3	38	-196.299	-259.93
3	39	1445.751	-252.462
3	40	1235.767	-115.038

3	41	348.48	-112.126
3	42	153.403	-149.928
3	43	1233.686	-232.293
3	44	2621.796	-188.181
3	45	4239.82	-416.947
3	46	1103.238	-185.143
3	47	-3.648	-9.046
4	14	-298.736	8247.421
4	15	333.52	923.366
4	16	0.792	-185.481
4	17	47.714	313.489
4	18	578.962	514.878
4	19	-1.308	835.332
4	20	193.175	357.282
4	21	4168.084	596.857
4	22	2973.467	784.872
4	23	1341.731	-232.39
4	24	-278.6	8048.857
4	25	-0.051	314.838
4	26	104.556	27.99
4	27	-249.904	1355.529
4	28	-206.443	104250.058
4	29	-261.698	1190.16
4	30	-332.668	499.955
4	31	182.934	461.247
4	32	-348.169	870.012
4	33	-320.899	668.009
4	34	67.107	378.835
4	35	478.932	614.086
4	36	-343.513	1012.296
4	37	-5450.164	-268.736
4	38	-263.415	517.502
4	39	259.91	384.997
4	40	-186.57	4531.5

4	41	-238.959	423.216
4	42	1341.731	-232.39
4	43	392.884	473.192
4	44	-169.706	38046.942
4	45	-5571.093	55868.68
4	46	-224.51	178357.139
4	47	3795.924	-172.089
5	14	-10.091	280.807
5	15	-9.108	4749.809
5	16	253.549	-5.903
5	17	-89.55	278.899
5	18	4256.602	-59.881
5	19	148.855	400.408
5	20	969.58	-783.708
5	21	4256.602	184.967
5	22	1875.066	-198.907
5	23	461.118	-240.522
5	24	-18.737	7.206
5	25	2.798	278.386
5	26	-238.859	665.253
5	27	209.31	27.638
5	28	743.088	-90.176
5	29	136.622	81.727
5	30	-109.887	86.568
5	31	3379.087	-136.601
5	32	7.332	7.332
5	33	354.457	-166.178
5	34	4256.602	-191.424
5	35	4256.602	-144.199
5	36	-125.994	210.676
5	37	4256.602	250.596
5	38	-281.065	-107.602
5	39	1154.77	-32.72
5	40	503.491	23.974

5	41	-283.169	241.422
5	42	461.118	-240.522
5	43	1879.571	-87.411
5	44	1207.856	-81.348
5	45	4256.602	-332.719
5	46	1051.446	-117.08
5	47	4180.497	7079.73
6	14	42.354	490.127
6	15	-403.316	-90.993
6	16	-40.789	-140.894
6	17	26.366	490.298
6	18	1634.741	63.195
6	19	-52.822	3192.207
6	20	156.799	-56.207
6	21	4136.467	-426.912
6	22	-0.039	-68.798
6	23	-368.121	894.809
6	24	-70.841	177.858
6	25	54.061	490.286
6	26	39.276	471.644
6	27	1812.862	32.995
6	28	-199.649	675.171
6	29	-279.903	1961212.888
6	30	-289.93	3353.024
6	31	4136.467	4.839
6	32	-297.971	277.036
6	33	-187.989	703.406
6	34	4136.467	35.01
6	35	4136.467	264.351
6	36	-267.101	976.449
6	37	-4897.479	436714.083
6	38	-612.98	206.624
6	39	-234.713	1133.741
6	40	-350.127	421582.72

6	41	-328.057	436.199
6	42	-368.121	894.809
6	43	4136.467	-27.422
6	44	3943.948	31.642
6	45	-5377.398	125102.611
6	46	-241.16	375727.545
6	47	-0.747	-68.788
7	14	42.55	432.014
7	15	3424.047	3664.642
7	16	-1.22E+03	1.32E+07
7	17	25.863	432.014
7	18	4030.273	54861.123
7	19	-742.21	-4266.787
7	20	10282.223	5322.84
7	21	93.099	570.138
7	22	268.497	111.867
7	23	4247.379	47.35
7	24	100.954	11248.809
7	25	53.96	432.015
7	26	39.623	392.064
7	27	282.321	169.088
7	28	-145.194	38.594
7	29	492.028	192.702
7	30	-236.958	628.692
7	31	3919.026	66.714
7	32	679.135	107.751
7	33	460.321	102.229
7	34	2022.735	48.706
7	35	93.109	570.14
7	36	32.179	350.701
7	37	1413.891	-1334.654
7	38	-643.581	3624.547
7	39	2095.702	259.387
7	40	-56.522	773.386

7	41	-416.773	9137.664
7	42	-420.634	7352.027
7	43	1761.682	25.251
7	44	1119.026	1.11
7	45	-5293.398	59070.726
7	46	-2.194	257.545
7	47	2148.896	2112.95
8	14	42.225	291.021
8	15	-247.236	-518.384
8	16	-1.02E+03	1.35E+04
8	17	25.39	291.034
8	18	-209.582	29648.442
8	19	102.186	2104517.225
8	20	218.187	-504.928
8	21	172.895	525.832
8	22	-97.014	260.1
8	23	-331.628	1139.383
8	24	41.482	343.757
8	25	54.234	291.063
8	26	79.419	380.279
8	27	114.765	107.476
8	28	-96.691	-53.739
8	29	-84.301	385.724
8	30	-178.903	488.452
8	31	1304.506	-95.54
8	32	179.423	179.423
8	33	56.127	151.4
8	34	4171.96	-111.778
8	35	172.933	525.831
8	36	126.331	176.636
8	37	-4381.852	871216.419
8	38	-28.913	-291.003
8	39	80.122	159.056
8	40	33.407	203.902

8	41	2.788	83.255
8	42	-331.628	1139.383
8	43	628.002	-48.352
8	44	727.741	13.344
8	45	-5343.402	8615.384
8	46	214.663	128.203
8	47	0.269	311.393
9	14	176.237	9659.82
9	15	-504.804	224.168
9	16	5.51E-01	1.83E+02
9	17	110.863	8842.652
9	18	-116.777	-419.186
9	19	3997.01	602.657
9	20	2.467	53891.279
9	21	520.345	78.893
9	22	1.745	-969.367
9	23	4129.06	1476.161
9	24	7.218	680.812
9	25	3729.56	565.976
9	26	131.065	1107.65
9	27	3997.01	518.471
9	28	108.257	210.074
9	29	3997.01	634.483
9	30	958.31	531.961
9	31	-445.941	1195.541
9	32	57.932	200.354
9	33	2155.194	586.693
9	34	3997.01	415.333
9	35	791.627	1038.964
9	36	3997.01	697.142
9	37	4198.101	10366.291
9	38	-429.161	336.192
9	39	3997.01	565.066
9	40	3796.013	725.463

9	41	922.719	542.783
9	42	4129.06	8900.065
9	43	-419.594	1294.847
9	44	3997.01	605.436
9	45	263.522	404.431
9	46	3997.01	590.967
9	47	0.062	-969.372
10	14	86.164	629.366
10	15	4153.946	7380.055
10	16	-3.95E+02	1.07E+03
10	17	93.491	629.359
10	18	3962.025	694.939
10	19	4153.946	8095.696
10	20	-429.187	10000
10	21	4153.946	169.288
10	22	2767.797	6230.621
10	23	-435.4	4498.29
10	24	-50.479	192.225
10	25	1517.692	47.224
10	26	-3.462	810.434
10	27	4153.946	414.262
10	28	2709.724	421.76
10	29	4153.946	470.29
10	30	4153.946	304.273
10	31	4153.946	360.135
10	32	124.76	629.363
10	33	2944.924	494.723
10	34	3961.427	311.283
10	35	4153.946	12137.834
10	36	995.06	480.802
10	37	4153.946	10000
10	38	1059.399	91.093
10	39	4153.147	421.648
10	40	1545.082	499.373

10	41	-382.828	292389.397
10	42	4291.181	977.639
10	43	872.432	420.079
10	44	76369.851	442.866
10	45	6.752	184.872
10	46	4153.946	437.881
10	47	1609.713	128.963
11	14	172.813	6484.134
11	15	682.323	-243.609
11	16	9.00E-03	-1.24E+02
11	17	284.981	247.54
11	18	321.75	127.187
11	19	4153.946	8095.696
11	20	7.04	302.24
11	21	19890.002	608.091
11	22	-0.078	206.987
11	23	370.789	-20.462
11	24	66.334	44.119
11	25	2.252	5.055
11	26	-69.908	580.668
11	27	942.336	-140.971
11	28	134.359	29.849
11	29	1844.917	-123.348
11	30	463.296	-191.048
11	31	317.645	-128.202
11	32	1027.556	1027.556
11	33	452.039	-109.58
11	34	-94.444	-14.325
11	35	73.42	57.796
11	36	705.566	-33.274
11	37	162.932	10000
11	38	101.058	-446.487
11	39	-52.528	88.067
11	40	266.543	3.863

11	41	-11.169	161.819
11	42	370.789	-20.462
11	43	143.007	1.293
11	44	350.558	-25.715
11	45	2002.641	-294.176
11	46	-79.24	208.841
11	47	4.852	467.967
12	14	604.247	264.834
12	15	-59.285	-35.036
12	16	4.78E+02	-2.46E+01
12	17	242.075	29.545
12	18	3025.238	5.209
12	19	-129.378	-196.204
12	20	-90.568	-25.657
12	21	3681.333	-433.094
12	22	-68.903	27.04
12	23	-359.258	1010.26
12	24	206.843	29.58
12	25	2711.998	324.408
12	26	440.116	684.522
12	27	-15.814	8539.921
12	28	4276.599	148.392
12	29	87.464	4959.592
12	30	112.473	5567.11
12	31	4276.599	163.791
12	32	4276.599	4276.599
12	33	267.067	479.021
12	34	2513.528	255.807
12	35	4276.599	4975.066
12	36	4084.079	242.091
12	37	4276.599	6384.249
12	38	4276.599	-29.083
12	39	296.807	6470.607
12	40	149.333	5042.962

12	41	210.78	227.71
12	42	-359.258	1010.26
12	43	4276.599	115.953
12	44	2926.128	140.431
12	45	-5012.139	6451.379
12	46	42.837	11626.275
12	47	4276.599	7592.187
13	14	258.39	3974.003
13	15	-514.794	-62.515
13	16	5.00E-03	2.11E+01
13	17	169.041	-1.647
13	18	924.883	-146.974
13	19	-201.59	652.927
13	20	-16.159	-113.733
13	21	652.424	1178.513
13	22	53.554	10000
13	23	-331.932	798.673
13	24	50.508	27.514
13	25	4224.442	7426.61
13	26	86.310	156.746
13	27	4373.324	-132.521
13	28	-6.514	323.938
13	29	4373.324	-129.099
13	30	586.021	-157.238
13	31	-197.709	986.655
13	32	4373.324	4373.324
13	33	531.119	-84.665
13	34	1312.896	-118.317
13	35	741.078	-264.308
13	36	976.865	-105.771
13	37	-4608.031	9.29E+07
13	38	4180.804	-379.729
13	39	55.855	117.319
13	40	-200.713	8243.01

13	41	212.932	5.904
13	42	-331.932	798.673
13	43	-228.575	2633.873
13	44	-158.839	850.366
13	45	-5411.572	2592.962
13	46	-204.807	6283.593
13	47	636.765	-255.245
14	15	986.500	156.400
14	16	251.500	83.360
14	17	65.080	134.110
14	18	-24.940	1269.620
14	19	6930.911	9252.789
14	20	7783.260	-791.240
14	21	9916.233	18350.253
14	24	19.680	300.610
14	25	703.250	8730.620
14	26	219.440	-34.640
14	27	154.79	816.71
14	28	16004.648	16474.475
14	29	154.79	816.71
14	30	694.19	-285.94
14	31	62147.194	8615.596
14	32	331.64	-19.44
14	33	595.73	-229.99
14	34	8196.014	5657.644
14	35	4517.704	4498.278
14	36	89.02	136.82
14	37	-4999.54	-594.89
14	38	183.605	8730.614
14	39	8204.35	8212.26
14	40	64315.474	9714.071
14	41	8195.99	-469.69
14	43	5186.583	5406.077
14	44	7799.171	8730.62

14	45	-5227.934	-4144.373
14	46	29403.075	8730.621
15	16	28.060	237.700
15	17	-199.990	737.690
15	18	-147.610	1789.950
15	20	5524.910	-417.340
15	24	-320.230	636.960
15	25	-223.620	32.290
15	26	-61.130	536.610
15	27	-33.36	64.06
15	29	-126.41	-28.95
15	30	91.85	220.7
15	32	-56.32	-57.35
15	37	-976.48	-678.25
15	38	-777.58	-941.81
16	17	-220.860	-376.850
16	18	-281.650	-15.870
16	20	895.420	1728.790
16	24	-7649.640	-113.900
16	25	3716.540	-13.820
16	27	804.02	77.16
16	30	469.89	197.5

APPENDIX C

VAPOR PRESSURE CALCULATION METHODS FOR GASES INVOLVED IN UNIFAC-IL-GAS MODEL

Gases	Methods	Equations (T/K, P ^s /Pa)	Parameters				
			A	B	C	D	E
CO ₂	DIPPR	$P^s = \exp \left[A + \frac{B}{T} + C \ln T + DT^E \right]$	47.0169	-2839	-3.86388	2.81E-16	6
CO	DIPPR	$P^s = \exp \left[A + \frac{B}{T} + C \ln T + DT^E \right]$	39.205	-1324.4	-3.4366	3.10E-05	2
SO ₂	DIPPR	$P^s = \exp \left[A + \frac{B}{T} + C \ln T + DT^E \right]$	47.365	-4084.5	-3.6469	1.80E-17	6
O ₂	DIPPR	$P^s = \exp \left[A + \frac{B}{T} + C \ln T + DT^E \right]$	39.205	-1324.4	-3.4366	3.10E-05	2
H ₂ S	DIPPR	$P^s = \exp \left[A + \frac{B}{T} + C \ln T + DT^E \right]$	85.584	-3839.9	-11.199	0.018848	1
NH ₃	Antoine	$\log_{10} P^s = A - B/(T + C)$	4.86886	1113.928	-10.409	--	--
N ₂	DIPPR	$P^s = \exp \left[A + \frac{B}{T} + C \ln T + DT^E \right]$	39.205	-1324.4	-3.4366	3.10E-05	2
N ₂ O	Antoine	$\log_{10} P^s = A - B/(T + C)$	4.37799	621.077	-44.659	--	--
H ₂	DIPPR	$P^s = \exp \left[A + \frac{B}{T} + C \ln T + DT^E \right]$	39.205	-1324.4	-3.4366	3.10E-05	2
CH ₄	Antoine	$\log_{10} P^s = A - B/(T + C)$	4.22061	516.689	11.223	--	--
C ₂ H ₄	Antoine	$\log_{10} P^s = A - B/(T + C)$	3.87261	584.146	-18.307	--	--
C ₂ H ₆	Antoine	$\log_{10} P^s = A - B/(T + C)$	3.93835	659.739	-16.719	--	--
C ₃ H ₈	Antoine	$\log_{10} P^s = A - B/(T + C)$	4.01158	834.26	-22.763	--	--

APPENDIX D

KINETICS MODEL OF ABE FERMENTATION PROCESS

The kinetics model of ABE fermentation process developed by Mulchandani and Volesky ⁸⁶ can be summarized as following equations:

$$r_X = \mu_m \frac{S}{S+K_S} f(I)X \quad D1$$

$$-r_S = k_3\mu_m X + k_4X + k_1 \frac{S}{S+K_S} \frac{BA}{BA+K_{BA}} X + k_2 \frac{S}{S+K_S} \frac{AA}{AA+K_{AA}} X \quad D2$$

$$r_{BA} = k_5 \left[k_3\mu_m \frac{S}{S+K_S} f(I)X + k_4X \right] - k_6 \frac{S}{S+K_S} \frac{BA}{BA+K_{BA}} X \quad D3$$

$$r_{AA} = k_8 \left[k_3\mu_m \frac{S}{S+K_S} f(I)X + k_4X \right] - k_9 \frac{S}{S+K_S} \frac{AA}{AA+K_{AA}} X \quad D4$$

$$r_B = k_7 \left[k_3\mu_m \frac{S}{S+K_S} f(I)X + k_4X \right] - k_{14} \frac{S}{S+K_S} \frac{BA}{BA+K_{BA}} X \quad D5$$

$$r_A = k_{10} \left[k_3\mu_m \frac{S}{S+K_S} f(I)X + k_4X \right] - k_{15} \frac{S}{S+K_S} \frac{AA}{AA+K_{AA}} X \quad D6$$

$$r_E = k_{11} \left[k_3\mu_m \frac{S}{S+K_S} f(I)X + k_4X \right] \quad D7$$

The symbols involved in these equations are listed in Table D1 and the inhibition function $f(I)$ can be found in Section 3.3 (expressed by Eqs.8-11). All assumptions used in the development of this kinetics model are summarized in Table D2.

Table D1. List of the symbols involved in Eqs.A1-A7

Symbols	
r_X	Rate of biomass growth, g/L·h
μ_m	Maximum specific growth rate, 1/h
S	Substrate concentration in the fermentor, mmol/L
K_S	Saturation constant for substrate (sugar), mmol/L
r_S	Total substrate consumption rate, mmol/L·h
BA	Butyric acid concentration in the fermentor, mmol/L
K_{BA}	Saturation constant for acetic acid, mmol/L
AA	Acetic acid concentration in the fermentor, mmol/L
K_{AA}	Saturation constant for acetic acid, mmol/L
X	Biomass concentration in the fermentor, g/L
r_{BA}	Rate of butyric acid accumulation, mmol/L·h
r_{AA}	Rate of acetic acid accumulation, mmol/L·h

r_B	Rate of butanol accumulation, mmol/L·h
r_A	Rate of acetone accumulation, mmol/L·h
r_E	Rate of ethanol accumulation, mmol/L·h
$k_{1,2,...15}$	Model constants

Table D2. Assumptions used in the devevopment of kinetics model of ABE fermentation process

Assumptions
1. Carbon substrate limitation only.
2. No nitrogen and nutrient limitation.
3. Product inhibition.
4. Acetic acid and butyric acid are intermediate metabolites and are reduced to acetone and butanol respectively.
5. Acetone and butanol are also synthesized directly from carbon substrate.
6. Ethanol is synthesized from carbon substrate only.
7. Fermentation is performed at, a) optimal temperature of 37°C; b) optimal pH of 4.5; c) under anaerobic conditions.
8. All the cells are metabolically active and viable.

Process and Systems Engineering Center (PROSYS)
Department of Chemical and Biochemical Engineering
Technical University of Denmark
Søltofts Plads, Building 229
DK - 2800 Kgs. Lyngby
Denmark

Phone: +45 45 25 28 00

Web: www.kt.dtu.dk/forskning/prosys